THE UNIVERSITY OF ADELAIDE

DEPARTMENT OF MECHANICAL ENGINEERING

HYDROJET
DUCTED PROPULSION SYSTEM

IMPELLER INDUCED VIBRATORY PRESSURES
and
PERFORMANCE CHARACTERISTICS

by

MALCOLM R. HALE B. E.

NOVEMBER 1966

Thesis for the degree of Doctor of Philosophy.

TABLE OF CONTENTS.

--ooOoo--

ABSTRACT.

Theoretical and experimental studies were conducted on a Hydrojet ducted impeller system with the aim of developing an efficient and vibration-free propulsion unit for ships. Initial estimates of the propulsive efficiency of the Hydrojet showed this to be a practical means of propulsion and further detailed investigations were undertaken.

A theoretical analysis of an impeller operating in an infinitely long duct was developed by assuming the impeller to be replaced by a simple bound vortex-line. The optimum geometry for an impeller was taken to be that design for which the induced and profile drags had minimum values, the maximum blade stress was equal to the design stress, and the blade sections operated free from cavitation at the design conditions.

Experimental and theoretical values of impeller efficiency showed that values in the order of 0.85 to 0.90 were possible.

Impeller-induced vibratory pressures on the inner duct surface were measured under various impeller loading conditions and different inflow velocity patterns to the impeller. An intense pressure field existed near the impeller plane but its magnitude rapidly attenuated with distance from the impeller. Pressure coefficients $\frac{P}{\rho n^2 D^2}$ in the order of 0.5 were measured at the impeller plane, but values of less than 0.01 existed at distances greater than 0.4 of the impeller diameter (D). The blade frequency harmonic content of the total pressure was extremely large, with the 2nd and 3rd harmonics being approximately 60% and 25% respectively of the 1st harmonic. The phase angle of all harmonics of the induced pressure were constant forward of the impeller and varied linearly with distance behind the impeller. The trailing vortices of the impeller blades appeared to originate near the mid-point

of the blade chord and had a tendency to move forward as the harmonic number increased. The helical vortex line at the duct surface had a constant pitch.

The pressure due to non-uniform flow were approximately dependant on the mean velocity taken over the blade length for a given angular position of the impeller.

In the course of the investigation the following studies were also conducted.

(a) An accurate method of machining impellers was developed. The impeller was machined with a spherical milling cutter which was controlled to move at all times tangential to the desired surface. The position of the cutter on the desired locus was limited to a rectangular grid pattern. A digital computer programme was developed to calculate the co-ordinates of points on the surface of an impeller blade of arbitrary shape.

(b) An analysis and associated technique was developed for the calibration of a five-hole spherical pitot in a flow whose direction is only approximately known.

(c) A complete analogue data-acquisition system was designed and developed capable of recording time-varying data with a flat frequency response from DC to 15 kc. The analogue data was recorded on to magnetic tape which was capable of being digitized at rates up to 12,000 samples per second.

STATEMENT

This thesis contains no material which has been accepted for the award of any other degree or diploma in any University. To the best of the author's knowledge and belief, this thesis contains no material previously published or written by another person, except where due reference is made in the test.

Malcolm R. Hale

Nov. 1966.

ACKNOWLEDGEMENTS

The author wishes to express his sincere appreciation to the following individuals and organizations:

Professor H.H. Davis, Dr. J. Mannam and the staff of the Mechanical Engineering Department, University of Adelaide and Professor D.H. Norrie of the Department of Mechanical Engineering, Calgary (formerly of Adelaide) for their guidance, assistance, suggestions and encouragement during this project.

Messrs. R. Schumann, R. Garnham, G. Morgan and H. Bode, who helped with the design and construction of the data acquisition system used for this investigation.

Mr. J. Dunne and his staff of the Computing Electronics Division of Weapons Research Establishment (W.R.E.) Salisbury, South Australia, for their guidance and assistance during the development of the voltage to frequency converters.

Messrs. R. Fitton, R. Trueman and the staff of the Mechanical Engineering workshop, for their co-operation in constructing the models and mechanical components used in this research project.

Messrs. J.H. Fowler of Mechanical Engineering Department and D. Knight of C.S.I.R.O. computing centre for their assistance whilst developing the computer programmes. Miss P. Yates of Mathematical Services Division of W.R.E. for processing the recorded information by converting the analogue data to digital. The use is greatly appreciated of the computing facilities and services of the Commonwealth Scientific and Industrial Research

Organization (C.S.I.R.O.) Computing Section, Adelaide and the Department of Computing Science (University of Adelaide).

Commonwealth Government of Australia and the C.S.I.R.O. for providing research scholarships, which the author was fortunate enough to hold during this post graduate study.

U.S. Government Department of the Navy and the David Taylor Model Basin for the financial assistance which made this research possible.

INTRODUCTION

Naval architects and marine engineers are continually endeavouring to improve the propulsive efficiency and power of ships to obtain higher speeds. Unfortunately, the increase in power and speed is accompanied by an increase in the unsteady forces which are created by the propeller and which act on the hull of a ship. The vibrations produced by these forces may reach magnitudes which will have a detrimental effect on the machinery as well as producing considerable discomfort to passengers and crew. Thus designers are faced with the problem of reducing these unwanted forces to more acceptable levels.

Two types of forces are generated:--

(a) bearing forces

(b) surface forces

The former forces are transmitted to the hull through the propeller shaft and bearings. They arise from the propeller operating in a ship's wake which has a non-uniform velocity field. This field is primarily caused by the viscous boundary layer of the hull and to lesser extent by the potential flow field.

The latter forces are created through the interaction of the pressure field with the hull surface. The pressure field surrounding the propeller is dependant on the instantaneous loading on the propeller, on the blade geometry and, in particular, on the blade thickness. The resultant surface force on the hull is governed by the geometrical relationship between the propeller and the surface.

A considerable number of experimental investigations have been carried out to determine comfortable enviromental levels of vibration, the levels existing in ships, the magnitude of the forces present, and

the effect the geometry of the afterbody has on these forces. (Ref. 0.1 and 0.2).

The results of these investigations lead to the conclusion that, with conventional hull form and propeller design, it is difficult to reduce the vibration to acceptable levels. It also suggests that it will be necessary to examine other forms of marine propulsion where the propeller-excited vibrations may be reduced and the propulsive efficiency increased. One such system is a ducted propulsion unit.

This thesis deals with a theoretical and experimental investigation into the feasibility of a ducted propulsion system, herein called a "Hydrojet". The Hydrojet consists of an impeller operating in a cylindrical duct of several impeller diameters in length. The following investigation was undertaken:--

(a) An estimate of the propulsive efficiency of the Hydrojet.

(b) A theoretical analysis of the impeller.

(c) A model impeller based on the above theory was constructed to a high dimensional accuracy by a new machining technique.

(d) The pressure induced by the impeller operating in a duct were measured at the inner duct surface.

(e) Experimental values of the impeller characteristics were measured and compared with those obtained by theory.

1.0 HYDROJET PROPULSION

1.1 ROTODYNAMIC PROPULSION UNITS.

Hitherto the screw propeller, which is a roto-dynamic device, has been accepted as the conventional propulsion unit for marine vessels. One of the problems encountered with this type of propulsion device is the generation of large fluctuating propeller-induced forces. As already mentioned in the Introduction, extensive investigations have been undertaken to understand this problem and thus make it possible to reduce the vibrations to acceptable levels.

It is known that these vibratory forces can be eliminated if the following two conditions are satisfied.

(a) The magnitude and direction of the forces, acting on the blades, must be independant of time. This will be the case when a rigid propeller operates in a uniform flow field.

On the other hand, if the propeller operates in a non-uniform flow field, the blade section pitch will have to be controlled if the above conditions are to be satisfied.

(b) The net force due to the pressure field acting on the boundaries of the propulsion unit must be invariant with time. This can only be achieved with a rotor having finite number of blades and the boundaries near the rotor being both rigid and symmetrical about the rotor axis.

Based on these requirements, rotodynamic propulsion units can be broadly divided into two groups:--

(a) An 'Open' configuration where the solid boundaries near the rotor are effectively outside the intense fluctuating pressure field which is generated by the rotor. Normal screw propulsion falls within this category.

(b) A 'Ducted' unit where the solid boundaries are within the intense pressure field of the rotor. Here the rotor operates in a rigid duct which is substantially symmetrical about the rotor axis near the plane of the rotor and the duct diameter approaches that of the rotor.

Many investigators have studied the open configuration with a view to increasing the efficiency and reducing the vibration levels due to the bearing and surface forces (Ref. 1.1). The factors governing the efficient operation of such a propeller are well known and can easily be adjusted when selecting a propeller for a given duty. The vibratory forces however are not easily controlled and in many instances it is difficult to obtain acceptable levels. Therefore it was decided to carry out a preliminary examination of various types of propulsive systems to see whether it would be possible to reduce the propeller-induced unsteady forces to even lower values.

For any new propulsion system to be suitable for large displacement vessels there are a number of requirements, in addition to those mentioned above (p 1.1), which must be satisfied, viz:--

(a) Propulsive efficiency must be comparable with that of a conventional screw propeller.

(b) Steering power must be adequate.

(c) The ability to maintain satisfactory performance in varying conditions of seaway must be maintained.

(d) The ability to withstand damage in exceptional conditions must be comparable with screw propellers.

The following configurations considered would have inherently low vibration characteristics:--

(a) A conventional screw propeller behind a hull with modified after-body.

(b) Various configurations with the propeller mounted at or forward of the bow.

(c) Various multi-hull configurations in which the propeller or propellers would operate in more uniform wakes than with the conventional screw system.

(d) A submersible hull consisting of a cigar-shaped main body completely submerged with a narrow stream-lined superstructure protruding above the water line.

(e) A hull with propulsive units in pods on outriggers.

(f) Various forms of internal duct system (hydraulic jet propulsion or Hydrojet).

Preliminary studies of the above configurations indicated that the type mentioned in (f) was most suited as a replacement for the screw propeller on large displacement vessels. For this reason it was considered profitable to carry out a more detailed analysis of this type of propulsion system.

1.2 PERFORMANCE OF A HYDROJET.

A Hydrojet or ducted impeller system is one in which the impeller operates in a duct or tunnel of dimensions comparable with the impeller diameter. The duct diameter (D_d) would be very nearly that of the impeller (D). The length would be of the order of several impeller diameters depending on its application.

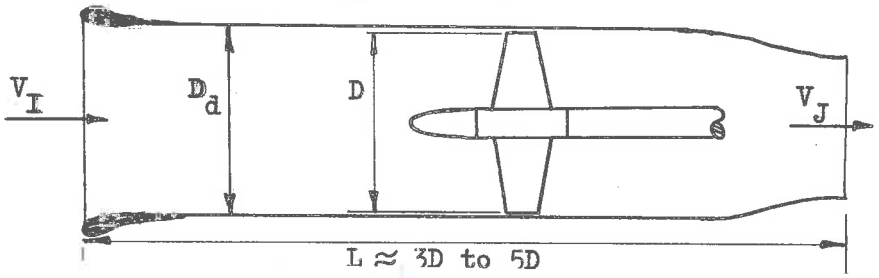

In order to develop the desired thrust by increasing the axial momentum of the fluid, there is a contraction at the exit of the duct so that the exit or jet velocity (V_J) exceeds that of the intake (V_I).

1.2.1 Propulsive Efficiency.

The fundamental nature of the energy losses in a Hydrojet is extremely complicated. To obtain an estimate of this, the hydrodynamic energy losses are divided into:-

(a) Impeller losses.

(b) The losses due to the intake, duct and nozzle.

(c) Loss due to the interaction of hull and duct.

The losses associated with the impeller are accounted for in the impeller efficiency η_E. The intake, duct and nozzle losses, termed the duct loss, may be expressed as a fraction of the intake kinetic energy.

ie. Ductwork losses per unit mass flow $= \zeta \frac{V_I^2}{2}$ ... 1.1

where ζ = the loss factor

V_I = intake velocity

The hull efficiency η_H takes into account the effect of operating the Hydrojet in the vicinity of a hull (Appendix A4). Hence the propulsive efficiency η_P can be expressed as follows:-
(See Appendix A4 for the derivation).

$$\eta_P = \eta_E \eta_H \frac{2\mu(1-\mu)}{[1-\mu^2(1-\zeta)]} \quad \text{... 1.2}$$

where $\mu = \frac{V_I}{V_J}$ = velocity ratio

and

V_J = velocity at exit of duct

A more useful relationship of η_P can be given in terms of the thrust load coefficient (C_{TL}) based on the area (Ao) and the relative axial velocity (Va) of the fluid at the impeller.

Thus

$$\eta_P = \eta_E \, \eta_H \, \frac{4(C_{TL} K_A)}{[(C_{TL} K_A)^2 + 4(C_{TL} K_A) + 4\xi]} \qquad \ldots 1.3$$

where $C_{TL} = \dfrac{T}{\frac{1}{2} \rho V_a^2 A_o}$

and T = thrust of the Hydrojet

K_A = ratio of area of impeller annulus to area of duct

Fig. 1.1 shows curves of propulsive efficiency (η_P) against thrust load coefficient (C_{TL}) for different duct loss factor (ξ) as expressed by equation 1.3. It will be observed that for a fixed value of ξ, the efficiency η_P will increase with increasing C_{TL} and reach a maximum; further increasing the C_{TL} results in a decrease of propulsive efficiency (η_P).

The maximum impeller efficiency (η_{Popt}) of a ducted propulsion system for a given duct geometry and hence loss factor is:-

$$\eta_{Popt} = \eta_E \, \eta_H \, \frac{1}{1 + \sqrt{\xi}}$$

$$= \eta_E \, \eta_H \, \frac{2}{(C_{TLopt} K_A) + 2} \qquad \ldots 1.4$$

This maximum efficiency occurs when

$$\mu_{opt} = \frac{1}{1 + \sqrt{\xi}} \qquad \ldots 1.5$$

and

$$C_{TLopt} = \frac{2\sqrt{\xi}}{K_A}$$

Drawing a line passing through the maximum efficiency (η_{Popt}) of each individual curve of ζ shows that the η_{Popt} will increase with decreasing thrust load coefficient and approach unity. Hence for high efficiency the duct loss factor and the thrust load coefficient must be kept as low as possible (Ref. 1.3 and 1.4).

It might be mentioned that below the maximum efficiency (η_{Popt}) line the propulsive efficiency is greatly dependant on the thrust load coefficient (C_{TL}) and hence the velocity ratio (μ) for a given ζ ; above this line, however, η_P is not significantly affected by a change in C_{TL}.

In order to apply the theoretical results shown in Fig. 1.1 it is necessary to estimate the duct loss factor (ζ) and the impeller efficiency (η_E).

1.2.2 Estimation of Duct Losses.

An initial estimate of the hydrodynamic loss can be made by first assuming the impeller does not effect the growth of the boundary layer in the duct. Therefore it is possible to replace the duct by a flat plate, having the same length and area as the inner surface of the duct. It is also assumed that the plate is in a uniform fluid stream having a velocity equal to the intake velocity of the propulsion unit. The loss factor (ζ), which is the ratio of energy loss to the kinetic energy of fluid at the leading edge, is expressed by the following equation:--

$$\zeta = \frac{\text{energy loss}}{\text{K.E. at inlet}}$$

$$= \frac{\left[\frac{1}{2} C_D \rho V_I^2 \left(\pi D_d L\right)\right] V_I}{\frac{1}{2}\left[\rho \left(\frac{\pi D_d^2}{4}\right) V_I\right] V_I^2}$$

$$= \frac{4 C_D L}{D_d} \qquad \ldots 1.6$$

where C_D = drag coefficient of the plate

and D_d = diameter of duct

and assuming $C_D = C_F + \Delta C_D$ ... 1.7

where C_F is given by the ATTC (1947) mean friction line as expressed in the relationship

$$(C_F)^{-0.5} = 4.132 \log_{10} (R_n C_F) \quad \text{... 1.8}$$

and R_n is Reynolds number of the plate based on its length.

also ΔC_D = 0.001 is an allowance for the surface and its coating.

The magnitude of ζ for varying duct geometry and operating conditions is given in Fig. 1.2. The values are based on the assumption that the density of fluid is 1.99 slugs/cub.ft.

The value of the duct loss factor (ζ) for a practical arrangement of ducting which has a length-to-diameter ratio of about 5 is, from Fig. 1.2, between 0.004 and 0.006. The corresponding value of the optimum performance ratio $\frac{\eta_P}{\eta_E \eta_H}$ from Fig. 1.1 is between 0.81 and 0.84.

The propulsive efficiency of the Hydrojet can be determined, if the impeller efficiency η_E and the hull efficiency η_H are known. An estimate for the impeller efficiency is of the order of 0.90, based on high specific-speed axial-pump data (Ref. 1.5). Assuming a value of 1.0 for the hull efficiency then the value of the propulsive efficiency for a practical Hydrojet system would be between 0.72 and 0.76.

2.0 IMPELLER DESIGN AND MANUFACTURE.

2.1 IMPELLER DESIGN.

2.1.1 Introduction.

Propeller design procedures in use today, do not attempt to determine the optimum propeller geometry for a given set of operating conditions, apart from one recorded exception given in Ref. 2.1.

The methodical series of propellers are based on an optimum value for one of the major variables and the optimum values for all other design variables are not determined. For example, from the design data for the NSMB (or Van Manen) screw series, the optimum diameter can be chosen and hence the corresponding pitch and mean blade area ratio can be determined to avoid cavitation under the operating conditions. In this series, the blade outline, blade sections, and variation of maximum blade thickness with radius have been previously fixed.

In some of the more theoretical design procedures, it is possible to calculate the circulation distribution, so that the energy loss caused by the induced flow is minimised. It is not possible, however, to determine from these theories an optimum blade shape for strength and for the desired circulation distribution.

The theoretical knowledge of propeller operation has progressed to a stage where an attempt should be made to develop a design technique based on these theories which would determine the

best propeller geometry to suit a given set of operating conditions. A technique of this magnitude would require many mathematical statements and decisions. If such a design is to be economical in both time and cost, the resources of a high-speed digital computer and store are necessary. With the advent of more rigorous and complex theoretical approaches to the design of propellers, a type of optimum design procedure will become necessary in the future, if full advantage is to be taken of the acquired theoretical knowledge.

A programme described in Appendix A 1 was an initial attempt at an optimizing design procedure. Although the design method used in this programme was not the most rigorous, the solutions given by the programme show that optimization could be usefully employed for more complex design theories. The programme was developed to study the feasibility of the Hydrojet propulsion unit.

2.1.2 Hydrodynamic Model of the Impeller.

Since the present research project was directed towards estimating the capabilities of a ducted propulsion system, it was considered that a simplified vortex-line theory could be satisfactorily applied to the design of the impeller.

The following theory is applicable to the design of ducted propellers where the induced circulation around the duct can be neglected. It can also be applied to the design of axial flow pump units.

Consider an impeller operating in a long cylindrical duct in which the fluid can be considered as irrotational upstream of the impeller. It is assumed that the impeller has neglible tip clearance. Thus the impeller diameter equals the duct internal diameter. The finite size boss is assumed to have neglible effect on the induced flow.

It is assumed that the axial velocity profile is uniform across the duct upstream of the impeller.

It is also assumed that for a sufficient distance upstream and downstream of the impeller, the duct is parallel. The impeller design is selected to have no axial component of induced velocity. The velocity diagram is as shown in Fig. 2.1.

It is considered to be sufficiently accurate for the interference flow to be assumed constant circumferentially at any radius. This is equivalent to assuming the interference flow is generated by an infinite number of lifting-lines of variable strength in the radial direction. Using the Betz's criteria for minimum induced energy loss in the wake of an inviscous fluid, and the Kutta-Joukowsky relationship, the ideal thrust and torque gradients at any section can be derived as follows:-- (see Fig. 2.1)

$$\frac{dT_i}{dr} = 4\pi \rho \omega^2 r^3 \eta_i (1 - \eta_i) \qquad \ldots 2.1$$

$$\frac{dQ_i}{dr} = 4\pi \rho \omega Va\, r^3 (1 - \eta_i) \qquad \ldots 2.2$$

If it is assumed that the circulation distribution for minimum energy loss is not greatly affected by the variation of profile drag with radius, then the actual thrust and torque gradient can be evaluated as follows:-- (see Fig. 2.1).

$$\frac{dT}{dx} = \frac{dT_i}{dx}\,(1 - \xi \tan \beta_i) \qquad \ldots 2.3$$

$$= K_1\, \eta_i\, (1 - \eta_i)\left(1 - \frac{\xi}{\delta x\, \eta_i}\right) x^3 \qquad \ldots 2.4$$

and

$$\frac{dQ}{dx} = \frac{dQ_i}{dx}\left(1 + \frac{\xi}{\tan \beta_i}\right) \qquad \ldots 2.5$$

$$= K_1 \frac{Va}{\omega}\,(1 - \eta_i)(1 + \xi\, \delta x\, \eta_i)x^3 \qquad \ldots 2.6$$

where

$$\delta = \frac{\omega R}{Va} \qquad \xi = \frac{C_D}{C_L}$$

$$x = \frac{r}{R} \qquad K_1 = \frac{4\pi\, \rho\, \delta^4\, Va^4}{\omega^2}$$

$$\tan \beta_i = \frac{1}{\delta\, \eta_i\, x}$$

The total thrust (T) and torque (Q) of the impeller can only be evaluated by summation over the blade length if the drag to lift ratio ξ is known at each section. Since this ratio depends on the blade profile which is in turn dependent on the strength, cavitation and hydrodynamic requirements, a simple expression for thrust and torque cannot be obtained.

An approximation to the impeller geometry can be obtained by assuming the drag to lift ratio constant with the radius. In this case integration gives the following equations for total thrust T and overall efficiency η_o.

$$T = A(1 - \eta_i)(\eta_i B - C) \quad \ldots 2.7$$

$$\eta_o = \frac{\eta_i B - C}{B + \eta_i D} \quad \ldots 2.8$$

$$= \frac{T}{A(1 - \eta_i)(B + \eta_i D)} \quad \ldots 2.9$$

where

$$A = \frac{\pi \rho \, Va^4 \, \delta^3}{\omega^2} \qquad C = \tfrac{4}{3} \xi (1 - K^3)$$

$$B = \delta (1 - K^4) \qquad D = \tfrac{4}{5} \xi \, \delta^2 (1 - K^5)$$

$$K = \frac{\text{radius of boss}}{R}$$

2.1.3 Blade Element Properties.

(1) Blade element characteristics.

The design lift coefficients of the section (C_L) can be expressed as,

$$C_L = \frac{dL}{\frac{1}{2} \rho V_R^2 \, c \, dr} = \frac{8\pi \, \delta (1 - \eta_i) x^2 R}{Zc \sqrt{(x \, \delta \, \eta_i)^2 + 1}} \quad \ldots 2.10$$

where c = chord of blade section.

The theoretical lift coefficient (C_{li}) required to develop the design lift is assumed to be greater than C_L by a factor μ_m, the viscosity factor. According to the potential theory of thin wing sections (see Chapter 5, Ref. 2.2), the theoretical lift coefficient of the section is a function of the camber to chord ratio $\frac{m_x}{c}$ only if the section operates at shock-free entry conditions, hence

$$C_{li} = l_m \frac{m_x}{c} \qquad \ldots 2.11$$

The blade section chosen for this impeller was an NACA-16 thickness distribution with a mean line of a = 1.0 and the values for viscosity factor (μ_m) and lift camber factor (l_m) at shock-free conditions are given in Appendix A 1, eqn. 18 to 20 and also in Table 5.6, p 175 in Ref. 2.2 .

(2) Blade strength.

The stresses at a blade section were calculated by the simple theory for bending of a beam as suggested by Tingey (Ref. 2.3, also Ref. 2.2).

It is important to note that this theory can be applied only to designs where chordwise bending due to the pressure distribution over a section can be ignored. This implies that the blades should have relatively large thickness to chord ratio ($\frac{t_x}{c}$) and not excessively wide chords. The blade geometry chosen for the impeller is consistent with the assumptions of the stress calculation by Tingey.

(3) Cavitation.

Using the theory of thin wings, the cavitation parameter, the "pressure minima cavitation number" σ_p is determined for the given blade section as follows: (Ref. 2.2 p 209)

$$\sigma_p = (1 + 1.14 \frac{t_x}{c} + \frac{C_{li}}{4})^2 - 1 \qquad \ldots 2.12$$

The sectional cavitation number σ_s is defined by

$$\sigma_s = \frac{(P_r - e)}{\frac{1}{2} \rho V_R^2} \qquad \ldots 2.13$$

where

p_r = pressure at blade section radius r and at minimum immersion

e = saturated vapour pressure

When applying these equations to an actual impeller an overall factor f_o which makes allowance for irregular and viscous flow is introduced to effectively increase σ_p.

Thus

$$\sigma_s \geqslant f_o \sigma_p \qquad \ldots 2.14$$

where f_o = 1.2 (Ref. 2.2 p. 209)

A similar method was used by Matthews and Straszak to estimate the inception of cavitation in screw propeller designs. (Ref. 2.4).

2.1.4 Optimum Design.

The optimum combination of blade sections for a Hydro-jet impeller was chosen to be that which satisfies the following:--

(a) The hydrodynamic equations for minimum energy loss.

(b) The lowest possible profile drag providing that:--

(c) The blade section is strong enough to limit the sectional stresses to a value equal to or less than the maximum design stress.

(d) The blades must also operate free from cavitation.

(e) As a consequence of meeting the above conditions, the weight of the impeller will be a minimum for the chosen operating conditions.

Details of the design procedure are given in Appendix A1.

Although the impeller dimensions calculated by this design method lead to an optimum blade section arrangement for the given conditions, it is not necessarily the optimum design for a given duty, for example, for a given thrust (T).

The optimum design must be selected by studying closely, the results of a series of systematically varied impellers, all designed for optimum arrangement and satisfying the requirements of a given duty. Before deciding upon the final impeller geometry, certain other factors

affecting the operation of an impeller or rotor-dynamic propulsion unit must also be taken into account - e.g.

(a) Is the largest diameter impeller that can be installed in the vessel also the optimum diameter?

(b) Is the number of blades and rotational speed conducive to exciting critical modes of vibration when the propulsion system is operating?

(c) What is the economical range of rotational speeds of the prime mover?

The sectional lift coefficient is another important variable which must be studied before selecting the final design.

The design programme given in this report does not achieve the ideal objective. This could be stated as "the selection of an optimum impeller geometry to suit a particular duty by considering every possible arrangement which satisfies all known laws, principles and facts associated with its operation." All these decision points could be inserted into a programme for the logical selection of the ideal impeller, and would require extremely careful planning. Although the complete optimum design is not specified directly by the programme of this report, it is considered that the technique given for selecting an optimum blade geometry is a radical departure from the usual propeller design procedures.

2.2 IMPELLER CHARACTERISTICS AND MODEL IMPELLER.

The impeller design method outlined in the previous section determines the optimum blade dimensions which satisfy the design assumptions and the given set of operating conditions. Unfortunately it is not possible to represent the parameters which govern the impeller characteristics by dimensionless groups, as for each set of operating conditions there is only one arrangement of blade dimensions which satisfy all the design requirements.

A design study was made of a twin Hydrojet propulsion unit to replace an existing single screw propeller on a 19,000 tdw ore carrier. A drawing of the proposed layout is given in the Appendix A5.

The main design requirements of the impeller were

Thrust/Unit - 44,800 lbf

Velocity at impeller disc - 19.3 fps

To meet the above operating conditions, a number of impellers were designed according to the procedure given in Section 2.1 by varying the impeller radius, rotational speed and blade area ratio. The impeller efficiency η_E for these various designs are shown in Figs. 2.2 to 2.4. The blade section chord was assumed linear with radius, varying from CID at the boss to COD at the blade tip.

A study of these characteristics shows the radius at which the impeller efficiency is a maximum is not significantly affected by blade-area ratio or geometry changes (Fig. 2.2). Similarly, the optimum rotational speed is not greatly affected by the varying impeller geometry (Fig. 2.3) for the fixed impeller diameter and rotational speed. Fig. 2.4 shows the small change in impeller efficiency due to a change in the blade geometry.

The impeller chosen to meet the design conditions was as follows:--

Thrust/Unit	44,800 lbf
Velocity at impeller disc	19.3 fps
Diameter	15 ft
Blades	4
Rotational Speed	1.5 rps
Expanded Blade Area Ratio	0.543
Linear chord distribution	
Tip chord	5.0 ft
Boss chord	3.0 ft
Chord section	NACA-16, a = 1.0
Theoretical efficiency of the impeller	0.87
Thrust load coefficient	0.688

An 8 inch diameter model of this impeller is shown in Fig. 2.5 and Fig. 2.9 and a list of dimensions of the impeller is given in Table 4 of Appendix A1.

The value of the theoretical impeller efficiency compares favourable with that taken in Section 1.2.2 as an initial estimate.

2.3 MACHINING TECHNIQUE FOR THE IMPELLER.

Manufacturing technology, in general has progressed rapidly over the past decade, but it has not significantly affected the machining techniques used to construct model or prototype propellers.

Changes in manufacturing processes are necessary if accuracy is to be increased and production time decreased. Accuracy is important where measured values of a variable from model experiments are to be used to predict the prototype values or are to be compared with theoretical values.

The common method of machining an impeller or propeller is to use a cutter which moves (relative to the blade) on a cylindrical path with centre on the axis of the impeller. The cutter motion is controlled by a follower moving over a series of templates which may be either cylindrical or expanded-cylindrical sections depending on the mechanism used to convert movement of the follower to the cutter.

Another method, which is suited for the majority of milling machines, is the spot-machining of points on the blade surface in either a polar or a rectangular grid pattern. This method requires considerable computation especially when cartesian co-ordinates are used, because the object is naturally defined by polar co-ordinates.

In all the machining techniques commonly employed it is usual to use only a small number of sections to define the complete blade shape. Hand machining is thus necessary to "fair in" between the machined regions.

Disadvantages of the above methods are:--

(1) The time taken to hand "fair in" between the accurately machined sections.

(2) The blade surface can only be as accurate as the templates.

(3) The accuracy is dependant on the size of the cutter since a correction should be made to the templates to define the locus of the cutter moving over a blade surface at the desired section. Because the template shape is usually that of a blade section, an appreciable error is introduced unless the cutter has a cutting edge radius small in comparison with the radius of curvature of the blade surface at the point being considered.

The ideal method of machining an impeller is by an automatically-controlled milling machine using a magnetic tape as an input medium for all machining instructions and control. The technique used to manufacture the model impeller associated with this research project, could be adapted to generate the above machining instructions.

Appendix A 2 gives a method of determining the co-ordinates of points on the locus-surface generated by the centre of a spherical cutter which would machine the surface of an arbitrarily defined impeller blade. The points are obtained in a rectangular grid pattern of a predetermined dimension.

The 8 inch diameter model impeller, Fig. 2.9, (scale ratio of 22.5) was machined in a Pantograph copying machine (Fig. 2.7 and 2.8) from a three-dimensional master template. This master template was four times larger than the model and was machined in a universal miller (Fig. 2.6) to dimensions calculated by the programme in Appendix A 2.

The master templates were used to increase the accuracy of the final impeller and to reduce the number of machining co-ordinates necessary to obtain the required accuracy.

The machined points were placed 0.25 of an inch in the radial direction and either 0.125 or 0.025 of an inch in a direction normal to it, depending on the rate of curvature of the surface at the point being machined. To define the blade surfaces 6550 points were used, ie. 3275 points for each blade surface. The spherical cutter used to machine the master templates was 1.25 of an inch in diameter.

The accuracy of the finished model impeller was within $\pm$ 0.001 of an inch. The accuracy of computation can be selected and depends on the size of the model and master templates.

A brief description of the machining technique used is given in Appendix A 3.

3.0 MODEL ARRANGEMENT AND TESTING PROCEDURE

3.1 MODEL ARRANGEMENT.

Investigations were conducted to determine the impeller characteristics and surface pressures on the duct of a simple two-dimensional Hydrojet model as shown in Fig. 3.1. This model was tested in the 18 inch diameter Research Water-Tunnel of the Department of Mechanical Engineering.

The model consisted of several plane cylindrical sections of 8 inch internal diameter, to which was attached a contoured entrance section and a converging exit nozzle. The duct from intake to exit was 4.625 impeller diameters in length and the impeller was located in a plastic section 2.75 diameters from the intake. The plastic section of the duct surrounding the impeller had a blade tip clearance of 0.0028 impeller diameters.

The entrance section was a portion of an NACA 0015 basic thickness profile with an NACA 250 mean line. (Ref. 3.1, Nozzle 19 in Table 2). The exit nozzle had an area ratio $\left(\frac{A_J}{A}\right)$ of 0.745 which corresponds to the design thrust load coefficient of the impeller as expressed in equation 1.5 of Section 1.2.1.

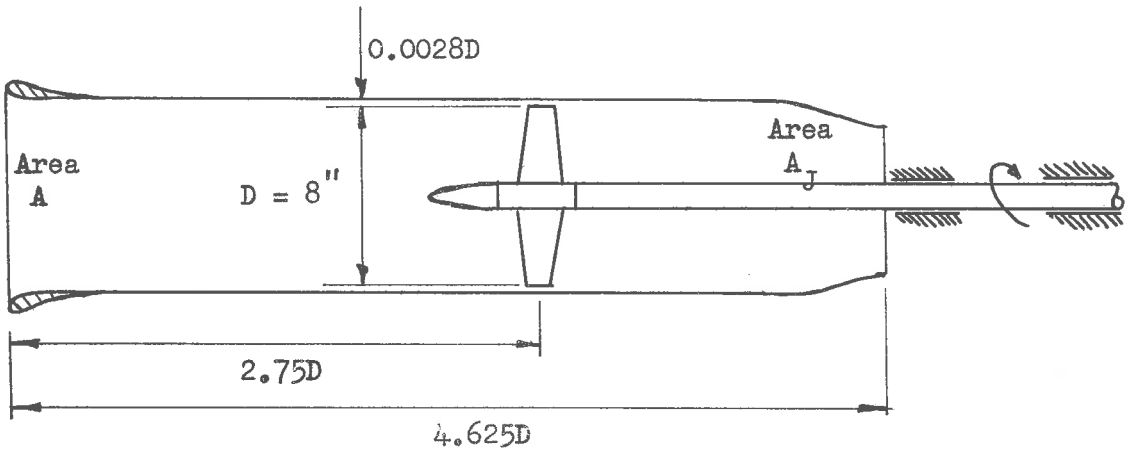

The pressure transducer (Section 4.1.2) could be mounted in any one of a series of locations placed on a plane parallel to the duct centre-line.

The other basic component of the model Hydrojet was the impeller dynamometer and drive shaft assembly. The drive shaft which housed the dynamometer was supported by bearings aft of the duct. Some difficulty was met with the design of these bearings because the impeller, dynamometer and drive shaft acted as a torsional pendulum and was excited by the slightest change in resistive torque of the bearing. However, the vibration of the dynamometer was reduced to workable levels by firstly inserting a carbon liner into the bearing and secondly by heavily damping the bearing supports. The damping was provided by lead weights which were attached to the supports and which were free to vibrate as dynamic absorbers.

3.2 DESIGN OF THE DYNAMOMETER.

The design requirements for the dynamometer were as follows,

(a) The new system had to fit into the existing drive shaft without modification.

(b) The system had to measure the mean values of torque and thrust.

(c) The fluctuating components of the torque and thrust had to be measured.

The arrangement finally selected for the dynamometer is shown in Fig. 3.2 and 3.3.

The bearing which carried the impeller was elastically connected to the drive shaft by a thin-walled cylindrical sensing element. This allowed relative motion between the shaft and impeller and at the same time effectively supported the impeller.

A tapered-land hydrostatic bearing (Ref. 3.2) was chosen because the change in eccentricity of the bearing and journal is very small for a

change in the bearing load. Thus the damping properties of the bearing were very nearly constant and the damping was viscous.

As the impeller was effectively supported by the bearing, the design of the sensing element was controlled by the maximum loading conditions of the impeller, providing the natural frequencies of the dynamometer were also acceptable. Also another design requirement of the sensing element was that its strain levels under normal operating conditions had to be large enough to be detected by the measuring instruments.

The characteristics chosen for the dynamometer were as follows:--

TABLE 3.1

	THRUST	TORQUE
Normal max. loading - (Limited at present by electronic instrumentation)	100 lbf	200 lbf ins
Max. Design Loading	400 lbf	350 lbf ins
Natural Frequency with impeller in air	2000 cps	370 cps
Sensitivity of dynamometer and amplifier (Sect. 4.2)	0.031 volts/lbf	0.043 volts/lbf.in
Sensing element dimensions	1.300 in. dia.	
	1.300 in. length	
	0.030 in. wall thickness	
	Material - Cast Monel.	

The forces acting on the dynamometer were detected by a fully active Wheatstone bridge circuit incorporating resistance wire strain gauges supplied with a DC voltage.

Because the sensing element initially was open to the surrounding water, the gauges were waterproofed by a thin coating (0.050 ins.) of a silicone rubber compound. This proved to be unsatisfactory because the moisture content gradually increased over a period of several weeks to a level that upset the balance of the D.C.

pre amplifiers in the recording instrumentation. (Appendix A7.). For this reason an alternative method was used, which consisted of forming an enclosed space above the strain gauges with a thin rubber diaphram (Fig. 3.3). The space was then filled with silicone oil to exclude the entry of water into the space. This arrangement was an improvement on the previous method.

Unfortunately after completing the model tests discussed herein it was found that a small amount of water had entered the cavity and that the silicone oil had affected the cement used to bond the strain gauges to the sensing element. During the tests however, the dynamometer behaved satisfactorily.

3.3 MODEL TESTING PROCEDURE.

Tests were conducted to determine the following:-

(a) The fluctuating pressures acting on the inner surface of the duct near the plane of the impeller for,

(i) Uniform flow at the impeller.

(ii) Non-uniform flow at the impeller.

(b) Impeller Performance Characteristics.

(i) Steady state values for thrust and torque.

(ii) Velocity in the wake of the impeller.

The above characteristics were investigated at both 15 and 20 cps of the impeller, for various advance coefficients J_I, where

$$J_I = \frac{V_I}{nD}$$

V_I = duct velocity at intake (fps)

n = impeller rotational speed (cps)

and D = impeller diameter (ft)

When the model was tested under non-uniform inflow conditions, a series of wire-mesh patches, which formed a velocity wake inducer

(Ref. 3.3), were located forward of the duct intake. The complete wake inducer could be rotated during these tests about a longitudinal axis of the duct. This enabled the complete pressure distribution on the duct surface to be measured by only one transducer which could be moved axially along the duct.

Since it is known that the induced vibratory pressure of an impeller is periodic in relation to impeller rotation, and that it has a fundamental frequency equal to the blade passing frequency (ie. rotational speed of the impeller times the number of blades), it was decided to express the pressure by a Fourier Series.

As facilities were available to process recorded analogue data into digital information, the Fourier components were determined analytically. The design and construction of a high-speed magnetic tape recording system with a Frequency Modulated (FM) recording mode was thus undertaken and is discussed in the following Section 4.0 and also in Appendix A7.

4.0 INSTRUMENTS AND APPLIED MEASURING TECHNIQUES.

The design and construction of much of the instrumentation for measurement and data recording was undertaken for this research project.

The recording mode selected for this project was F.M. (frequency modulated) to I.R.I.G. specifications.

The recorded F.M. analogue signal was converted to digital information before analysing the data on a digital computer.

The recording instruments can be divided into the following basic groups:--

(1) Sensing elements - transducers

(2) Signal amplifiers and conditioning units

(3) Recording system - high-speed tape recorder

A simplified block diagram of the instrumentation is given in Fig. 4.1.

Details of each unit and its calibration are given in the following sections and Appendix A7.

4.1 SENSING ELEMENTS - TRANSDUCERS.

4.1.1 Torque and Thrust Transducers.

Torque and thrust transducers were mounted in the dynamometer, details of which are given in Section 3.2.

The impeller which was supported on a hydrodynamic tapered bearing was elastically attached to the drive shaft via a thin-walled cylindrical tube, or strain shell.

The sensing elements, resistance wire strain gauges, were cemented to the strain shell in the directions of the principal stresses, and were connected to form a fully-active Wheatstone bridge circuit which was sensitive to either axial or torsional loading.

The strain gauges in the torque and thrust bridges consisted of four 600 Ω Phillips strain gauges, PR 9812 with a nominal gauge factor of K = 2.0.

A direct current (D.C.) strain-gauge system was adopted, and the signals were voltage amplified in D.C. pre-amplifiers attached to the flywheel of the impeller drive shaft.

Monel-metal slip-rings with silver carbon brushes were used to transmit the signals to MOVADAS, the recording system.

4.1.2 Pressure Transducer.

The pressure transducer used was a Statham PM 222 TC ± 5-200 Bi-directional Differential Pressure Transducer which had a nominal output of 370 μV/psi/volt and a maximum excitation voltage of 3 volts. The diaphragm of the transducer which was 0.25 of an inch in diameter, was flush mounted as an external surface of the transducer. Because of its construction, the transducer had to be enclosed in a water-proof holder with only the sensing diaphragm and the signal leads open to the atmosphere. It was found necessary, during the tests, to apply an internal pressure to the transducer diaphragm in excess of the static pressure at that particular point to ensure no possible entry of water into

the holder.

Before and after each series of measurements, the transducer was statically calibrated. The following is a brief specification of the transducer.

Table 4.1.

PRESSURE TRANSDUCER SPECIFICATION.

Model	Statham PM 222 TC ± 5-200
Pressure Range	± 5 psid
Transduction	Resistance, balanced complete unbonded strain gaige bridge
Normal Bridge Resistance	200 Ω
Excitation	3 volts D.C.
Nominal Output	370 μV/psi/volt.

4.1.3 Event Marker - Transducer.

This simple transducer, namely a photo-electric cell was arranged to give a voltage spike once per revolution at a known position of the impeller. This voltage signal, after amplification, triggered a monostable multivibrator to generate a square pulse which was recorded, in F.M. form, on a track of the tape-recorder.

In the subsequent mathematical analysis, the phase of the Fourier components of the wave were determined with respect to the Event Marker signal.

The Units comprising the Event Marker are discussed in Appendix A 7.

4.2 SIGNAL AMPLIFIERS AND CONDITIONING UNITS.

The signal amplifier and conditioning units form a data acquisition system which is called MOVADAS (Modulated Voltage Analogue Data Acquisition System).

MOVADAS consists of the following units (see Fig. 4.1.).

(1) D.C. voltage pre-amplifiers and mean-reading instruments.

(2) High-pass filter

(3) Driver amplifier

(4) Voltage to Frequency (V-F) Converter

(5) Programming Switch

Details of these units are given in Appendix A 7.

In order to obtain a signal capable of driving the Voltage to Frequency (V-F) Converter, the voltage output of the transducers were firstly D.C. amplified using balanced push-pull stages to gain stability and a satisfactory common mode rejection ratio. High-pass filtering was necessary to remove tunnel noise before further amplifying the AC components and converting the signal to a modulated frequency in the V-F Converters.

Prior to recording the desired F.M. signal on the tape, the programming switch inserted binary coded pulses to identify the

type of data and the data set or number. Calibration signals were also fed into the V-F converter to give an instantaneous calibration of the converter. The identification and calibration signals were applied to all active data channels simultaneously so that the resultant digital information could be cross correlated between channels.

The F.M. signals in the range 54 Kc $\pm$ 40% were recorded at 60 ips. The analogue tape was later converted to digital information at a rate of 4000 samples per second of actual recording time.

The major difficulties encountered while developing the measuring instrumentation are as follows:--

(1) D.C. Pre-amplifiers.

Because the voltage gains of the torque and thrust amplifiers were approximately 2500 and 4000 respectively, any small voltage change on the input side of the amplifier caused large signal changes at the output.

Originally, the rotating pre-amplifiers and strain gauges were supplied with power from external batteries via slip-rings. This arrangement was found to be unsatisfactory because:--

(i) Changes in brush to slip-ring resistance caused the strain gauge supply voltage to fluctuate.

(ii) Thermal emf's were generated on the slip-rings.

(iii) Power leads cutting stray magnetic fields generated small voltages.

The noise was cut to acceptable limits by attaching to the rotating amplifiers, the complete power-supply unit, including batteries and a voltage regulation circuit.

The output from the amplifiers were the only signals transmitted through the slip-rings.

(2) Mean Reading Instrument.

Large fluctuations in the thrust and torque signals were recorded after the D.C. pre-amplifiers. It was not possible to record consistant mean readings on a normal volt-meter.

A consistant average was obtained by counting the number of cycles on the output of the V-F converter over a period of 10 seconds. For this test, the high-pass filter was removed from the normal recording circuit.

It was thought that the large fluctuations in the signals were caused by non-uniform flow at the impeller.

(3) High-pass Filter.

The level of the background tunnel noise was approximately equal to the magnitude of the maximum pressure signals due to the impeller. A frequency analysis of the total pressure showed that most of its components were below 60 cps. The major component of the pressure noise occurred between 30 and 35 cps.

The noise was due to changing static pressure in the working section caused by :--

(i) Average flow rate changing with time.

(ii) Vibrations transmitted to the working section and water tunnel structure from the drive motors, pumps and auxiliary units.

Since the frequency of the major component of the noise was below the blade passing frequency, filtering was adopted. After filtering out 50 cps and below, the pressure signal showed properties of a stationary periodic wave (refer Section 5.1).

The simple filter used did not have a sharp cut-off frequency, as it was only a single stage T filter. It was thus necessary to measure the complete transfer function of the filter and correct the measured signal. A typical plot of the transfer function components of one of the filters is shown in Fig. 4.2.

4.3 MATHEMATICAL ANALYSIS OF RECORDED INFORMATION.

After analogue to digital (A-D) conversion, the recorded digital information was identified and converted into words compatible to the word structure of the digital computer, CDC 6400 which was used in subsequent analyses (see Appendix A 7 and A 8 for details).

The list of digits which constituted a single experimental reading of one variable was termed a file. In each file there were a number of revolutions of the impeller, depending on the recording time. It was possible to choose from a complete file a list of numbers which corresponded to any one or more of the recorded revolutions of the impeller. This was possible because the identification pulses, from the programming switch, were recorded simultaneously on all active channels.

A Fourier analysis of the recorded signals was performed by considering the points as constituting a series of pseudo square waves whose Fourier coefficients can be expressed mathematically. The Fourier coefficients of the complex wave were determined by summing the coefficients of the pseudo square waves (see Ref. 4.1 and Appendix A 8)

The orientation of the reference axes used to describe the position of the impeller or a point on the duct surface is as follows:--

Consider a right handed set of axes OX, OY, and OZ with origin on the impeller axis and axes OY and OZ in the plane of the impeller (see Fig. 5.1). The plane YOZ was taken in these model studies to be the plane which contains the centroids of all the blade sections. (Section 2.3 of Appendix A 1 shows this to be a property of the impeller design).

The OX axis is in the same direction as the axial displacement of the impeller with respect to the fluid. The OY axis is

taken as the reference line for all angular measurements. The angular position of a given blade from the OY axis is θ and the position of a point in space is given by the coordinates X, r, γ.

4.3.1 Pressure Field.

The Fourier components of the pressure fluctuations at a point on the duct surface X, R_d, γ (see Fig. 5.1) were reduced to the following form, where R_d is the duct radius,

$$p = \sum_{i=1} A_i \cos (4\, i(\theta - \gamma) + \varepsilon_i) \qquad \ldots 4.1$$

where A_i = modulus of pressure component of the i^{th} harmonic of blade frequency, ie. single amplitude of vibratory pressure

θ = blade angle with respect to axis, Fig. 5.1

ε_i = phase-lead angle of i^{th} harmonic

The magnitude of the pressures are also given in the form of non-dimensional coefficients K_{pi} and K_{Pt} where

$$K_{Pi} = \frac{A_i}{\rho\, n^2\, D^2} \quad \text{and} \quad K_{Pt} = \frac{P_t}{\rho\, n^2\, D^2} \qquad \ldots 4.2$$

where P_t = single amplitude of total (all frequencies) vibratory pressure, peak to peak

n = propeller revolutions per second

D = propeller diameter

ρ = density of fluid

4.3.2 Vibratory Impeller Forces.

The direct measurement of fluctuating forces acting on an impeller propulsion system is extremely difficult because the forces must be determined from a knowledge of the vibrations of the propulsion system. This requires the complete dynamic properties of the impeller, drive and supporting system to be known. A further complication arises, however, due to a fundamental property of an impeller. The various modes of vibration of a propulsion system are cross coupled by the impeller.

The dynamics of this type of system are investigated, in part, in Ref. 4.4. Here a theoretical analysis is undertaken of an elastically supported impeller being excited by a sinusoidal gust velocity. Experimental values of the dynamic coefficients mentioned in this report are given in Ref. 4.5.

Consider a simple, elastically supported impeller vibrating about its longitudinal axis (ie. axial and torsional). The complete transfer function of an impeller-mass-spring system is not only dependent on the mechanical properties of the mass-spring system, but also on the geometry of the impeller.

The equations of motion describing this coupled system can be expressed in the following:-

$$\left[\ddot{\varepsilon}_Z M_Z + \dot{\varepsilon}_Z C_Z + \varepsilon_Z C^F_Z\right] + \left[\ddot{\varepsilon}_Z \left[\frac{F_Z}{\ddot{\varepsilon}_Z}\right] + \dot{\varepsilon}_Z \left[\frac{F_Z}{\dot{\varepsilon}_Z}\right] + \ddot{\varphi}_Z \left[\frac{F_Z}{\ddot{\varphi}_Z}\right] + \dot{\varphi}_Z \left[\frac{F_Z}{\dot{\varphi}_Z}\right] + \varphi_Z C^{FT}_Z\right] = F_Z \quad \ldots 4.8$$

$$\left[\ddot{\varphi}_Z I_Z + \dot{\varphi}_Z G_Z + \varphi_Z C_Z^T\right] +$$

$$+ \left[\ddot{\varphi}_Z \boxed{\frac{T_Z}{\ddot{\varphi}_Z}} + \dot{\varphi}_Z \boxed{\frac{T_Z}{\dot{\varphi}_Z}} + \ddot{\varepsilon}_Z \boxed{\frac{T_Z}{\ddot{\varepsilon}_Z}} + \dot{\varepsilon}_Z \boxed{\frac{T_Z}{\dot{\varepsilon}_Z}} + \varepsilon_Z C_Z^{TF}\right] = T_Z \qquad \ldots 4.9$$

The first group of terms in both equations refer to an elastically supported impeller vibrating in air. These coefficients are called the dynamic mechanical coefficients. The second group of variables refer to the hydrodynamic and cross coupling properties of the impeller system, the dynamic hydro-mechanical coefficients. The definitions of the above quantities are given below in Table 4.2.

Combining the second group of variables in equations 4.8 and 4.9 as:-

$$\left[\ddot{\varepsilon}_Z \boxed{\frac{F_Z}{\ddot{\varepsilon}_Z}} + \dot{\varepsilon}_Z \boxed{\frac{F_Z}{\dot{\varepsilon}_Z}}\right] + \left[\ddot{\varphi}_Z \boxed{\frac{F_Z}{\ddot{\varphi}_Z}} + \dot{\varphi}_Z \boxed{\frac{F_Z}{\dot{\varphi}_Z}} + \varphi_Z C_Z^{FT}\right] =$$

$$= \left[\frac{1}{H_{H\varepsilon}}\right]\varepsilon_Z + \left[H_4\right]\varphi_Z \qquad \ldots 4.10$$

$$\left[\ddot{\varphi}_Z \boxed{\frac{T_Z}{\ddot{\varphi}_Z}} + \dot{\varphi}_Z \boxed{\frac{T_Z}{\dot{\varphi}_Z}}\right] + \left[\ddot{\varepsilon}_Z \boxed{\frac{T_Z}{\ddot{\varepsilon}_Z}} + \dot{\varepsilon}_Z \boxed{\frac{T_Z}{\dot{\varepsilon}_Z}} + \varepsilon_Z C_Z^{TF}\right] =$$

$$= \left[\frac{1}{H_{H\varphi}}\right]\varphi_Z + \left[H_3\right]\varepsilon_Z \qquad \ldots 4.11$$

and assuming that differential equations 4.8 and 4.9 are linear, with constant coefficients, they can be expressed as:-

Table 4.2 PROPERTIES OF THE ELASTIC SYSTEM.

Symbol	Description	Units.
	Dynamic Mechanical Coefficients	
ε_Z	Longitudinal displacement	ft.
φ_Z	Angular displacement	rad.
F_Z	Axial load - thrust	lbf.
T_Z	Torsional load - torque	lbf.ft.
M_Z	Effective mass of vibratory system in air	slug
C_Z	Damping in longitudinal direction	lbf.sec/ft.
C_Z^F	Stiffness in longitudinal direction	lbf/ft.
I_Z	Effective inertia of system in air	lbf.ft.sec^2
G_Z	Damping in torsional direction	lbf.ft.sec.
C_Z^T	Stiffness in " "	lbf.ft/radian
C_Z^{FT}	Cross coupling stiffness between ε_Z and	"
C_Z^{TF}	φ_Z displacements	lbf/ft.

Table 4.2 continued.

Dynamic Hydro-mechanical Coefficients (Ref. 4.4, Table 1.3)

Symbol	Description	Units
$\left[\frac{F_Z}{\dot{\varphi}_Z}\right] = \left[\frac{T_Z}{\dot{\varepsilon}_Z}\right]$	Velocity coupling	lbf.sec.
$\left[\frac{F_Z}{\ddot{\varphi}_Z}\right] = \left[\frac{T_Z}{\ddot{\varepsilon}_Z}\right]$	Acceleration coupling	$lbf.sec^2$
$\left[\frac{F_Z}{\dot{\varepsilon}_Z}\right]$	Axial damping	lbf.sec/ft
$\left[\frac{F_Z}{\ddot{\varepsilon}_Z}\right]$	Axial entrained mass	slugs
$\left[\frac{T_Z}{\dot{\varphi}_Z}\right]$	Torsional damping	lbf.ft.sec
$\left[\frac{T_Z}{\ddot{\varphi}_Z}\right]$	Entrained moment of inertia	$lbf.ft.sec^2$

$$\left[\frac{1}{H_{\varepsilon}} + \frac{1}{H_{H\varepsilon}}\right] \varepsilon_Z + H_4 \varphi_Z = F_Z \qquad \ldots 4.12$$

$$\left[\frac{1}{H_{\varphi}} + \frac{1}{H_{H\varphi}}\right] \varphi_Z + H_3 \varepsilon_Z = T_Z \qquad \ldots 4.13$$

Here H_i represent the transfer function of a particular section i of the vibratory system

where

i = ε simple longitudinal system in air

i = φ simple torsional system in air

i = Hε hydrodynamic system for longitudinal displacement

i = Hφ hydrodynamic system for torsional displacement

and i = 3,4 coupling between longitudinal and torsional displacement

A further simplification can be made by substituting

$$\frac{1}{H_1} = \frac{1}{H_{\varepsilon}} + \frac{1}{H_{H\varepsilon}} \qquad \ldots 4.14$$

and

$$\frac{1}{H_2} = \frac{1}{H_{\varphi}} + \frac{1}{H_{H\varphi}} \qquad \ldots 4.15$$

into equation 4.12 and 4.13

$$F_Z = \frac{\varepsilon_Z}{H_1} + H_4 \varphi_Z \qquad \ldots 4.16$$

$$T_Z = \frac{\varphi_Z}{H_2} + H_3 \varepsilon_Z \qquad \ldots 4.17$$

This permits the impeller-mass spring system and associated hydrodynamic effects to be illustrated by a block diagram as follows:--

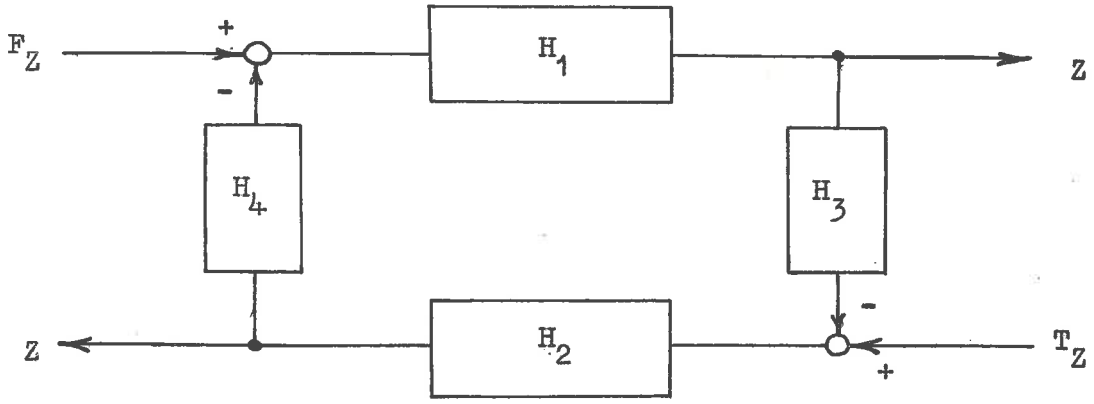

The actual impeller loading can be calculated from measured displacements ε_z , φ_z by equations 4.16 and 4.17 once the respective transfer functions have been determined either mathematically or experimentally.

It was intended that the fluctuating forces acting on the impeller of the Hydrojet model would be measured in these studies, but this was not possible because of a faulty dynamometer (Section 3.2).

An outline of the method used to calibrate the dynamometer is given in Section 4.5.

4.4 SPHERICAL 5-HOLE PITOT AND ITS CALIBRATION.

Until now, the claibration of the 5-hole spherical pitot was conducted in a fluid in which the relative direction of flow was known accurately. This necessitated the use of a towing tank, in which the relative motion of carriage and water was precisely known, or the use of a very accurate wind or water tunnel.

A method was devised to accurately calibrate a spherical pitot in a flow whose direction is only approximately known. Calibration is thus possible in a small wind tunnel, water tunnel or duct.

The calibration procedure and theoretical analysis which is given in detail in Appendix A 6, is briefly discussed in the following section.

4.4.1 Theory.

The potential solution of the flow around a sphere gives the pressure at a point as:--

$$\frac{p - p_o}{\frac{1}{2}\rho V^2} = 1 - \frac{9}{4}\sin^2\beta \qquad \ldots 4.3$$

where p = pressure at point considered

p_o = free stream pressure

V = magnitude of velocity vector $\bar{V}$ of free stream

ρ = fluid density

β = angular position of point from stagnation point

For three equispaced holes a, b, c on a great circle of a sphere Pien (Ref. 4.2) has shown that (see Fig. 4.3) --

$$C_{ph} = \frac{p_a - p_b}{\frac{1}{2}\rho V_h^2} = \frac{9}{4} \sin 2\alpha \sin 2\beta_h \qquad \ldots 4.4$$

$$C_{Ph} = \frac{p_a - p_b}{2P_c - p_a - p_b} = \frac{\sin 2\alpha}{1 - \cos 2\alpha} \tan 2\beta_h \qquad \ldots 4.5$$

where

p_a, p_b, p_c = pressures at a, b, c.

C_{ph}, C_{Ph} = pressures coefficients

α = angle between adjacent holes

V_h = orthogonally projected component of the velocity $\bar{V}$ onto the plane of the great circle

β_h = angle between V_h and the stagnation point

From measurements of p_a, p_b, p_c the value of β_h can be calculated from equation 4.5, whence V_h can be obtained from equation 4.4. If on the great circle through c orthogonal to that through a, b, c, two equispaced holes a' and b' are placed as shown in Fig. 4.3, the component V_v of the velcoity $\bar{V}$ in the plane of this circle can be determined from measurement of p_a', p_c', p_b' by equations analogous to 4.4 and 4.5. The three components V_x, V_y, V_z along the sphere axes OX, OY and OZ of the velocity $\bar{V}$ are then given by:--

$$V_x = V_h \cos \beta_h$$

$$V_y = V_h \sin \beta_h$$

$$V_z = V_v \sin \beta_v \qquad \ldots 4.6$$

In Ref. 4.2 and 4.3 in place of equation 4.4 the appropiate relations for

$$\frac{p_c - p_a}{\frac{1}{2} \rho V_h^2} \quad , \quad \frac{p_c - p_b}{\frac{1}{2} \rho V_h^2} \qquad \ldots 4.7$$

are used. The first or second of these pressure coefficients is taken depending on whether V_h is on one side or the other side of the centre hole. This introduces an unnecessary complication. Use of equation 4.4 is also recommended because its pressure coefficient has a greater variation at any given value of β_h than these other two coefficients, thus giving a greater sensitivity.

4.4.2 Calibration.

4.4.2.1 Initial Angular Calibration.

The pitot is set up in a flow whose direction is approximately known, so that it can be rotated about two axes OY, OZ which are normal to each other and to the nominal flow direction. OY and OZ pass through the sphere centre and lie approximately in the plane of the holes. The axis OX also passes through the sphere centre and is orthogonal to OY and OZ. The axes OX, OY, OZ are

are called the pitot axes.

Values of the expression for C_{ph} and C_{Ph} versus β_h and C_{pv} and C_{Pv} versus β_v are obtained by rotating the pitot axes 0Y and 0Z respectively.

The error introduced by the flow velocity $\bar{V}$, not being in the calibration plane will be quite small since the velocity in the calibration plane will differ from V only by $V(1 - \cos\phi)$ where ϕ is the angle of $\bar{V}$ to the calibration plane. Usually ϕ will not be more than a few degrees.

4.4.2.2 Orientation of Pitot Axes with reference to Datum Instrument Axes.

On the pitot base there will have been machined location faces. These can be used to define a set of orthogonal axes at the sphere centre, which will be called the datum instrument axes 0XX, 0YY and 0ZZ. The problem is now to determine the orientation or position of the pitot axes with reference to these known instrument axes. As shown below, this orientation can be determined in a stream whose flow direction is only approximately known, by three inversions of the sphere position, providing the pitot is set up in the flow so that the sphere can be rotated about 0XX , 0YY or 0ZZ without the centre of the sphere moving in space.

(1) Rotation about 0XX Axis.

The sphere is initially positioned so that the flow vector $\bar{V}$ is at some estimated angle Ψ to the centre hole (of between 5° and 10°). The sphere is then rotated

successively by 90° about the instrument axis OXX.

By solving equations 12 to 15 of Appendix A 6 the orientation of the pitot axis OX with respect to the instrument axes can be determined.

(2) Inversion about OYY axis

The sphere is positioned so that the velocity $\bar{V}$ will make an angle $\theta \simeq 5^{\circ}$ with the XXYY plane as shown in Fig. 4.4. Since the flow direction is known approximately, an estimate of the value of θ can be made. The sphere is then rotated about OYY so that $\bar{V}$ will make an angle of approximately $-\theta$ with the XXYY plane. Using values of the pressures at the initial and final positions, the orientation of pitot axis OZ with respect to the instrument axes can be determined (by solving equations 24 and 25, Appendix A.6).

(3) Inversion about OZZ axis

By repeating the procedure outlined in the section above, but in this case, for inversion about the OZZ axis, the orientation of OY axis can be determined.

4.4.2.3 Calibration Assumptions.

The initial calibration referred to in section 4.4.2.1 is based on an assumption, that the flow velocity is in the calibration plane. The accuracy of calibration can be increased by repeating the calibration procedure now that the fluid direction with respect to the instrument can be calculated.

Another assumption is that the pressure relationship between the holes is only dependent on the velocity component which can be considered as existing in the respective plane of calibration and that the pressure distribution is independent of the magnitude of the velocity component in the other calibration plane.

This is true for a perfect sphere having infinitely small holes which lie on a great circle through the centre hole.

The calibration of this instrument should include a check on its accuracy for fluid velocities whose directions are not in in the calibration plane.

The velocity gradient of the free stream is also assumed to be small over the area of cross section of the sphere.

4.4.3 Construction Details.

The diameter of the spherical head was chosen to be 0.375 of an inch. An angular distance between the centre hole and the side holes of 20° and a hole diameter of 0.024 of an inch was selected.

The major difficulty in constructing an accurate spherical pitot is to accurately position the pressure tapping holes in the sphere. The following method of manufacture was used to partly alleviate this problem.

(1) The head was rough machined to a cylindrical form.

(2) This blank was mounted on a precision vertical drilling machine and pressure tapping holes were drilled parallel to the axes of the pitot head.

These holes were positioned so that a point on their centre line would be 20° to the axis of the spherical head when the head was machined spherical to 0.375 of an inch in diameter.

(3) Small bore stainless steel tubes were inserted into the holes and soldered in place.

(4) The head was accurately machined spherical.

4.5 DYNAMIC CHARACTERISTICS OF THE DYNAMOMETER.

Before a dynamic calibration could be undertaken, the linearity of the dynamometer had to be proven for various loading combinations of thrust and torque. This test was conducted, and the dynamometer and associated recording instruments were shown to be linear with load.

The dynamic properties of an impeller-dynamometer system, as discussed in Section 4.3.2, can be broadly divided into the determination of -

(a) The dynamic mechanical coefficients

(b) The dynamic hydro-mechanical coefficients

4.5.1 Dynamic Mechanical Coefficients.

A common method of determining the transfer function of a dynamic system is to excite the system with a sinusoidal force and measure the overall response of the system. This method can be applied in nearly all cases, but certain restrictions and experimental procedures must be met, depending on the physical properties of the system and the force exciter.

However, the only possible way of applying an exciting force to the dynamometer, (Section 3.2) was by an external force exciter. If the connection of this force exciter to the dynamometer, was to have a neglible effect on the actual transfer function of the latter, then the mass, stiffness and damping of the exciter had to be small in comparison with that of the dynamometer.

This was true for the axial mode but in the torsional mode, which had a low stiffness and natural frequency, this situation did not exist. In this case, the dynamometer-plus-exciter system had to be considered as a compound system, each component of which had its own transfer function.

Here the torsional transfer function of the dynamometer was obtained by a vectorial substraction of the transfer function for the exciter from that of the exciter plus dynamometer system. This method of determining the vibration characteristics of a compound system is discussed in Ref. 4.6.

(a) Transfer Function of the Exciter.

The force exciter, which was used to determined the transfer functions, was an electro-magnetic loud-speaker coil assembly.

Two methods can be used to determine the transfer function of of electro-magnetic exciters. The experimental method was adopted for these studies in preference to a theoretical derivation. This required connecting the exciter to a known vibratory system and measuring the complete transfer function of the combined system.

A simple cantilever beam was selected as the known vibratory system. Its natural frequency and stiffness was chosen to be approximately equal to that of the dynamometer.

A certain portion of the mass of the exciter appeared to behave as a point mass loading on the beam. The magnitude of this mass was determined from a knowledge of the natural frequency of the system. Knowing this and the physical properties of the beam, the transfer function for the beam and effective mass loading was calculated. Now the vibratory characteristics of the exciter can be obtained by vectorial substraction of the transfer function of the beam from that of the combined system.

It was found that the exciter had only a small influence on the combined system and that it behaved as an extra mass loading.

(b) Transfer Function of the Dynamometer in Air.

Tests, similar to those above, were conducted to determine the dynamic mechanical coefficients of the dynamometer as expressed in equation 4.9. of Section 4.3.2.

The dynamometer-plus-exciter system was considered as a compound system, as discussed previously.

The mass or inertia added to replace the impeller during these tests was equal to that of the impeller.

4.5.2 Dynamic Hydro-Mechanical Coefficients.

It was anticipated that the following tests would be undertaken, but as previously mentioned, a fault in an electrical component of the dynamometer terminated these.

The values of dynamic hydro-mechanical coefficients were to be computed theoretically (Ref. 4.4) and compared with those determined experimentally from a knowledge of the free vibrations of the impeller-dynamometer when immersed in water (Ref. 4.7).

It is worthwhile to mention that the theory of Wereldsma (Ref. 4.4) is based on an unsteady two-dimensional airfoil theory presented by Von Karman and Sears (Refs. 4.8 and 4.9). This theory may be better adapted to ducted impellers than open water propellers, because in a ducted impeller the radial velocities and the velocity gradients over the blade length are small.

5.0 RESULTS OF MODEL EXPERIMENTS.

5.1 PRESSURE ON DUCT SURFACE.

The reference axis used to describe orientation of the impeller and the position of a point P (X, r, γ) is shown in Fig. 5.1. The right handed set of axes OX, OY, OZ with origin on the impeller axis has the axes OY and OZ in the reference plane of the impeller.

The reference plane, in this case, is the plane which contains the centroids of all the blade sections.

The direction of the OX axis is opposite to the fluid motion. All angular measurements are taken from the OY axis. The angular position of the impeller is given by θ (Fig. 5.1). The coordinates of a point on the duct surface are X, R_d, γ.

The induced fluctuating pressures p measured on the duct for the uniform in-flow conditions were taken at a fixed angular position of $\gamma = 0$ and various axial distances (X). The pressures at these points were expressed by the following equation --

$$p = \sum_{i=1} A_i \cos [4 i (\theta - \gamma) + \varepsilon_i] \qquad \ldots 5.1$$

where A_i = magnitude of the i^{th} harmonic of blade frequency pressure (i.e. single amplitude of the vibratory pressure).

θ = impeller blade angle with respect to the axes in Fig. 5.1.

γ = angular position of the point being considered (Fig. 5.1).

ε_i = phase-lead angle of i^{th} harmonic component.

For the uniform flow conditions, the relationship above applied to all values of γ on the same axial section at X, because A_i and ε_i were independent of γ.

For the non-uniform in-flow to the impeller, however, the pressure

measurements were taken for various values of γ and X. The pressures were again expressed by equation 5.1, but for this type of pressure distribution the values of A_i and ε_i were dependent on γ.

The test results are presented in a non-dimensional form which has been justified by other investigators (Ref. 5.1 and 5.3).

$$K_{Pi} = \frac{A_i}{\rho n^2 D^2} \quad \text{and} \quad K_{Pt} = \frac{P_t}{\rho n^2 D^2} \qquad \ldots 5.2$$

where K_{Pi} = pressure coefficient of i^{th} harmonic of blade frequency.

K_{Pt} = Pressure coefficient of total pressure.

P_t = half the peak to peak value of the total pressure (all frequencies) (lbf/ft^2).

n = impeller rotational speed (rpm).

D = impeller diameter (ft).

ρ = density of fluid ($slug/ft^3$).

5.1.1 Effect of Filtering the Signal and of its Periodicity.

The pressure measured by the transducer had two components. The periodic component in Fig. 5.2 was due to the induced pressure field of the impeller and the lower frequency component, apparently non-periodic, was generated by various external mechanisms remote from the impeller-duct system. The latter component had major frequencies between 30 and 35 cps. This was due to the excitation of the working section and supporting structure of the water tunnel at its natural frequency. The vibration was excited by force transmission through the pipe work from the main pumps and drive motors.

Because the level of the unwanted pressure fluctuations above 50 cps approached the noise level of the recording amplifiers, it was decided to select the operating conditions of the impeller so that the fundamental frequency of the induced pressure exceeded 50 cps. The impeller rotational speeds were thus chosen to be 15 and 20 cps, which corresponded to a fundamental frequency for the fluctuating pressure of 60 and 80 cps respectively.

It was decided to filter out the unwanted pressure component electronically, because without the use of a filter, it was difficult to study the induced pressure at distances greater than $\frac{X}{D} = 0.15$ where the noise to signal ratio exceeded 2. With the unwanted signal component removed it was possible to monitor the impeller induced pressure signal prior to recording. The recording accuracy was also improved becasue the signal due to the induced pressure was capable of driving the recording instruments over their full operating range.

A Fourier analysis of the filtered pressure signal was performed on the digital information obtained from the recording instruments. Over a period of 8 revolutions of the impeller, various samples of the recorded information were analysed and compared with those obtained from an analysis over the 8 revolutions. Fig. 5.3 shows the results of the Fourier analysis where the pressure coefficient for various samples (⊡ , ⊙, △) are compared with the average pressure coefficient (▽) at the different harmonics of blade frequency. The pressure coefficients in Fig. 5.3 for the samples were computed from digital information between the NPI^{th} and the $(NPI + NP)^{th}$ revolution of the impeller. The values of NPI and NP for the samples are given in Fig. 5.3.

The results given in Fig. 5.3 show remarkable agreement with each other for the various harmonics of the blade frequency. Thus the pressure signals detected were stationary. A frequency analysis of the measured pressure is given in Fig. 5.4 for an impeller rotational speed of 20 cps. It can be seen that the pressure is periodic with a fundamental frequency of 80 cps. As this corresponds to the blade passing frequency, the results of Figs. 5.3 and 5.4 show that the pressure fluctuations were stationary and periodic.

Although the computed Fourier components were not significantly affected by the sample length, the results discussed in the following sections were the average components taken over 8 revolutions of the impeller for the uniform flow condition, and the average over 4 revolutions in the non-uniform flow conditions.

5.1.2 Effect of Reynolds Number.

The Fourier components of the pressure, namely the pressure coefficient and the phase angle, for impeller rotational speeds of 15 and 20 cps are given in Figs.5.8 and 5.12 for various values of advance coefficient (J_I).

The values for the measured pressure components are independant of the rotational speed. Thus it is assumed that the Reynolds number, at least over the small range applicable to model impellers, has no effect on the induced vibratory pressures of a ducted impeller.

It has also been shown (Ref. 5.1) that the free-space pressures of model open-water propellers are independant of Reynolds number.

5.1.3 Vibratory Pressures with Uniform Flow.

The pressure on the duct was measured for three advance coefficients J_I, equal to 0.74, 0.80 and 0.85 where

J_I = intake advance coefficient

$= \frac{V_I}{nD}$ where V_I = duct velocity at intake (fps)

n = impeller rotational speed (cps)

D = impeller diameter (ft)

The test results are presented in Figs. 5.5 to 5.17 and are discussed under the following headings:--

(a) Vibratory pressure of the blade frequency harmonics.

(b) Peak-to peak values of the total pressure.

(c) Phase angle of the blade frequency harmonics.

(d) Phase angle of the maximum pressure.

(a) Vibratory Pressure of the Blade Frequency Harmonics.

The magnitude of the Fourier components of the induced vibratory pressure acting on the duct surface is shown in Figs. 5.5 to 5.7 for the various advance coefficients.

The axial pressure distribution of the ducted impeller system shows similar characteristics to the free space pressures of an open-water propeller, (Ref. 5.2) but the absolute value of the pressure is far greater. The attenuation in magnitude with axial distance from the impeller is also greater than that of an open-water propeller.

The major pressure region of a Hydrojet extends over a relatively small distance between + 0.3 to - 0.1 of the impeller diameter.

This length is comparible with the projected length of the impeller blade in the axial direction of $\frac{X}{D}$ =+0.043 to-0.048. The magnitude of the pressure outside this region is of the same order as the pressure which exists at much larger tip clearances ($\frac{r}{D}$ = 0.6 to 0.7) for an open-water propeller.

It is known (Ref. 5.2 and 5.3) that the pressure distribution near an open-water propeller in a uniform velocity field is dependent on,

(i) the blade loading

(ii) the blade thickness

The pressure distribution associated with blade loading is symmetrical about the propeller, while that attributed to the blade thickness effect is asymmetrical. The effect of this same asymmetrical pressure distribution was detected for the ducted impeller. (Figs. 5.5 to 5.8). For this reason, the pressure due to the blade thickness effects must have a significant influence on the resulting vibratory pressures of a ducted impeller.

The magnitude of the pressure coefficients (K_{Pi})for the higher harmonics are large in relation to the fundamental. Values of the $K_{Pi}$for the second and third harmonics were approximately 60% and 25% respectively of the fundamental value. This large harmonic content is not present in the near pressure field of an open-water propeller with the same number of blades. (Fig. 21 of Reference 5.1).

For a ducted impeller however the blade frequency harmonics are important and must be considered if the peak to peak amplitudes

are to be measured or calculated.

It can also be seen (Figs. 5.5 to 5.7) that for a given blade frequency harmonic, the axial distance at which the maximum pressure occurs moves forward as the harmonic number increases. The phase angle of the harmonics also reveal a forward shift of the harmonics with increasing harmonic number (Fig. 5.9 to 5.11). A discussion of this is left to a following section (c).

(b) Peak to Peak Values of the Total Pressure.

In Fig. 5.8 the magnitude of half the peak-to-peak pressure coefficient is given for the total pressure at various advance coefficients. The peak-to-peak values of the total pressure were determined by synthesizing the actual total pressure from its Fourier components.

As the blade frequency harmonics are very nearly in phase behind the impeller and are definitely in phase forward of the impeller plane, (see following section) the peak-to- peak values of the total pressure (Fig. 5.8) are approximately the sum of the pressures for the odd harmonic components.

(c) Phase Angle of the Blade Frequency Harmonics.

The blade frequency pressure harmonics lead the impeller blade position by an angle ε_i, where i is the harmonic number (eqn. 5.1). Therefore, the maximum pressure of the harmonic components on the duct surface are at an angle ε_i to the impeller blade position in the direction of the angular motion of the impeller.

The determination of the phase angle of any experimentally

derived signal is difficult, and this was the case with the measured pressure signals (Section 5.15). After carefully studying the results and relating them to the hydrodynamics of an impeller, the following interpretation of the results is given.

It can be seen from Figs. 5.9 to 5.17 that the pressure field consists of two separate regions, one forward and the other behind the impeller. Near the plane of the impeller there is a discontinuity in phase of the induced pressure.

(i) Forward of the Impeller, the phase angle of each blade frequency is very nearly independant of axial distance $\frac{X}{D}$ and of advance coefficient of the impeller. This is clearly shown in Figs. 5.9 to 5.11 where the results for $J_I = 0.74$ are given. The pattern of variation of the phase angle for the higher harmonics and higher advance ratios is not so well defined but the results do appear to follow the same trend as the lower harmonics.

As previously mentioned on p.5.6, the induced pressure is dependant on the blade thickness and on the blade loading. For an open-water propeller, the effect of blade thickness has been estimated from a source-sink distribution over the blade surface (Ref. 5.2). Also the pressure due to blade loading is effectively the pressure distribution of an array of doublets whose axes are perpendicular to the helicoidal surface swept out by the advancing blade. Thus the phase angle of the blade thickness pressure component at any axial position is constant with respect to the blade position while

the phase angle due to the blade loading component is dependant on the distance from the propeller.

For a ducted impeller, however, the blade thickness must control the total pressure field ahead of the impeller because the phase angle of the pressure harmonics are constant with distance.

It has been shown by Breslin (Ref. 5.2, Figs. 2a to 3b) that the blade thickness effect controls the magnitude of the pressure field forward of a propeller. However, only limited evidence has been put forward for the phase relationship of the pressure in this region. Other investigations (Refs. 5.3 and 5.4) have indicated that there is a region forward of a propeller where the phase is substantially independant of distance from the impeller.

However, the phase angle of the harmonic components of the pressure for the ducted impeller ceases to be constant as the blade frequency harmonic number increases. The phase angle for the 3rd blade frequency harmonic, shown in Fig. 5.11 decreases with axial distance from the impeller. The pressure component due to blade thickness effect in this case must have a reduced influence on the total pressure field.

(ii) In the Region of the Impeller Plane, the trailing vortices or blade loading effect suddenly affects the pressure field and the phase angle of the Fourier components show a discontinuity (Fig. 5.9). The point at which this discontinuity occurs is not constant but moves forward slightly with increasing blade frequency harmonic.,(Figs. 5.9 to 5.11). As the maximum pressure peak also moves forward with increasing blade frequency harmonic, the effective location of the bound vortices emanating from the impeller blades would appear to move forward.

(iii) Aft of the Impeller. Although the phase angle (ε_i) of the harmonics components (Figs. 5.9 to 5.15) are for values between 0 and 2π, they may also be expressed by the addition of multiples of 2π, i.e. ($\varepsilon_i \pm 2\pi n$) where $n = 1,2,3,...$ This is possible because the fluctuating pressures are periodic over 2π radians. For this reason, the value of phase angles in the above figures are not discontinuous at 0 and 2π, but the values do, in fact, represent a continuous function.

Aft of the impeller, the phase angles of the pressure harmonics decrease linearly with axial distance from the impeller plane (Figs. 5.9 to 5.15). The phase change is in the same direction as the helicoidal wake pattern generated by the impeller. This indicates that the pressure field is mainly governed by the pressure associated with the blade loading, i.e. the pressure due to the trailing vortices. The trailing vortices have approximately constant pitch equal to that of the impeller. It is expected that the pitch of the trailing vortices should be constant in this ducted impeller case, because previous investigators have shown theoretically and experimentally that they are constant for most open-water propellers.

It is difficult to determine from the results a relationship between the phase angle of various harmonic components after the impeller. The indication is that they are not in phase (Figs. 5.9 to 5.11) This may be due to --

(a) The effective location of the bound vortex lines moving forward.

(b) Inaccuracies in measurement and computation of the phase angle.

With increasing advance coefficient J_I, the phase angle of the pressure has a tendency to be continuous from forward of the impeller to well aft (Fig. 5.16). For this to occur, the pressure field due to the trailing vortices must be insignificant in comparison with that due to the blade thickness. This is possible because at $J_I = 0.85$ the impeller loading, which in fact controls the magnitude of the pressures associated with the trailing vortices, is extremely small compared with the loading value at $J_I = 0.74$ (Fig. 5.25).

(d) Phase Angle of Maximum Pressure.

The phase angle of the maximum pressures shown in Figs. 5.12 5.15, and 5.17 are very nearly equal to that of the first blade frequency harmonic, because there is little variation in phase angle between the harmonics.

5.1.4 Vibratory Pressures with Non-uniform Flow.

Pressure measurements were taken with the impeller operating in a non-uniform flow. The velocity distribution at the intake of the duct and forward of the impeller is shown in Figs. 5.18 and 5.19. From these figures it can be seen that the velocity distribution

is effectively unchanged from the intake to the impeller.

Measurement of the fluctuating pressure on the duct was taken at only one advance coefficient $J_{I_{avge}} = 0.74$. The operating conditions were selected to maintain the same mass flow through the duct as in the previous test at $J_I = 0.74$ for a uniform flow condition. It would have been better to maintain a constant thrust loading condition between these two tests, but this was not possible due to the malfunction of the dynamometer. The pressure was measured at various angular positions between $\gamma = 0$ and $\frac{\pi}{2}$ (Fig. 5.1) because the velocity pattern was basically symmetrical about two normal diametral axes.

A frequency analysis of the pressure revealed that only blade frequency harmonics were significant as was the case for the uniform flow condition. It was difficult to determine a relationship between the pressure and the wake velocity from the limited number of experimental readings. However it can be said that the pressure at a given angular position (γ) is dependant, to the first approximation, on the average velocity over the radial line to that position.

The pressure near the impeller plane between $\frac{X}{D} = 0.15$ and -0.10 is influenced by the velocity distribution (Fig. 5.20 to 5.22). Outside the region the pressure is substantially constant and equals that for the uniform flow condition. In contrast to this, the pressure field of an open-water propeller operating in a wake is greatly dependant on the wake pattern even at extremely large distances from the propeller (Ref. 5.4, Fig 4). It has been stated by Breslin (Ref. 5.4) that the "non-uniform inflow velocities persist to larger distances since the signal associated with the non-uniform conditions

decays more slowly than the corresponding signal associated with the uniform conditions."

This statement, however, was based on a limited number of calculations at a considerable distance from the propeller where $\frac{r}{D} = 0.6$. The assumptions of this theory may not apply to a region extremely close to a ducted impeller.

On the other hand the phase angle of the pressure on the duct at various axial distances was not dependant on the wake pattern at the impeller (Figs. 5.23 and 5.24).

5.1.5 Possible Measurement Errors.

Factors which affected the accuracy of the measured pressure components were --

(a) Recording instrumentation and analysis.

(b) A finite size pressure transducer.

(c) Static pressure drop across the model.

(a) Recording Instrumentation and Analysis.

Although the analogue pressure signal and the event signal were recorded simultaneously on different tracks of a magnetic tape (Appendix A7),, the sampling of the analogue signal and subsequent conversion to digital information was executed for each track in turn. Thus the digital data from each track was within one sample of the true event. When comparing information from two tracks, the phase relationship between them may be in error by up to $\pm$ one sample in the total number of samples per period of the event. As the analogue to digital conversion was 4000 samples per second

for all the tests, this corresponded to $\pm$ 1.8 degrees of phase shift at 20 cps of the impeller. Unfortunately the phase error in the harmonics of the blade frequency was considerably greater and equal

$$\pm 1.8 \, Z \, i \text{ degrees,} \qquad \ldots 5.3$$

where Z = number of blades (4)

and i = blade frequency harmonic number.

This represents a significant phase error for the higher harmonics. It should be noted that the magnitudes of the pressure components are not affected by this inaccurate phase relationship.

The accuracy of the recording instrumentation and subsequent analogue to digital (A-D) conversion was extremely high. The voltage to frequency (V-F) converters were linear to 0.5% of the correct value. For an input voltage of $\pm$ 1.4 volts to the V-F converters, i.e. the normal input voltage range, the digital information after A-D conversion had a range of approximately 700 units. Also, at 4000 samples per second, which was the digital sampling rate for these tests, there were at least 8 digital samples per cycle of the 6th blade frequency harmonic. Thus the computational errors due to aliasing were small even for the higher harmonics that were considered.

(b) Pressure Transducer.

The measured signal from the transducer was not a true 'point measurement' but was in fact a reading which was dependant on the pressure distribution on the diaphragm of the transducer. As

previously discussed, the pressure distribution in the region of the impeller showed considerable change in both magnitude and phase with axial distance and it is in this region the accuracy of the measured signal was doubtful.

In order to estimate analytically the accuracy of the recorded pressure, the transducer diaphragm is assumed to be a uniform circular plate, rigidly supported at the edge. Also the measured signal is assumed to be proportional to the deflection of the centre of the plate.

Consider the deflection of the plate due to the following pressure distributions acting on it.

(i) Linear pressure variation across the plate.

(ii) Fluctuating pressure with a linear change in its magnitude and phase across the plate.

(i) Linear Pressure Variation.

Consider a linear pressure variation from P_1 to P_2 across the disc.

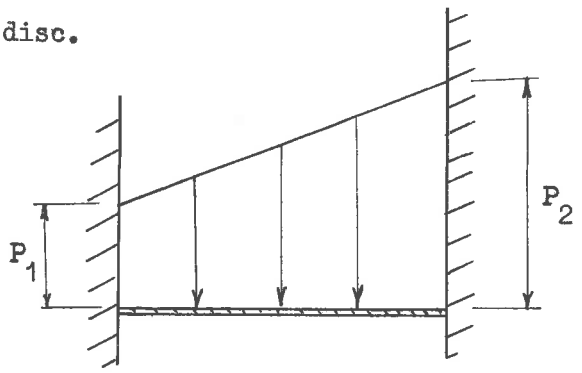

The deflection of a simply supported plate under the above loading conditions is given in Ref. 5.5 (p.256 eqn(f)). There the deflection of the plate at the centre is dependant on the mean pressure i.e. $\frac{1}{2}(P_1 + P_2)$ and not on the

distribution, providing it is symmetrical.

This solution will also apply to the centre of a plate with fixed edges as above.

Forward of the impeller, the pressure on the transducer was approximately linear with constant phase, Therefore the measured components of the pressure in this region are effectively point measurements. However, the pressure measurements behind the propeller where large variations in magnitude and phase were detected, are inaccurate as shown in the following.

(ii) Linear Change in Magnitude and Phase on the Plate.

Consider a slowly varying sinusoidal pressure acting on a plate with the same boundary conditions as for (i) above. The magnitude and phase of this pressure is assumed to vary linearly across the disc. The deflection at the centre of the disc (w) due to this pressure (P) acting on a small unit area dx by dy is given in Ref. 5.5, p.290 viz.

$$w = \frac{P}{8 \pi D} \left(b^2 \log \frac{b}{a} + \frac{a^2 - b^2}{2} \right) \qquad \ldots 5.4$$

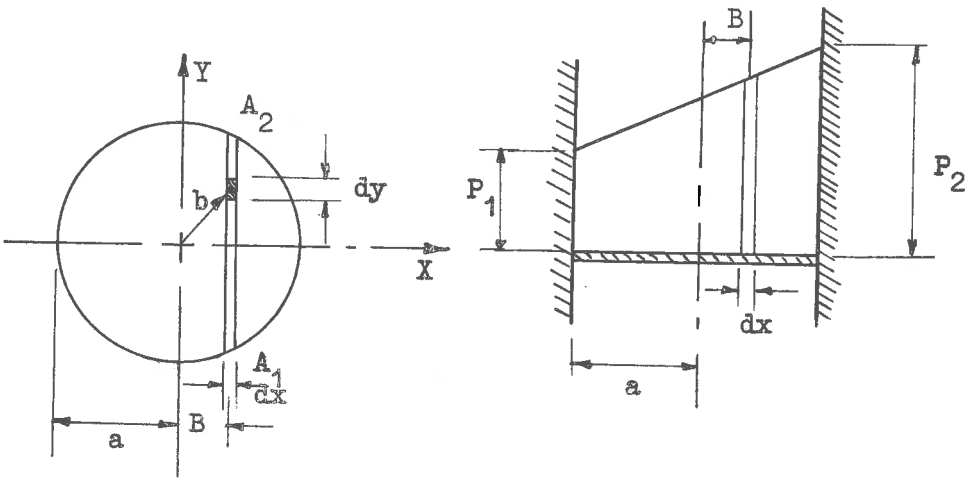

Assuming the pressure is linear with distance x i.e. between A_1 and A_2, the magnitude and phase are constant. The resultant deflection (w') of the centre of the plate due to the pressure loading from A_1 to A_2 is;

$$w' = \frac{P}{8\pi D}\int_{A_1}^{A_2} (b^2 \log \frac{b}{a} + \frac{a^2-b^2}{2})dx\,dy \qquad ...5.5$$

where D = flexural rigidity of the plate.

Substituting $b = B \sec\theta$ and $y = B \tan\theta$ into equation 5.5 and evaluating between A_1 and A_2

$$w' = \frac{PB^3}{4\pi D}\left[\sqrt{(\frac{a^2 - B^2}{B^2})}\ (\frac{2a^2}{9B^2} - \frac{8}{9}) + \frac{2}{3}\text{arc cos}\ \frac{B}{a}\right] dx \qquad ...5.6$$

Assuming a phase distribution similar to that measured aft of the impeller, then the response of the transducer can be determined by an integration in the x direction.

From Fig. 5.10 the change in phase for a change in $\frac{X}{D}$ of 0.031 (i.e. dimension of the transducer)is approximately 0.6π for the region aft of the impeller.

A numerical solution of equation 5.6 with the above distribution of pressure was obtained. Under these conditions the deflection of the centre of the plate was reduced by 4.8% and the phase lead by 1.8 degrees compared to a uniform pressure distribution equal to $\frac{1}{2}(P_1 + P_2)$ and no phase change across the plate.

Thus the size of the transducer does affect the accuracy of the pressure measurements in a region aft of the impeller. Here the recorded pressures of the Hydrojet should be

increased by approximately 5%.

(c) Static Pressure Drop Across the Model.

A large pressure drop was experienced along the length of the model during the tests. This resulted from the model being situated in a bounded fluid, where the model duct diameter was large in comparison with the diameter of the working section of the water tunnel. However, it was assumed that the fluctuating pressure induced by the impeller was not affected by the change in static pressure along the model. Thus the vibratory pressure on this model can be assumed to equal that of a model which operates in an infinite fluid.

5.2 IMPELLER CHARACTERISTICS.

5.2.1 Impeller Performance Characteristics.

Unfortunately the values of thrust and torque coefficients given in Fig. 5.25 may be significantly in error. As mentioned in Section 4.1.1 the voltage signals from the dynamometer were amplified by the rotating D.C. pre-amplifiers before the voltage signals were measured. Due to the extremely large voltage gain of these amplifiers, there was considerable voltage drift during the measurement of the thrust and torque signals. The zero readings of the amplifiers taken before and after each experimental reading showed a voltage drift equivalent to approximately 10% and 2% of the measured values of thrust and torque respectively. In determining the values of torque and thrust, the drift was assumed linear with time. However, assuming the experimental values given in Fig. 5.25 are true values, then the experimental values are lower than the theoretical values at the design advance coefficient as shown below,

		Theoretical	Experimental
Intake Advance Coefficient	$J_I = \frac{V_I}{nD}$	0.82	0.82
Thrust Coefficient	$K_T = \frac{T}{\rho n^2 D^4}$	0.198	0.123
Torque Coefficient	$K_Q = \frac{Q}{\rho n^2 D^5}$	0.0311	0.0204
Impeller Efficiency (at $J_I = 0.82$)	$E = \frac{J_I K_T}{2 \pi K_Q}$	0.834	0.77
Maximum Experimental Impeller Efficiency (at $J_I \approx 0.74$)		--	0.95

Although there is a large variation between the theoretical and the experimental values for thrust and torque, the value of advance coefficient, at which the theoretical value of thrust is produced, is only 0.792. This represents a decrease of less than 4% in the design advance coefficient. Assuming the measured values are correct, the results indicate that the pitch of the impeller should be increased by approximately 1.04 to maintain the design conditions.

Although the measured impeller efficiency, at the design advance coefficient, was considerable less than that calculated, the maximum experimental efficiency was considerably greater and was equal to 0.95. If the measurements were in error by 12% then the maximum efficiency would be approximately 0.79. This value, although much lower than the theoretical efficiency, is considerably greater than an equivalent open-water propeller. For example, an open-water efficiency of 0.64 can be expected for a propeller of the Troost B-55 Series, which has approximately the same dimensions and operating conditions as the impeller tested in these studies.

The results indicate that a favourable impeller efficiency is obtainable from a ducted impeller, but further tests must be conducted to accurately determine the correlation between the theoretical and experimental performance characteristics.

5.2.2 Velocity in the Wake of the Impeller.

By measuring the velocities in the wake behind the impeller, the calculated load distribution along the blade may be checked. The results of such a wake survey with a 5-hole spherical pitot (Section 4.4) are given in Fig. 5.26.

In Fig. 5.26 the axial velocity (V_A) and the tangential velocity (V_T) are given for various radial distances at two advance coefficients. These velocities are not as predicted in Section 2.1. The theoretical design assumed the axial velocity distribution was constant and the tangential velocity was linear with radial distance. This variation between theory and practice is to be expected because of the limitations of the simple theoretical analysis.

It has also been shown that large differences do exist between calculated and theoretical values of the wake velocities for open-water propellers, even when they are compared with the most rigorous propeller theories (Ref. 5.6).

6.0 CONCLUSIONS.

6.1 IMPELLER-INDUCED VIBRATORY PRESSURES.

Although the fluctuating pressures induced by a ducted impeller are similar in nature to that of an open-water propeller, several important differences do exist.

(1) The harmonic content of the 2nd and 3rd blade frequency harmonics of the impeller-induced pressure is approximately 60% and 25% respectively of the 1st harmonic pressure. Thus theoretical and experimental determination of pressures at points which are extremely close to an impeller, i.e. about 0.3% of the impeller diameter, must include the blade frequency harmonic components.

(2) Although the maximum pressure coefficient $\frac{P_t}{\rho n^2 D^2}$ is approximately 0.5, its magnitude rapidly attenuates to 10% of its maximum value at distances of $\frac{X}{D}$ equal to + 0.2 and - 0.1 from the impeller plane.

(3) The blade thickness controls the pressure field forward of the impeller and results in a constant phase angle with respect to the blade position for all the harmonic components of the pressure.

(4) Aft of the impeller, both the blade thickness and the blade loading, influence the pressure field. When the blade loading is high, the pressures associated with the trailing vortices control the pressure, but as the thrust loading approaches zero, the blade thickness effects become significant.

(5) A marked discontinuity in the pressure distribution occurs near the plane which contains the mid-points of the blade sections of the impeller. Behind the impeller plane, the phase is constant

with respect to a uniform pitch helical surface which is, in fact, the trailing vortices of the blades. The position of the discontinuity in the pressure field, i.e. where the trailing vortices appear to emanate from the blade, has a tendency to move forward with an increase in the blade frequency harmonic component.

For this reason, the bound vortex lines, which represent the impeller in a theoretical model, must be situated at the mid-point of the blade sections.

(6) For a non-uniform inflow velocity distribution at the impeller, the resultant induced pressure is dependant, to a first approximation, on the mean velocity component existing over blade length.

(7) Care must be excercised when measuring pressures aft of an impeller, because the response of a finite size transducer is dependant on the phase relationship of the pressures across the diaphragm of the transducer. For example, the pressure measured behind the impeller with a transducer which has a diaphram diameter of 0.03 of the impeller diameter, is approximately 4% lower than the true pressure. However, the phase of the pressure is only in error by about 2 degrees.

6.2 IMPELLER EFFICIENCY.

There is substantial evidence that impeller efficiencies in the order of 0.90 are possible from a ducted impeller. The experimental value of the maximum impeller efficiency was 0.95, but this unfortunately may be an optimistic estimate because of instrumentation errors. A simple vortex-line analysis of the impeller predicted an efficiency

of only 0.83.

However, further experimental studies must be conducted to determine the actual performance characteristics of the ducted impeller.

6.3 FEASIBILITY OF A HYDROJET.

Only two characteristics of a Hydrojet propulsion unit were considered in these studies. They were the propulsive efficiency and the impeller-induced vibratory pressures on the duct surface.

The propulsive efficiency of a Hydrojet suitable for large displacement vessels is expected to exceed 0.75 providing the ratio of duct length can be reduced to twice its diameter, then the propulsive efficiency is significantly increased to approximately 0.80.

Before accurate predictions can be made for the propulsive efficiency of a Hydrojet propulsion unit, detailed investigations into the frictional resistance of a duct-impeller system and also into the characteristics of the impeller are necessary.

The other characteristic of the Hydrojet that was considered was the impeller induced pressures on the duct surface. Although the magnitudes of these pressures were extremely high, the extent of this intense fluctuating pressure field was very small. Before it is possible to say whether the resultant forces due to the pressure and hence the vibration levels of the ship are acceptable, detailed studies of the duct structure surrounding such an impeller must be undertaken. It is anticipated that such a structure can be designed to effectively cancel the cyclic forces due to the induced pressures of an impeller operating in a uniform velocity field. This would then leave only those forces due to the non-uniformity of the wake to force excite the hull.

REFERENCES.

0.1 NORRIE, D.H. Studies in Marine Propulsion Vibration.
Doctor of Philosophy Thesis, University of Adelaide, Mechanical Engineering Department. July, 1964.

0.2 BROWN, N.A. Periodic Propeller Forces in Non-uniform Flow.
Massachusetts Institute of Technology, Dept. of Naval Architecture and Marine Engineering. Report No. 64-7, June, 1964.

1.1 BRESLIN, J.P. Review of Theoretical Predictions of Vibratory Pressures and Forces Generated by Ship Propellers.
Stevens Institute of Technology, Davidson Laboratory, Note 717.
(Prepared for the Second International Ship Structures Congress, Delft. July 1964.)

1.2 HALE, M.R. and NORRIE, D.H. Hydrojet Propulsion Reduces Vibration.
Engineering, 24th July, 1964.

1.3 GASUINAS, A and LEWIS, W.P. Hydraulic Jet Propulsion - A Theoretical and Experimental Investigation into the Propulsion of Seacraft by Water Jets.
Presented to Ordinary Meeting of the Institution of Mechanical Engineers, Portsmouth, 24th. October, 1963.

1.4 GONGWER, C.A. The Influence of Duct Losses on Jet Propulsion Devices.
Jet Propulsion, Vol. 24 No.6, 1954, p385-6.

References Continued--

1.5 VAN MANEN, J.D. Fundamentals of Ship Resistance and Propulsion. Part B. p120. Netherlands Ship Model Basin, Publication 132a.

2.1 BRITISH PROPELLER DESIGN. Marine Engineer and Naval Architects, Vol.88 No.1069, April, 1965

2.2 O'BRIEN, T.P. The Design of Marine Screw Propellers. Hutchinson & Co., Ltd. London, 1962.

2.3 TINGEY, R.H. Marine Engineering, Vol.1 Chap. IX (Editor - Seward, H.L.) Society of Naval Architects and Marine Engineers, 1942.

2.4 MATTHEWS, S.T. and STRASZAK J.S.C. Optimum Length and Thickness of Propeller Blade Sections for Cavitation and Strength Considerations. National Research Council of Canada. Mech. Eng. Report, M. B.-231 April, 1961.

3.1 VAN MANEN, J.D. and SUPERINA, A. The Design of Screw Propellers in Nozzles. International Shipbuilding Progress. Vol.6, No.55, March 1959.

3.2 MANNAM, J; FOWLER, J.H. and CARPENTER, A.L. Tapered Lands Hydrostatic Journal Bearings. I. Mech. E. Lubrication and Wear, 3rd Convention, London, 1965.

References continued --

3.3 McCARTHY, J.H. A Method of Wake Production in Water Tunnels.
David Taylor Model Basin, Report 1785, October, 1963.

4.1 CLARKE, A.P. Computation of the Coefficients of a Fourier Series Expansion of a Function defined by Sampled Data Points.
Weapons Research Establishment, Tech. Memo. T.RD 71, ADDS.

4.2 PIEN P.C. The Five-Hole Spherical Pitot Tube.
David Taylor Model Basin. Report 1229. May, 1958.

4.3 SILOVIC, V. The Five-Hole Spherical Pitot Tube for Three Dimensional Wake Measurements.
Hydro-Og Aerodynamisk Laboratorium, Lyngby, Denmark.
Report No. Hy-3, May, 1964.

4.4 WERELDSMA, R. Dynamic Behaviour of Ship Propellers.
Internationale Periodieke Pers, Rotterdam. April, 1965.

4.5 WERELDSMA, R. Experiments on Vibrating Propeller Models.
Journal of Ship Research, 1965
also Netherlands Ship Model Basin Publication No. 252.

4.6 PENDERED, J.W. and BISHOP, R E,D, Extraction of Data for a Sub-system from Resonance Test Results.
Journal Of Mechanical Engineering Science, Vol.5 No.4, 1963.

References continued -

4.7 LEIBOWITZ R C. and KENNARD, E.H. Theoretical and Experimental determination of Damping Constants of One-to Three Dimensional Vibrating Systems.
David Taylor Model Basin. Report 1770, June 1964.

4.8 KARMAN, TH. VON and SEARS, W,R, Airfoil Theory for Non-uniform Motion.
Journal of Aeronautical Sciences, 1938.

4.9 SEARS, W.R. Some Aspects of Non-stationary Airfoil Theory and its Practical Application.
Journal of Aeronautical Sciences, 1941.

5.1 TACHMINDJI, A.J. and DICKERSON, M.C. The Measurement of Oscillating Pressures in the Vicinity of Propellers.
David Taylor Model Basin, Report 1130. April, 1957.

5.2 BRESLIN, J P. Review and Extension of Theory for Near-Field Propeller Induced Vibratory Effects.
Fourth Symposium on Naval Hydrodynamics, Vol.2 Washington DC August, 1962.

5.3 BRESLIN, J.P. and KOWALSKI, T. Experimental Studies of Propeller-Induced Vibratory Pressures on Simple Surfaces and Correlation with Theoretical Predictions.
Journal of Ship Research, Vol.8, No.3, December 1964.

5.4 TSAKONAS, S; BRESLIN, J.P. and JEN, N. Pressure Field around a Marine Propeller Operating in a Wake.
Steven Institute of Tech. Davidson Laboratory, R-857, May 1962.

References continued --

5.5 TIMOSHENKO, S and WOINOWSKY-KRIEGER, S. Theory of Plates and Shells.
McGraw - Hill Book Company.

5.6 JOHNSSON C.A. Comparison of Propeller Design Techniques.
Fourth Symposium on Naval Hydrodynamics.
Washington DC. August 1962.

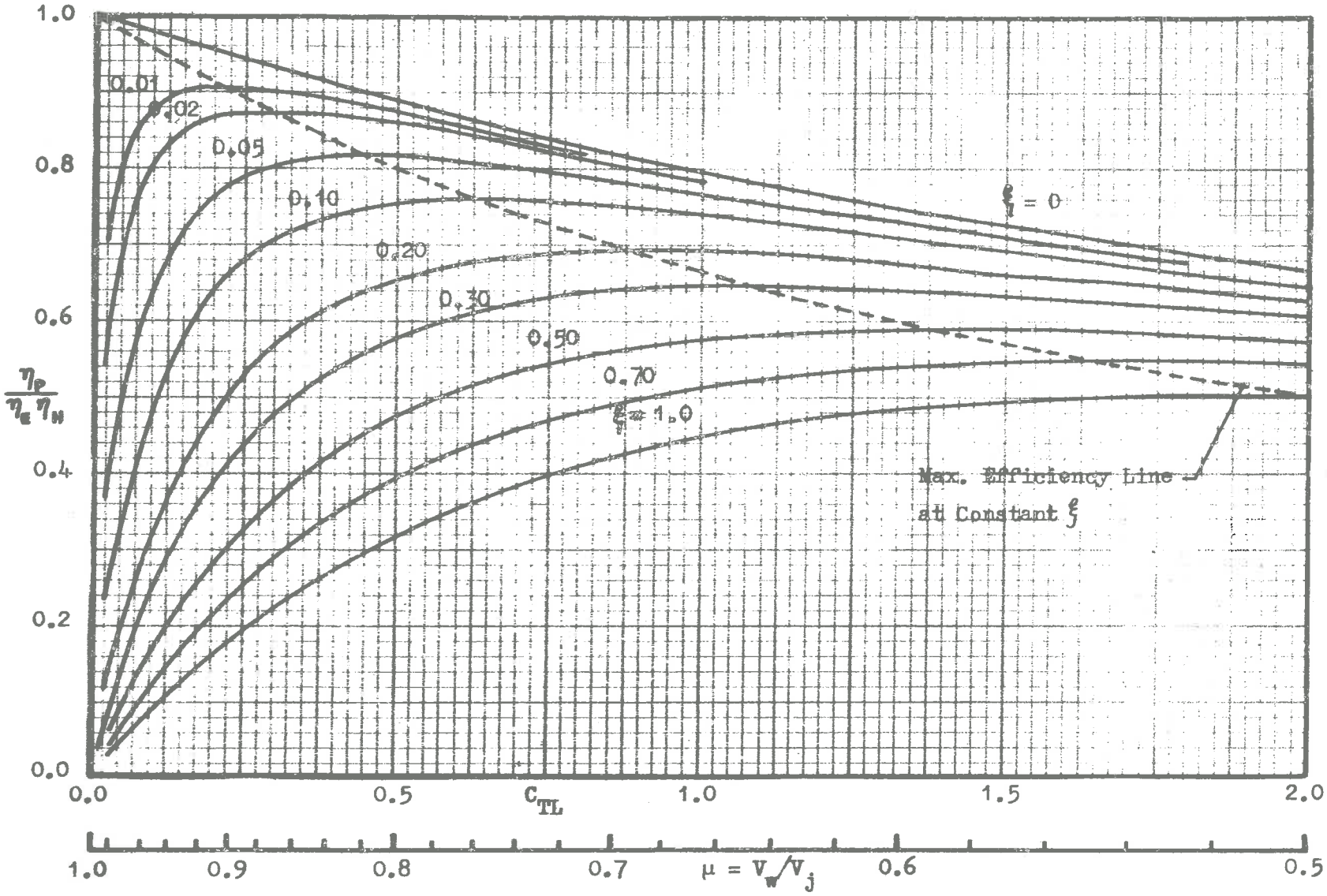

Fig. 1.1

Fig. 1.1 - Estimated Performance of Hydrojet Propulsion Unit. (Assuming $K_A = 1$)

Fig. 1.2

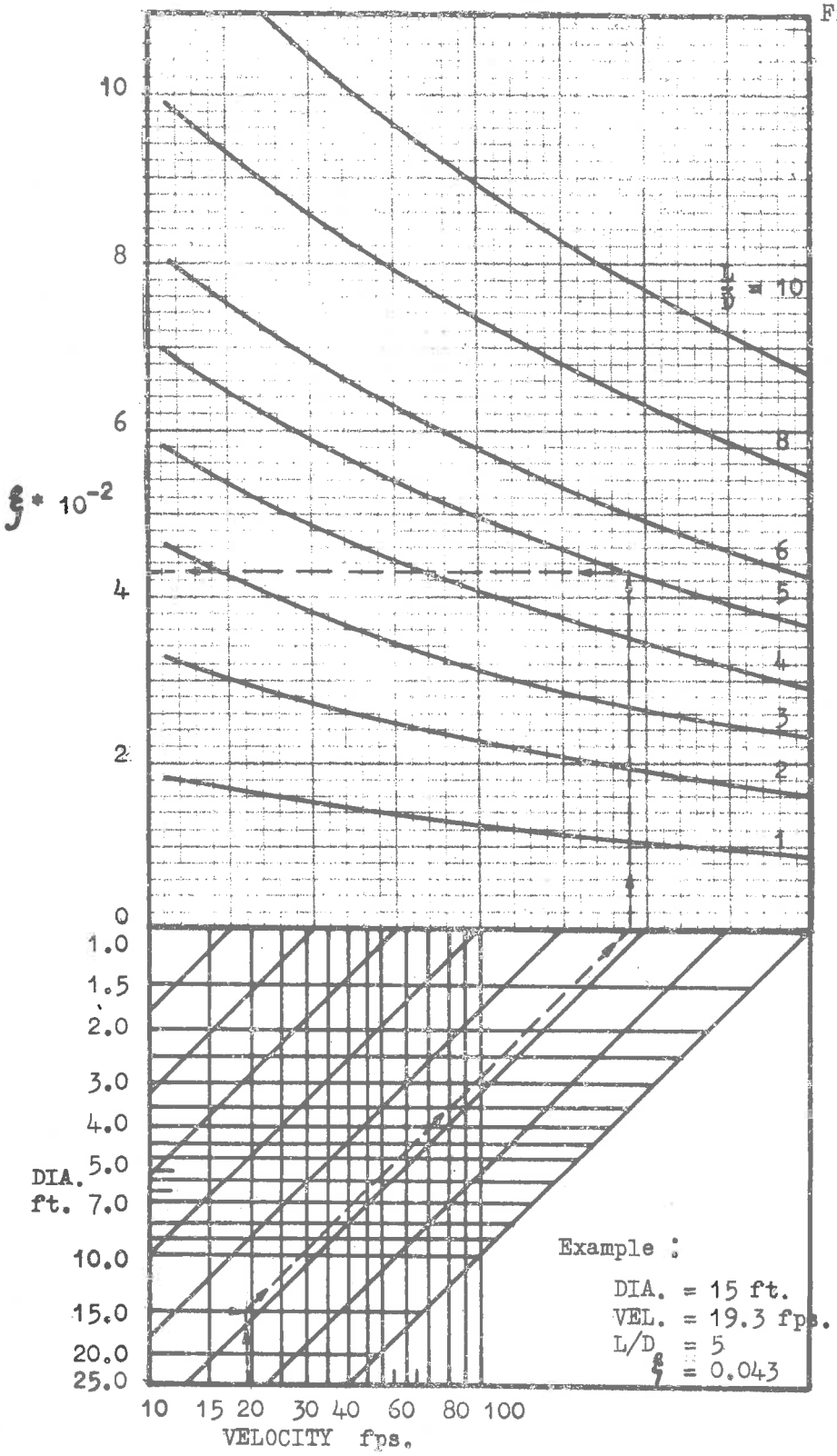

Fig. 1.2 - Estimated Ducting Loss Factor ξ.

Based on, (1) ρ = 1.99 slug/cubft.
(2) C_F ATTC. (1947) Mean Friction Line.
(3) Equivalent straight duct.

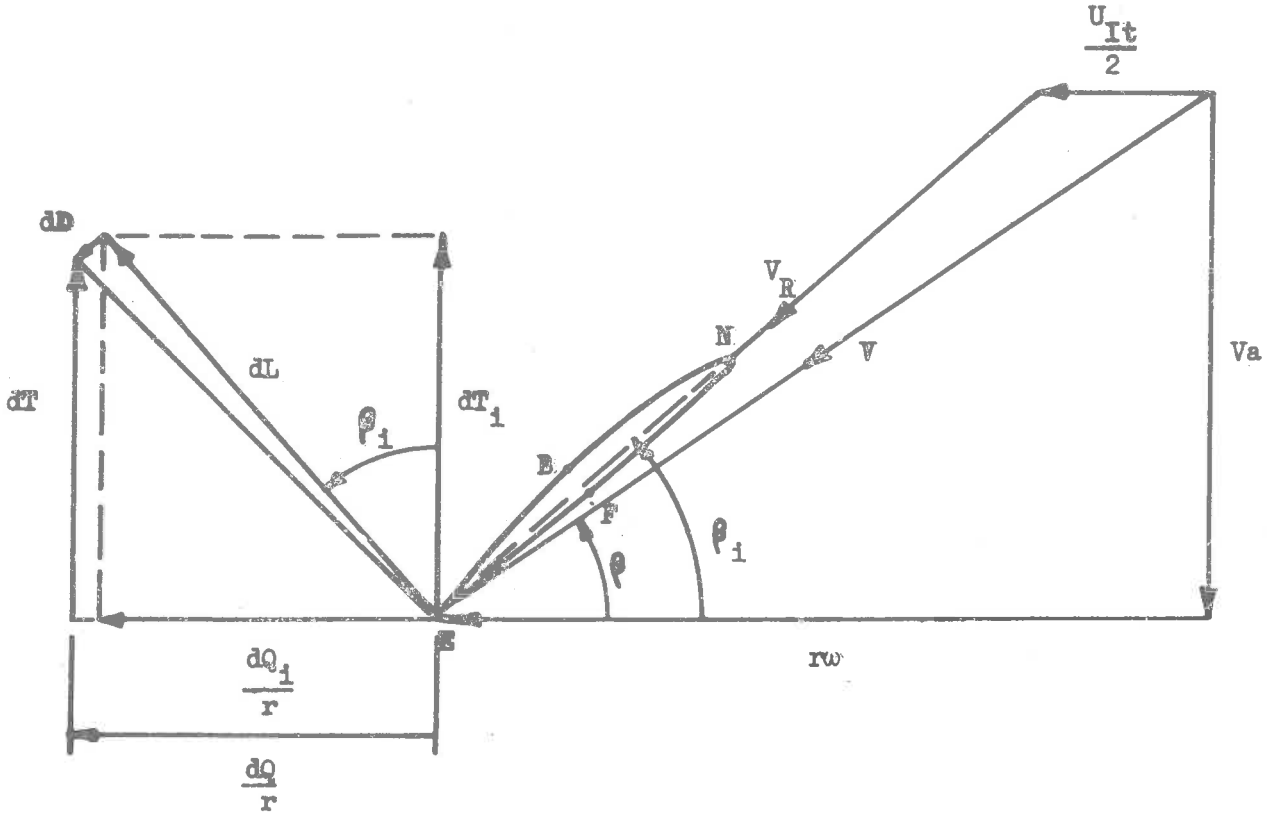

Fig. 2.1 - Velocities and Forces at Blade Section.

Fig. 2.1

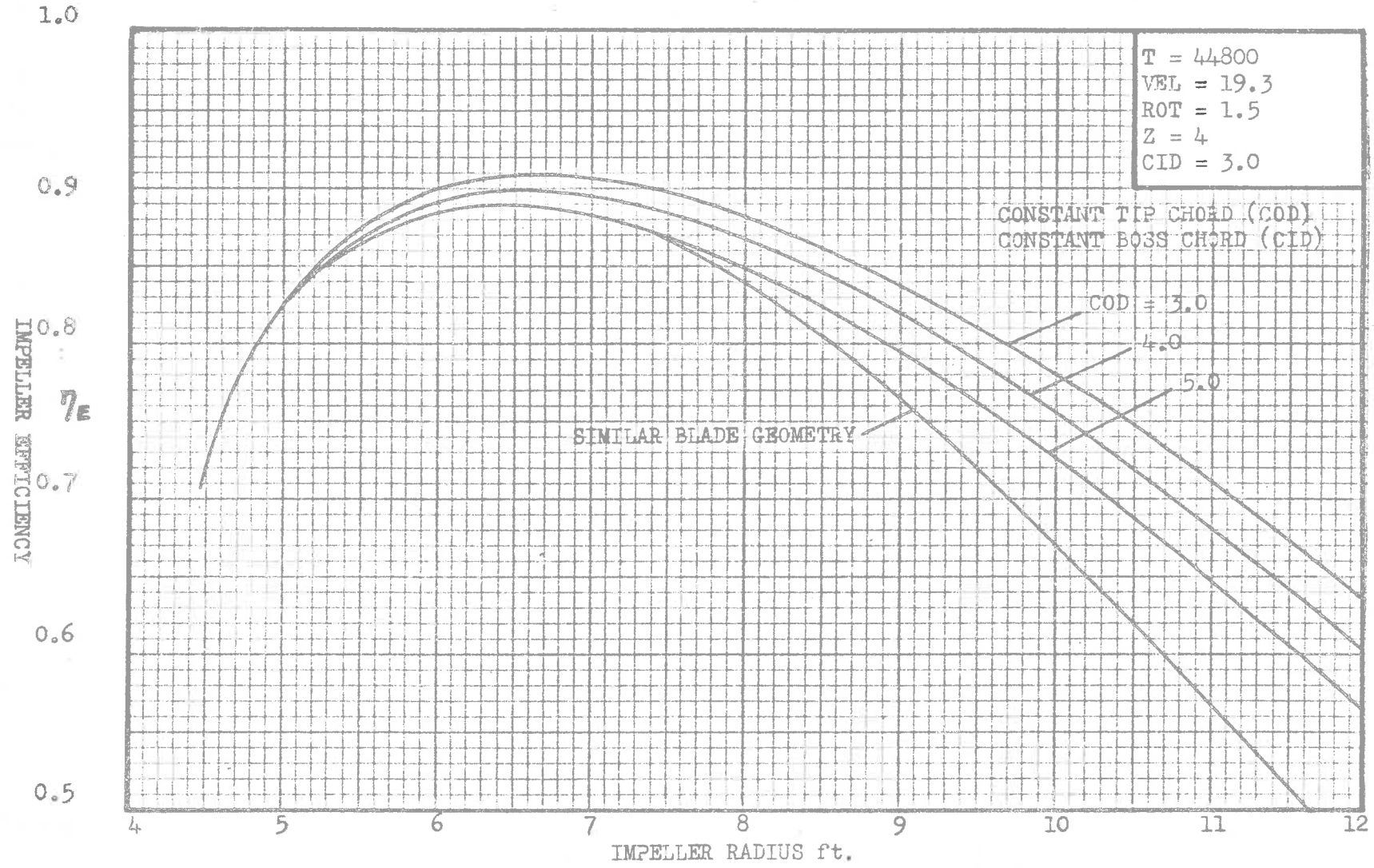

Fig. 2.2 - Optimum Efficiency for Varying Radius.

Fig. 2.2

Fig. 2. 3

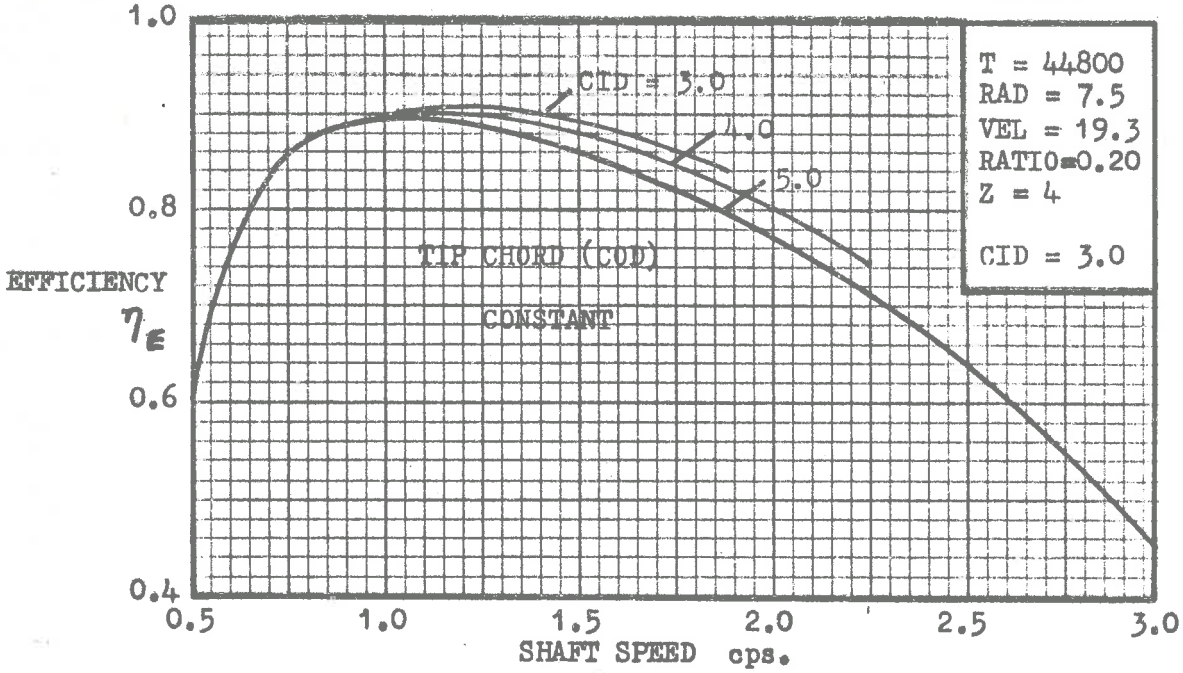

Fig. 2.3 - Optimum Efficiency at Varying Shaft Speed.

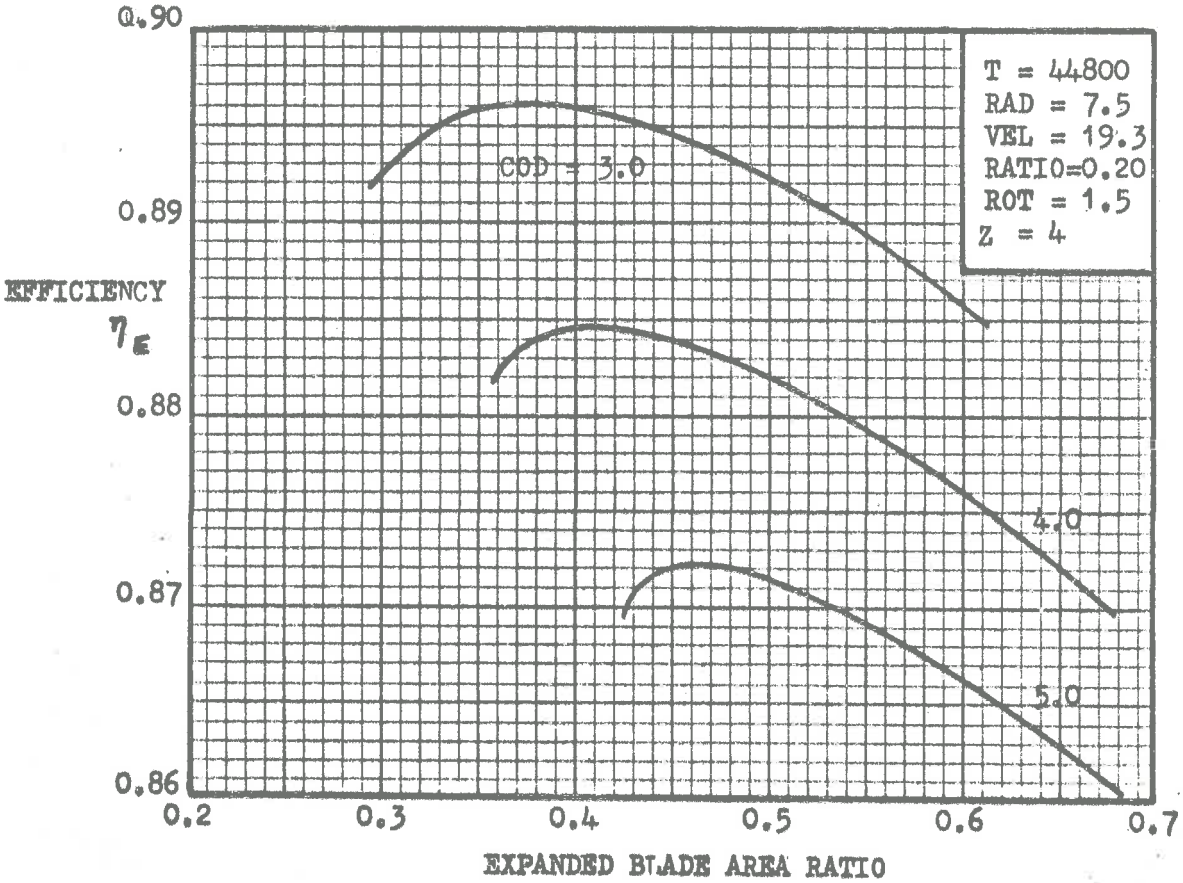

Fig. 2.4 - Optimum Efficiency with Varying Blade Geometry.

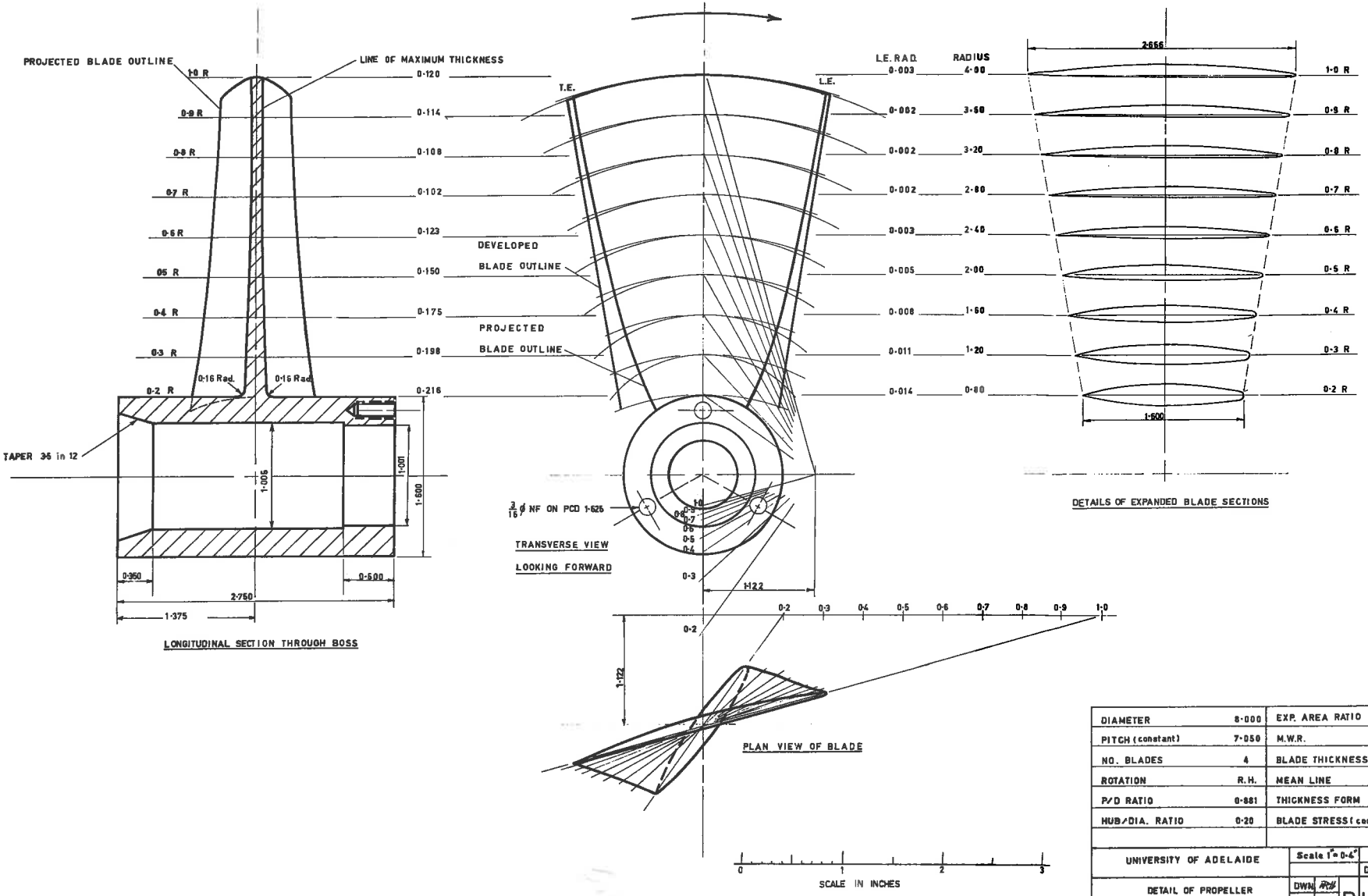

DIAMETER	8·000	EXP. AREA RATIO	0·543
PITCH (constant)	7·050	M.W.R.	0·668
NO. BLADES	4	BLADE THICKNESS RATIO	·027(02R
ROTATION	R.H.	MEAN LINE	a=1·0
P/D RATIO	0·881	THICKNESS FORM	NACA 16
HUB/DIA. RATIO	0·20	BLADE STRESS (constant)	7250psi

UNIVERSITY OF ADELAIDE		Scale 1"=0·4"	Date 25-8-84
DETAIL OF PROPELLER NO. 0003	DWN. PDS TCD. CKD.	B	HYDRO-6

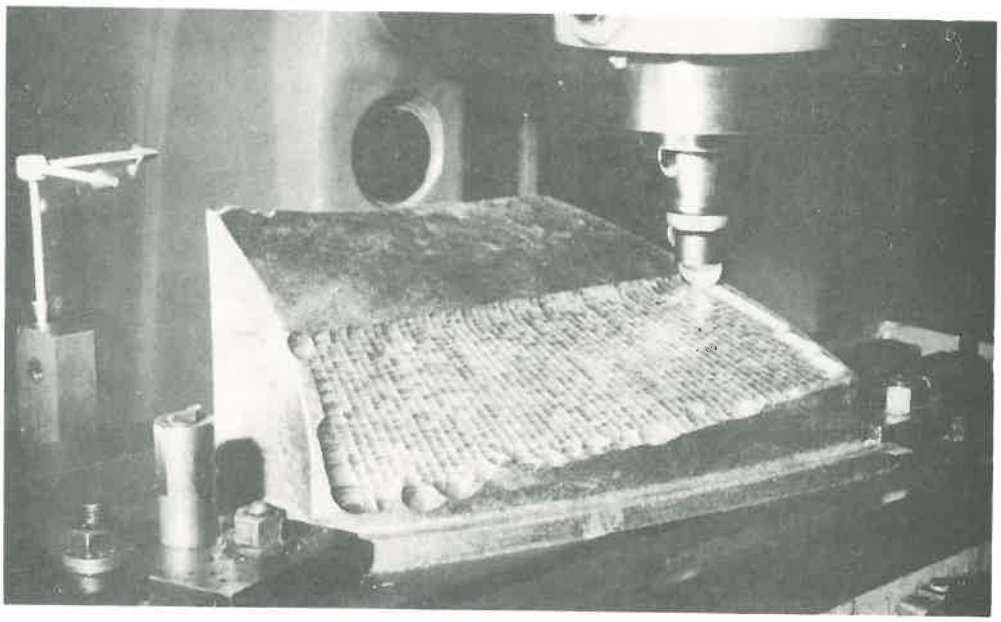

Fig. 2.6 - MACHINING MASTER TEMPLATES FOR IMPELLER.

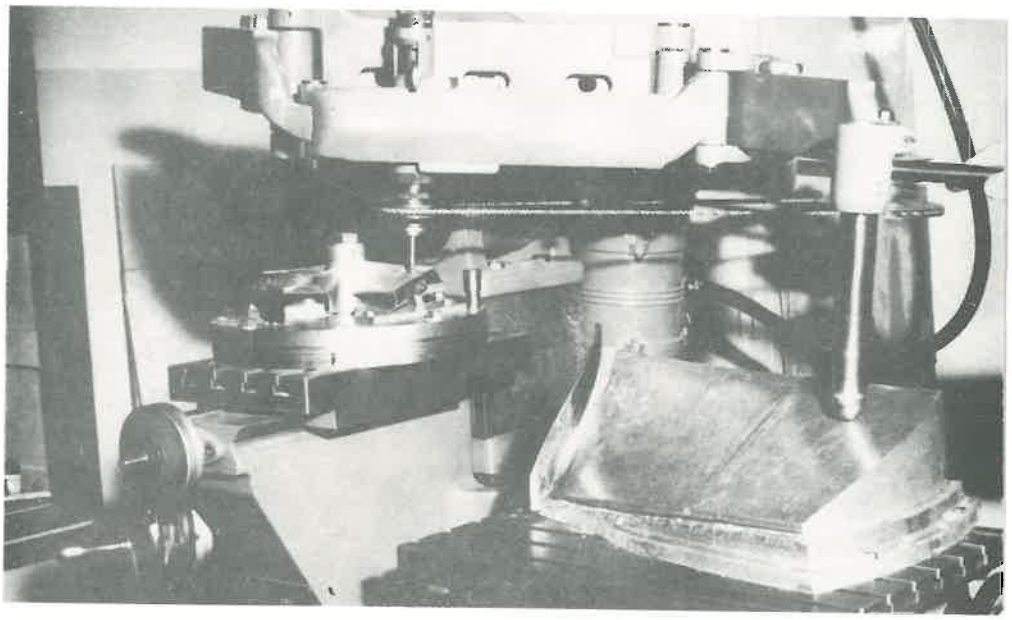

Fig. 2.7 - MACHINING MODEL IMPELLER IN COPYING MACHINE.

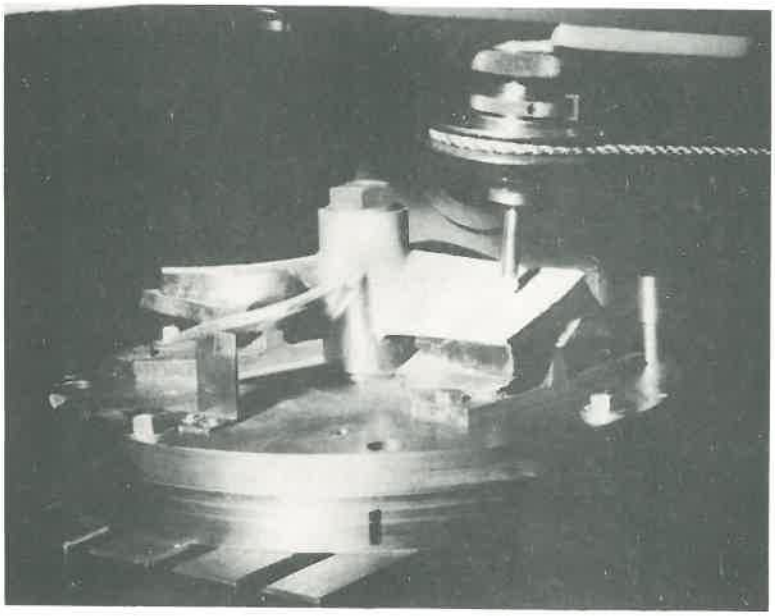

Fig. 2.8 - MACHINING MODEL IMPELLER.

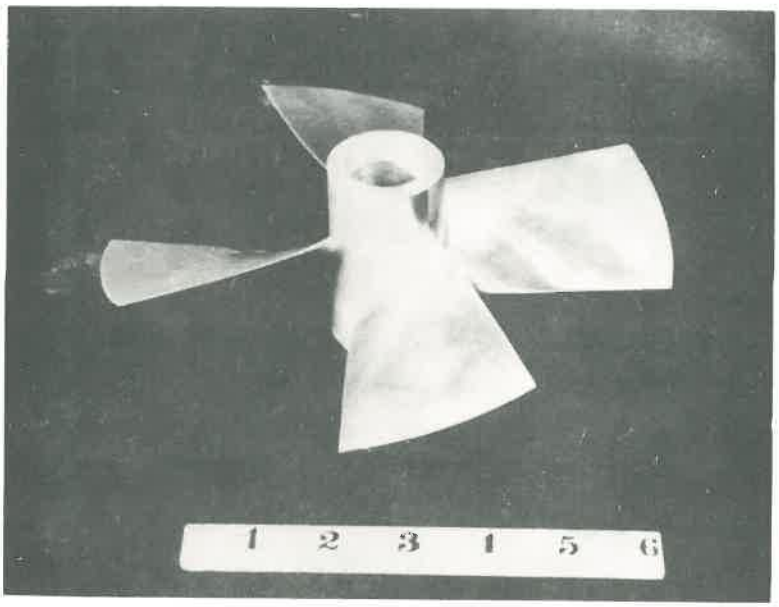

Fig. 2.9 - MODEL IMPELLER.

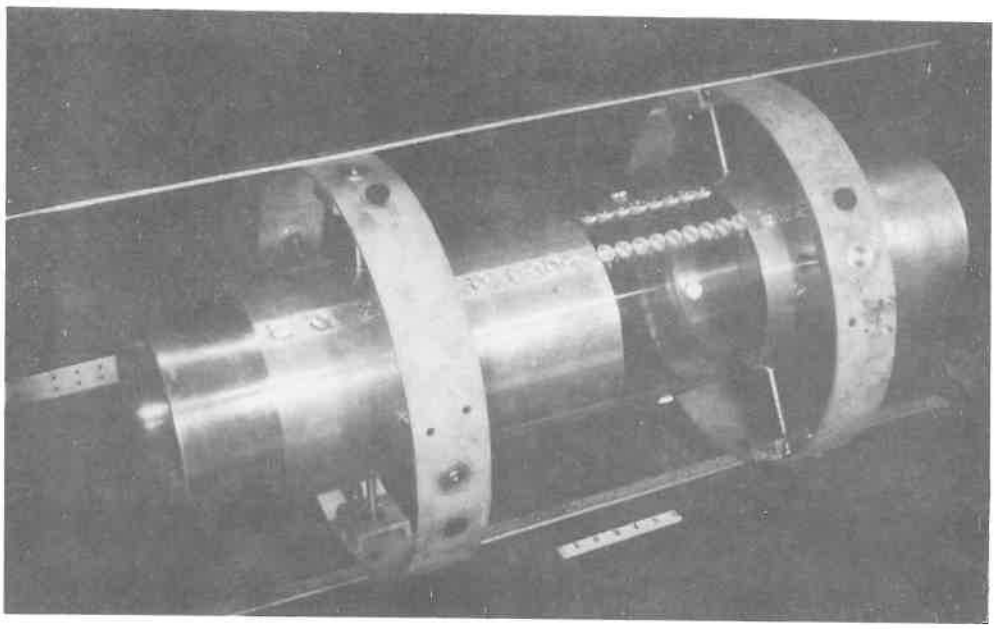

Fig. 3.1 – MODEL DUCT ARRANGEMENT.

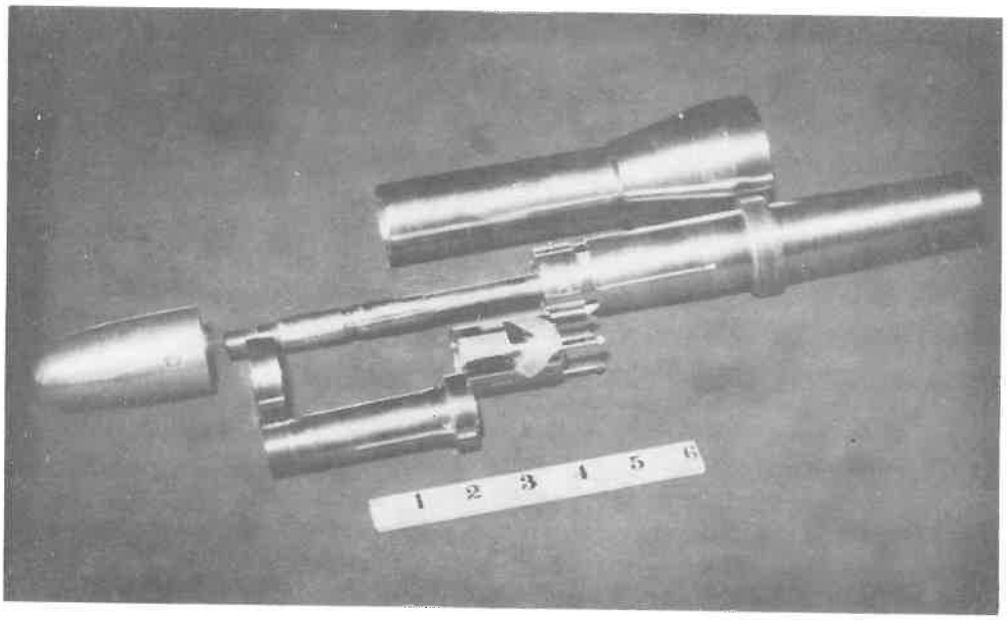

Fig. 3.2 – VIEW OF DYNAMOMETER BEFORE ASSEMBLY.

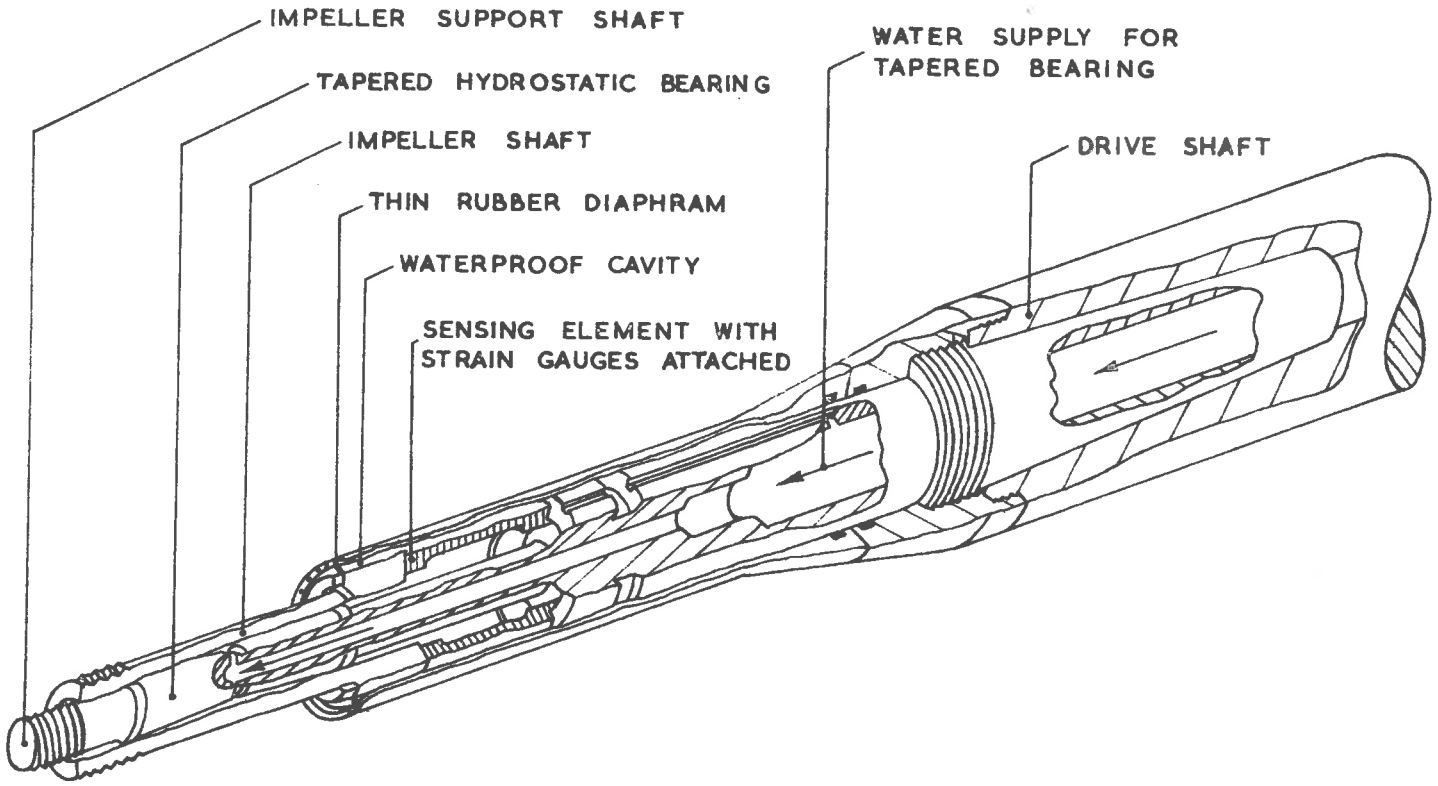

FIG. 3.3 CROSS SECTION OF DYNAMOMETER

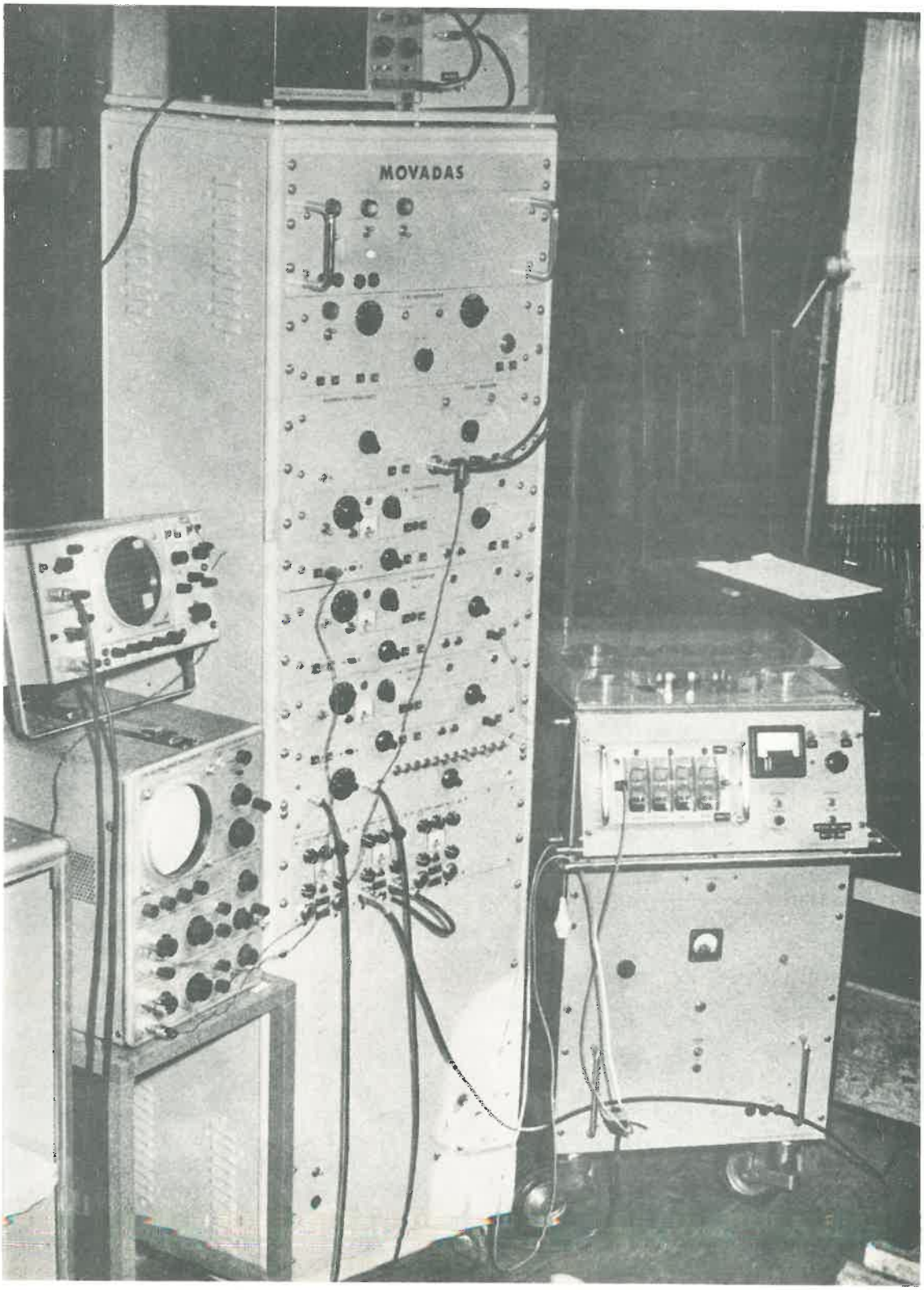

Fig. 4.0 – GENERAL VIEW OF THE INSTRUMENTATION.

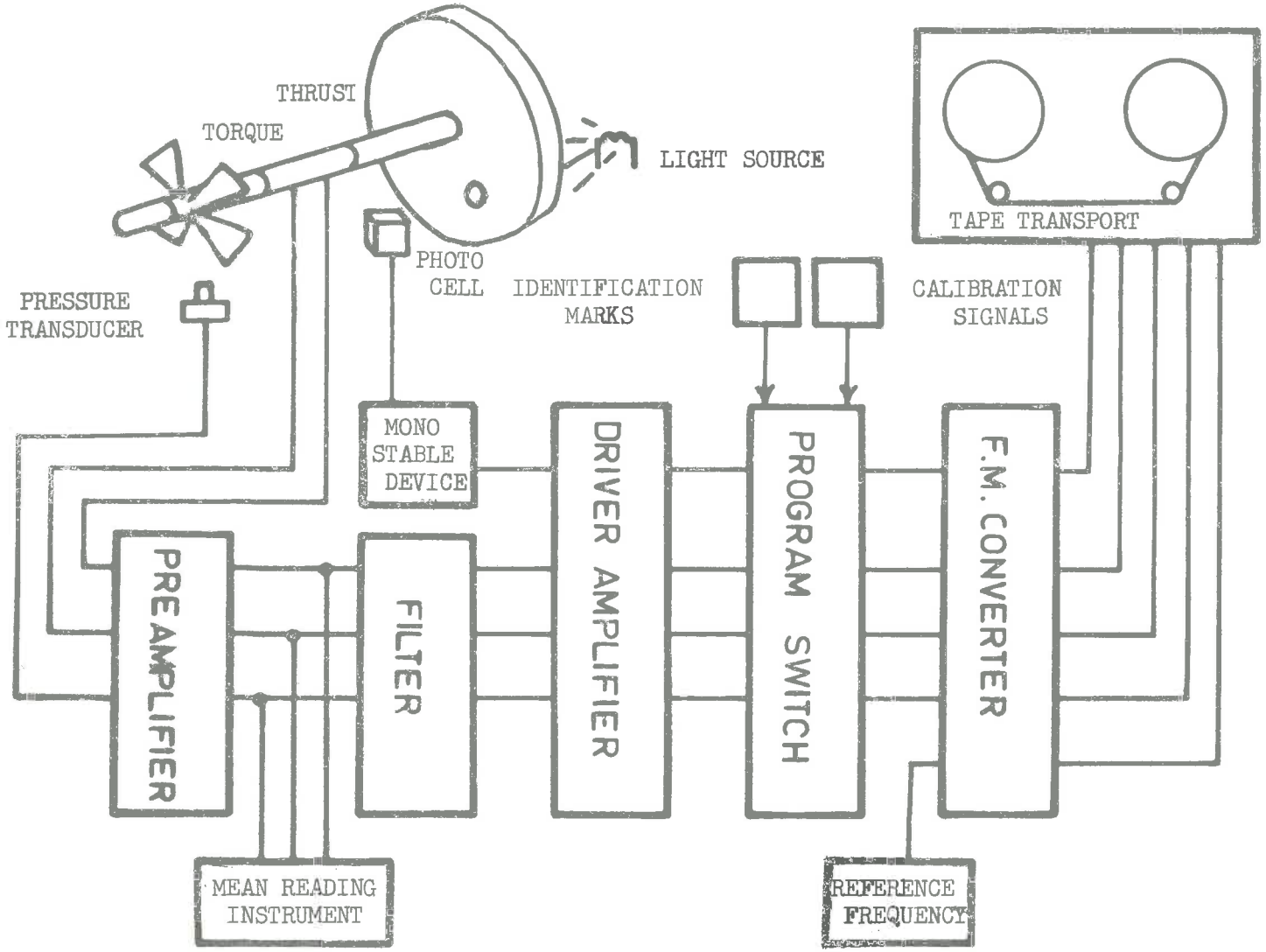

Fig. 4.1 - Block Diagram of Instrumentation

Fig. 4.1

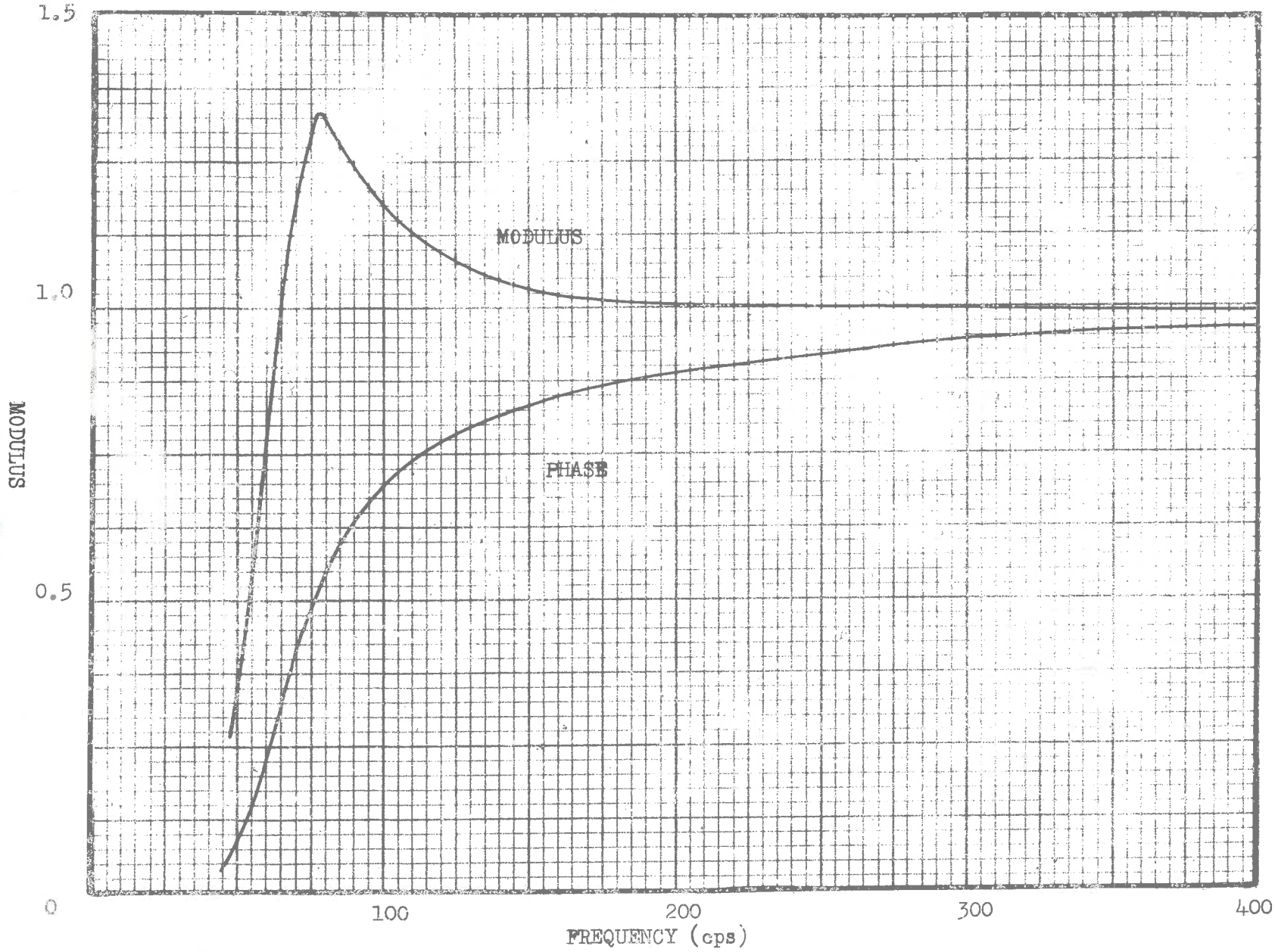

Fig. 4.2 - Typical Transfer Function Characteristics of the High-pass Filter.

Fig. 4.2

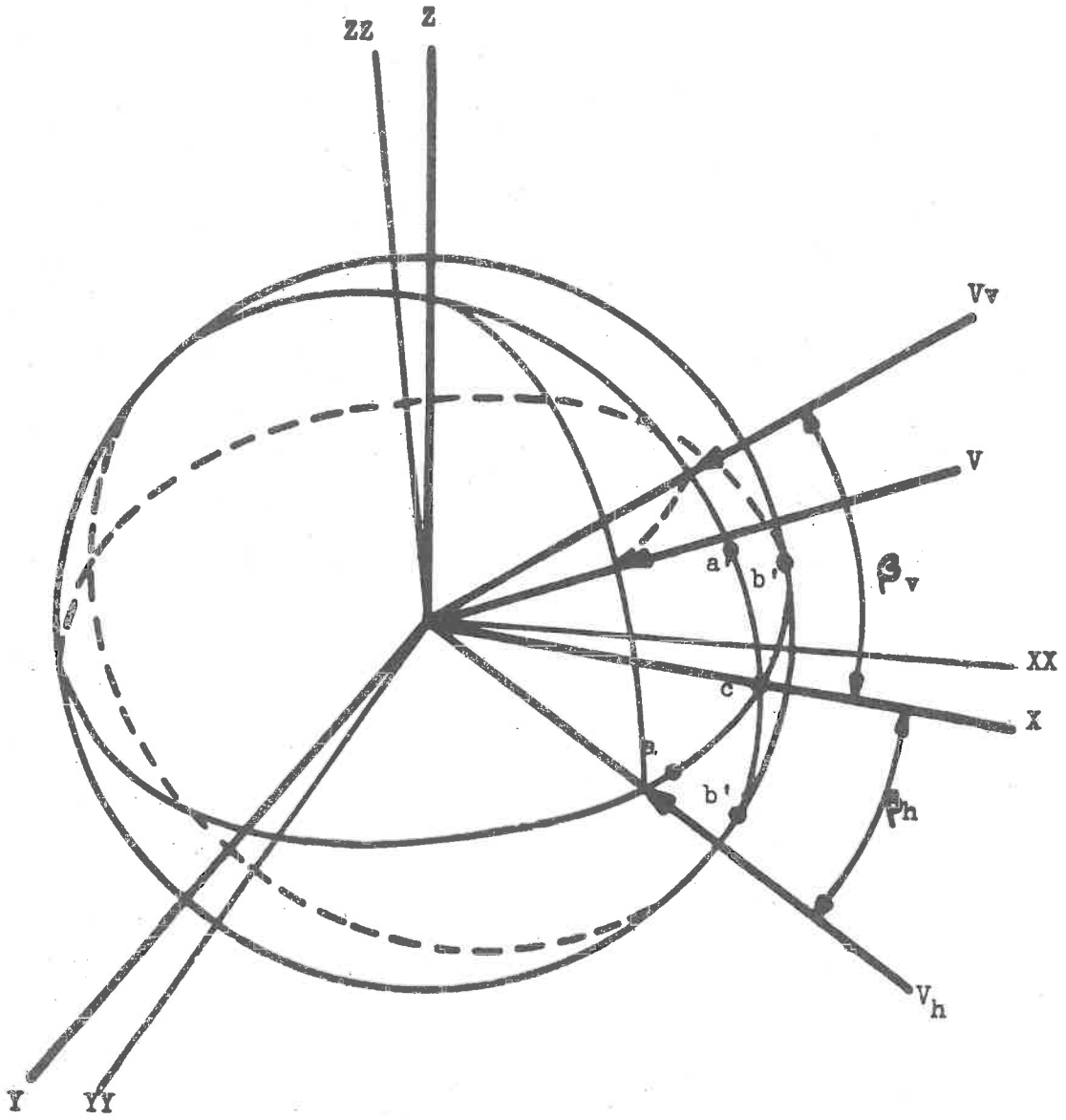

Fig. 4.3 - Orientation of Velocity components and pressure points to the Axes.

Fig. 4.4

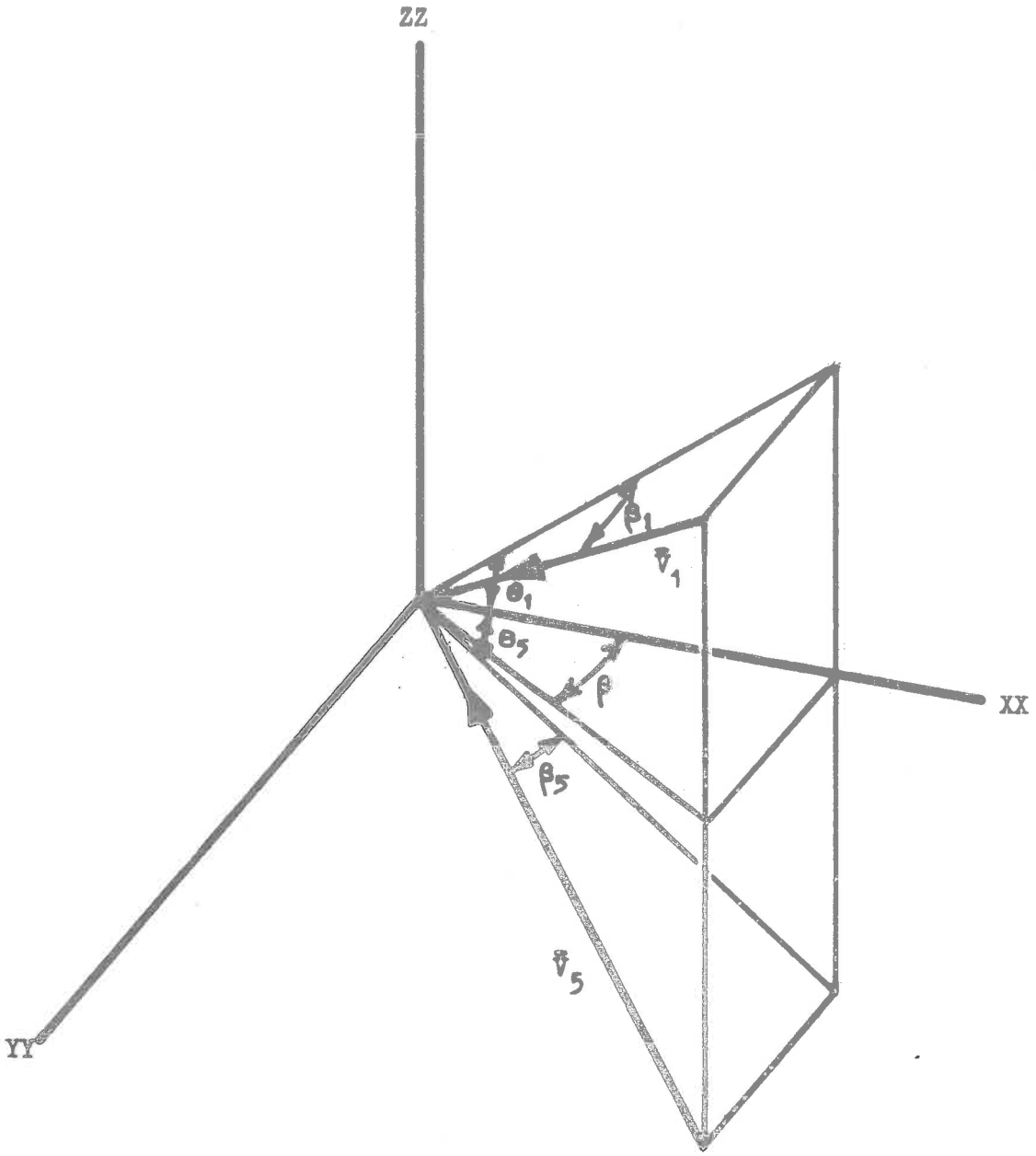

Fig. 4.4 - Inversion about OYY Axis.
Notation of Velocity Components with respect to the Instrument Axes.

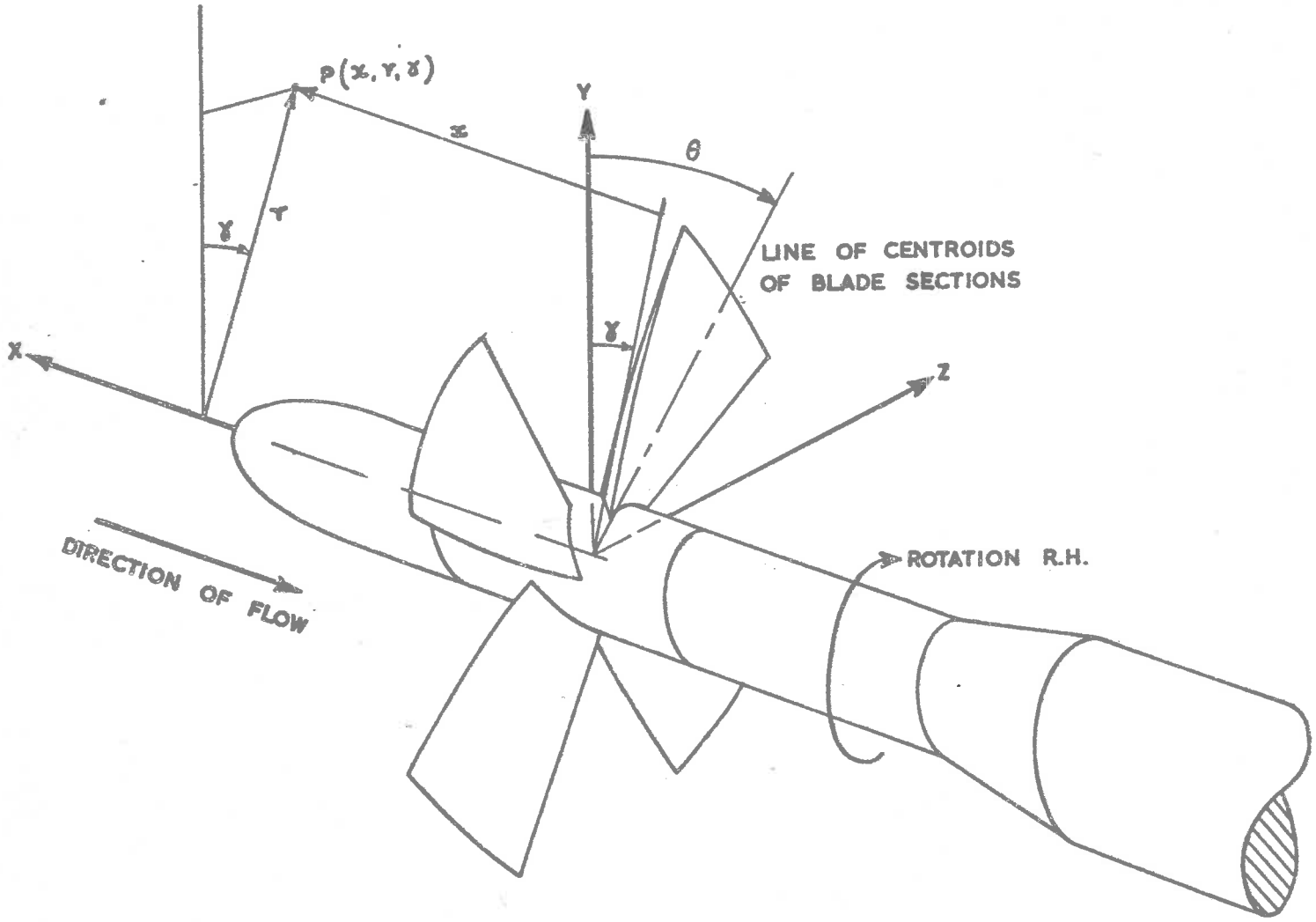

Fig. 5.1 - Orientation of axes of impeller

Fig. 5.1

Fig. 5.2

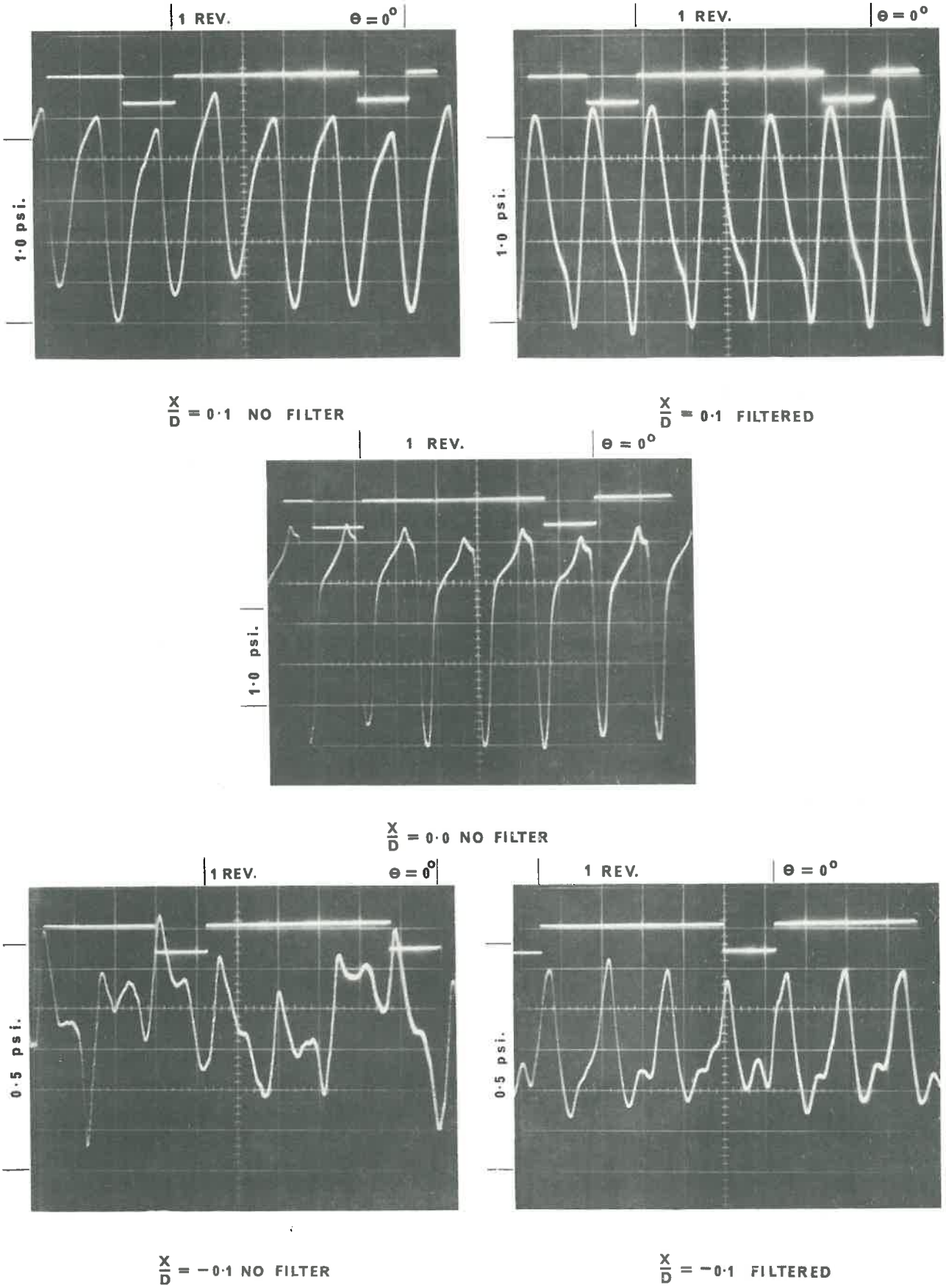

Fig. 5.2 – TYPICAL PRESSURE SIGNALS FOR UNIFORM FLOW $J_1 = 0{\cdot}74$, N = 1200 rpm., $\frac{Rd}{D} = 0{\cdot}5028$

Fig. 5.3

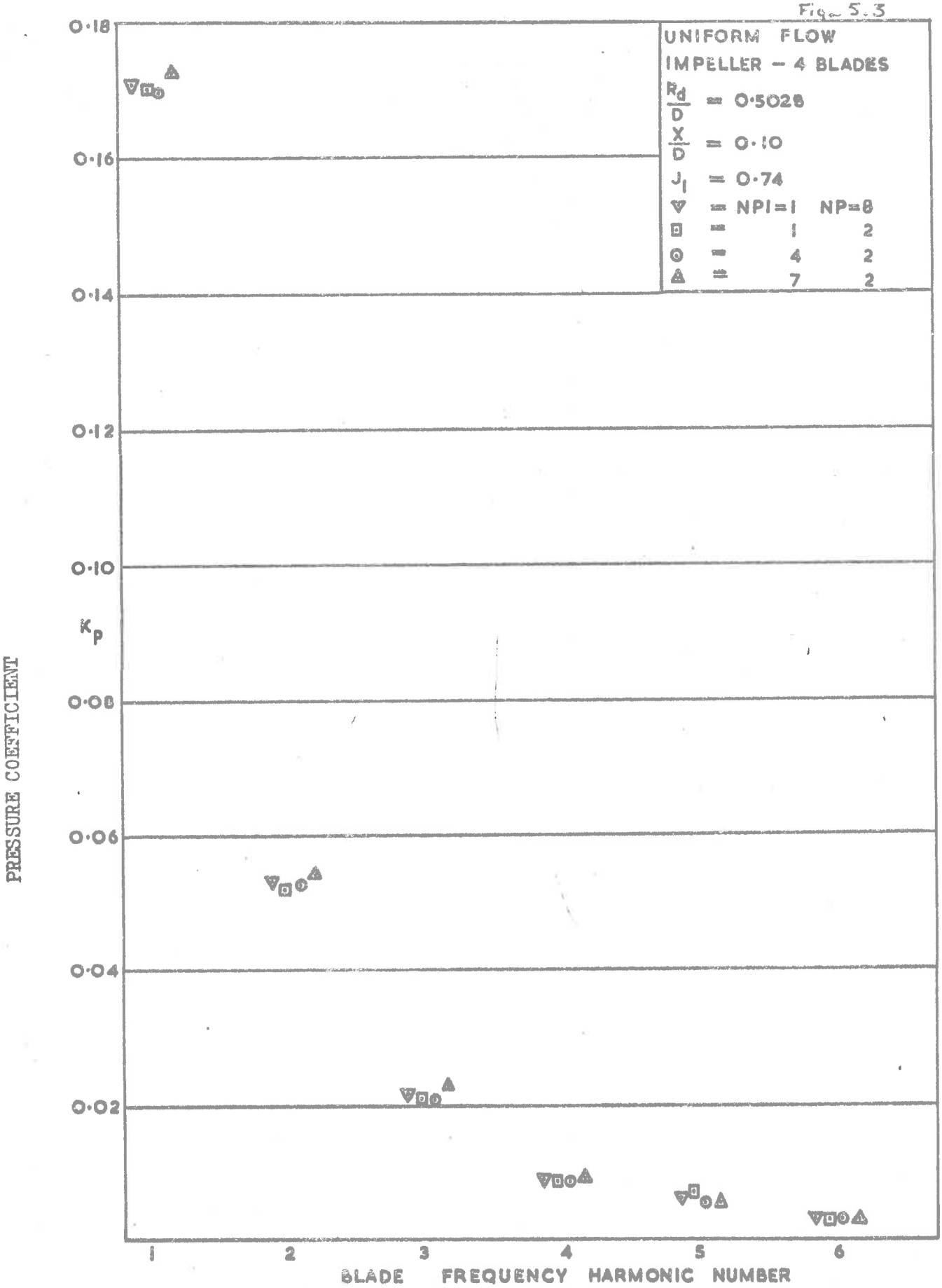

Fig. 5.3 - Periodicity of Recorded Pressure.

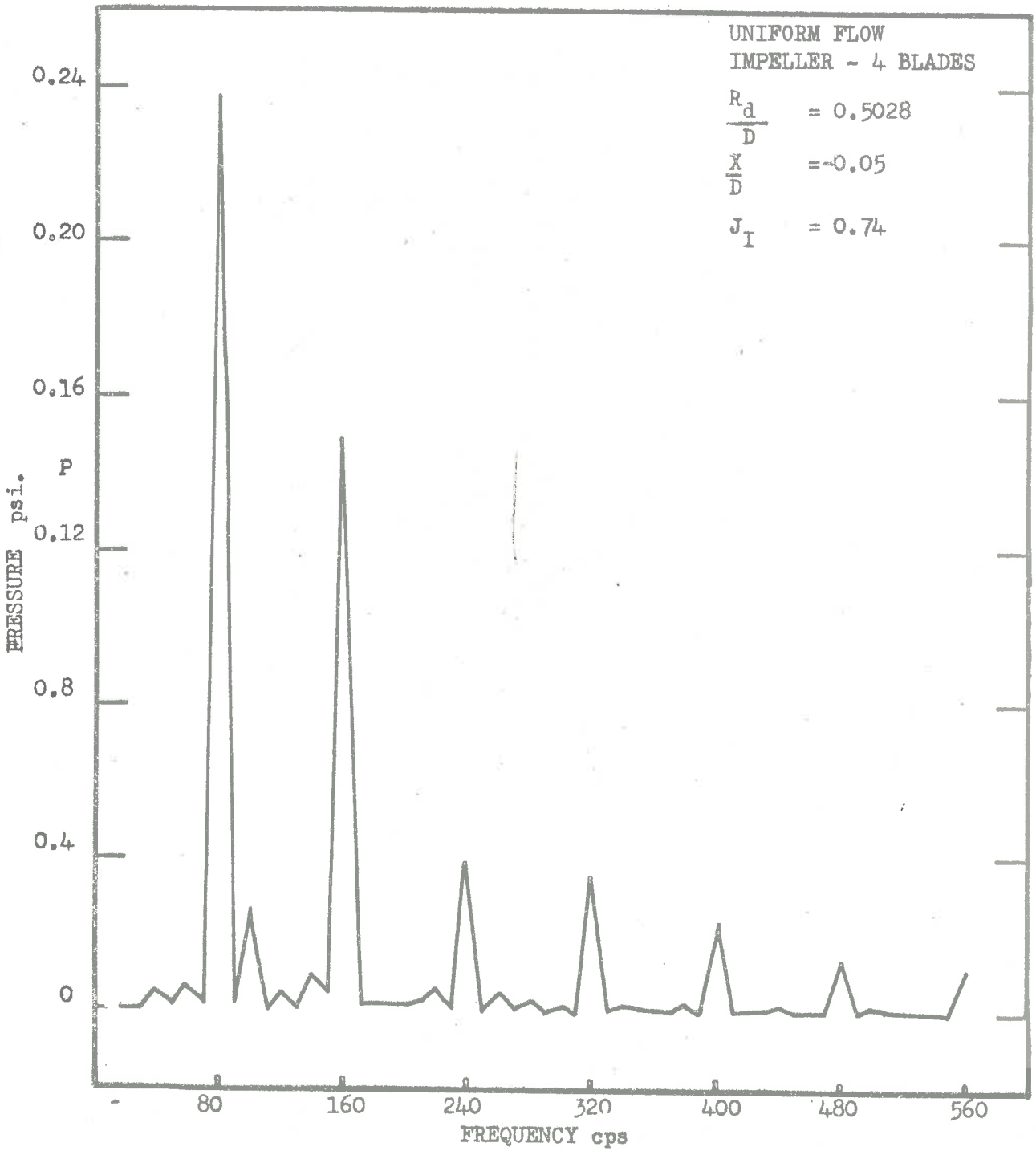

Fig. 5.4 - Frequency Spectra of Pressure

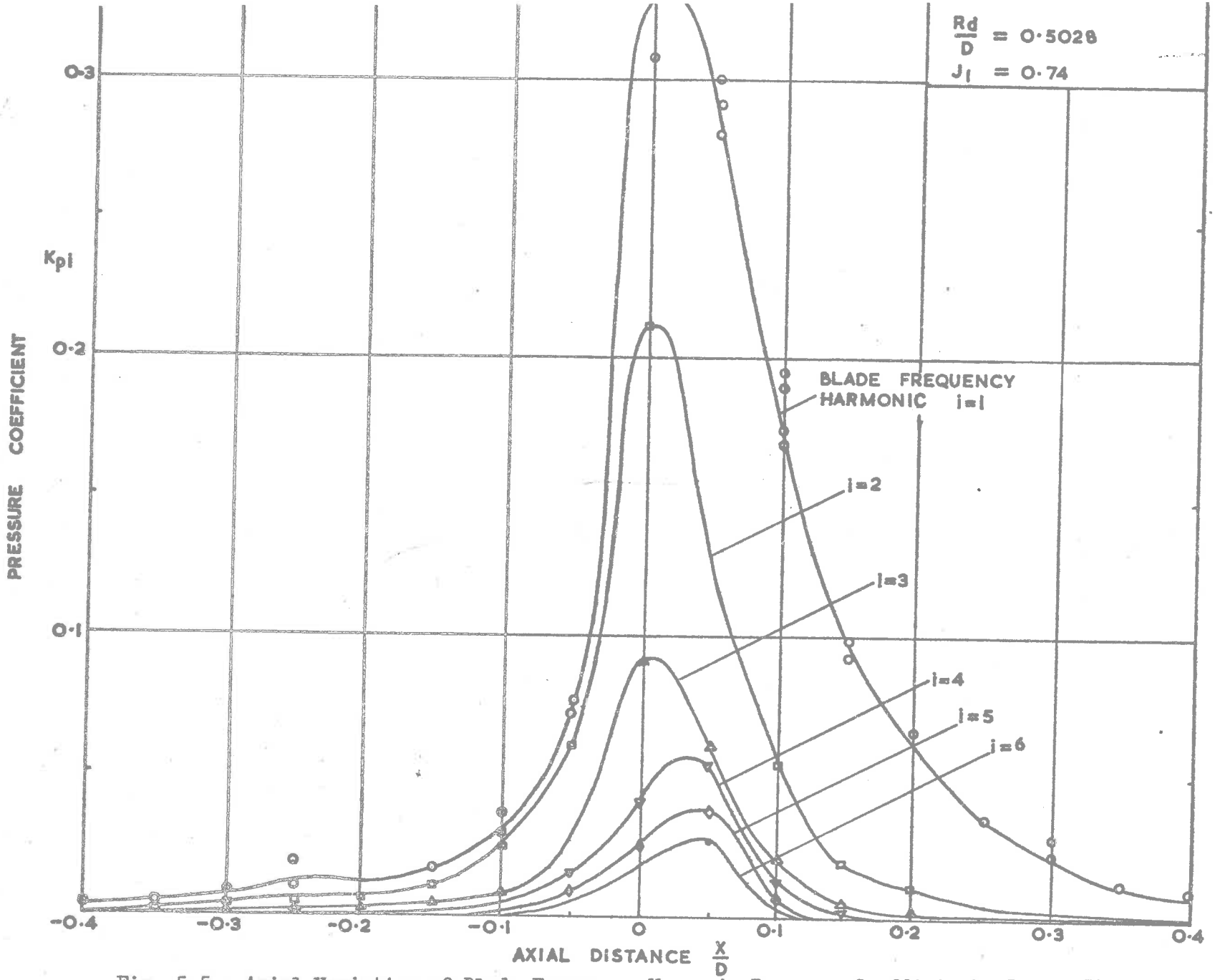

Fig. 5.5 - Axial Variation of Blade Frequency Harmonic Pressure Coefficient. $J_I = 0.74$.

Fig. 5.5

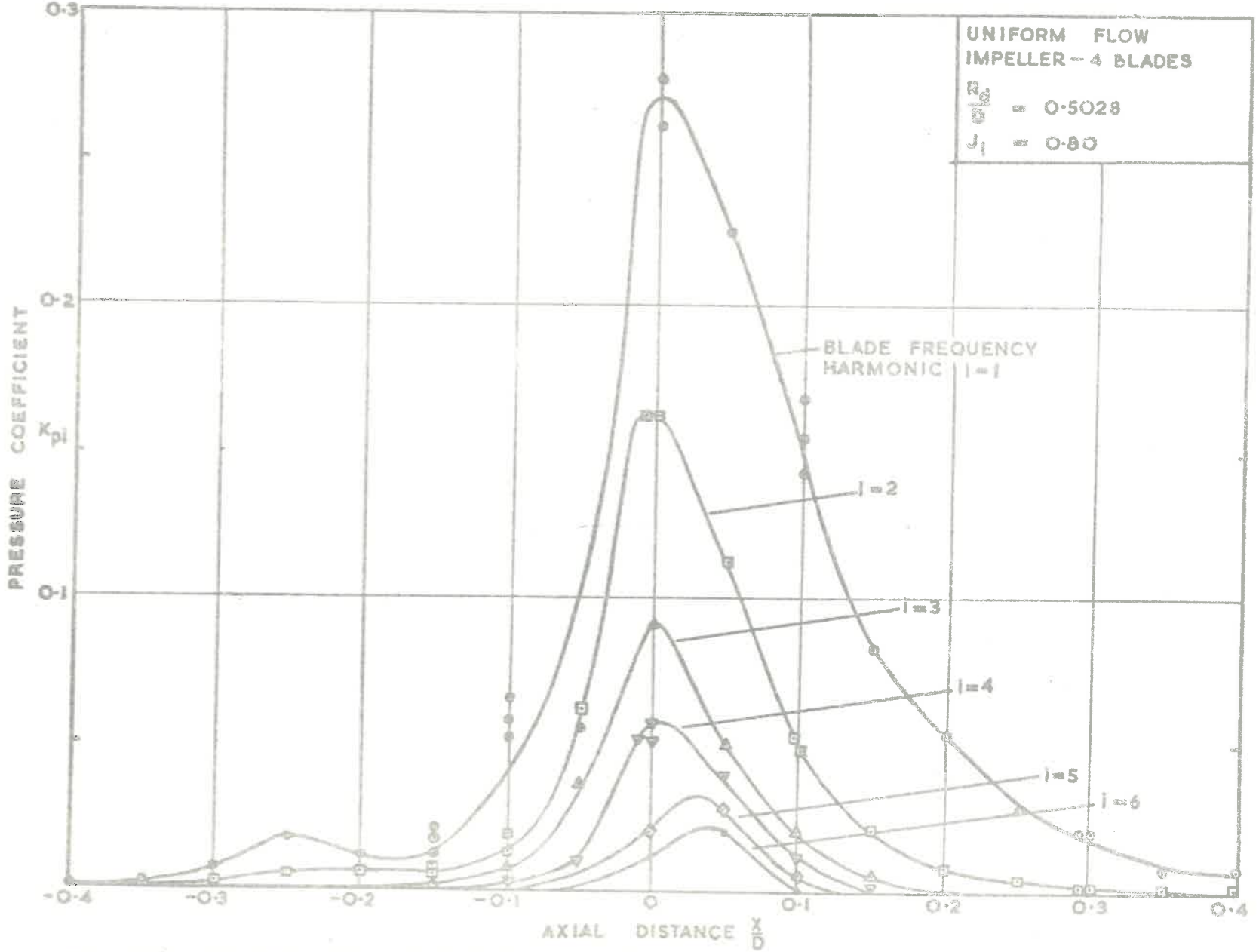

Fig. 5.6 - Axial Variation of Blade Frequency Harmonic Pressure Coefficient. J_I = 0.80.

Fig. 5.6

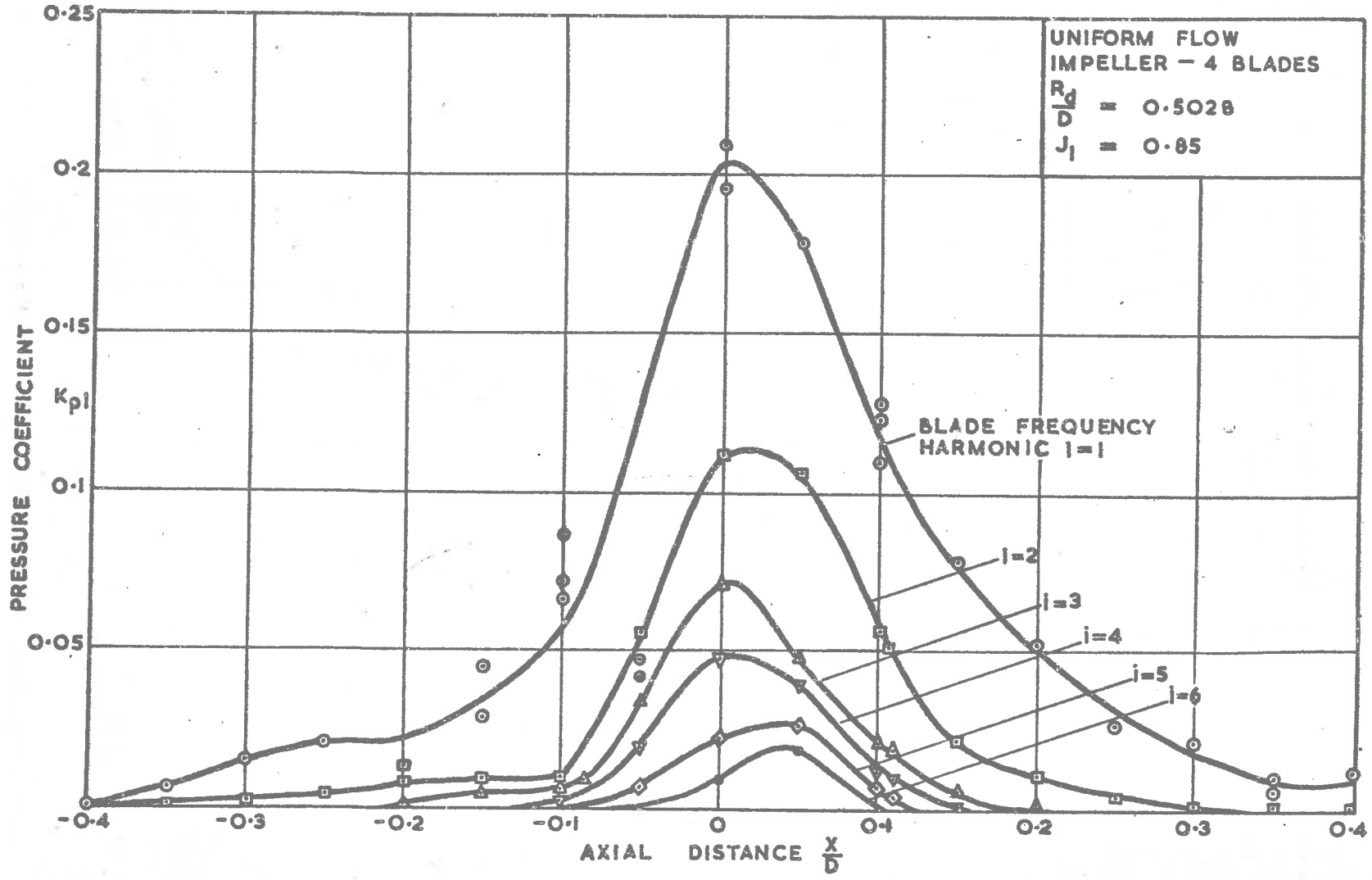

Fig. 5.7 - Axial Variation of Blade Frequency Harmonic Pressure Coefficient. J_I = 0.85.

Fig. 5.7

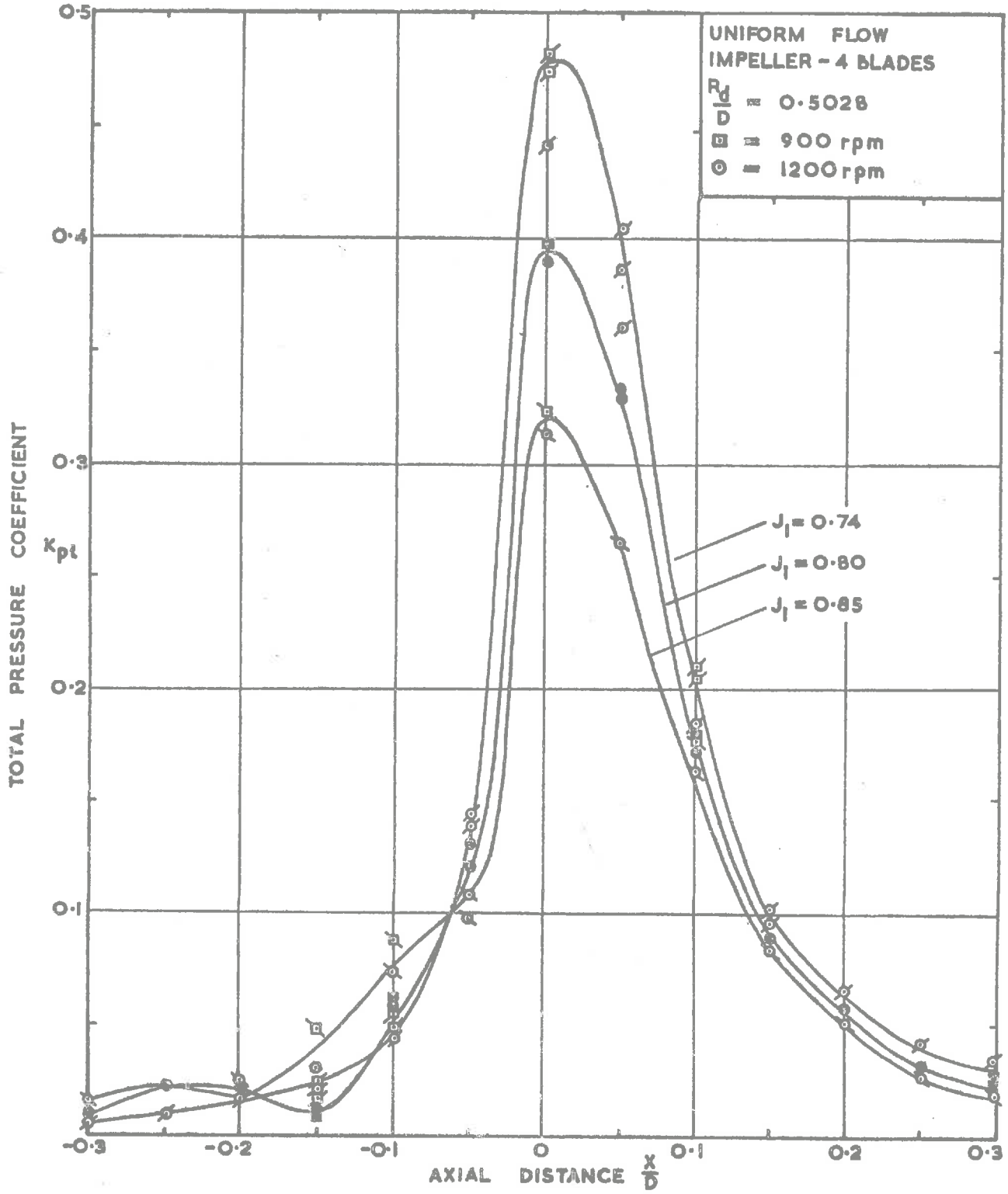

Fig. 5.8 - Axial Variation of the Total Pressure Coefficient.

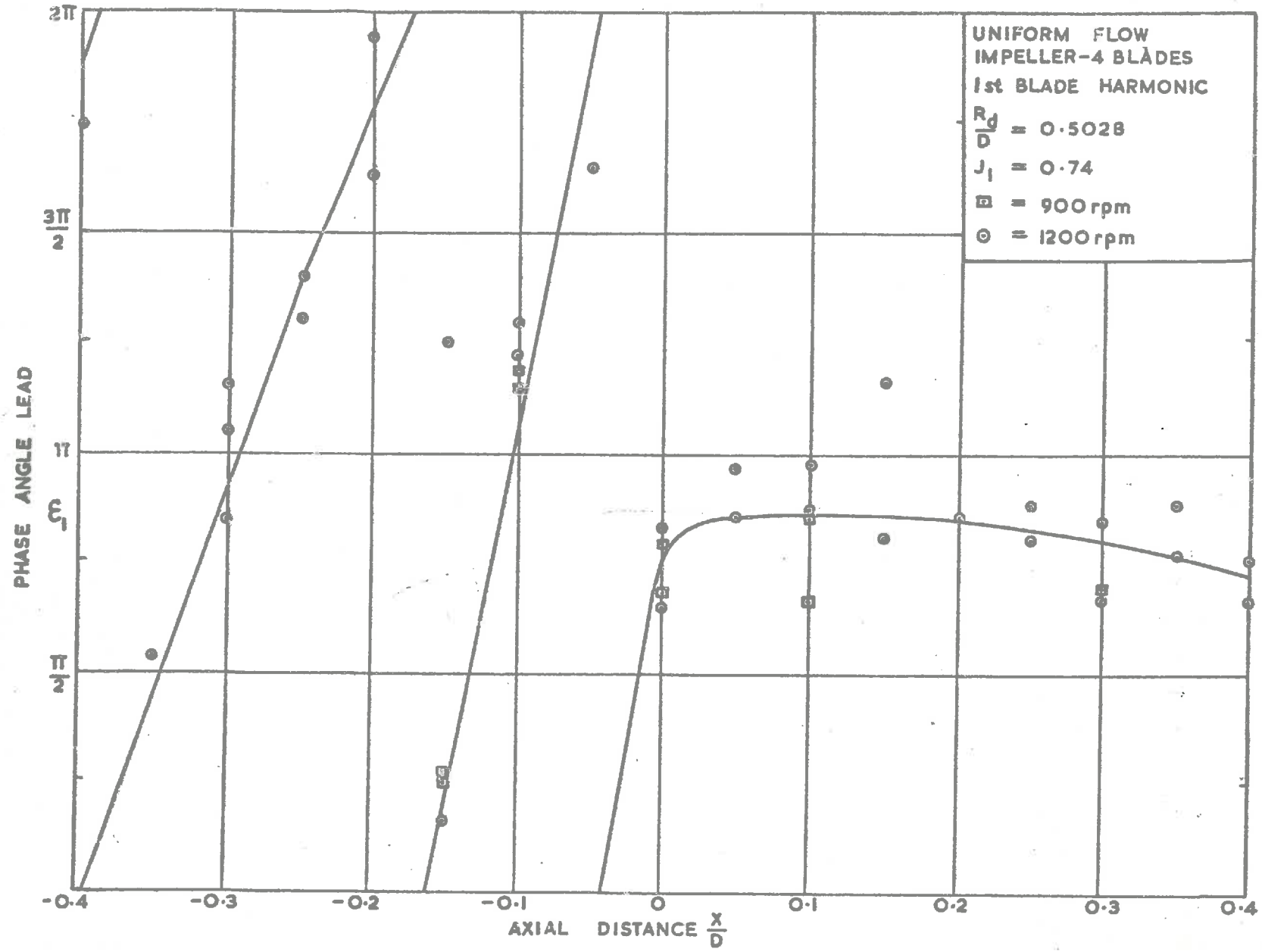

Fig. 5.9 - Axial Variation of Phase Angle (Lead) For 1st Blade Frequency Harmonic. $J_I = 0.74$

Fig. 5.9

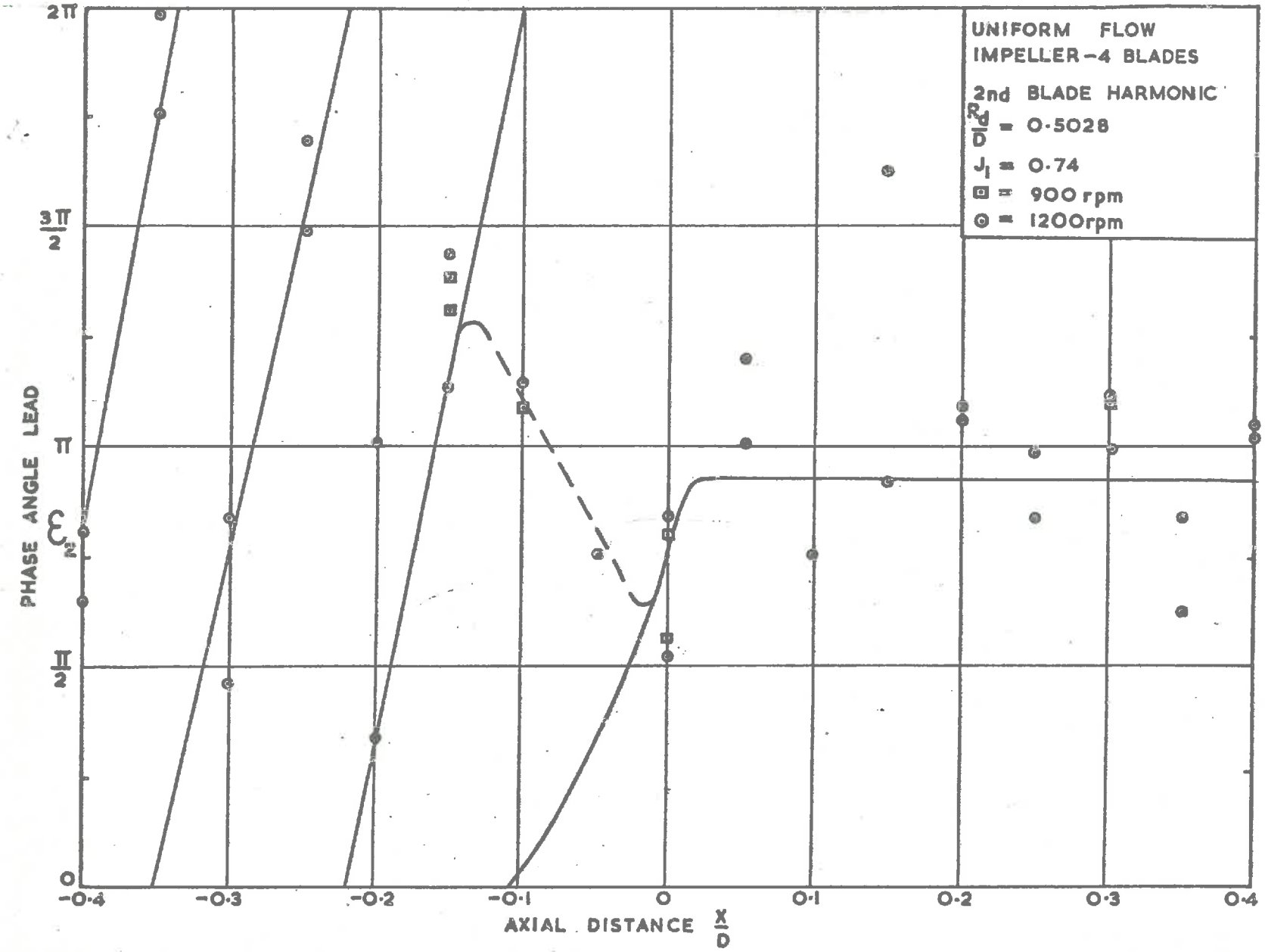

Fig. 5.10 - Axial Variation of Phase Angle (Lead) for 2nd Blade Frequency Harmonic. J_I = 0.74.

Fig. 5.10

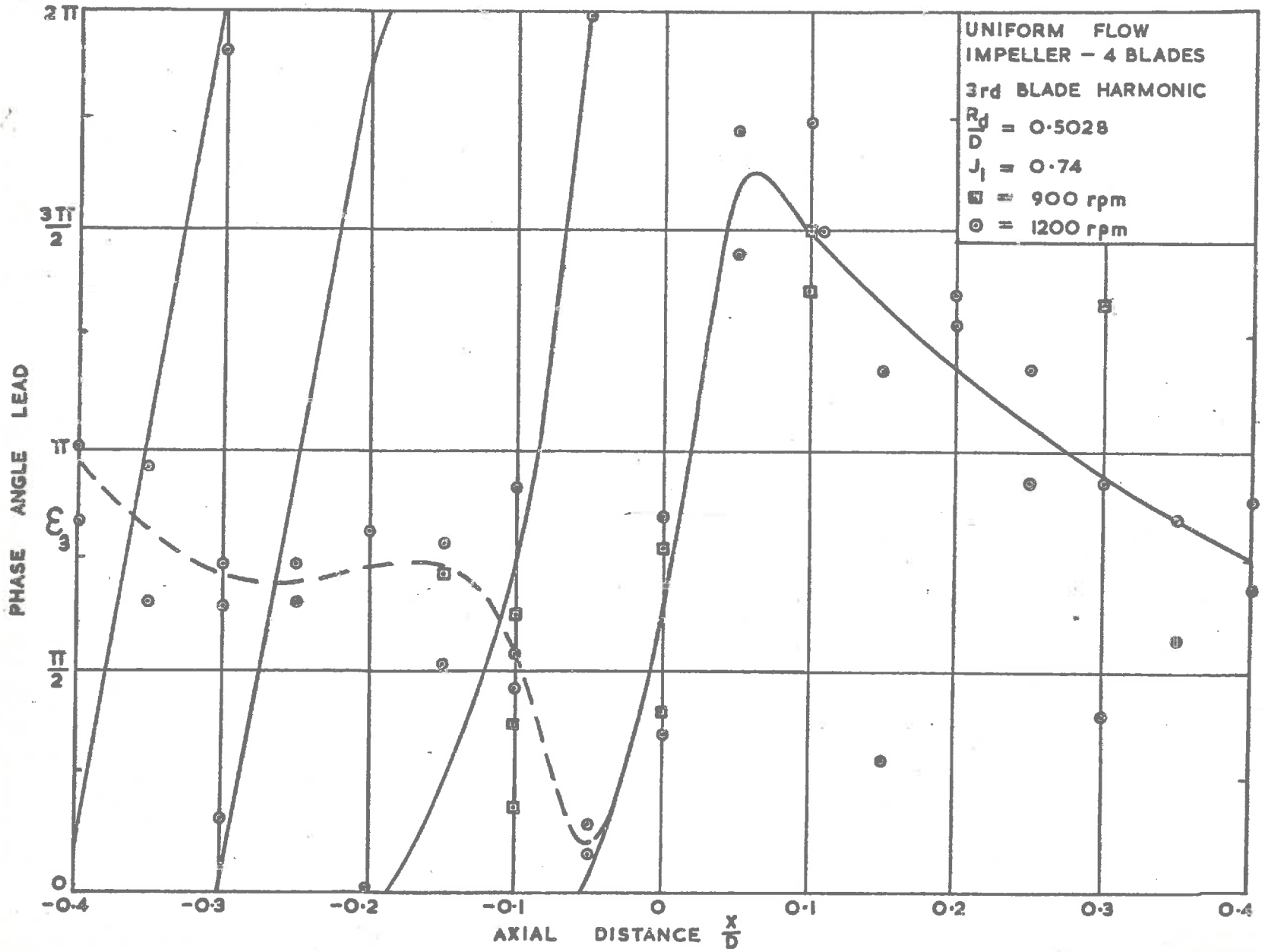

Fig. 5.11 - Axial Variation of Phase Angle (Lead) for 3rd Blade Frequency Harmonic. J_I = 9.74

Fig. 5.11

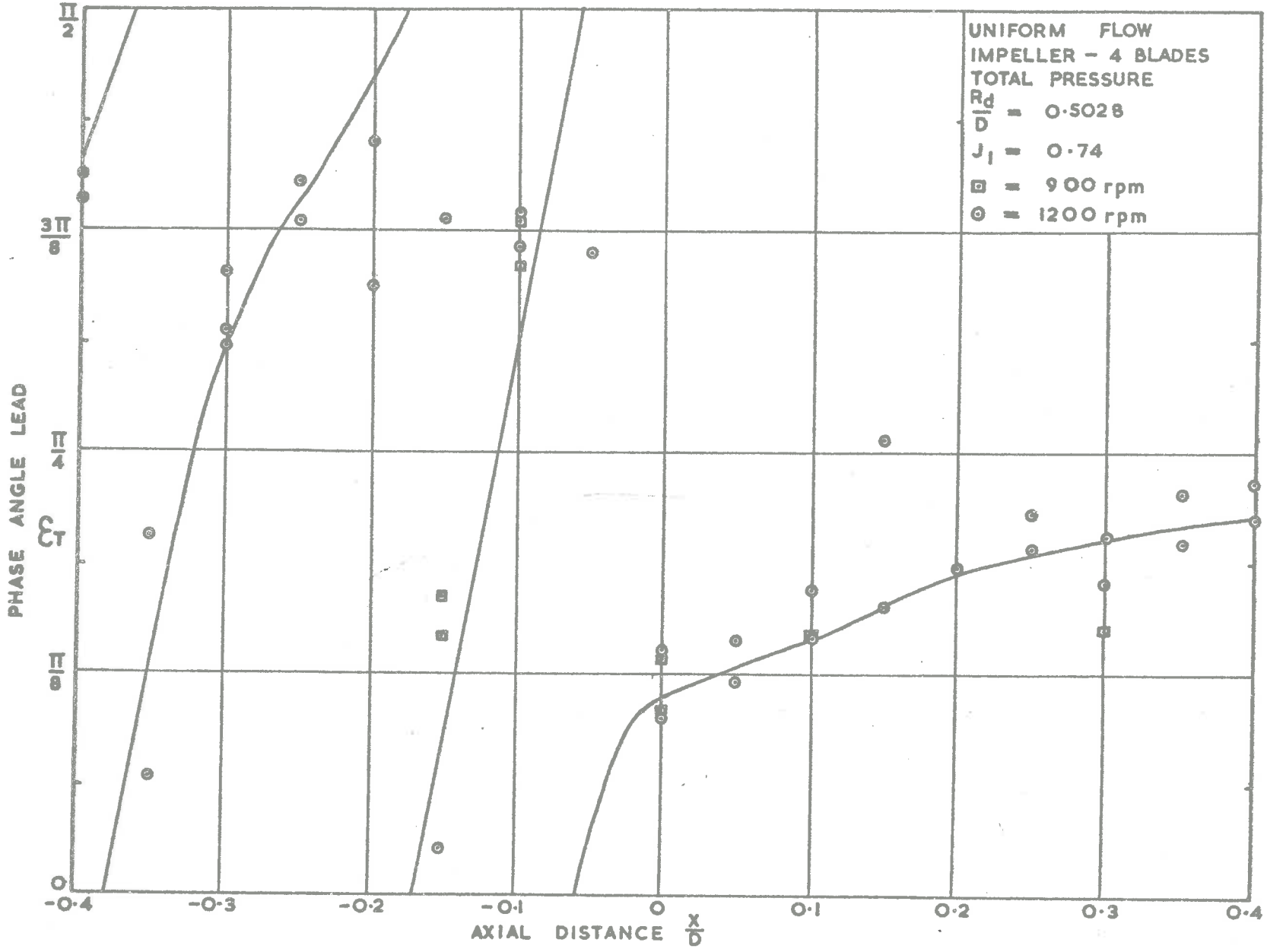

Fig. 5.12 - Axial Variation of Phase Angle (Lead) for Total Pressure.

Fig. 5.12

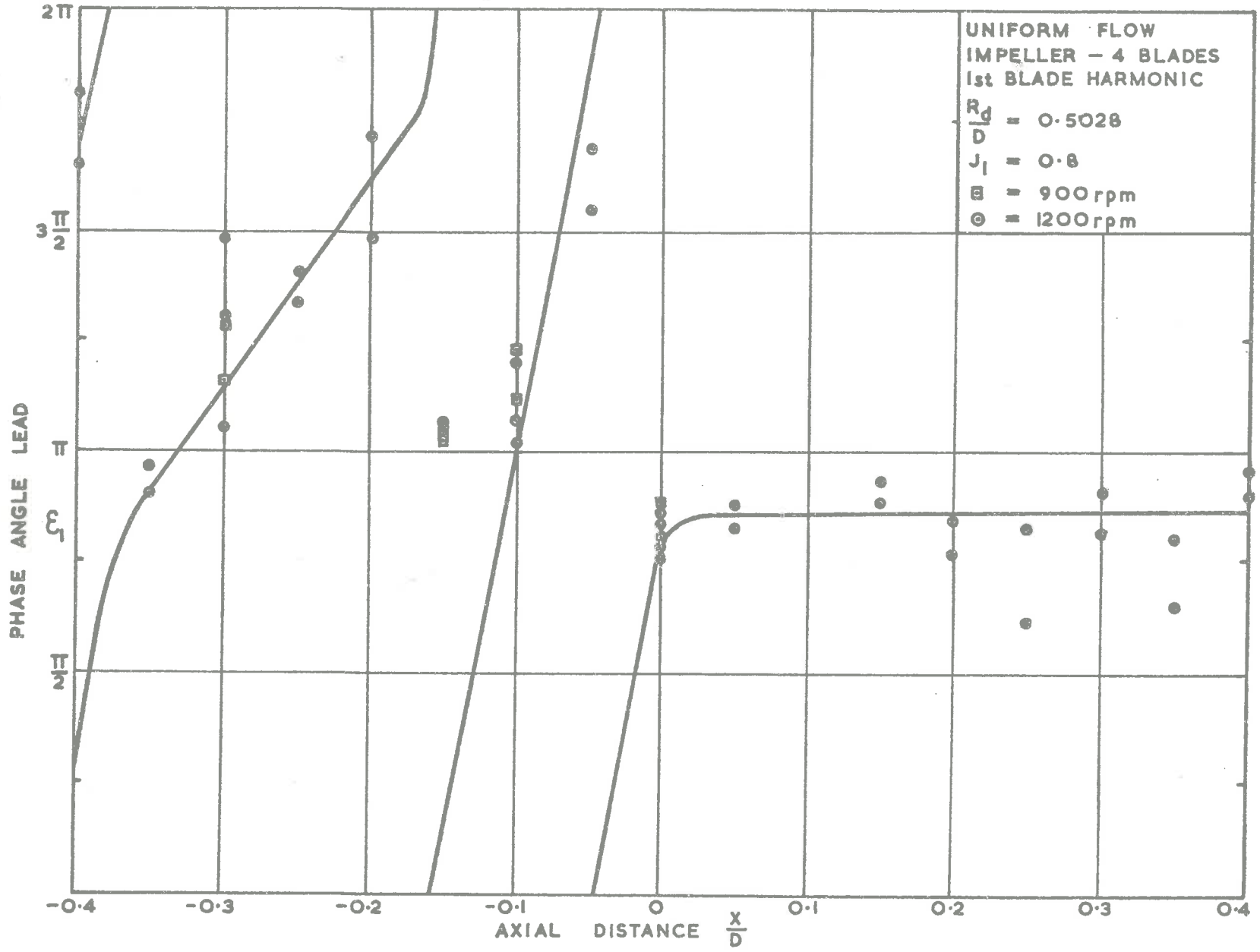

Fig. 5.13 - Axial Variation of Phase Angle (Lead) for 1st Blade Frequency Harmonic. J_I = 0.80.

Fig. 5.13

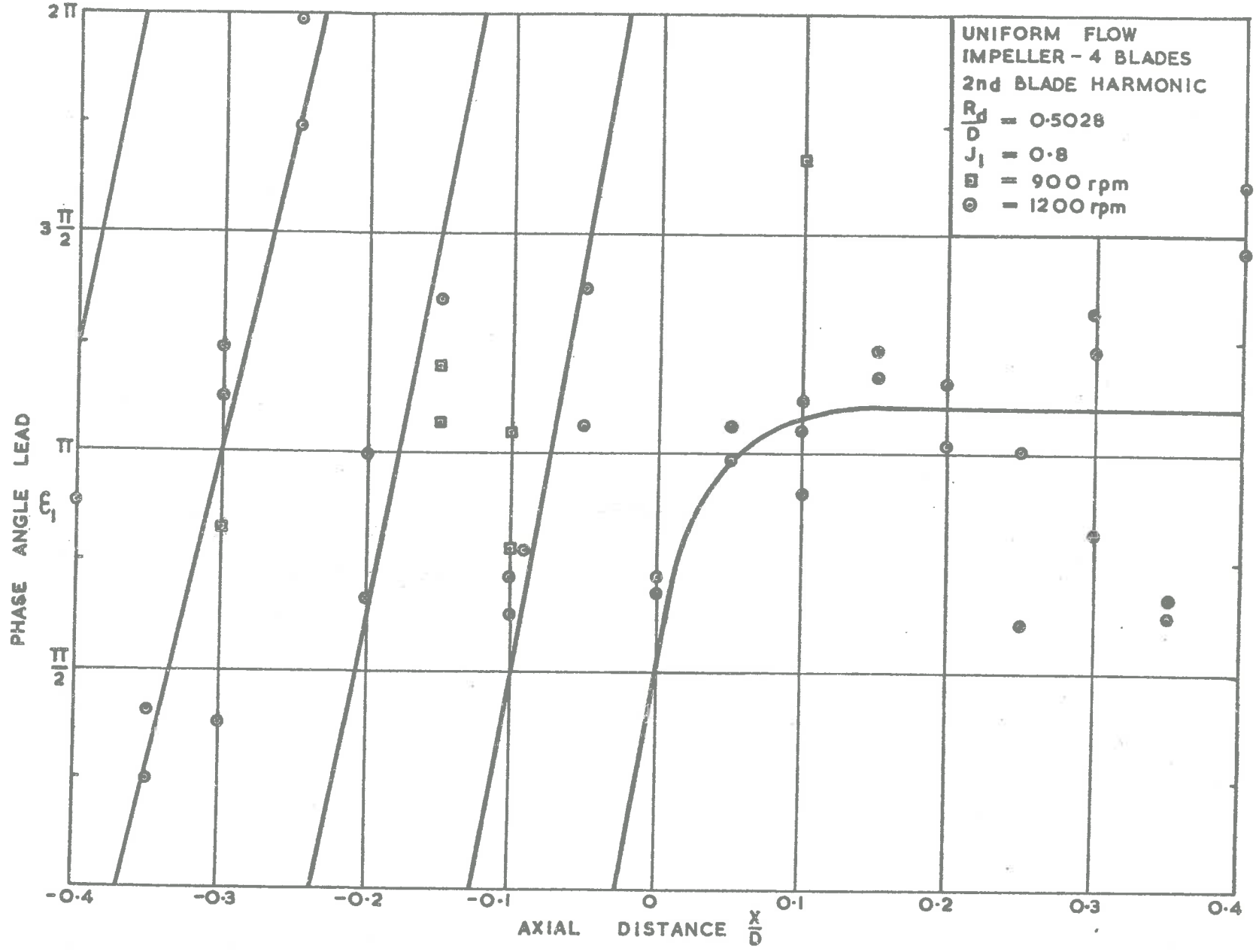

Fig. 5.14 - Axial Variation of Phase Angle (Lead) for 2nd Blade Frequency Harmonic. J_I = 0.80.

Fig. 5.14

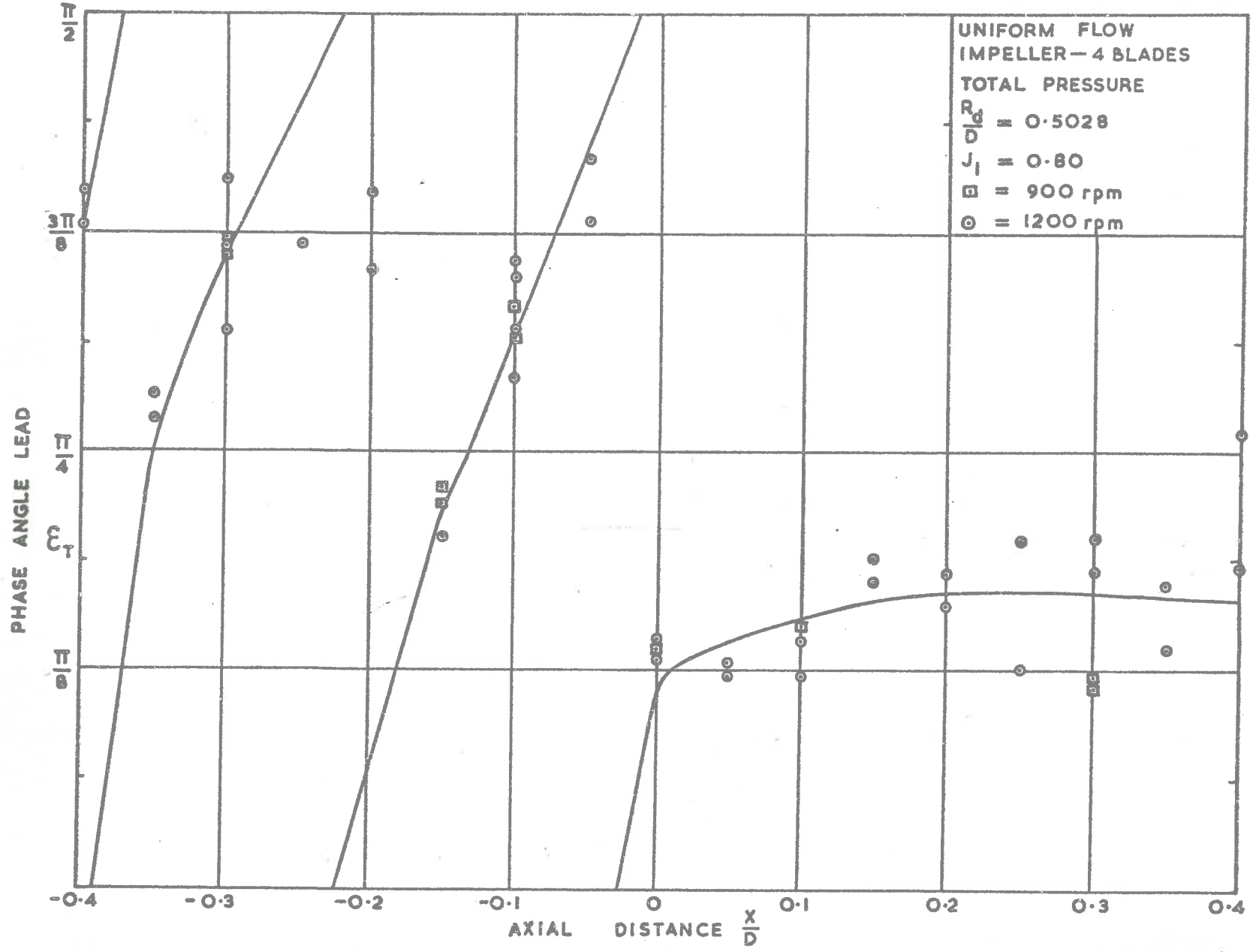

Fig. 5.15 - Axial Variation of Phase Angle (Lead) for Total Pressure. J_I = 0.80.

Fig. 5.15

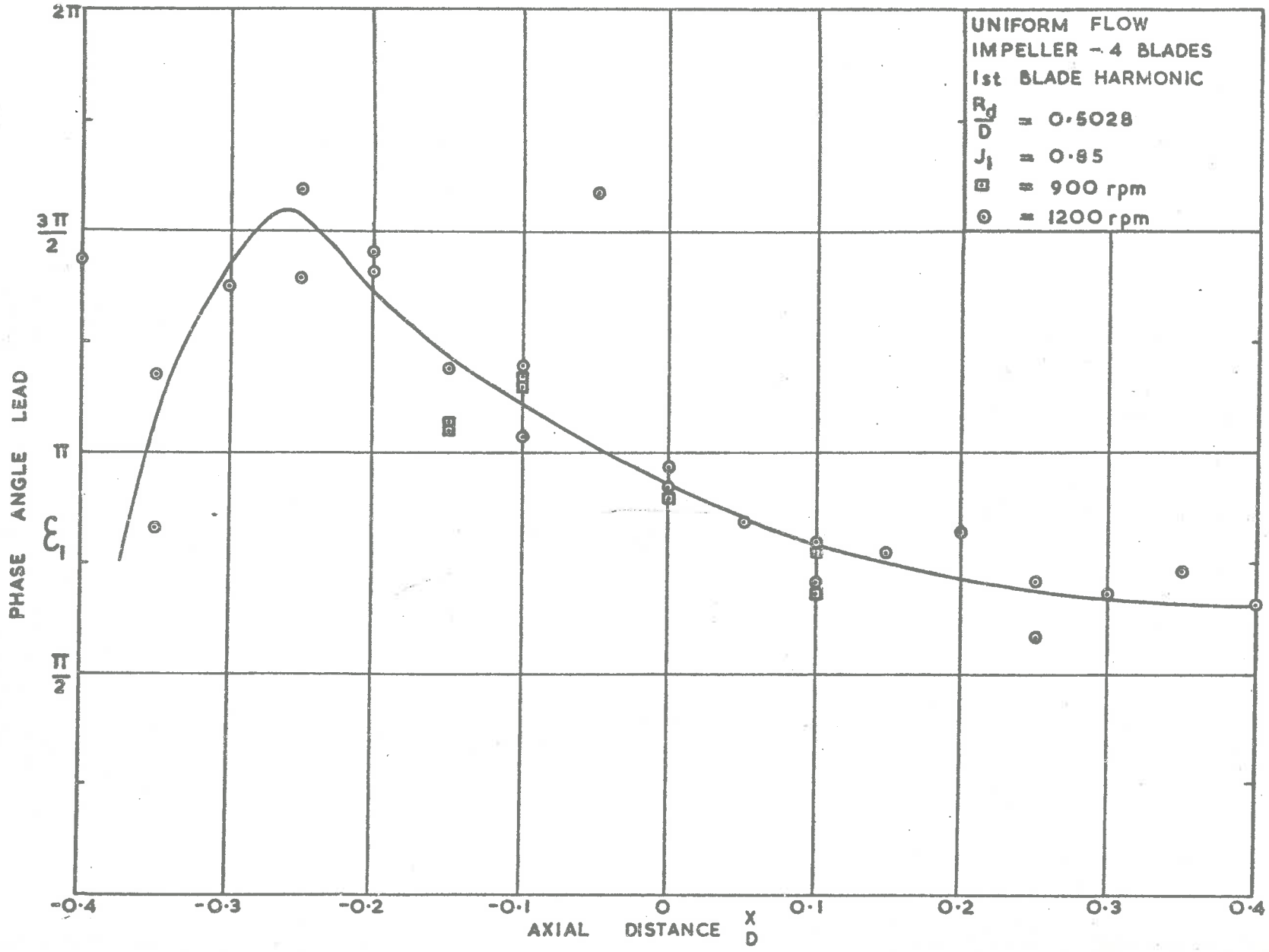

Fig. 5.16 - Axial Variation of Phase Angle (Lead) for 1st Blade Frequency Harmonic. J_I = 0.85.

Fig. 5.16

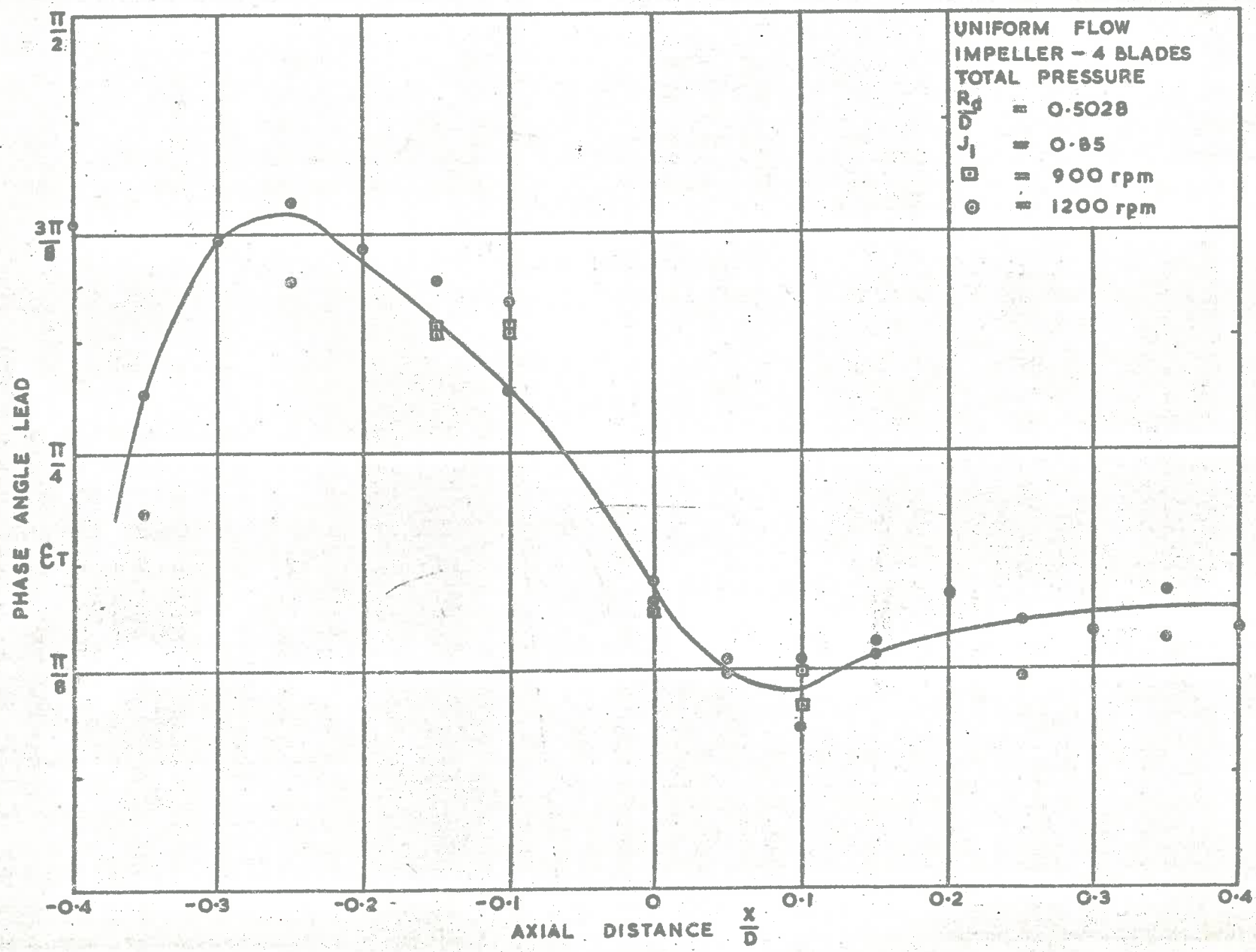

Fig. 5.17- Axial Variation of Phase Angle (Lead) for Total Pressure. J_I = 0.85.

Fig. 5.17

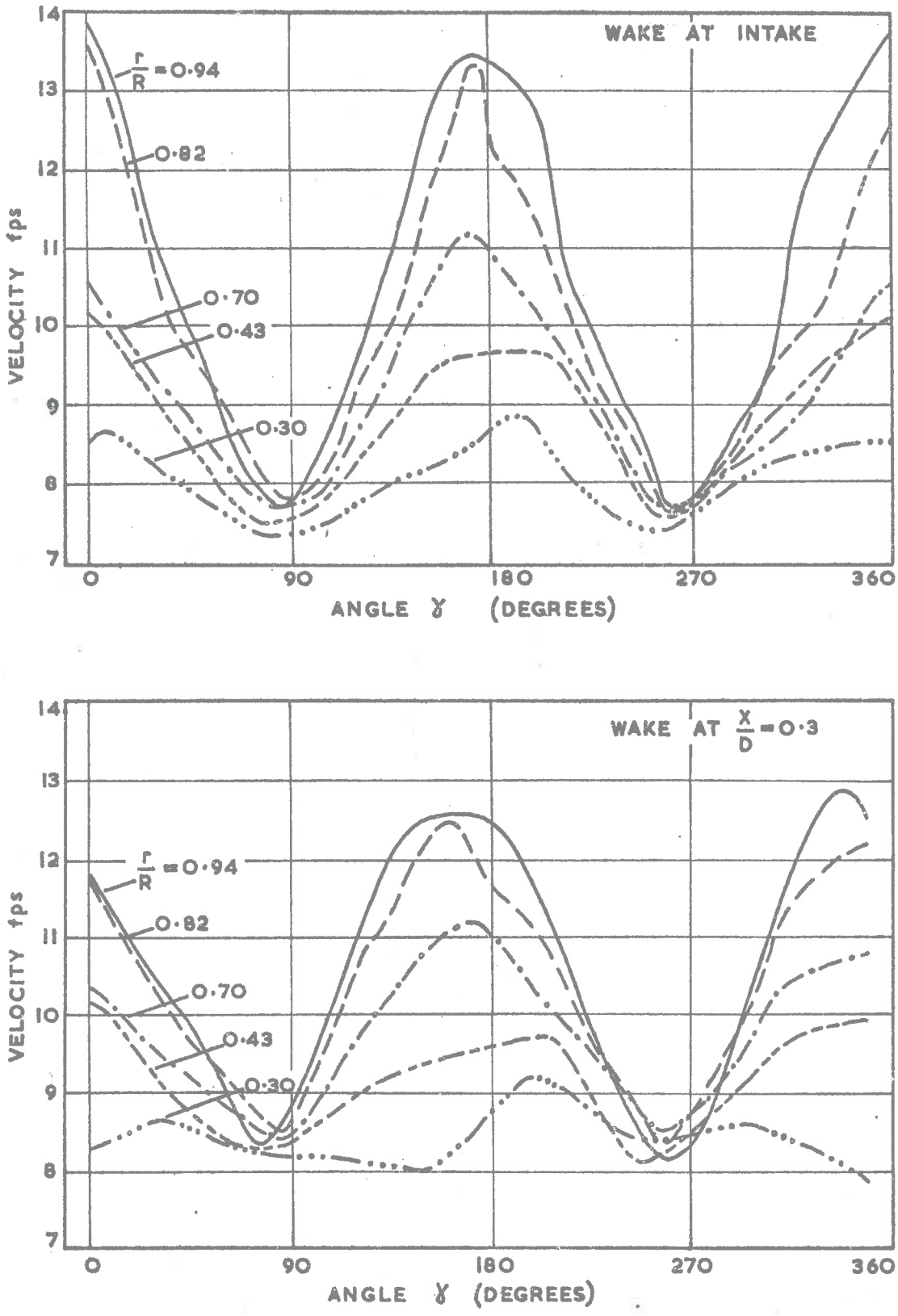

Fig. 5.18 - Velocity Profile in the Duct for Wake-2.

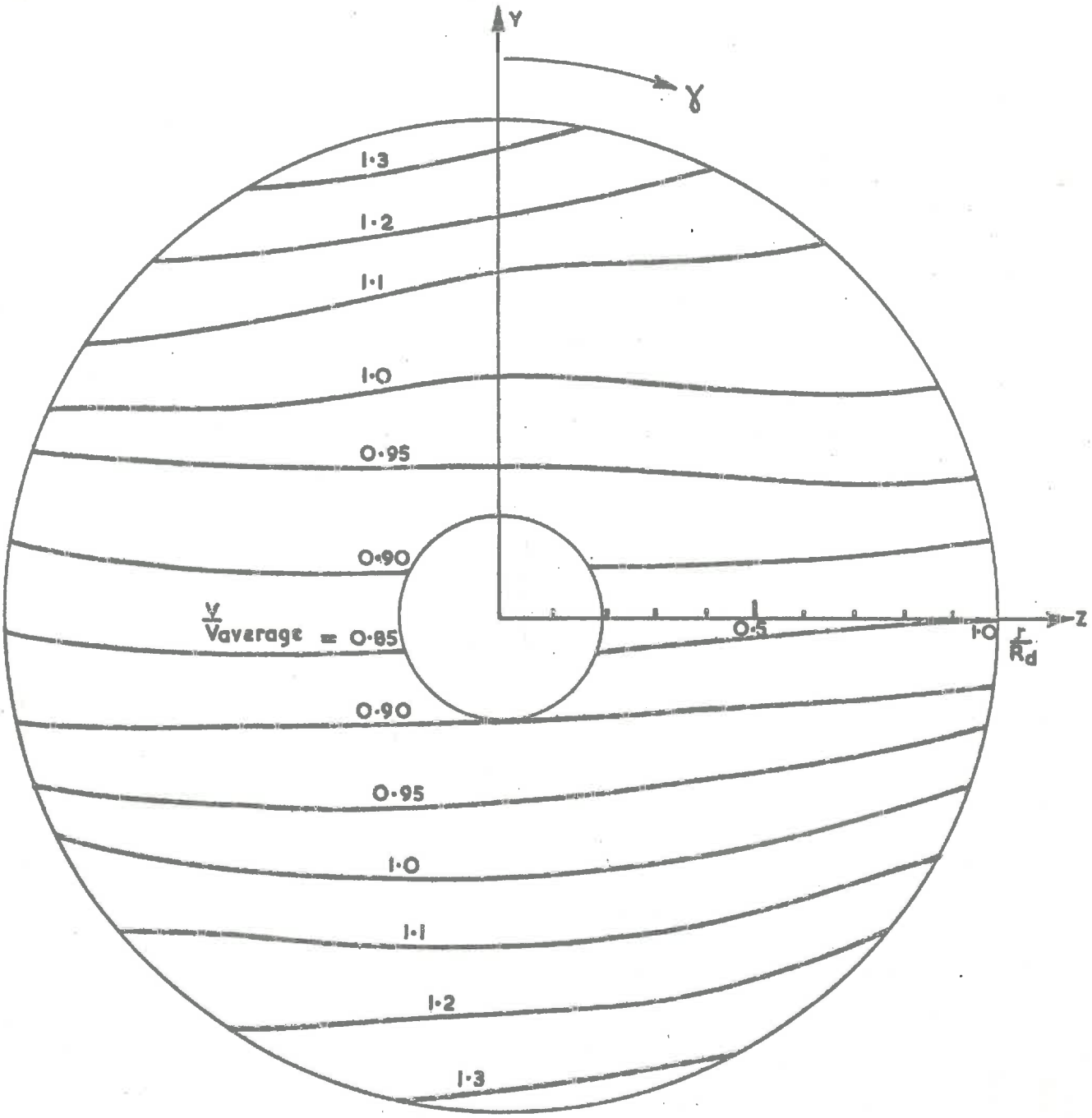

Fig. 5.19 - Velocity Profile at the Impeller for Wake - 2.

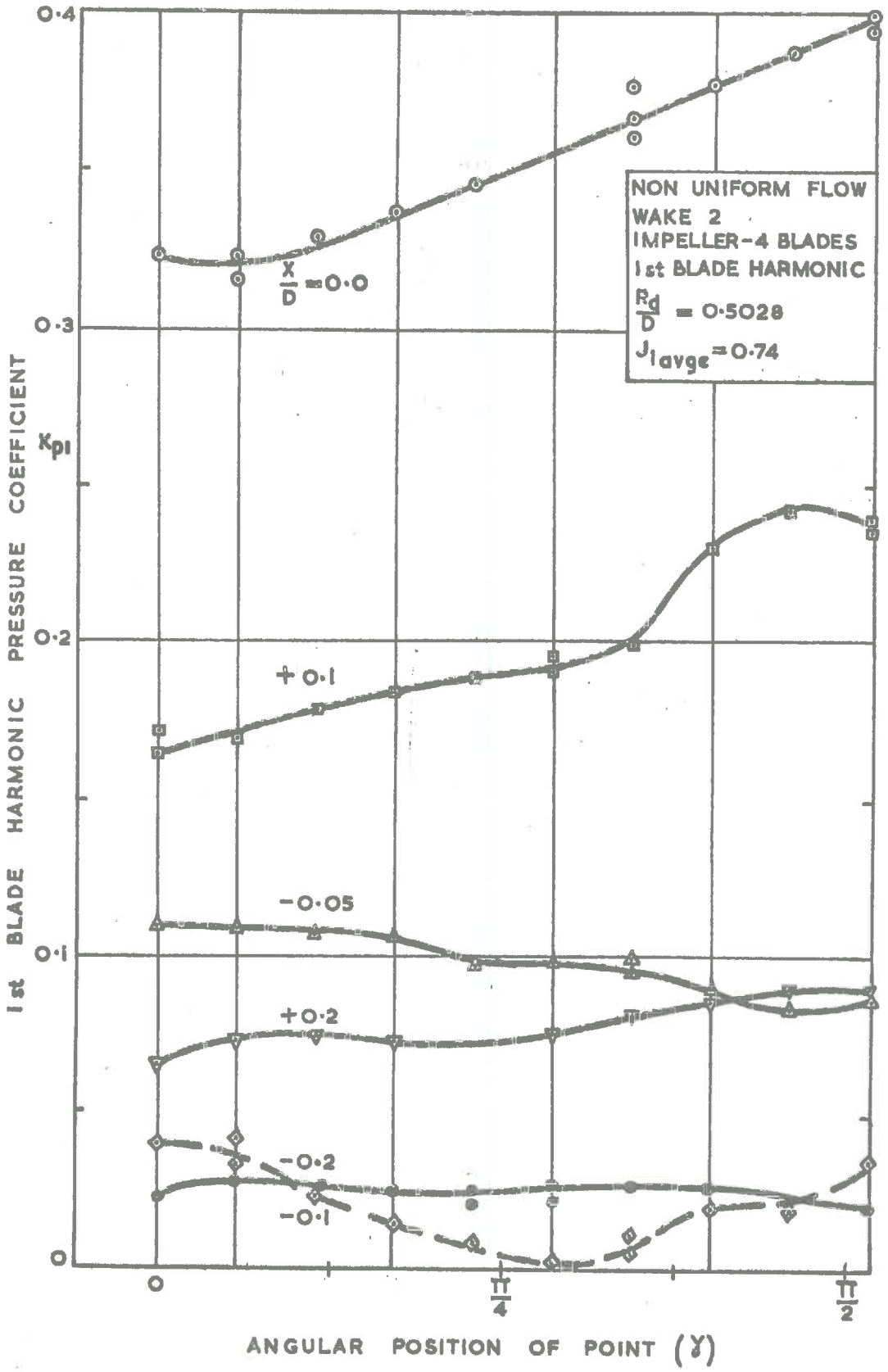

Fig. 5.20 - Pressure Coefficient for the 1st Blade Frequency Harmonic with Wake-2.

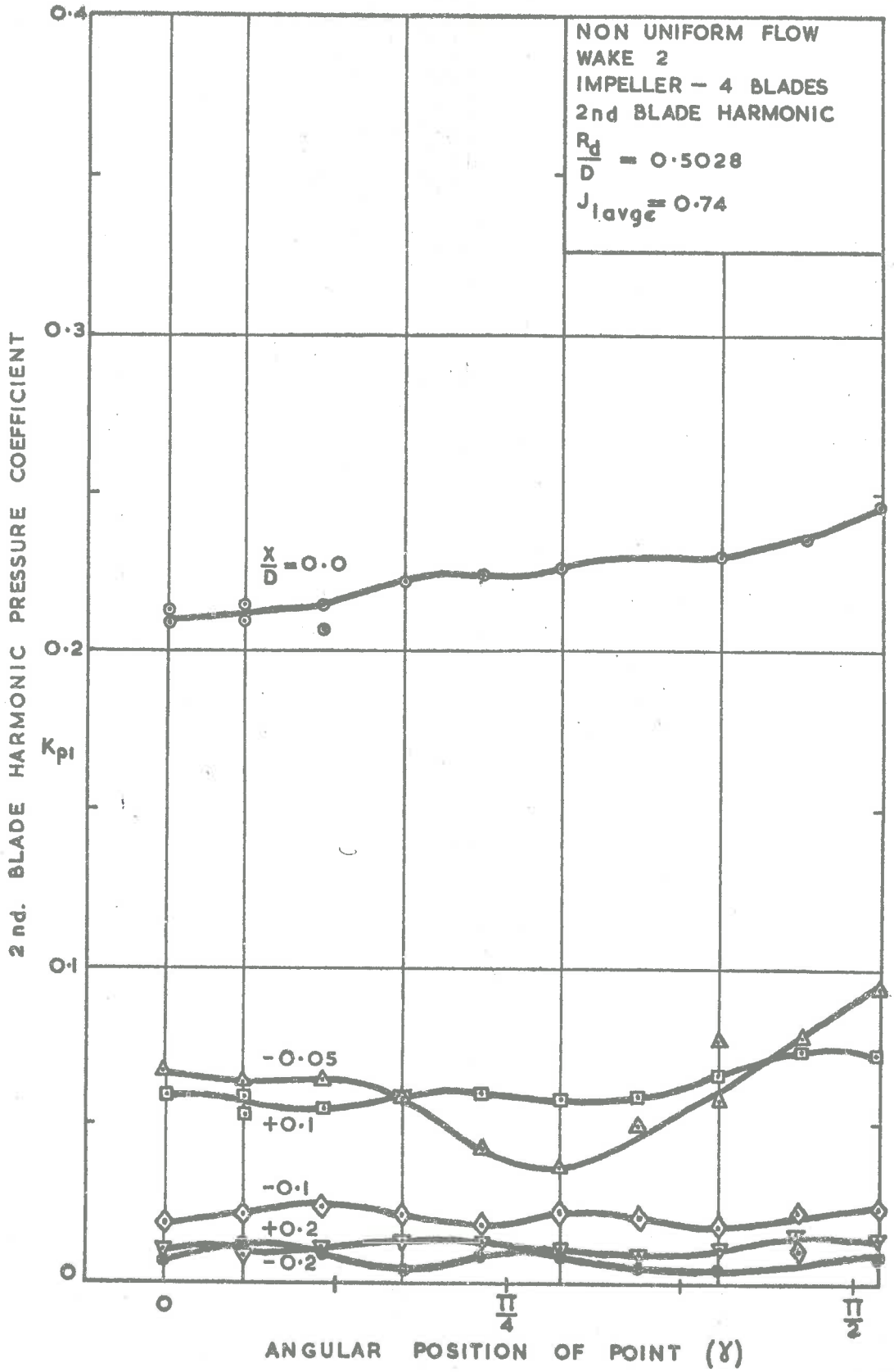

Fig. 5.21 - Pressure coefficient for the 2rd Frequency Harmonic with Wake-2.

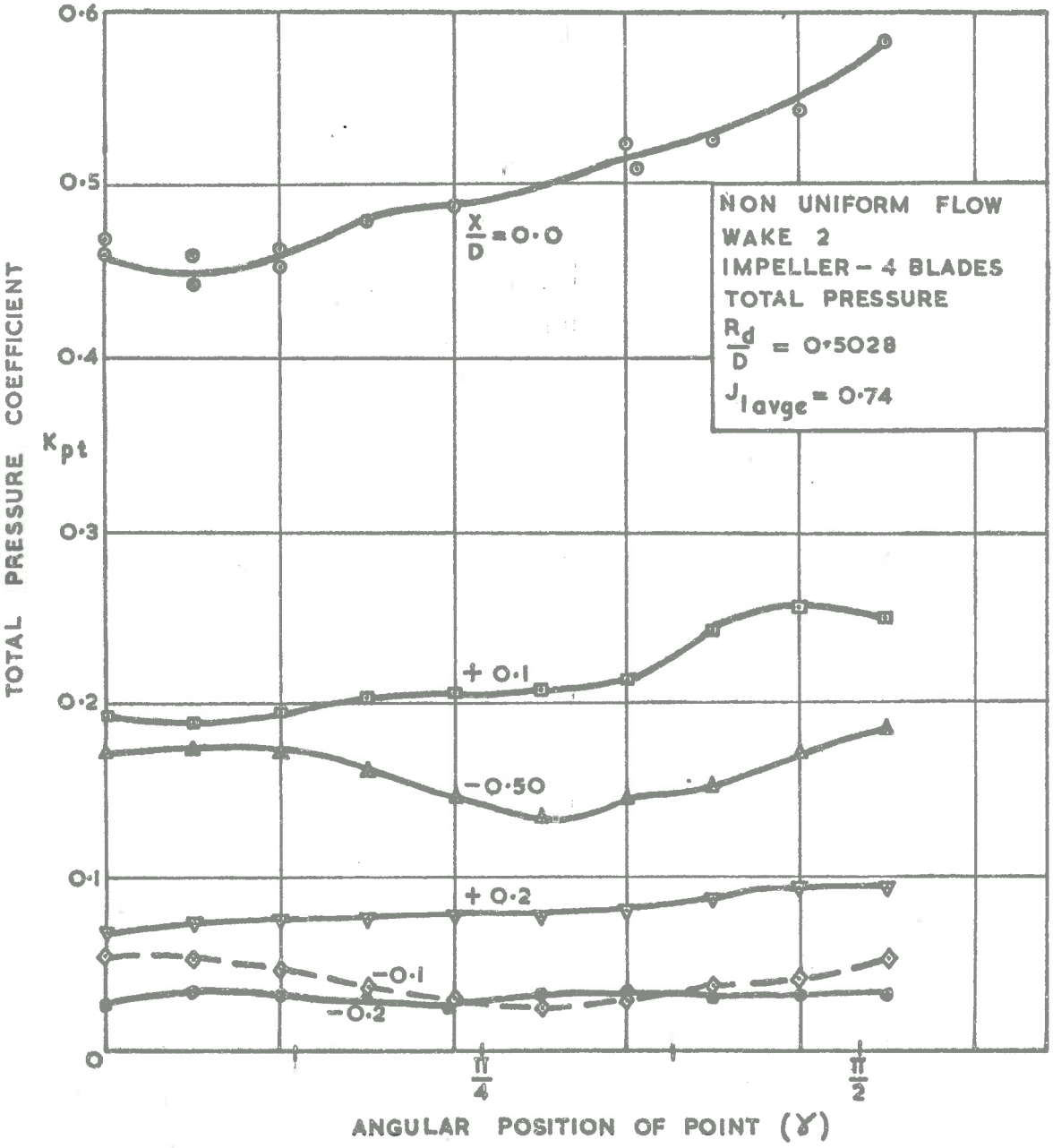

Fig. 5.22 - Pressure Coefficient of the Total Pressure with Wake-2.

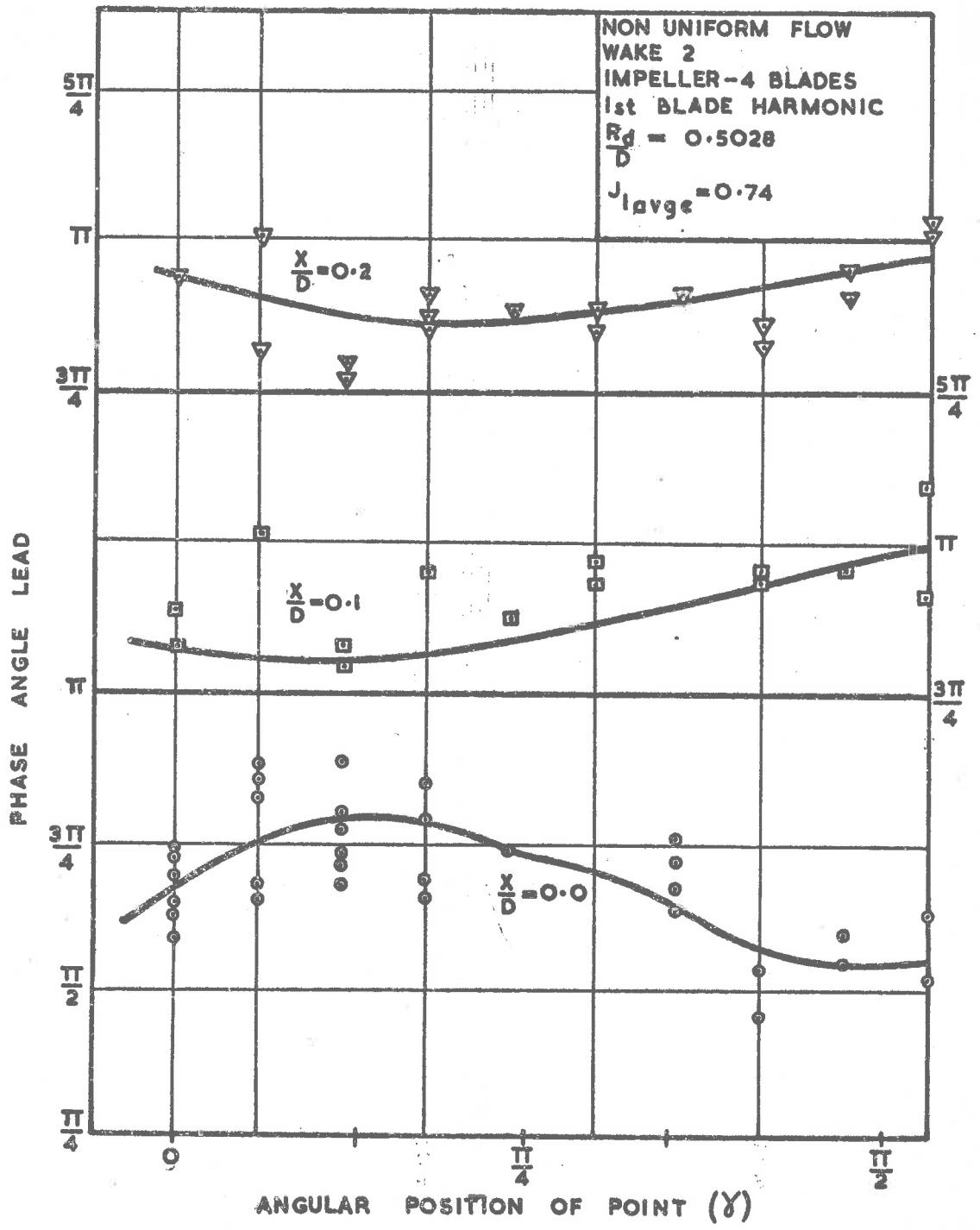

Fig. 5.23 - Phase Angle (Lead) for the 1st Blade Frequency Harmonic with Wake-2.

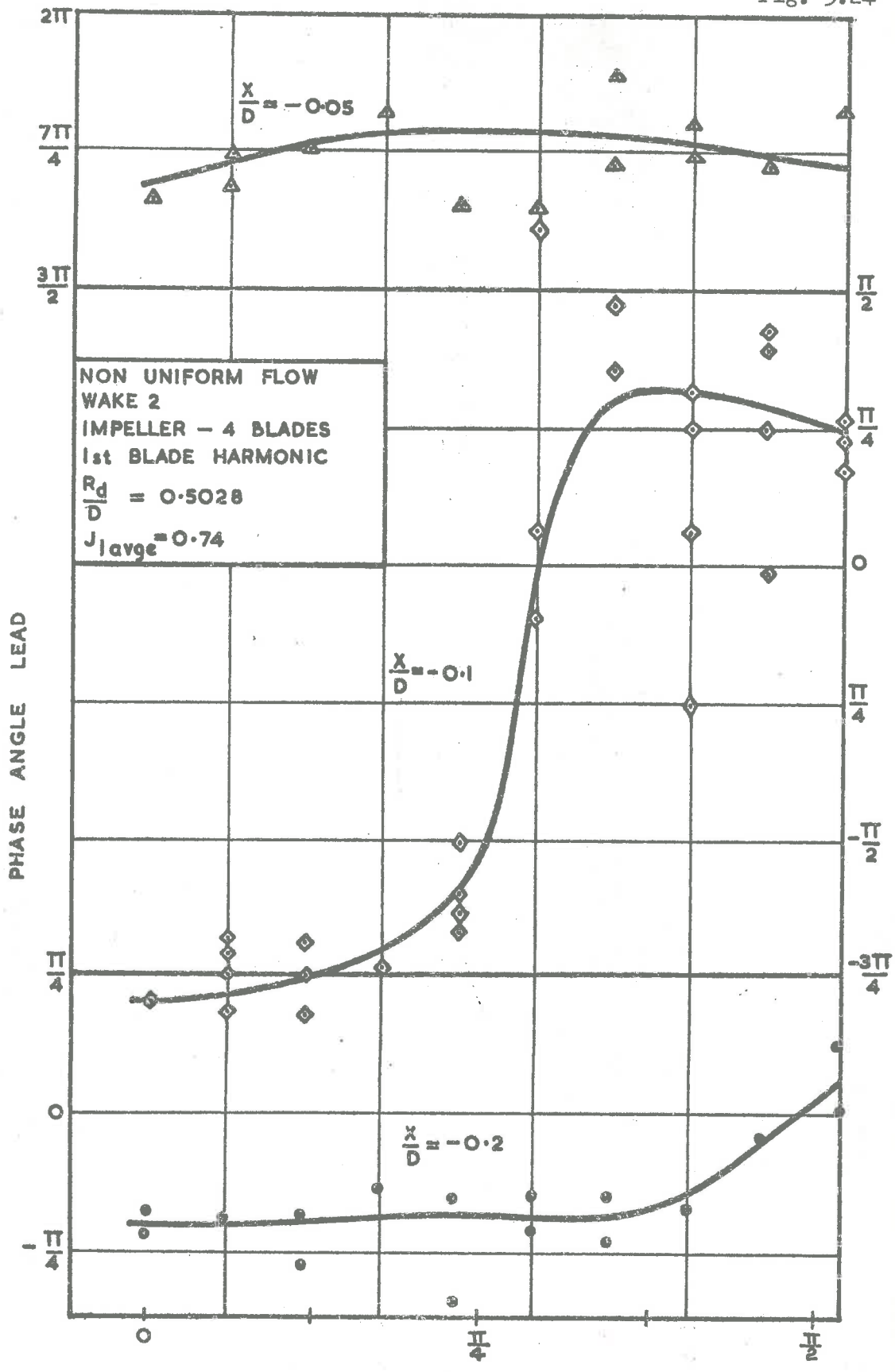

Fig. 5.24 - Phase Angle (Lead) for the 1st Blade Frequency Harmonic with Wake-2.

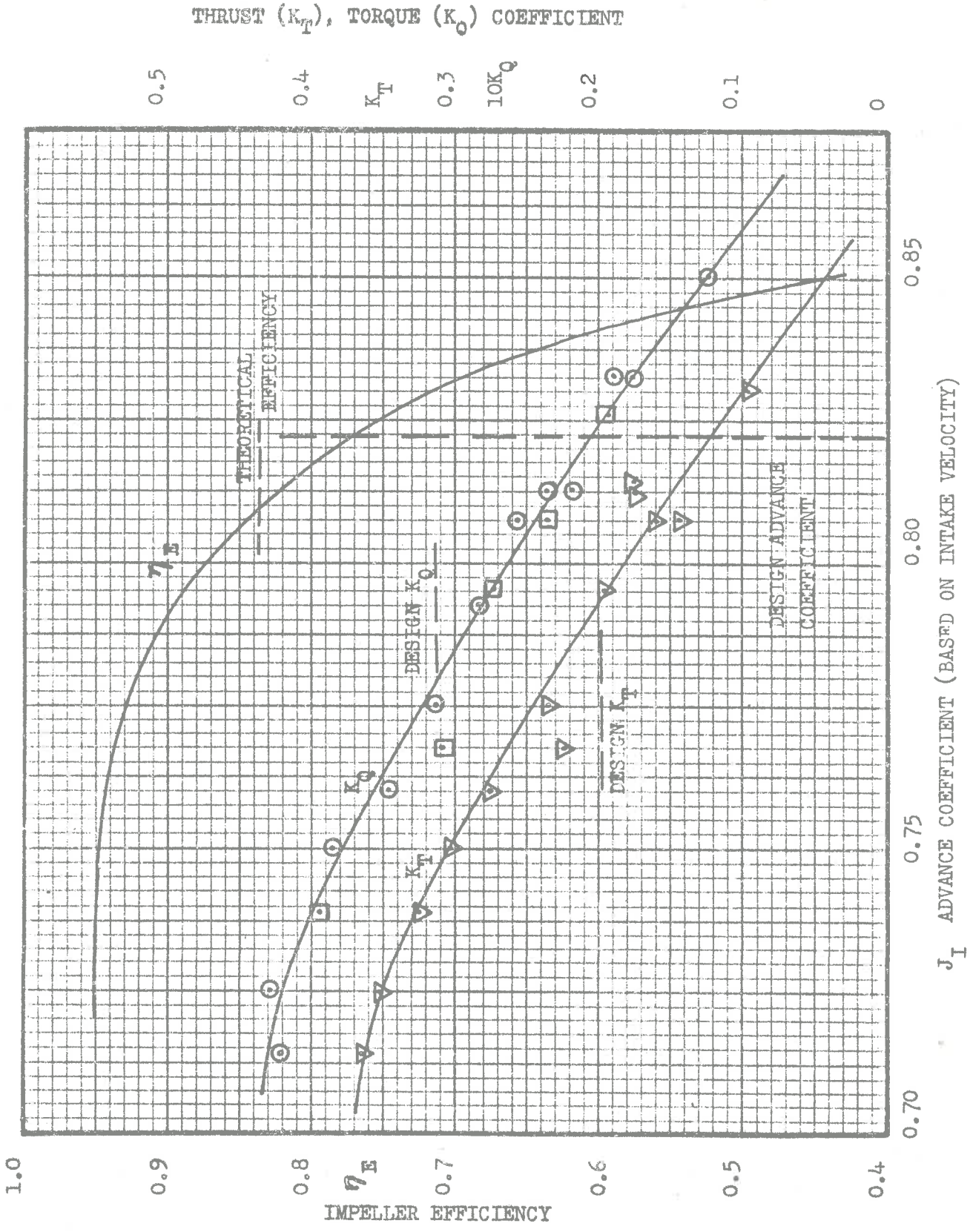

Fig. 5. 25 - Impeller Performance Characteristics

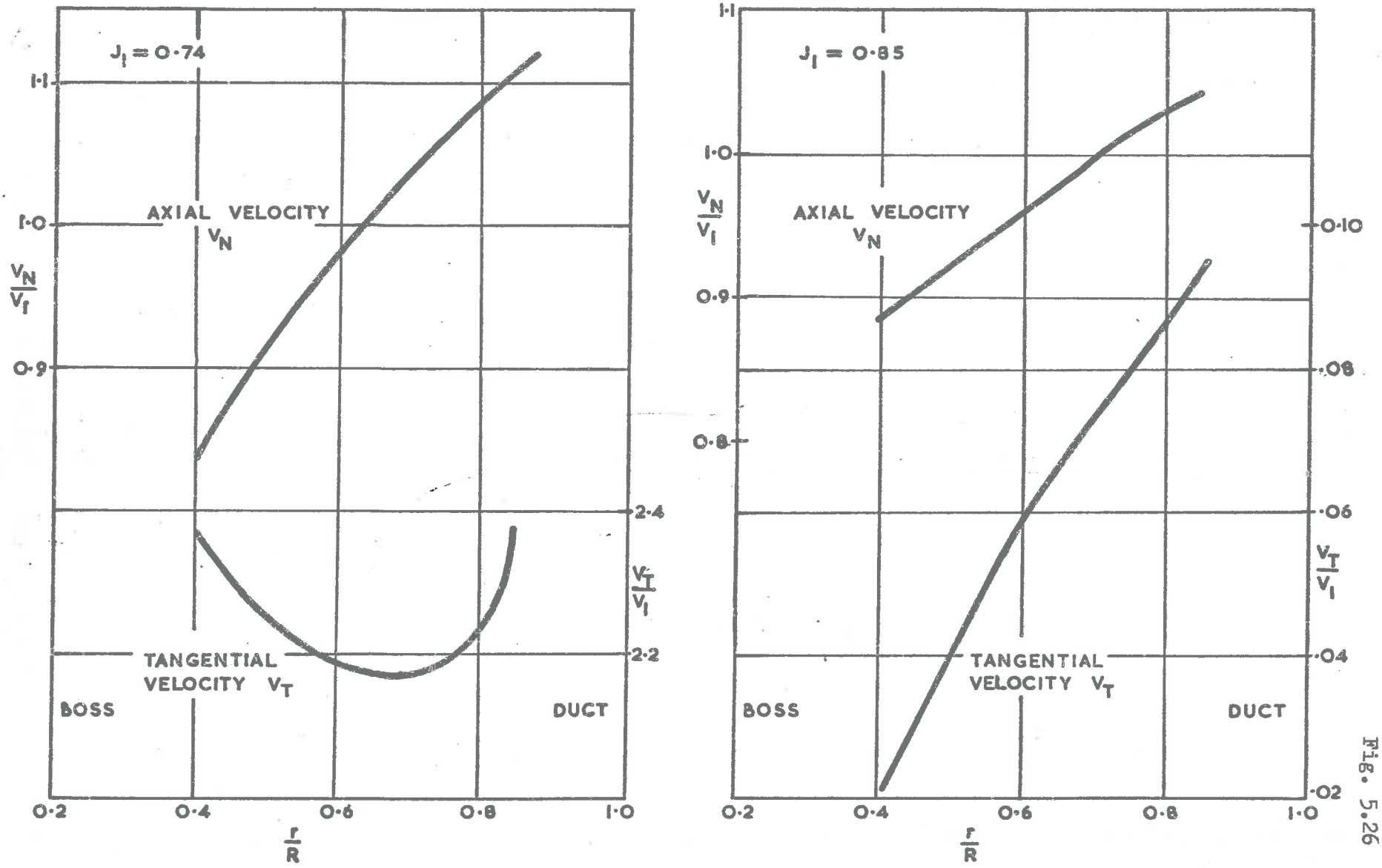

Fig. 5.26

Fig. 5.26 - Induced Velocities behind the Impeller at $\frac{X}{D} = -0.49$.

APPENDIX A1

THE DESIGN OF DUCTED IMPELLERS USING A VORTEX LINE ANALYSIS and AN OPTIMIZING COMPUTER TECHNIQUE

by

M.R.Hale

UNIVERSITY OF ADELAIDE

DEPARTMENT OF MECHANICAL ENGINEERING

Report Mech. Eng. R65/2

March, 1965.

TABLE OF CONTENTS

1.0 INTRODUCTION

Propeller design procedures in use today (with one recorded exception - Ref. 1) do not attempt to determine the optimum propeller geometry for a given set of operating conditions. The methodical series of propellers are based on an optimum value for one of the major variables, such as diameter or blade area. The optimum values for all the other design variables are not determined. For example, from the design data for the NSMB (or Van Manen) screw series the optimum diameter can be chosen and hence the corresponding pitch and mean blade area ratio can be determined to avoid cavitation under the operating conditions. But in this series the blade outline, blade sections and variation of maximum blade thickness with radius has previously been fixed.

In some of the more theoretical design procedures, it is possible to calculate the circulation distribution so that the energy loss caused by the induced flow is minimized. It is not possible however to determine from these theories a blade shape which is an optimum from the point of view of strength and other requirements yet capable of producing the desired circulation distribution.

The theoretical knowledge of propeller operation has progressed to a stage where an attempt should be made to develop a design technique based on these theories which would determine the best propeller geometry to suit given operating conditions.

A technique of this magnitude would require many mathematical statements and decisions. If such a design is to be economical in both time and cost, the resources of a high-speed digital computer and store are necessary. With the advent of more rigorous and complex

theoretical approaches to the design of propellers, this type of optimum design procedure will become necessary in the future, if full advantage is to be taken of the acquired theoretical knowledge.

The programme described in this report was an initial attempt at an optimizing design procedure. Although the design method used in this programme was not the most rigorous, the solutions given by the programme show that this type of optimization could be usefully employed for more complex design theories. The programme was developed as part of a feasibility study of a hydrojet propulsion unit in which an impeller operates in a cylindrical duct.

The design technique given in this report determines the optimum geometry for an impeller having minimum induced drag energy loss and minimum profile-drag energy loss. The blade thickness required to maintain the maximum stress at any section constant and equal to the design stress is determined. Blade surface pressure and cavitation margin are also taken into account in selecting the blade sections.

The impeller design as given by the optimum solution will, within the limitations of the theory used, have the maximum possible efficiency, the maximum utilization of material and the minimum weight.

2.0 THE DESIGN OF THE IMPELLER

2.1 Hydrodynamic model of the impeller

Since the present research project was directed towards estimating the capabilities of a ducted propulsion system, it was considered that a simplified vortex-line theory could be satisfactorily applied to the design of the impeller.

Consider an impeller operating in a long cylindrical duct in which

the fluid can be considered as irrotational upstream of the impeller. It is assumed that the impeller has negligible tip clearance. Thus the impeller diameter equals the duct internal diameter. The finite size boss is assumed to have negligible effect on the induced flow.

It is assumed that the axial velocity profile is uniform across the duct upstream of the impeller. It is also assumed that for a sufficient distance upstream and downstream of the impeller the duct is parallel. The impeller design is selected to have no axial component of induced velocity. The velocity diagram is as shown in Fig. 1.

It is considered to be sufficiently accurate for the interference flow to be assumed constant circumferentially at any radius. This is equivalent to assuming the interference flow is generated by an infinite number of lifting-lines of variable strength in the radial direction. Using the Betz's criteria for minimum induced energy loss in the wake, and the Kutta-Joukowsky relationship, the ideal thrust and torque gradients at any section can be derived as follows. (See Fig. 1).

Betz's theory can be stated as:-- "When the distribution of circulation along the blade is such that, for a given thrust, the energy lost per unit time is a minimum, then the flow far behind the screw is the same as if the screw surface formed by the trailing vortices was rigid, and moved backwards in the direction of its axis with a constant velocity, the flow being that of classical hydrodynamics in an inviscid fluid, continuous, irrotational and without circulation." (See Ref. 2).

The Betz minimum energy condition is expressed as (Ref. 3)

$$\frac{\tan \beta}{\tan \beta_i} = \eta_i = \text{constant with radius} \quad \ldots \quad 1.$$

where β = the advance angle

β_i = the hydrodynamic pitch angle

η_i = the ideal blade element efficiency

Substituting for $\tan\beta$ and $\tan\beta_i$ from Fig. 1 gives

$$\frac{\tan\beta}{\tan\beta_i} = 1 - \frac{U_{It}}{2r\omega} \quad \ldots 2$$

where U_{It} is the circumferential component of induced velocity at a sufficient distance downstream of the impeller.

The expression for thrust grading $\frac{dT_i}{dr}$ and torque grading $\frac{dQ_i}{dr}$ (see Ref. 3) become in the present case:-

$$\frac{dT_i}{dr} = \rho \Gamma Z(r\omega - \frac{U_{It}}{2}) \quad \ldots 3$$

$$= 4\pi \rho \omega^2 r^3 \eta_i(1 - \eta_i) \quad \ldots 4$$

$$\frac{dQ_i}{dr} = \rho \Gamma Z Va\, r \quad \ldots 5$$

$$= 4\pi \rho \omega Va\, r^3 (1 - \eta_i) \quad \ldots 6$$

where $\Gamma = \frac{2\pi r U_{It}}{Z}$ is the circulation around a blade.

Z = the number of blades ... 7

If it is assumed that the circulation distribution for minimum energy loss is not greatly affected by the variation of profile drag with radius, then the actual thrust and torque gradient can be evaluated as follows. (See Fig. 1).

$$\frac{dT}{dx} = \frac{dT_i}{dx}(1 - \xi \tan\beta_i) \quad \ldots 8$$

$$= K_1 \eta_i (1 - \eta_i)(1 - \frac{\xi}{\delta x \eta_i}) x^3 \quad \ldots 9$$

and $$\frac{dQ}{dx} = \frac{dQ_i}{dx}\left(1 + \frac{\xi}{\tan \beta_i}\right) \quad \ldots \quad 10$$

$$= K_1 \frac{Va}{\omega}\,(1 - \eta_i)(1 + \xi \delta x \eta_i)\, x^3 \quad \ldots \quad 11$$

where $\delta = \frac{\omega R}{Va}$ $\qquad \xi = \frac{C_D}{C_L}$

$x = \frac{r}{R}$ $\qquad K_1 = \frac{4\pi \rho \delta^4 Va^4}{\omega^2}$

$\tan \beta_i = \frac{1}{\delta \eta_i x}$

The total thrust (T) and torque (Q) of the impeller can only be evaluated by summation over the blade length if the drag to lift ratio ξ is known at each section. Since this ratio depends on the blade profile which is in turn dependent on the strength, cavitation and hydrodynamic requirements, a simple expression for thrust and torque cannot be obtained.

An approximation to the impeller geometry can be obtained by assuming the drag to lift ratio constant with the radius. In this case integration gives the following equations for total thrust T and overall efficiency η_o.

$$T = A(1 - \eta_i)(\eta_i B - C) \quad \ldots \quad 12$$

$$\eta_o = \frac{\eta_i B - C}{B + \eta_i D} \quad \ldots \quad 13$$

$$= \frac{T}{A(1 - \eta_i)(B + \eta_i D)} \quad \ldots \quad 14$$

where $A = \frac{\pi \rho Va^4 \delta^3}{\omega^2}$ $\qquad C = \frac{4}{3}\xi(1 - K^3)$

$B = \delta(1 - K^4)$ $\qquad D = \frac{4}{5}\xi\delta^2(1 - K^5)$

$$K = \frac{\text{radius of boss}}{R}$$

2.2 Blade-element lift and drag characteristics

The lift on a blade element is given by the Kutta-Joukowski relationship:

$$dL = \rho \Gamma V_R \, dr \qquad \ldots \quad 15$$

where $$V_R = \sqrt{(r\omega - \frac{U_{It}}{2})^2 + Va^2}$$

Using equations 2, 7, 11, 15, the design lift coefficient of the section (C_L) can be expressed as,

$$C_L = \frac{dL}{\frac{1}{2}\rho V_R^2 \, c \, dr} = \frac{8\pi \delta (1 - \eta_i) x^2 R}{Zc\sqrt{(x \delta \eta_i)^2 + 1}} \qquad \ldots \quad 16$$

where c = chord of blade section

The theoretical lift coefficient (C_{li}) required to develop the design lift is assumed to be greater than C_L by a factor μ_m, the viscosity factor. According to the potential theory of thin wing sections (see Chapter 5, Ref. 4) the theoretical lift coefficient of the section is a function of the camber to chord ratio $\frac{m_x}{c}$ only if the section operates at shock-free entry conditions, hence

$$C_{li} = l_m \frac{m_x}{c} \qquad \ldots \quad 17$$

The blade section chosen for this impeller was an NACA-16 thickness distribution with a mean line of a = 1.0, and the following are the values for viscosity factor (μ_m) and lift camber factor (l_m) at shock-free conditions. (Table 5.6, p.175 in Ref. 4).

$$\mu_m = 0.74 \qquad \ldots \quad 18$$

$$l_m = 18.13 \qquad \ldots \quad 19$$

hence $$\frac{m_x}{c} = \frac{C_{li}}{l_m} = \frac{C_L}{\mu_m l_m} = 0.0745 \, C_L \qquad \ldots \quad 20$$

The above method of calculating blade section geometry to obtain a desired lift coefficient has been experimentally proven valid by O'Brien of the National Physics Laboratory, (Ref. 5). Unfortunately there is no corresponding derivation at present available for the analysis of blade-section profile drag. The usual assumption that the profile drag is a function of the thickness to chord ratio $\frac{t_x}{c}$ and angle of incidence was therefore adopted. The values of drag coefficient C_D used in the design were taken from the data of Hill (Ref. 6). A 10th order polynomial of the form

$$C_D = \sum A_i \left(\frac{t_x}{c}\right)^i \qquad \ldots \quad 21$$

where $i = 0, 1, 2, \ldots, 10$

was fitted to the data for aerofoil sections at zero angle of incidence. The coefficients A_i are given in Table 1. These coefficients were calculated using IBM Programme Library No. 7.0.002 in which a set of simultaneous equations representing the condition for least square deviation is solved using a modified Gaussian elimination technique followed by a back substitution.

A tenth order polynomial was necessary to determine the value of C_D to an accuracy of 0.2% over the range of $\frac{t_x}{c}$ from 0.0 to 0.3.

This C_D relationship will apply to the NACA - 16, a = 1.0 section used in the design since the ideal angle of incidence is constant and equal to zero at shock-free entry conditions. (Ref. 4, Table 5.6).

2.3. Blade Strength

The stresses at a blade section were calculated by the simple theory for bending of a beam as suggested by Tingey (Ref. 7, also Ref. 4).

It is important to note that this theory can only be applied to designs where chordwise bending due to the pressure distribution over a section can be ignored. This implies that the blades should have

relatively large thickness to chord ratio $(\frac{t_x}{c})$ and not excessively wide chords.

The assumptions made by Tingey for the determination of stresses in a propeller with zero rake are:-

(1) The section through which the blade would fracture if overstressed (which is a plane section approximately parallel to the axis of rotation) has the same geometric properties as a corresponding cylindrical blade section at the same radius from the axis of rotation.

(2) The centres of area of all the cylindrical blade sections (or the centres of gravity of all the cylindrical blade sectional elements) are on a straight line intersecting the axis of rotation and normal to this axis.

(3) The simple theory of the bending of beams can be applied in assessing the stresses due to the bending moments caused by hydrodynamic forces acting on the blades.

(4) The principal axes of inertia of a cylindrical blade sectional element coincide with two perpendicular axes in the plane of the expanded element. One axis is parallel to the chord line, and the other intersects it at the centre of the element.

(5) The blades do not deflect.

The stress σ at a given point on the section due to the hydrodynamic loading and the centrifugal force is then given by

$$\sigma = y \frac{M_n}{I_n} + h \frac{M_p}{I_p} + \frac{F_c}{A_s} \qquad \ldots \quad 22$$

where $M_n = M_T \cos \phi + M_Q \sin \phi$

$$M_p = M_T \sin \phi - M_Q \cos \phi$$

ϕ = Blade element pitch angle

$= \beta_i$ in this design

The relevant geometrical properties of the NACA - 16, a = 1.0 blade section is given in Table 2. Information for other sections can be found in Table 8.4 in Ref. 4.

2.4 Cavitation

Using the theory of thin wings, the cavitation parameter "pressure minima cavitation number" σ_p can be determined for a particular geometry of blade section.

$$\sigma_p = \frac{(p - p_1')}{\frac{1}{2}\rho V_R^2} \quad \ldots \quad 23$$

where p = free stream pressure

p_1' = minimum value of local pressure p_1 on surface of section.

For the blade section under discussion, (Ref. 4, p.209)

$$\sigma_p = (1 + 1.14 \frac{t_x}{c} + \frac{C_{li}}{4})^2 - 1 \quad \ldots \quad 24$$

The sectional cavitation number σ_s is defined by

$$\sigma_s = \frac{(p_r - e)}{\frac{1}{2}\rho V_R^2} \quad \ldots \quad 25$$

where p_r = pressure at blade section radius r and at minimum immersion

e = saturated vapour pressure

When applying these equations to an actual impeller an overall factor f_o which makes allowance for irregular and viscous flow is introduced to effectively increase σ_p.

Thus $\sigma_s \geq f_o \sigma_p$ ... 26

where f_o = 1.2 (Ref. 4 p.209)

A similar method was used by Matthews and Straszak to estimate the inception of cavitation in screw propeller designs. (Ref. 8).

For simplicity in calculating the static pressure at a blade section it was assumed that there is negligible head loss in the intake up to the impeller, and that the operating conditions of the impeller-duct system are such that the fluid velocity at the intake equals the fluid velocity just forward of the intake. If the duct is uniform in diameter, the static pressure at the impeller plane equals the static pressure at the corresponding point at the intake.

For a non-uniform duct, and other operating conditions, the impeller static pressure would need to be estimated from parameters of the system. The influence of duct friction could also be allowed for if applicable.

2.5 Applicability of the Design Analysis.

It should be noted that the hydrodynamic design of the impeller used in this paper differs in a number of significant respects from that commonly used for axial-flow pumps, and to a lesser extent from methods used for axial flow fans and compressors.

The design analysis was developed for a feasibility study of a ducted impeller (i.e. axial-flow pump) operating at conditions far removed from the normal range for axial-flow pumps. The application was for propulsion of large ships, where the unit would have a large diameter, extremely high capacity, low head, and low static head at the impeller. The specific speed would thus be very large, a typical value of

$$N_s = \frac{NQ^{0.5}}{H^{0.75}} \quad \text{(N in rpm, Q in gpm, H in ft)} \qquad \ldots 27$$

being 40,000. An impeller designed for such conditions has very low values of induced tangential velocities, these being of the order of 2% and 10% of the axial velocities at hub and tip respectively.

Further differences from axial pump practice arise because the design uses an optimizing procedure. This also has the incidental effect of reducing the impeller weight since not only is the distribution of maximum stress along the blade uniform but also the profile drag (and hence blade sectional area) is minimized.

In axial-flow machines, the impeller can be designed for any arbitrary variation of tangential velocity with radius, i.e. vortex distribution. If there is to be no radial flow ("simple radial equilibrium") it can be shown (Ref. 9, p.427) that the axial velocity must satisfy the relation.

$$\left(\frac{V_a}{V_{a_o}}\right) = 1 - \left(\frac{n-1}{n}\right)\left(\frac{U_{It_o}}{V_{a_o}}\right)^2 \left[\left(\frac{r_o}{r}\right)^{2n} - 1\right] \qquad \ldots 28$$

where V_a = axial velocity at radius r

V_{a_o} = axial velocity at hub

U_{It_o} = induced tangential velocity at hub

and where n is the index in the vortex distribution, described in the form

$$U_{It} r^n = \text{constant} \qquad \ldots 29$$

For axial-flow pumps, free-vortex design (i.e. n = 1) is often used and 28 shows this leads to the design condition of constant axial velocity. Such a design does not necessarily result in the highest overall efficiency at the design condition (Refs. 10, 11).

The aim of the present design is to maximise the overall efficiency. This requires minimizing the energy losses i.e. profile drag losses and induced energy losses. The former are minimized in the hydrodynamic analysis of Section 2.1 by using the Betz condition of minimum energy loss. This latter condition

expressed in equations 1 and 2 leads to the requirement $U_{It} r^{-1} =$ constant i.e. forced-vortex or solid-rotation design for which $n = -1$ in equation 29. Substitution of the representative design values of $V_{a_o} = 25$ f.p.s. and $U_{It_o} = 0.5$ f.p.s. into equation 28 shows that V_a varies only 0.5% from hub to tip, and hence be assumed constant in this design. The design thus ensures radial equilibrium, for the application considered.

Solid-rotation gives a non-constant total-energy distribution with radius after the impeller. For axial-compressors, as noted in Ref. 12, this does not lead to a decreased efficiency as compared with the free-vortex design with its constant total-energy distribution, and there appears to be no reason to believe that the same will not be true for the present design. In any case the total-energy variation is small in this design. It is also noted in Ref. 12 that the solid-rotation design has for the same diameter and speed, the advantage of a greater work capacity than the free-vortex design.

It is interesting to note that several axial-flow compressor designs which are commonly used do violate the simple radial equilibrium condition (Ref. 9, pp.424--425; Ref. 13). The same is true for marine propellers. These two types of machine bracket as it were the axial-flow pump and ducted-impeller, and indicate that departure from simple-radial equilibrium may not necessarily introduce an efficiency penalty in pump design. Removal of the radial-equilibrium restriction would allow greater flexibility in design. Some of the design types discussed in Ref. 14 might lead to a higher overall efficiencies for pumps and ducted impellers.

(It is noted on p.435 of Ref. 9 that pump efficiencies are not as high as might perhaps be expected). Optimizing programs of the type described in this paper could be developed for the various kinds of design, and could facilitate comparison of their merits.

The present analysis assumes the interference flow to be constant circumferentially at any radius (i.e. assumes an infinite number of blades). The effect of a finite number of blades could be taken into account by incorporating into the analysis a "blade-number factor" for circumferential induced velocity similar to the Goldstein factor used in open-water screw-propeller design. Such a factor can be computed from equation 32 of Ref. 15 The analysis could then be used to optimize the number of blades.

It should be noted that the optimizing technique can be adapted to other impeller design methods, such as those commonly used for axial-flow pumps or compressors. It could also be adapted to turbines of various kinds.

3.0 THE OPTIMUM DESIGN OF AN IMPELLER

The optimum combination of blade sections for a hydrojet impeller must satisfy the conditions expressed in the hydrodynamic equations for minimum energy loss, have the lowest profile drag that is possible, but still be strong enough to limit the sectional stresses to a value equal to or less than the maximum design stress. The blades must also operate free from cavitation. For this design, the weight of the impeller will be a minimum for the chosen operating conditions of T, n and D.

Although the impeller calculated by this design method has an optimum blade section arrangement for the given conditions it is not necessarily the optimum design for a given duty, i.e. given T. The optimum design must be selected by studying closely the results of a series of systematically varied impellers, all designed for optimum arrangement and satisfying the requirements of a given duty. Before deciding upon the final impeller geometry, certain other factors affecting the operation of an impeller or rotor-dynamic propulsion unit must also be taken into account - e.g. --

(1) What is the largest diameter that can be installed in the vessel, and is this greater than the optimum diameter?

(2) Is the number of blades and rotational speed conducive to exciting critical modes of vibration when the propulsion system is operating?

(3) What is the economical range of rotational speeds of the prime mover?

The sectional lift coefficient is another important variable which must be studied before selecting the final design since the value of lift

coefficient selected in the programme is not limited. Under certain circumstances, the sectional lift coefficient as computed may exceed the stall value. Usually this only occurs when the operating conditions differ greatly from the optimum operating conditions.

The design programme given in this report does not achieve the ideal objective which could be stated as "the selection of an optimum impeller geometry to suit a particular duty by considering every possible arrangement which satisfies all known laws, principles and facts associated with its operation." All these decision points could be inserted into a programme for the logical selection of the ideal impeller and would require extremely careful planning. Although the complete optimum design is not specified directly by the programme of this report, it is considered that the technique given for selecting an optimum blade geometry is a radical departure from the usual propeller design procedures. It is felt to be a worthwhile step towards designing the most efficient unit possible using available design techniques and aids.

3.1. The Optimizing Ducted-Impeller Design Technique

An outline is given below of the major steps in the design programme. The bold-type letters in the margin refer to sections of the programme (see a listing of the programme in Table 3). The flow diagram of the programme given in Fig. 2 shows the major computing steps and the information flow paths.

The impeller design method is an iterative process in which the blade sectional variables $\frac{dT}{dx}$, $\frac{dQ}{dx}$, C_L, t_x, etc. and the impeller efficiency are computed using successive estimated values for the blade element efficiency η_i until the impeller efficiency calculated is to within a small pre-determined percentage of its preceding value.

The design then has the maximum impeller efficiency, since it is assumed that curves of impeller efficiency versus the sectional variables are smooth single-maximum curves with no points of inflection.

D. INITIALIZATION

Before commencing the main calculation, an initial estimate of η_i is computed by solving equation 11 in which the drag to lift ratio is assumed constant with radius.

It has been found from previous experience that a value for drag to lift ratio ξ of 0.03 determines the initial value of η_i to within a few per cent of its final value (for which profile drag is considered a variable).

E. Using the estimated value of η_i and the assumed value of ξ, the blade sectional variables are computed from the hydrodynamic equations 1 - 11, 15 - 20 for a selected number of circumferential sections at radius fractions x.

F. SELECTION OF BLADE SECTIONS

The aim of this section of the routine is to determine the blade section geometry necessary to satisfy the hydrodynamic requirements. The calculation commences at the blade tip where some of the variables are known or can be selected, and then proceeds with the selection of blade sections properties towards the boss.

The tip and root chords widths are selected values which form part of the input to the programme. The remaining chord widths are then calculated using a given input chord distribution which for simplicity was assumed linear for the hydro-jet impeller design.

These chords widths may be adjusted later to prevent cavitation causing departure from the initially assumed linear chord distribution.

Because stress on the tip section is not a limiting factor, the tip thickness is selected for minimum profile drag ($\frac{t_x}{c}$ = 0.045 from equation 21).

With the above selected blade sectional variables and those calculated from part E above, the sectional cavitation number σ_s at the tip is determined and compared with the pressure minimum cavitation number σ_p of the section. If the conditions at this section induce cavitation, the chord width must be increased to reduce the lift coefficient. This will result in a decrease in the pressure minimum cavitation number i.e. an increase in the minimum value of local pressure on the section at which the inception of cavitation occurs. The width is progressively adjusted until cavitation free operation of the section is obtained.

G. BLADE STRESS CALCULATION

This routine is progressively applied from tip to root to all the chosen radial stations or radius fractions, excluding the tip station.

The first estimate of blade thickness at the station being considered is based on the blade thickness at the preceding station (i.e. the next station radially outwards) and maintains the thickness to chord ratio constant. Since the maximum-sectional stress is zero at the tip and increases with decreasing radius, the thickness to chord ratio can be maintained constant over the outer portion of the blades until a section is reached where the maximum stress is equal to the design stress. These outer sections, therefore, operate with

minimum profile drag.

I. The stress at four points on the blade section is calculated and the maximum numerical value is compared with the allowable stress. These four points are - the leading and trailing edges and the maximum ordinate position on both the back and face. If the calculated maximum stress is equal to or less than the allowable design stress, the section must now be checked for cavitation. If cavitation exists, the chord at the section must be increased and the stress calculation for that radius fraction repeated. However , if the maximum stress at the section is greater than the design stress, the thickness is increased and the stress calculation repeated until the maximum sectional stress is equal to the design stress at which point the section is checked for cavitation. If cavitation exists, the chord is increased and the stress calculation repeated on the basis that thickness to chord ratio is the same as that of the preceding station. After successive calculations, a stage is reached at which the working stress equals the design stress, and the section is free of cavitation.

H. The method used to determine the required thickness is a combined iterative and convergence procedure called "Regula Falsi". The independent variable, thickness, is progressively increased by a known amount until the dependent variable, maximum sectional stress minus design stress, changes its numerical sign. When this state has been reached, the desired value of the independent variable lies between the last two consecutive values, providing there is not more than one root of the equation in this interval. As the equation for blade thickness has only one solution, a solution is always possible no matter what stepping interval is selected.

Having located the solution within a range of values a forced convergence is applied. The convergence method used computes the dependent variable for a value of the independent variable midway between the two values surrounding the solution. The numerical sign of the value of dependent variable obtained is investigated. Two values of the independent variable, thickness, for which the corresponding values of dependent variables have opposite numerical signs are then selected from the last three consecutive values. The forced convergence is repeated until the desired accuracy of the solution is reached. Since the convergence is based on the mid-point value, the accuracy of the computation is governed by the number of complete passes through the calculating routine, after the initial values spanning the solution have been determined.

J. The stress calculation, blade thickness determination and cavitation estimate are repeated for every station up to the boss, using the estimated value of the blade element efficiency. Having now determined the blade thickness distribution, the values of the following variables lift coefficient and drag-to-lift ratio at the selected radial stations can be evaluated.

K. A position has now been reached where a close estimate of the blade element efficiency is required.

Since the blade element efficiency cannot be expressed as a simple function of thrust and blade section properties, the "Regula Falsi" method of convergence must again be employed to determine the design blade element efficiency. The efficiency is progressively decreased from an assumed value of 99.9% until the computed thrust obtained by summing the values of thrust gradient at each station over the complete blade length equals the design thrust. The

thrust gradient at each station is calculated using the current value of blade element efficiency and the sectional characteristics determined in Section J. above.

L. The final value from section K above is now used to re-compute the torque gradients, lift coefficients, and maximum ordinate of the mean line.

If the final value of blade efficiency from Section K is not equal to the initial value chosen in Section D to the desired accuracy, further convergence is necessary and the calculation from Section F to Section K must be repeated using the newly determined value of the blade element efficiency from Section K as an input variable. This calculation yields a new output value of blade element efficiency which must be compared with the input value. If the two values are not equal to within the desired accuracy, the process must be repeated until this condition is satisfied whence the computation is complete.

4.0 INPUT INSTRUCTIONS

The input data is divided basically into two groups: one group for constant data, such as blade section properties, material densities etc., and the other group for variable impeller design conditions and geometry.

The variable input data - characters TT to NTEST (see Table 3) form a group. Any number of such groups may be placed after the constant data - characters DTOL to A10, if systematically varied impellers are to be investigated.

LSTEP is a control on the number of stations chosen to satisfactorily define the impeller. LSTEP must be odd and

for most calculations it is suggested that LSTEP be selected equal to 17.

NTEST controls the type of print-out from the programme;

NTEST - ve causes print-out of impeller characteristics and geometry after each estimate of η_i.

NTEST = 0 causes print-out of impeller characteristics and geometry after η_i has been determined to the required accuracy.

NTEST + ve causes progressive print-out of all major decisions and relevant variables as well as the impeller characteristics and geometry.

The definitions of the characters defined in the input statements of Table 3 are given in the nomenclature list Table 6. The form of the input can be seen from the example given in Table 5.

The programme as written in FORTRAN for CDC 3200 occupies about 2,100 words of storage, not including the storage required for the total number of subscripted variables. The execution time for the CDC 3200 machine is approximately 3 minutes per single set of data.

REFERENCES

1. BRITISH PROPELLER DESIGN
Marine Engineer and Naval Architect
Vol. 88 No.1069, April 1965.

2. GOLDSTEIN, S. On the Vortex Theory of Screw Propellers
Proceedings of the Royal Society of London,
Series A. Vol. 123, 1929.

3. van MANEN, J.D. Fundamentals of Ship Resistance and
Propulsion. Part B.
Netherlands Ship Model Report. 132a.

4. O'BRIEN, T.P. The Design of Marine Screw Propellers
Hutchinson & Co. Ltd., London, 1962.

5. SILVERLEAF A. & O'BRIEN T.P. Some Effects of Blade Section
Shape on Model Screw Performance.
Transactions of the North-East Coast Institution of
Engineers & Shipbuilders. Newcastle-on-Tyne Vol.77, 1955.

6. HILL, J.G. The Design of Propellers.
Trans. Society of Naval Architects & Marine Engineers,
Vol. 57, 1949.

7. TINGEY, R.H. Marine Engineering, Vol.1, Chap. IX,
(Editor - Seward, H.L.) Society of Naval Architects
and Marine Engineers, 1942.

References continued:

8. MATTHEWS, S.T. & STRASZAK, J.S.C. Optimum Length and Thickness of Propeller Blade Sections from Cavitation and Strength Considerations. National Research Council of Canada Mech.Eng. Report. M.B. - 231, April, 1961.

REFERENCES

9. SHEPHERD D.G

Principles of Turbomachinery

MacMillan 1956

10. BARNA P.S.

Equilibrium of Flow in Axial Flow Fans Designed for Constant Lift-Drag Ratio

Proceedings of First Australasian Conference on Hydraulic and Fluid Mechanics,

Pergammon Press 1964.

11. BARNA P.S.

Preliminary Aerodynamic Design Considerations of Axial Flow Fans.

Auburn University, Engineering Experiment Station,

Bulletin 50, April 1965

12. de KOVATS A. & DESMUR, G.

Pump Fans & Compressors,

Blackie 1958, p.288

13. COHEN H. & ROGERS G.F.C.

Gas Turbine Theory,

Longmans Green 1951, pp. 144-145.

References continued --

14. WATTENDORF F.L.

Simplified Design Comparisons of Axial Compressors, Journal of Aeronautical Sciences, Vol.18, 1951, p.447

15. TACHMINDJI, A.J.

Potential Problem of the Optimum Propeller with Finite Number of Blades - Operating in a Cylindrical Duct Journal of Ship Research, December, 1958.

Table 1 - Coefficients of Polynomial for Drag Coefficient of an Aerofoil at Zero Incidence

i	Ai
0	.9299158 E-02
1	- .3499790 E-01
2	- .2191732 E+01
3	.7515442 E+02
4	- .8086659 E+03
5	.3367858 E+04
6	.6849617 E+04
7	- .1329265 E+06
8	.5739262 E+06
9	- .1119756 E+07
10	.8516336 E+06

$$C_D = \sum Ai \left(\frac{t}{c}\right)^i \left(\frac{x}{c}\right)$$

where $i = 0, 1, 2, \ldots, 10$

Table 2. Geometrical Properties of NACA-16, a = 1.0 Profile

(Ref. 4, Table 8.4)

	Area factor	Co-ordinates of Centroids		Moment of Inertia Factors		Distance from Centroid to -	
						Max. Thick-ness	Chord line
Mathematical Symbol	a_s	$\frac{-h}{c}$	$\frac{-y}{t_x}$	i_p	i_n	$\frac{-h_t}{c}$	$\frac{-y_c}{t_x}$
Programme Symbol	AS	HBC	YBTA YBTB	PPIP	PPINA PPINB	HBTC	YBCT
Numerical Value	0.736	0.516	$0.5-0.182\frac{m_x}{t_x}$	0.0418	$0.0445+0.029(\frac{m_x}{t_x})^2$	-0.016	$0.818\frac{m_x}{t_x}$

where $A_s = a_s\, t_x\, c$ = AAS

$I_n = i_n\, t_x^3\, c$ = PIN

$I_p = i_p\, t_x\, c^3$ = PIP

Table 3 - Programme Listing.

```
C      1330 M R HALE/FOWLER MECH ENG DEPT U OF A  TEL 461
C      PROGRAMME NO 0017/CDC  3200
C      DESIGN PARAMETERS OF A HYDROJET IMPELLER
A      010 FORMAT(1H1/1X,38H  DESIGN PARAMETERS  HYDROJET IMPELLER/1H0,3X,18H
          1DESIGN ASSUMPTIONS/1H ,4X,25HBETZ MIN ENERGY CONDITION/1H ,4X,23HC
          2ONSTANT AXIAL VELOCITY/1H ,4X,30HNACA PROFILE  SHOCK FREE ENTRY//)
       020 FORMAT(1HC,72H  RADIUS  VELOCITY  ROTATION  BLADES  IDEAL EFF  TOT
          1AL EFF  THRUST   SHP)
       030 FORMAT(F7.3,F6.4,F8.4,F8.3,E10.3,F7.2)
       040 FORMAT(F7.3,2F8.4,F7.3,F5.1,4F7.3,F8.4/F6.2,F8.4,F8.1,F7.2,4E10.2)
       045 FORMAT(5E14.7/5E14.7/ E14.7)
       046 FORMAT(F9.1,F7.2,2F6.2,E16.8,F5.1,2F7.3,I4,I2)
       050 FORMAT(1H ,F7.2,F10.2,F9.2,I7,6X,F6.4,5X,F6.4,F10.0,F8.0)
       055 FORMAT(1H0,66HTIP CHORD  BOSS CHORD  BOSS RATIO  TIP IMMERSION  AL
          1LOWABLE STRESS)
       056 FORMAT(1H ,F7.3,5X,F7.3,4X,F7.3,7X,F7.2,9X,F7.0/)
       060 FORMAT(1H-,69HRAD FRAC  CHORD  THICKNESS  MEAN LINE  ANGLE BI  LIF
          1T COEF  DRAG/LIFT)
       070 FORMAT(1H ,F6.2,F9.3,F8.4,6X,F6.4,5X,F6.2,F10.3,F9.3)
       080 FORMAT(1H-,79HRAD FRAC  ST F  ST B  ST E  ST N  CAVT S  CAVT P
          1  THRUST GRAD  TORQUE GRAD)
       090 FORMAT(1H ,F6.2,2X,4F7.0,2F8.3,2X,E10.3,4X,E10.3)
       094 FORMAT(1H ,6H EFFI=,F7.4,4X,2HT=,F9.1)
       095 FORMAT(1H-,50H  SCAN EFF  BOSS THICKNESS  BOSS CHORD  MAX STRESS)
       096 FORMAT(1H ,F9.4,5X,F6.4,10X,F6.3,6X,F6.0)
       097 FORMAT(1H ,10H RAD FRAC=,F6.2)
       098 FORMAT(1H ,6H STEP=,I3,4X11HMAX STRESS=,F7.0,4X,6HCHORD=,F7.3,
          14X,10HTHICKNESS=,F7.4)
       099 FORMAT(1H ,11H CAVITATION,4X,7HCAVT S=,F8.3,2X,7HCAVT P=,F8.3,F8.3
          1)
           DIMENSIONDL(17),T(17),Q(17),CX(17),CL(17),AM(17),ST(17,4),ANG(17),
          1TX(17),CAVS(17),CAVP(17),X(17)
B          READ(60,030)DTOL,TCOD,DENW,DENM,STAL,HTIP
           READ(60,040)AS,PPIP,PPINA,PPINB,YBTA,YBTB,HBTC,YBCT,HBC,CLI,CAV1,
```

Table 3 - Continued.

```
     1CAV2,PAT,VAP,DEVN1,DEVN2,DEVN3,STEP1
      READ(60,045)A0,A1,A2,A3,A4,A5;A6,A7,A8,A9,A10
  100 READ(60,046)TT,VEL,ROT,RAD,DX,Z,COD,CID,LSTEP,NTEST
      CALLEOFCK(60,J)
      GOTO(450,460),J
  460 WRITE(61,010)
      IF(NTEST)102,102,101
  101 WRITE(61,095)
C     102 PI=3.1415927
      OMEG=2.0*PI*ROT
      DEL=OMEG*RAD/VEL
      RSTEP=LSTEP-1
      RATIO=1.0-DX*RSTEP
      CON1=4.0*PI*DENW*(DEL**4)*(VEL**4)/(OMEG*OMEG)
      CON2=DENM*OMEG*OMEG*RAD*RAD*AS
      CON3=8.0*PI*DEL*RAD/Z
      CON4=PAT+HTIP*32.2*DENW-VAP
D     A=(PI*DENW*((DEL*VEL)**3)*VEL)/(OMEG*OMEG)
      B=(1.0-RATIO**4)*DEL
      C=(1.0-RATIO**3)*DTOL*1.3333333
      D=(1.0-RATIO**5)*DTOL*DEL*DEL*0.8
      ROOT=SQRTF((1.0-C/B)**2-(4.0*TT)/(A*B))
      ETAI=(1.0+C/B+ROOT)*0.5
E     DO103K=1,LSTEP
      XD=K-1
      X(K)=1.0-XD*DX
      DL(K)=DTOL
      T(K)=CON1*(X(K)**3)*ETAI*(1.0-ETAI)*(1.0-DL(K)/(DEL*X(K)*ETAI))
      Q(K)=CON1*VEL*(X(K)**3)*(1.0-ETAI)*(1.0+DL(K)*DEL*X(K)*ETAI)/OMEG
      CX(K)=COD-(COD-CID)*(1.0-X(K))/(1.0-RATIO)
      CL(K)=CON3*X(K)*X(K)*(1.0-ETAI)/(SQRTF((X(K)*DEL*ETAI)**2+1.0)*
     1CX(K))
  103 AM(K)=CLI*CL(K)*CX(K)
F     TX(LSTEP)=0.0
      STRES=0.0
  104 ETA=ETAI
```

Table 3 - Continued.

```
      EFFI=ETA
      MSTEP=0
      IF(NTEST)106,106,105
  105 WRITE(61,096)EFFI,TX(LSTEP),CX(LSTEP),STRES
  106 CX(1)=COD
      TX(1)=TCOD*COD
      ANGB=ATANF(1.0/(DEL*EFFI))
      ANG(1)=ANGB*180.0/PI
      CAVS(1)=(CON4+(1.0-X(1))*32.2*DENW*RAD)*2.0*(SINF(ANGB)**2)/
     1(VEL*VEL*DENW)
  107 CAVP(1)=(1.0+1.14*TX(1)/CX(1)+CL(1)/(0.74*CAV2))**2-1.0
      IF(CAVS(1)-CAVP(1)*CAV1)108,109,109
  108 CLA=CL(1)
      CL(1)=0.74*CAV2*(SQRTF(CAVS(1)/CAV1+1.0)-1.0-1.14*TX(1)/CX(1))
      CX(1)=CLA*CX(1)/CL(1)
      TX(1)=TCOD*CX(1)
      IF(NTEST)107,107,119
  119 WRITE(61,099)CAVS(1),CAVP(1),CX(1)
      GOTO107
  109 IF(NTEST)111,111,110
  110 WRITE(61,097)X(1)
      WRITE(61,098)MSTEP,STRES,CX(1),TX(1)
  111 DL(1)=(A0+A1*TCOD+A2*(TCOD**2)+A3*(TCOD**3)+A4*(TCOD**4)+A5*(TCOD*
     1*5)+A6*(TCOD**6)+A7*(TCOD**7)+A8*(TCOD**8)+A9*(TCOD**9)+A10*(TCOD*
     2*10))/CL(1)
      ST(1,1)=0.0
      ST(1,2)=0.0
      ST(1,3)=0.0
      ST(1,4)=0.0
G     DO280I=2,LSTEP
      CX(I)=COD-(COD-CID)*(1.0-X(I))/(1.0-RATIO)
      IF(NTEST)113,113,112
  112 WRITE(61,097)X(I)
  113 STA=0.C
      STB=0.0
      STM=0.0
```

Table 3 - Continued.

```
      STAB=0.0
      STRES=0.0
      TX(I)=TX(I-1)*CX(I)/CX(I-1)
      MSTEP=0
  114 MSTEP=MSTEP+1
      IF(NTEST)116,116,115
  115 WRITE(61,098)MSTEP,STRES,CX(I),TX(I)
  116 IF(I/2-(I-1)/2)450,130,120
  120 NSTEP=I-2
      BMT=T(I-1)*DX*DX*0.5*RAD/Z
      BMQ=Q(I-1)*DX*DX*0.5/(Z*X(I-1))
      FC=CON2*(X(I)*TX(I)*CX(I)+X(I-1)*TX(I-1)*CX(I-1))*0.5*DX
      GOTO140
  130 NSTEP=I-1
      BMT=0.0
      BMQ=0.0
      FC=0.0
  140 IF(I-2)450,170,150
  150 DO160L=2,NSTEP,2
      TM1=T(L-1)*(X(L-1)-X(I))
      TM2=T(L)*(X(L)-X(I))
      TM3=T(L+1)*(X(L+1)-X(I))
      BMT=BMT+(TM1+4.0*TM2+TM3)*RAD*DX/(3.0*Z)
      QM1=Q(L-1)*(1.0-X(I)/X(L-1))
      QM2=Q(L)*(1.0-X(I)/X(L))
      QM3=Q(L+1)*(1.0-X(I)/X(L+1))
      BMQ=BMQ+(QM1+4.0*QM2+QM3)*DX/(3.0*Z)
      F1=X(L-1)*TX(L-1)*CX(L-1)
      F2=X(L)*TX(L)*CX(L)
      F3=X(L+1)*TX(L+1)*CX(L+1)
  160 FC=FC+CON2*(F1+4.0*F2+F3)*DX/3.0
  170 ANGB=ATANF(1.0/(DEL*EFFI*X(I)))
      BMN=BMT*COSF(ANGB)+BMQ*SINF(ANGB)
      BMP=BMT*SINF(ANGB)-BMQ*COSF(ANGB)
      ANG(I)=ANGB*180.0/PI
      AAS=AS*TX(I)*CX(I)
```

Table 3 - Continued.

```
      PIP=PPIP*TX(I)*(CX(I)**3)
      PIN=(TX(I)**3)*CX(I)*(PPINA+PPINB*((AM(I)/TX(I))**2))
      YB=TX(I)*(YBTA+YBTB*AM(I)/TX(I))
      HBT=HBTC*CX(I)
      YBC=YBCT*AM(I)
      HB=HBC*CX(I)
      ST(I,1)=YB*BMN/PIN+HBT*BMP/PIP+FC/AAS
      ST(I,2)=ST(I,1)-TX(I)*BMN/PIN
      ST(I,3)=YBC*BMN/PIN+HB*BMP/PIP+FC/AAS
      ST(I,4)=ST(I,3)-CX(I)*BMP/PIP
H     STM=ABSF(ST(I,1))
      DO190M=2,4
      STAB=ABSF(ST(I,M))
      IF(STM-STAB)180,190,190
180   STM=STAB
190   CONTINUE
      STRES=STM/144.0
      IF(STM-STAL)200,260,220
200   IF(MSTEP-1)450,260,210
210   STA=STM-STAL
      TXX=TX(I)
      GOTO240
220   STB=STM-STAL
      TXY=TX(I)
      IF(STA)240,230,450
230   TX(I)=TXY+STEP1
      GOTO114
240   IF(TXX-TXY-DEVN1)260,260,250
250   TX(I)=(TXX+TXY)/2.0
      GOTO114
I     260 TC=TX(I)/CX(I)
      DL(I)=(A0+A1*TC+A2*(TC**2)+A3*(TC**3)+A4*(TC**4)+A5*(TC**5)+A6*(TC
     1**6)+A7*(TC**7)+A8*(TC**8)+A9*(TC**9)+A10*(TC**10))/CL(I)
      CAVS(I)=(CON4+(1.0-X(I))*32.2*DENW*RAD)*2.0*(SINF(ANGB)**2)/
     1(VEL*VEL*DENW)
      CAVP(I)=(1.0+1.14*TX(I)/CX(I)+CL(I)/(0.74*CAV2))**2-1.0
```

Table 3 - Continued.

```
      IF(CAVS(I)-CAVP(I)*CAV1)270,280,280
  270 CLA=CL(I)
      CL(I)=0.74*CAV2*(SQRTF(CAVS(I)/CAV1+1.0)-1.0-1.14*TX(I)/CX(I))
      CX(I)=CLA*CX(I)/CL(I)
      IF(NTEST)113,113,275
  275 WRITE(61,099)CAVS(I),CAVP(I),CX(I)
      GOTO113
  280 CONTINUE
J     CALTA=0.0
      CALTB=0.0
      EFFI=0.999
  290 CALT=0.0
      DO300K=2,LSTEP,2
      T(K-1)=EFFI*(X(K-1)**3)*(1.0-EFFI)*(1.0-DL(K-1)/(DEL*X(K-1)*EFFI))
     1*CON1
      T(K)=EFFI*(X(K)**3)*(1.0-EFFI)*(1.0-DL(K)/(DEL*X(K)*EFFI))
     1*CON1
      T(K+1)=EFFI*(X(K+1)**3)*(1.0-EFFI)*(1.0-DL(K+1)/(DEL*X(K+1)*EFFI))
     1*CON1
  300 CALT=CALT+(T(K-1)+4.0*T(K)+T(K+1))*DX/3.0
K     IF(NTEST)306,306,305
  305 WRITE(61,094)EFFI,CALT
  306 IF(TT-CALT)330,360,310
  310 CALTA=TT-CALT
      EFFA=EFFI
      IF(CALTB)340,320,450
  320 EFFI=EFFA-0.0010
      GOTO290
  330 CALTB=TT-CALT
      EFFB=EFFI
  340 IF(EFFA-EFFB-DEVN2)360,360,350
  350 EFFI=(EFFA+EFFB)/2.0
      GOTO290
L     360 ETB=EFFB
      CALQ=0.0
      DO380K=2,LSTEP,2
```

Table 3 - Continued.

```
      Q(K-1)=(X(K-1)**3)*(1.0-ETB)*(1.0+DL(K-1)*DEL*X(K-1)*ETB)
     1*CON1*VEL/OMEG
      Q(K)=(X(K)**3)*(1.0-ETB)*(1.0+DL(K)*DEL*X(K)*ETB)
     1*CON1*VEL/OMEG
      Q(K+1)=(X(K+1)**3)*(1.0-ETB)*(1.0+DL(K+1)*DEL*X(K+1)*ETB)
     1*CON1*VEL/OMEG
  380 CALQ=CALQ+(Q(K-1)+4.0*Q(K)+Q(K+1))*DX/3.0
M     IF(NTEST)410,385,410
  385 IF(ABSF(ETA-ETB)-DEVN3)410,410,400
  400 ETAI=ETB
      DO390K=1,LSTEP
      CX(K)=COD-(COD-CID)*(1.0-X(K))/(1.0-RATIO)
      CL(K)=CON3*X(K)*X(K)*(1.0-ETB)/(SQRTF((X(K)*DEL*ETB)**2+1.0)*CX(K)
     1)
  390 AM(K)=CLI*CL(K)*CX(K)
      GOTO104
N     410 ETAO=TT*VEL/(CALQ*OMEG)
      SHP=CALQ*OMEG/550.0
      N=Z
      WRITE(61,020)
      WRITE(61,050)RAD,VEL,ROT,N,ETB,ETAO,TT,SHP
      WRITE(61,055)
      ALST=STAL/144.0
      WRITE(61,056)CX(1),CX(LSTEP),RATIO,HTIP,ALST
      WRITE(61,060)
      DO420J=1,LSTEP
  420 WRITE(61,070)X(J),CX(J),TX(J),AM(J),ANG(J),CL(J),DL(J)
      WRITE(61,080)
      DO440J=1,LSTEP
      CAVP(J)=CAVP(J)*CAV1
      DO430I=1,4
  430 ST(J,I)=ST(J,I)/144.0
  440 WRITE(61,090)X(J),ST(J,1),ST(J,2),ST(J,3),ST(J,4),CAVS(J),CAVP(J),
     1T(J),Q(J)
      IF(ABSF(ETA-ETB)-DEVN3)100,100,400
  450 STOP
      END
```

Table 4 - Output for HYDRO - 1 Impeller.

DESIGN PARAMETERS HYDROJET IMPELLER

DESIGN ASSUMPTIONS
BETZ MIN ENERGY CONDITION
CONSTANT AXIAL VELOCITY
NACA PROFILE SHOCK FREE ENTRY

RADIUS	VELOCITY	ROTATION	BLADES	IDEAL EFF	TOTAL EFF	THRUST	SHP
7.50	19.30	1.50	4	0.9733	0.8699	44800.	1807.

TIP CHORD	BOSS CHORD	BOSS RATIO	TIP IMMERSION	ALLOWABLE STRESS
5.000	3.000	0.200	11.50	7250.

RAD FRAC	CHORD	THICKNESS	MEAN LINE	ANGLE BI	LIFT COEF	DRAG/LIFT
1.00	5.000	0.2250	0.0926	15.67	0.249	0.030
0.95	4.875	0.2194	0.0876	16.45	0.241	0.031
0.90	4.750	0.2137	0.0826	17.31	0.233	0.032
0.85	4.625	0.2081	0.0776	18.26	0.225	0.033
0.80	4.500	0.2025	0.0726	19.32	0.217	0.034
0.75	4.375	0.1969	0.0675	20.51	0.207	0.036
0.70	4.250	0.1912	0.0625	21.84	0.197	0.038
0.65	4.125	0.2035	0.0574	23.34	0.187	0.040
0.60	4.000	0.2302	0.0523	25.06	0.175	0.044
0.55	3.875	0.2562	0.0471	27.02	0.163	0.049
0.50	3.750	0.2813	0.0419	29.29	0.150	0.056
0.45	3.625	0.3056	0.0367	31.94	0.136	0.066
0.40	3.500	0.3289	0.0315	35.04	0.121	0.080
0.35	3.375	0.3508	0.0263	38.71	0.104	0.100
0.30	3.250	0.3723	0.0211	43.08	0.087	0.130
0.25	3.125	0.3915	0.0160	48.29	0.069	0.178
0.20	3.000	0.4056	0.0112	54.51	0.050	0.264

Table 4 - Continued.

RAD FRAC	ST F	ST B	ST E	ST N	CAVT S	CAVT P	THRUST GRAD	TORQUE GRAD
1.00	0.	0.	0.	0.	0.555	0.347	0.181E 06	0.425E 06
0.95	140.	-127.	113.	113.	0.615	0.340	0.155E 06	0.363E 06
0.90	505.	-550.	385.	386.	0.685	0.333	0.132E 06	0.308E 06
0.85	1149.	-1330.	834.	834.	0.766	0.325	0.111E 06	0.259E 06
0.80	2089.	-2476.	1444.	1441.	0.861	0.317	0.922E 05	0.216E 06
0.75	3392.	-4061.	2229.	2216.	0.973	0.309	0.759E 05	0.177E 06
0.70	5095.	-6113.	3168.	3139.	1.106	0.300	0.616E 05	0.144E 06
0.65	6204.	-7246.	3300.	3246.	1.265	0.303	0.492E 05	0.115E 06
0.60	6454.	-7248.	2758.	2673.	1.457	0.318	0.386E 05	0.906E 05
0.55	6657.	-7247.	2330.	2201.	1.690	0.334	0.296E 05	0.699E 05
0.50	6829.	-7248.	1989.	1800.	1.975	0.349	0.221E 05	0.528E 05
0.45	6976.	-7249.	1717.	1446.	2.327	0.365	0.159E 05	0.387E 05
0.40	7101.	-7247.	1503.	1122.	2.762	0.381	0.110E 05	0.274E 05
0.35	7211.	-7247.	1346.	816.	3.303	0.397	0.719E 04	0.185E 05
0.30	7247.	-7184.	1236.	507.	3.969	0.415	0.433E 04	0.118E 05
0.25	7247.	-7099.	1191.	194.	4.779	0.432	0.228E 04	0.695E 04
0.20	7251.	-7030.	1230.	-135.	5.727	0.446	0.920E 03	0.365E 04

Table 5 - Input for HYDRO - 1 Impeller.

```
 0.030 .0450  1.9905  14.907 1.044E+06  11.50
 0.736  0.0418  0.0445  0.029  0.5 -0.182 -0.016  0.818  0.516  0.0745
 1.20  4.0000  2116.2  35.28  0.10E-03  0.10E-04  0.10E-03  0.10E-01
0.9299158E-02-0.3499790E-01-0.2191732E+01 0.7515442E+02-0.8086659E+03
0.3367858E+04 0.6849617E+04-0.1329265E+06 0.5739262E+06-0.1119756E+07
0.8516336E+06
 44800.0  19.30  1.50  7.50  0.50000000E-01  4.0  5.000  3.000  17 1
```

Table 6 List of Symbols

PROGRAMME SYMBOL	DESCRIPTION	UNIT	MATHEMATICAL SYMBOL
A1,..A10	Coefficients of polynomial $C_D = \sum A_i \frac{(t_x)^i}{c}$		A_i
AM(I)	Max. ordinate of mean line	ft	m_x
ANG(I)	Hydrodynamic pitch angle of blade element	degree	
ANGB	" " " " "	radian	β_i
AS	Blade area factor (Table 2)		a_s
AAS	Area of section	ft^2	A_s
BMN	Section bending moment about axis normal to chord	lbf ft	M_n
BMP	Section bending moment about axis parallel to chord	"	M_p
BMQ	Section bending moment due to Q	"	M_Q
BMT	" " " " " T	"	M_T
CALQ	Calculated torque of impeller	"	Q
CALT	Calculated thrust of impeller	lbf	T
CAV1	Overall factor for non potential flow eqn 26		f_o
CAV2	Constant in 3rd term of eqn. 24		
CAVP(I)	Pressure min. cavitation no. at a section		σ_p
CAVS(I)	Cavitation no. of a section		σ_s
CID	Section chord width at boss	ft	
CL(I)	Sectional lift coefficient		C_L
CLI	Constant in eqn. 20 (for NACA-16, =0.0745)		
COD	Section chord width at tip	ft	
CON1	Force parameter (see Section 2.1)	lbf	K_1

Table 6 cont. List of Symbols

PROGRAMME SYMBOL	DESCRIPTION	UNIT	MATHEMATICAL SYMBOL
CX(I)	Sectional chord width of section	ft	c
DEL	Advance coefficient		δ
DENM	Density of impeller material	slug/ft^3	ρ_m
DENW	Density of working fluid	"	ρ
DEVN1	Calculation accuracy of TX	ft	
DEVN2	" " " EFFI from thrust gradient		
DEVN3	Calculation accuracy of η_i		
DL(I)	Drag to lift ratio of section		$= \frac{C_D}{C_L}$
DTOL	Drag to lift ratio for initial approximation		
DX	Distance between sections as percentage of R		
EFFI	Ideal blade element efficiency		η_i
ETAI	" " " " estimation at beginning of calculation		η_i
ETAO	Impeller efficiency		η_o
FC	Centrifugal force acting on a section	lbf	F_c
HB	Blade section property (Table 2)	ft	$\bar{h}$
HBC	" " " "		$\frac{\bar{h}}{c}$
HBT	" " " "	ft	$\bar{h}_t$
HBTC	" " " "		$\frac{\bar{h}_t}{c}$
HTIP	Depth of immersion of blade tip	ft	H
LSTEP	Number of stations (see section 4.0)		
NTEST	Control for progressive print out of intermediate calculated variables		
OMEG	Angular velocity of impeller	rad/s	ω

Table 6

Table 6 cont. List of Symbols

PROGRAMME SYMBOL	DESCRIPTION	UNIT	MATHEMATICAL SYMBOL
PAT	Atmospheric pressure	lb/ft^2	P_A
PIN	Section moment of inertia about an axis through centroid parallel to chord line	in^4	I_n
PIP	Section moment of inertia about an axis through centroid normal to chord line	"	I_p
PPINA	Blade section property (Table 2)		i_n
PPINB	" " " "		
PPIP	" " " "		i_p
Q(I)	Torque gradient at section	lbf/ft	$\frac{dQ}{dx}$
RAD	Radius of impeller	ft	R
RATIO	Hub radius to impeller radius		
ROT	Rotational speed	rps	n
SHP	Shaft horse power at impeller	hp	
STAL	Allowable design stress	lbf/ft^2	σ_{design}
STEP1	Increase in blade thickness in "Regula Falsi" routine	ft	
STM	Maximum numerical stress at a section	lbf/ft^2	$\lvert\sigma_{max}\rvert$
ST(I J)	Stress at extremities of a section	"	
T(I)	Thrust gradient at a section	lbf	$\frac{dT}{dx}$
TCOD	Thickness to chord ratio for minimum profile drag		
TT	Design thrust	lbf	T
TX(I)	Maximum thickness of a section	ft	t_x

Table 6

Table 6 cont. List of Symbols

PROGRAMME SYMBOL	DESCRIPTION	UNIT	MATHEMATICAL SYMBOL
VAP	Vapour pressure of working fluid	lb/ft^2	e
VEL	Axial velocity of fluid at impeller	ft/s	V_a
X(I)	Radius fraction of section		x
YB	Blade section properties (Table 2)	ft	$\bar{y}$
YBC	" " " "	"	$\bar{y}_c$
YBCT	" " " "		$\frac{\bar{y}_c}{t}$
YBTA	" " " "		$\frac{\bar{y}}{t}$
YBTB	" " " "		
Z	No. of blades		Z

TABLE 6

Table 6 cont. List of Symbols

DESCRIPTION	UNIT	MATHEMATICAL SYMBOL
Sectional drag coefficient (2-dimensional flow)		C_D
Diameter of impeller	ft	D
Profile drag of blade element	lbf	dD
Actual lift " " "	"	dL
Actual torque " "	lbf ft	dQ
Ideal " " "	"	dQ_i
Actual thrust " "	lbf	dT
Ideal " " "	"	dT_i
Distance of point on section from centroid parallel to chord line	ft	h
Lift camber factor, eqn. 20		l_m
Free stream static pressure	lbf/ft^2	P
Min. value of local pressure p_e on surface of section	lbf/ft^2	p_e
Pressure at blade section radius r at minimum immersion	"	p_r
Radius of blade element	ft	r
Circumferential component of induced velocity in fully developed wake	ft/s	U_{It}
Velocity of flow relative to blade including induced flow effects	"	V_R
Normal distance of point on section from a line through centroid parallel to chord line	ft	y
Advance angle of blade element	rad	β
Circulation	ft^2/s	Γ
Viscosity factor eqn. 20		μ_m
Fibre stress at a point on a section	lbf/ft^2	σ
Pitch angle of blade element equals β_i in the example impeller	rad	ϕ

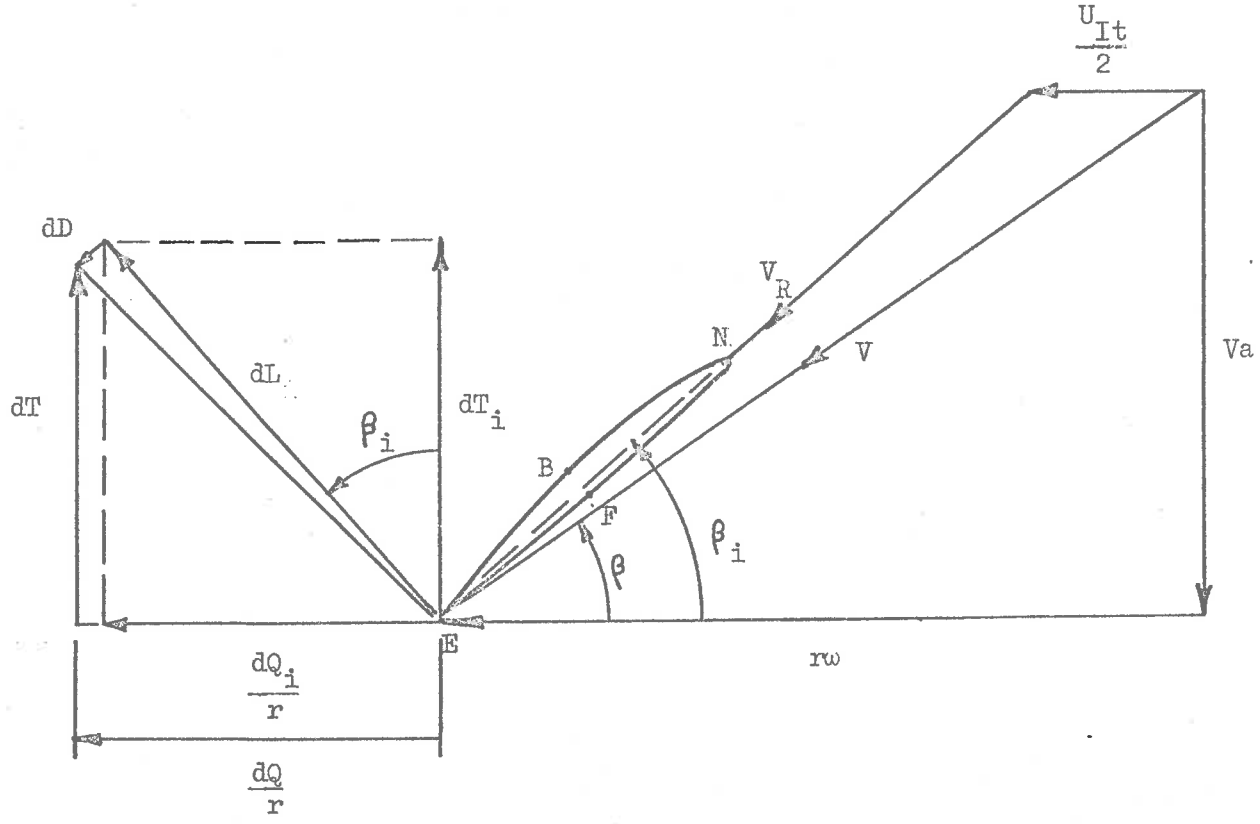

Fig. 1 - Velocities and Forces at Blade Section.

Fig. .2

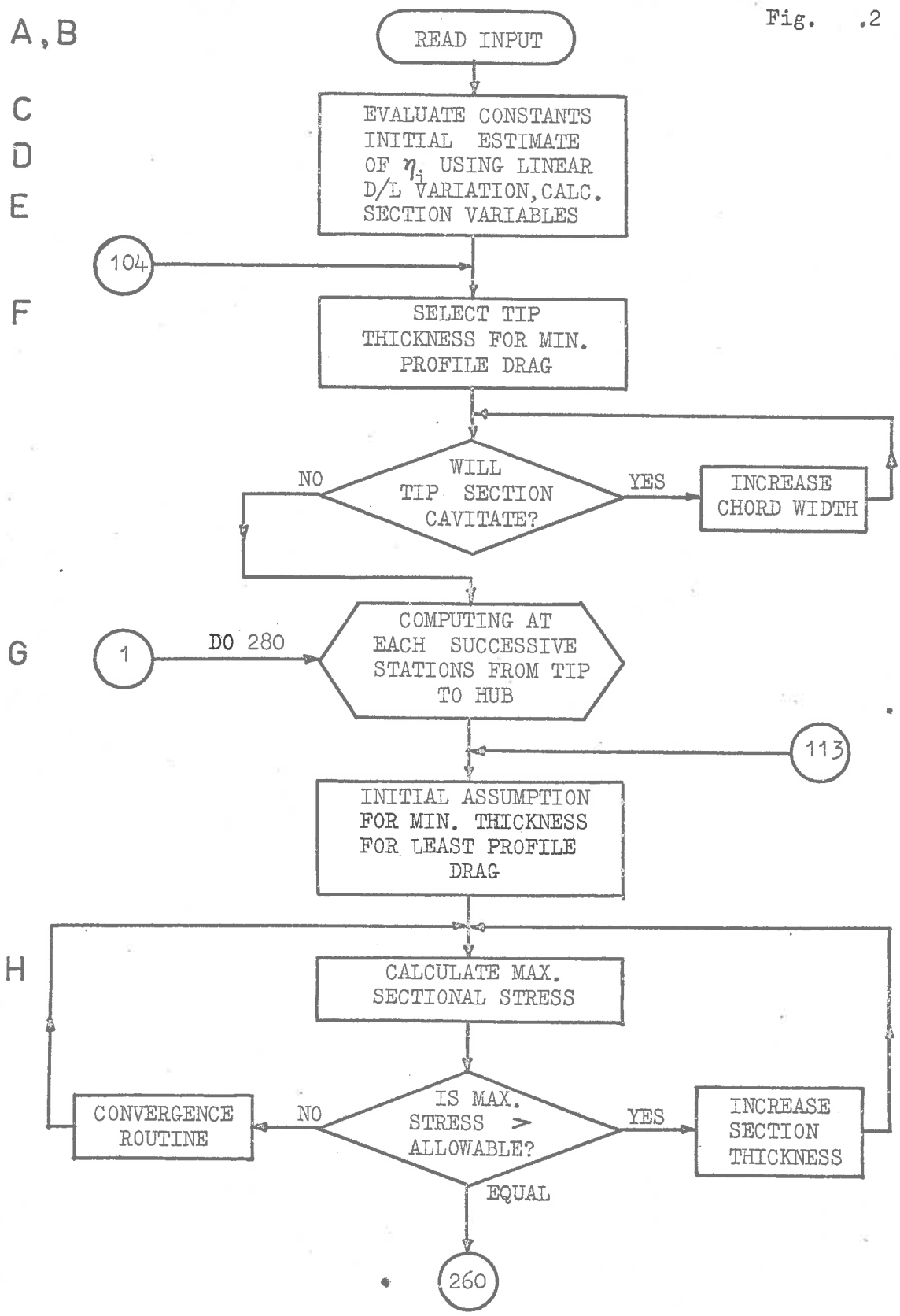

Fig. .2 - Programme Flow Diagram.

Fig. .2

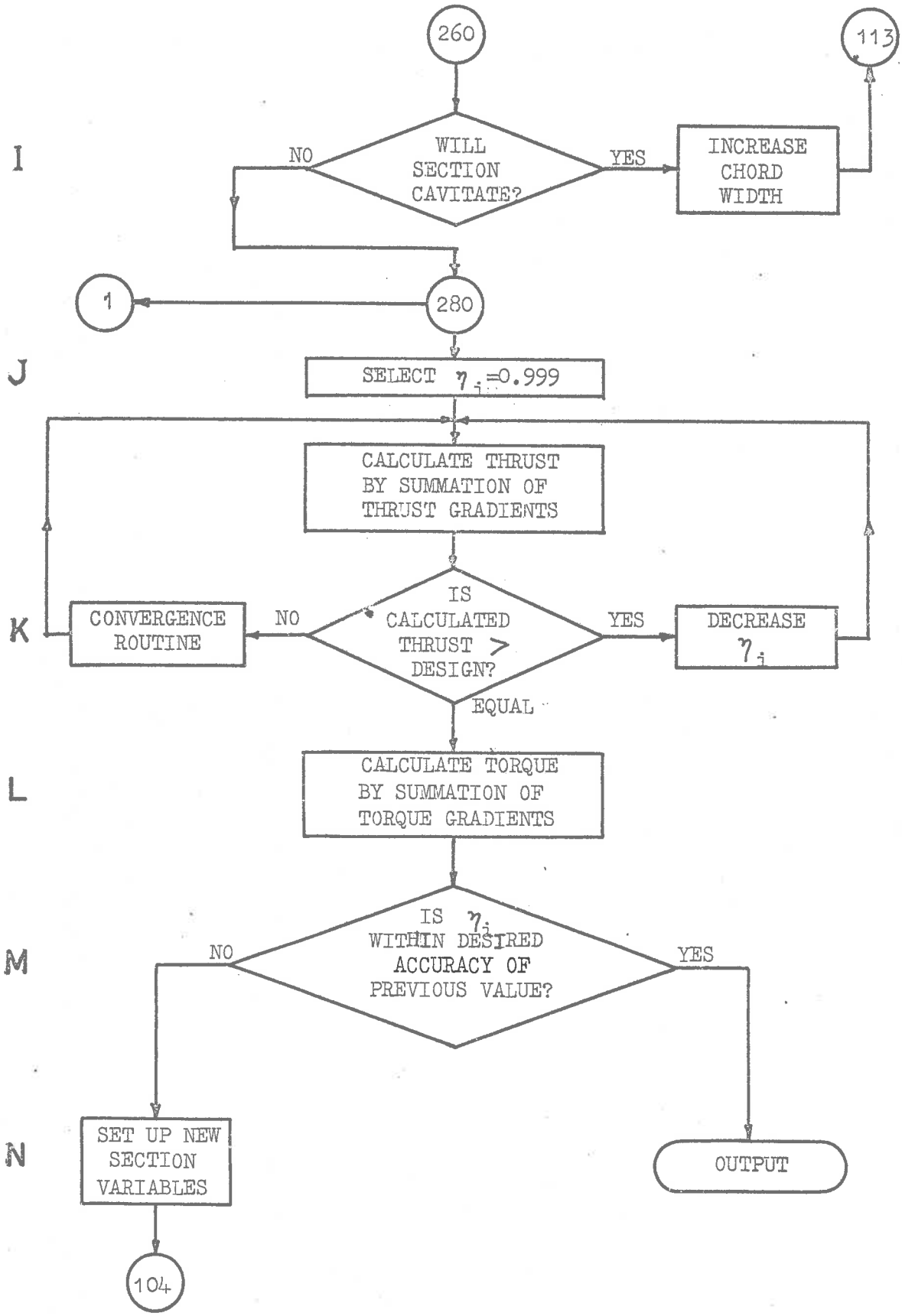
260
113
I
NO
WILL SECTION CAVITATE?
YES
INCREASE CHORD WIDTH
1
280
J
SELECT η_i=0.999
CALCULATE THRUST BY SUMMATION OF THRUST GRADIENTS
K
CONVERGENCE ROUTINE
NO
IS CALCULATED THRUST > DESIGN?
YES
DECREASE η_i
EQUAL
L
CALCULATE TORQUE BY SUMMATION OF TORQUE GRADIENTS
M
NO
IS η_i WITHIN DESIRED ACCURACY OF PREVIOUS VALUE?
YES
N
SET UP NEW SECTION VARIABLES
OUTPUT
104

Fig. .2

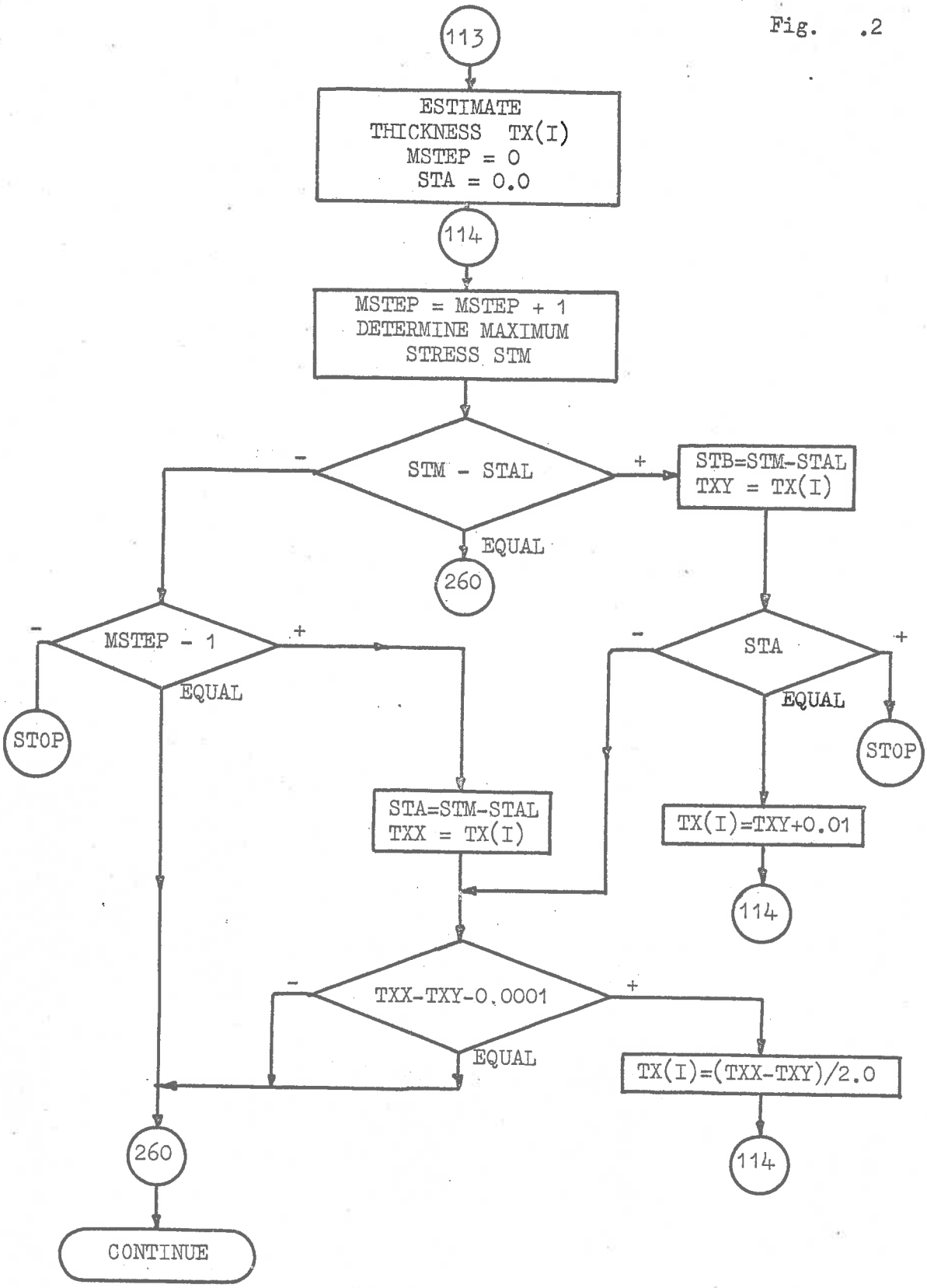

Fig. .2 - Continued. "Regula Falsi" Convergence Routine for Blade Thickness.

APPENDIX A2

COMPUTATION OF RECTANGULAR MACHINING CO-ORDINATES for AN ARBITRARY IMPELLER DESIGN

by

M.R.Hale

UNIVERSITY OF ADELAIDE

DEPARTMENT OF MECHANICAL ENGINEERING

Report Mech. Eng. R65/2

March, 1965.

TABLE OF CONTENTS

COMPUTATION OF RECTANGULAR MACHINING CO-ORDINATES FOR AN ARBITRARY IMPELLER DESIGN

by M.R. Hale

ABSTRACT

A digital-computer programme in FORTRAN has been developed to calculate the co-ordinates of points on the surface of an impeller (or propeller) blade of arbitrary shape from a series of specifying equations. The programme then computes the co-ordinates of points on the locus-surface of the centre of a spherical cutter which would machine the prescribed surface. All the points calculated lie on a rectangular grid. Although the impeller shape can be arbitrary, it must be possible to define the blade shape by a series of equations of given form. Certain minor restrictions on impeller geometry must also be satisfied.

The blade-shape equations which are required are those which define the following:-

(1) Radial chord distribution.

(2) Maximum-sectional-thickness distribution.

(3) Maximum-ordinate of mean line distribution.

(4) Blade angle distribution.

(5) Thickness form of the blade sections.

(6) Profile of the mean line.

The restrictions placed on the impeller geometry are the following:-

(1) The blade profiles at all sections must have a similar basic form, superimposed on the mean line.

(2) The mean lines must be similar at all sections, but may have varying maximum ordinates.

(3) The centroids of all sections must lie on a straight radial line, i.e., the blades must have no rake or skew.

The number of computed surface points is limited by the storage capacity of the computer. With the IBM 709/7090 II computer, having a total storage capacity of 32,561 words (about 28,000 usuable words) a matrix of points 53 by 120 can be calculated for each side of the blade.

The output of the programme is a typewritten list of machining co-ordinates and instructions in a form suitable for the operator of a hand-operated vertical miller.

The programme can be modified to cope with impeller or propeller designs which do not satisfy the above restrictions. It can also be extended to generate machining instructions for an automatic miller with magnetic tape control.

1.0 INTRODUCTION

The most common method of machining an impeller or propeller is to use a cutter which moves (relative to the blade) on a cylindrical path with centre on the axis of the impeller. The cutter motion is controlled by a follower moving over a series of templates which may be either cylindrical or expanded-cylindrical sections depending on the mechanism used to convert movement of the follower to movement of the cutter.

Another method, which is suited for the majority of milling machines, is based on spot-machining of points on the blade surface using either a polar or a rectangular grid. This method requires considerable computation to transform an object naturally defined by polar co-ordinates into one defined by cartesian co-ordinates if the latter are used.

In all the machining techniques commonly employed it is usual to use only a small number of sections to define the complete blade shape. Hand machining is then used to "fair in" between the machined regions.

Disadvantages of the above methods are:-

(1) The time consumed in hand-fairing between the accurately machined sections.

(2) The blade surface can only be as accurate as the templates.

(3) The accuracy is dependent on the size of the cutter. It is not usual to attempt to define the locus of a cutter moving over the blade surface at the desired section. As the template shape is usually that of a blade section, an appreciable error is thus introduced unless the cutter has a cutting-edge radius small in comparison with the radius of curvature of the blade surface at the point being considered.

Perhaps the ideal method of machining an impeller would be to make use of an automatically-controlled milling machine using a magnetic tape as an input medium for all machining instructions and control. The technique described in the paper does not satisfy this ideal completely but is a step towards the final objective.

This paper outlines a method of determining the co-ordinates of points on the locus-surface of the centre of a spherical cutter, such that the surface being machined would be the surface of an arbitrarily defined impeller blade. The machined points are obtained in a rectangular grid pattern.

The use of the programme is illustrated by considering the design of impeller which is being used in a model study of a Hydrojet Propulsion Unit (Ref. 1). The 8 inch model impeller (scale ratio of 22.5) was machined in a Pantograph copying machine from a three-dimensional master template. This master template which was four times larger than the model, was machined in a universal miller to demensions calculated by this programme. The intermediate stage of using a master template was introduced to reduce hand-fairing errors, and to reduce the number of machining co-ordinates necessary to obtain the required accuracy.

2.0 THE DEFINITION OF BLADE SHAPE

2.1 Restrictions on blade shape.

The programme as described in the following sections restricts the blade shape by requiring zero rake and skew, and requiring that the centroids of all sections lie on a straight radial line. This restriction could easily be removed by inserting extra equations defining these parameters in terms of the radius.

The most important limitation concerns the distribution of blade section

shapes. Corresponding ordinates of blade sections at all radii from tip to boss must be proportional to the maximum thickness of the sections. The mean line shape must also be similar at all sections i.e. corresponding ordinates of the mean line must be proportional to the maximum displacements of the mean lines. These restrictions simplify the problem of defining the whole impeller blade by a series of related equations.

2.2 Blade shape equations

The following shape parameters must be defined in terms of equations:

(1) Chord-width distribution with respect to radius.

(2) Maximum sectional thickness with respect to radius.

(3) Maximum ordinate of the mean line with respect to radius.

(4) Blade angle distribution with respect to radius.

(5) Thickness form of the blade section with respect to unit thickness and unit chord width.

(6) Profile of the mean line with respect to unit chord width.

The form of these equations expressing the blade shape parameters is not restricted in any way. If any of the equations differ from those used for the Hydrojet impeller, as expressed below, then these equations must replace the corresponding equations in the programme as written in Table 2. The majority of statements which refer to the shape parameters are found between statements numbered 600 and 660.

In the case of the Hydrojet impeller some of these relationships were expressed in the form of polynomial expansions. A previous programme (Ref. 1) had carried out the design of the impeller. From its output tabular values defining the above distributions (See Table 1) were taken. For some of the blade-shape distributions polynomials were fitted to the tabular values using the least-square-deviation technique. The

polynomial coefficients were calculated with the aid of IBM Library Programme No. 7.0.002. This uses a modified Gaussian elimination method to solve equations representing the condition for least-square deviation, the polynomial coefficients then being calculated by back substitution.

The equations representing the design data for the impeller under consideration are given below. Reference should be made to Table 5 for the nomenclature used.

(1) Chord width: The impeller design chosen has a linear chord distribution and this was represented by the following relationship between the chord at the tip COD, and the chord at the boss CID, for varying radii RX

$$CX = COD - (COD - CID) * (RADM - RX) / (RADM * (1.0 - RATIO) \quad \ldots 1$$

This assumes a hub to diameter ratio of RATIO.

(2) Maximum Section Thickness: The thickness distribution with respect to radius was expressed by three different equations, each being applicable over a certain region.

Between the radius fraction 0.7 and 1.0, where the maximum thickness TX of the section was determined by minimum profile drag conditions, the relationship was

$$TX = 0.045 * CX \quad \ldots 2.$$

Over the interval between radius fraction 0.65 and 0.7 where the working stress is made equal to the allowable stress, but where the change in design thickness is small, the thickness to be used in the programme was assumed constant.

For the region between radius fraction 0.2 and 0.65 where the thickness is determined by the design stress, a third-order-polynomial expression was used to specify the thickness to within an accuracy of 0.00012 ft. or 0.3%.

$$TX = \sum T_i \, (XR)^i \qquad \ldots \quad 3.$$

where $i = 0, 1, 2, 3$

and $XR =$ radius fraction

(3) Maximum mean-line ordinate: This distribution was defined by a fourth-order polynomial to an accuracy of 0.5%, the equation being

$$AM = \sum A_i \, (XR)^i \qquad \ldots \quad 4.$$

where $i = 0, 1, 2, 3, 4.$

(4) Blade angle: The impeller was designed to have the chord line at all sections lying on a helical surface. The blade angle was defined as:

$$ANG = \text{Arctan} \, \frac{(PITCH)}{(2\pi \, RX)} \qquad \ldots \quad 5.$$

(5) Thickness form of the blade section: The blade section used for the impeller was a NACA - 16 profile. (Ref. 2, p155). Because of the large change in curvature from the leading edge to the trailing edge, an equation, differing in form from a polynomial, had to be found to describe the shape of the section.

An equation was first chosen to give the correct curvature on the leading edge. The profile was assumed in this region to be given (See Ref. 3) by a parabola of the form

$$y_o^2 = 2K \, x$$

where y_o is the y ordinate at a fractional distance x along the chord.

Since radius of curvature $= \rho = \dfrac{\left[1 + \left(\frac{dx}{dy}\right)^2\right]^{3/2}}{\frac{d^2x}{dy^2}}$ ... 6.

then at the L.E. where $y_o = 0$, $x = 0$ ... 7.

$$\rho = K$$

For this profile $\rho = K$ may be calculated at the L.E. as

0.4888% of chord for unit thickness

At the T.E. where $x = 1.0$ the profile equation must satisfy

$y_o = 0$, $x = 1.0$

To satisfy this condition the parabolic equation is modified to

$$y_o = (1 - x)\sqrt{2K\,x} \qquad \ldots \quad 8.$$

The ordinates given by equation 8, if subtracted from the corresponding ordinates of the NACA - 16 profile give residual ordinates which can be approximated by a polynomial expansion. The final equation for the profile thus has the following form:-

$$Y0 = (1 - XX)[\sqrt{0.98879XX}] + \sum Y_i\, XX^i \qquad \ldots \quad 9.$$

where $i = 0, 1, \ldots, 9$

A tenth-order polynomial was necessary if the maximum percentage error was to be limited to 0.17%. The overall accuracy of this method for defining such an aerofoil section can be judged from the deviations shown in Fig. 1.

The ideal trailing edge thickness of the blade is zero. As this is impractical, and in any case is impossible to machine, the edge thickness of the model impeller was made equal to the smallest machinable dimension. Hence the blade section ordinates on the trailing edge half of the blade were increased above the calculated theoretical value

Y0 for this region to the value Y0' given by

$$Y0' = Y0 + ALTE * SCALM * (XX - 0.5) / (SCALE * TX) \quad \ldots \quad 10.$$

This equation applies to the model in question, which has a scale ratio of SCALM (1:22.5). The allowable edge thickness ALTE was chosen to be 0.020 of an inch. The factor SCALE in equation is the scale ratio of the master template to the prototype.

(6) Profile of mean line: The NACA a = 1.0 mean line was used in the impeller design. The equation representing the shape of the mean line is (Ref. 4, equation 4.26)

$$\frac{y_m}{c} = \frac{C_{li}}{4\pi} [(1 - x) \log_e (1 - x) + x \log_e x] \quad \ldots \quad 11.$$

where y_m = YM = y ordinate of mean line

C_{li} = Ideal lift coefficient for non-viscous fluid

c = Chord width

x = XX = Fractional distance along chord.

but $\frac{f}{c} = 0.05515\ C_l i$

where f = AM = Max. ordinate of mean line

thus $$\frac{YM}{AM} = \frac{1}{4\pi} (0.05515) [(1 - XX) \log_e (1 - XX) + XX \log_e XX] \quad \ldots \quad 13.$$

2.3 The Blade Shape of the Hydrojet Impeller

The dimensions of the Hydrojet impeller are given together with the estimated operating characteristics of the impeller in Table 1. From this data equations representing the blade shape parameters were determined in the form described in Section 2.2 These equations formed part of the input to the machining co-ordinate programme.

3.0 THE METHOD OF COMPUTING THE MACHINING CO-ORDINATES

3.1 Computing Stages

The programme can be divided into two major stages:-

(1) From the blade shape equations previously discussed, the co-ordinates of the following surface points are calculated:

(i) Points on the leading and trailing edges of the blade surface.

(ii) Points on the face and back surfaces of the blade.

(2) The direction cosines of the normal to the surface at each of the above points are determined. By making the length of each normal equal to the radius of the spherical cutter, the extra-surface points on the required locus-surface described by the cutter centre are obtained. For convenience of the machinist the co-ordinates of the bottom of the cutter are specified in the programme output.

A flow diagram representing the important steps in the computation is given in Fig. 2.

The complete programme listing is given in Table 2.

3.2 Points, Reference Planes and Axes

To describe the position of any point in space four sets of axes were used. These can be divided into two groups - one groups being used in Stage (1) of Section 3.1 and the other in Stage (2) of the same Section.

3.2.1 Surface Points

For the calculation of surface points (Stage 1) the following pairs of reference axes are used (See Fig. 3):-

(1) A set of right-handed cartesian axes X,Y,Z, aligned so that X lies along the line of centroids of the blade sections and Z along the axis of the impeller.

(2) A set of right-handed cartesian axes XB, YB, ZB, aligned parallel to X, Y, Z, and with YB co-linear with Y, as shown in Fig. 3. The distance between the X, Z plane and XB, ZB plane is denoted YD.

To simplify the computation, the points chosen to define the blade surface were those resulting from the intersection of a two-dimensional fundamental mesh (Ref. 6) with the blade surface. The planes forming the fundamental mesh were aligned respectively parallel to X, Z axes and the Y, Z axes.

Planes parallel to X, Z axes are called column planes and planes parallel to Y, Z, axes are called row planes or stations. The distance between column planes is not equal (See below). The distance between row planes is equal, and has a value DX.

The row planes are identified as I = 1, 2, 3, ... as shown in Fig. 5. It was necessary to select I = 1 outside the blade surface to simplify the computing routine. Thus the row plane passing through the tip of the impeller on the X axes (see Fig. 5) was chosen to be I = 5 row plane.

The column planes associated with each row plane are named separately (Fig. 5) and by two different methods:-

(1) <u>Nomenclature of column planes</u> - <u>Method 1.</u>

The plane containing the axes X, Z, is chosen as the datum plane N = 0 and planes on either side are named by N = 1, 2, 3 ..., an additional identification of M = 1 or 2 being required

to indicate which side of the datum is being considered. This distance between planes is (up to a certain distance from N = 0) equal, and of value SPACX. At a predetermined distance from the N = 0 plane the spacing between the column planes is changed to SPACN (one fifth of SPACX) and the identification of the planes continued numerically without further interruption. The predetermined distance is chosen to be equal to or greater than a given fractional distance of the value of the Y ordinate of the point on the leading or trailing edge on the same row plane. This fractional value PCX is given as an input instruction to the programme. The reason for using planes with a smaller spacing (SPACN) over part of the blade is to define more accurately the blade surface in the region where the surface curvature is increasing rapidly near the blade edges.

The numerical value of N associated with the column planes where the spacing distance changes from SPACX to SPACN is recorded as the value of MLE (I) and of MTE (I) where these correspond to the leading and trailing edge respectively at a given row plane I. The total number of N planes on either side of X, Z plane are recorded as NLE (I) and NTE (L) for the leading and trailing edge side at a given row plane I (Fig. 5).

It should be noted that column planes are not equally spaced over the entire blade surface, and also that points on the same plane parallel to the X, Z axes but in different row planes may not have the same numerical value of N.

Associated with any point on the blade surface a curved plane YR, ZR (Figs. 3, 5) passing through the point can be defined as a portion of a cylindrical surface with its axis coincident with the impeller axis.

The above identification of column planes applies only to the computation in Stage (1). The following nomenclature was used in the programme to store values associated with these planes:-

(2) Nomenclature of column planes - Method 2.

The column planes N are identified in another way by being num bered consecutively from the trailing edge to the leading edge with the identifier (subscript) of NNN. The values of NNN are chosen so that the numerical value of the NNN plane containing the X, Z axes (i.e. N = 0 plane) is made equal to a specified value NN. The value of NN must be chosen so that the identifier NNN for any column planes on the blade surface is positive and at least greater than NNN = 5. The chosen value of NN must be specified as an input statement. For the Hydrojet impeller, the value of NN was chosen to be 60.

It should be noted that although the column plane NNN are numbered consecutively their spacing is not constant and that for different row planes the column planes which hold the same value of NNN are not necessarily co-planar.

A point on the blade surface can be identified by the numerical values of the row and column planes which pass through it. The additional subscript J = 1 indicates back or face surface of the blade. Thus a point (I, NNN, J) = (6, 13, 2) would be a point on the face surface of the blade at I = 6 whose identifier has a value of NNN = 13.

The co-ordinates of points associated with the axes XB, YB, ZB are given by XB(I, NNN, J), YB(I, NNN, J) and ZB(I, NNN, J). For example ZB(I, NNN, J) is the distance from the point (I, NNN, J) to the XB, YB plane.

Before the direction cosines of the normal to the surface at a point can be calculated, a number of neighbouring points must be located from the complete array of points which was located in the store of the computer. To aid the identification of points in this section of the programme, each point is now renamed according to its distance from the N = 0 plane.

Consider a series of planes parallel to N = 0 plane, which have a spacing interval of SPACN. On the trailing-edge side of the axes X, Z a column plane is chosen as a datum plane NK = 0 and all the column planes spaced SPACN are identified consecutively from the datum as NK = 1, 2, 3, ... (Fig. 5). The numerical value of the NK plane containing the X, Y axes (i.e. N = 0 plane) is represented by NKKN in the programme. The value of NKKN is controlled by an input statement and its value is further discussed in Section 5.1.

Thus in the centre of the blade surface where the spacing of the surface points is SPACX, every fifth NK plane will be an N plane. Points which hold the same value of the identifier NK will be physically on the same column plane, and hence are easily distinguished from the complete array of points.

The 16 points which surround a given mesh point from which a normal is to be erected are located using the NK identification above. These points are then re-identified by a separate nomenclature KA. The mesh point is chosen to be the point KA = 5. The points on the row plane passing through KA = 5 are identified as L = 1 amd KA = 1 to 9 in the same sense as the positive direction of NNN (See Fig. 5). The points on a column plane through KA = 5 are denoted by L = 2 and KA = 1 to 9 in the same sense as the positive X direction. Each of these points KA = 1 to 9 must have the same spacing interval.

3.2.2 Extra - Surface Points

To identify points outside the blade surface in the section of the programme which computes the direction cosines of the normals, and the machining co-ordinates, (i.e. Stage (2) Section 3.1) the following pair of reference axes are used (Fig. 4).

(1) A set of right-handed cartesian axes XN, YN, ZN which are parallel to the X, Y, Z ares but with XN displaced a distance YD from X, and with YN displaced a distance ZD from Y (See Fig. 4). This set of axes is only used to identify the machining points associated with the face surface.

(2) A set of right-handed cartesian axes XM, YM, ZM obtained by rotating bodily the set of axes XN, YN, ZN about the X axis as shown in Fig. 4. This set of axes identifies machining points associated with the back surface.

The co-ordinates of points related to these axes are specified as XXX(J), YYY(J), ZZZ(J) where J = 1 or 2 refers to the back or face and hence identifies which set of axes is being considered.

3.3 Computation of Surface Points

The computation of the co-ordinates of points on the blade surface from the blade shape equations is divided into two sections:-

(1) Computation of points on the boundary edge of the blade surface for each row plane.

(2) Computation of points on the blade surface at the intersection of each row and column plane.

3.3.1 Computation of Boundary Points

The co-ordinates of points on the leading and trailing edges on a

given row plane are calculated and stored so that the calculation of points in the following section 3.3.2 can be confined to only the blade surface (See Fig. 2/1).

The iterative convergence procedure called "Regular Falsi" is used to compute these boundary points (See Fig. 2/13). Here the independant variable, radius RX, is adjusted to make the dependent variable, length-of-the-arc CA equal to CB a known proportion of the chord at the radial distance RX. These distances are shown in Fig. 5. Before entering the "Regular Falsi" routine the distance RX (See Fig 2) was approximated by

$$RX = RADM * PERCR + X \qquad \ldots \quad 14.$$

where X = X ordinate of the row plane

The value of PERCR must be selected to produce CA just greater than CB for all row planes of the impeller.

The Regular Falsi procedure is as follows.

The value of RX is progressively decreased until the difference between CA and CB changes its numerical sign. At this stage, the desired value of RX is between the two previous values. The calculation is then repeated for a value of RX midway between these two values. The values of RX which surround the desired value are again selected from the preceeding two values of RX and the current value. The convergence procedure is continued until the required accuracy is obtained.

At each station, the leading and then trailing edge co-ordinates are computed and then stored as subscripted variable in I (the row plane number).

The computation in this section is shown diagramatically in the flow diagrams Fig. 2/1 and 2/13.

3.3.2 Computation of Surface Points

Before entering the computing routine for the surface points, the subscripted variable YB(I,NNN) (i.e. the Y ordinate) for each point on the two-dimensional fundamental mesh which covers the blade surface is equated to zero. This is a necessary condition for the calculation stage to be described in Section 3.4.

The geometry of each blade section is specified by three variables CX, TX, AM and by equations for the thickness form and mean line profile (See Fig. 6). From this data the Z ordinate (of the surface) at a given surface point is computed by an iterative procedure (See Figs. 2/2 to 2/6). By considering a cylindrical blade section passing through a point (I, N) an initial approximation of the distance along the chord line to the desired surface point at (I, N) is made by assuming this distance to be equal to XC the distance between E and Q (See Fig. 6).

At this cylindrical distance XC from the leading edge, the co-ordinates for the points on the blade surface are computed and compared with the desired values. The value of XC is then progressively adjusted using the "Regular Falsi" iterative convergence technique until the co-ordinates are determined to within the desired accuracy.

The calculated co-ordinates of the chosen points on the surface are designated by the subscripted variable (I, NNN). The subscripted index NNN refers to the numerical order of the points in the positive YB direction from the trailing edge to the leading edge, and is centred about a point on the X, Z plane where NNN = NN. This method of subscripting is in contrast with the more usual method of naming points according to their distance for a reference axis. The former method was chosen because the available storage locations in the main store of

the IBM 709/7090 II computer were limited. The execution time for this programme would have been greatly increased if these variable had to be placed on a magnetic tape store. These factors necessitated keeping a numerical count of the number of points on each row plane (I) which had spacing intervals SPACX and SPACN. A knowledge of this numerical count was also necessary before the co-ordinates of points surrounding any given point could be selected from the stored variables specifying the given point.

3.4 Direction Cosine at a Point

Since the mesh of points set up to cover the blade surface is rectangular, some of the mesh points lie in a region outside the blade area and are therefore disregarded in the following computational routine. These points are easily distinguished because their YB ordinates have previously been equated to zero (Section 3.3.2) whereas all other points on the surface have values of YB(I,NNN, J) greater than zero (Fig. 2/7)

In turn, at each surface mesh points (I, NNN, J) the co-ordinates of sixteen points arranged about the given mesh points as shown in Fig. 5 are selected from the complete store of points (See Fig. 2/7 to 2/12). The spacing distance between points in the row plane and the column plane must be equal. These points are re-identified as KA = 1 to 9 on both the row plane and the column plane, in both cases being centred about the given mesh point (KA = 5). From these sixteen selected points, the most symmetrical array of eight points surrounding the given mesh point on the blade surface is selected (Fig. 2/12).

The intersection of the row plane through the mesh point, and the surface of the blade, determines a space curve through the point - the "row space curve". Similarly the intersection of the column plane through the mesh point, and the blade surface, determines the "column space curve". The gradient (i.e. differential coefficient) of the row space curve at the mesh point, can now be found by substituting the ordinates of the four selected points on the row plane plus the ordinate of the mesh point into the appropriate equation for a five-point Gregory-Newton differentiation. Similarly, the gradient of the column space curve at the mesh point can be found. Each gradient is of course, equal to the slope of the tangent to the curve.

By combining the gradients of the two space curves through the mesh point, the direction cosines of the normal to the surface is calculated as follows.

Equation of tangent to row space curve at mesh point XB, YB, ZB is given by,

$$z = a(y - YB) + ZB \qquad \ldots \quad 15.$$

where a = GRAD(1,J) = Slope of tangent to surface in YB direction

Similarly the equation to column space curve at mesh point is given by,

$$z = b(x - XB) + ZB \qquad \ldots \quad 16$$

where b = GRAD(2,J) = Slope of tangent to surface in XB direction

Hence equation of plane containing both tangents is given by,

$$ax + by - z = aXB + bYB - ZB \qquad \ldots \quad 17$$

The direction cosines COSA, COSB, COSC of the outward pointing normal to the back surface are

$$\frac{-\,GRAD(2,J),\ -\,GRAD(I,J),\ +1}{\sqrt{GRAD^2(2,J) + GRAD^2(I,J) + 1}} \qquad \ldots \quad 18$$

Note that:-

$$\left.\begin{array}{l}\text{Direction cosines of normal}\\ \text{to back surface}\end{array}\right\} = -\ \text{Direction cosines of normal to face surface} \qquad \ldots \quad 19$$

The position of the centre of the milling cutter along the normal to the given surface at the mesh point is now calculated, and specified in terms of the machining axes (Fig. 4). The information required by the machinist is not the blade surface dimensions, but the motions of the three lead screws necessary to traverse the cutter from the known origin of the axes to the point in question. Hence it was necessary to convert each co-ordinate of the cutter centre into an equivalent number of complete turns and parts of a turn (i.e. thousandths of an inch) of the appropriate lead screw. Since the machinist can easily check the position of the bottom of the cutter, it is more useful for the position of this point to be specified than the position of the cutter centre. Thus the final print-out is in terms of the position of the bottom of the cutter.

Since the blade surface has so far only been determined accurately up to but not at the blade edge, further points are required to define the actual blade edge. These points are calculated by a similar differentiation technique to that used for the points on the surface. These edge points are then specified with reference to the same machining axes described above and illustrated in Fig. 4. The corresponding

positions of the cutter are also calculated. The blade shape is further defined by specifying the radius of the leading edge (RLE(I)) at each row plane.

4.0 STABILITY OF CALCULATIONS

When applying this computing technique to an impeller or propeller design, care must be taken to ensure that the iterative routines incorporated in the solution do in fact converge. The rate and accuracy of the convergence must also be checked.

The two iterative procedures in the programme are considered separately in the following.

4.1 Convergence in computing boundary points. (Ref. Section 3.3.1)

This routine is convergent provided that the initial value assumed for RX is greater than the actual value of RX at a given row plane. This is governed by statement number (170 + 0002) Table 2.

```
RX = X + RADM * PERCR                                    ...  20
```

The value of PERCR can be adjusted for each impeller design and is submitted to the programme by an input statement.

The rate of convergence is governed by statement

```
230  RX = RX - STEP1                                     ...  21
```

The accuracy of the calculation of the boundary point is determined by the test statement

```
IF(ABSF(CA - CB) - DEVN1)270, 270, 260                   ...  22
```

This terminates the calculation of CB when an accuracy of less than + or - (DEVN1) of an inch is obtained.

4.2 Convergence in computing points on surface (Ref. Section 3.3.2) 22.

(1) In Stage 1 of the computation the N plane on which the surface point is located is progressively moved closer to the trailing edge of the blade. The position of the surface point on an N plane near the trailing edge needs careful investigation. This surface point must be located on the actual blade surface, i.e. the face or back surface, and not on the square region of the edge (See detail A Fig. 6).

In statement (430 + 0001) Table 2, the Y ordinate of the N^{th} plane is tested to determine whether the plane cuts the blade on the blade surface or not. The significant variable in this expression is YYTE. This variable represents the value of the distance, parallel to the X, Y plane, from the intersection of the chord line and the trailing edge to the intersection of the face surface of the blade and the trailing edge, at a given row plane. The value of YYTE is derived from the allowable edge thickness ALTE, and the actual blade thickness Y0, at XC = 1.0. This value Y0 is referred to in the programme as DEVN2. (See statement 348, Table 2). DEVN2 exists because of the inaccuracies in the equation defining the thickness form. The actual value of Y0 at XC = 1.0 for the NACA - 16 profile is zero. The extra factor of 1.0001 in statement 348 increases the distance YYTE to allow for accumulated errors in the computation.

If another thickness form is used in place of the NACA - 16, the value of DEVN2 submitted as input to this programme should be a zero or positive value although its actual value may be

negative.

(2) By choosing an initial value of XC as given in statement (654 + 0004) (Table 2) a solution is always possible provided --

$0 \leqslant XX \leqslant 1.0$ where $XX = XC/CX$ ... 23.

i.e. XX must be within the blade section.

If during the iteration the value of XX (See statements 790, 810) falls outside the above range, it is forced to hold one of the limiting values.

As with the first convergence routine, the rate of convergence and accuracy are governed by statements 790, 810, and 820, (Table 2) and values of STEP2 and DEVN3.

5.0 INPUT/OUTPUT INSTRUCTIONS AND EXECUTION TIME

5.1 Input instructions

The programme as written (Table 2) will accept data for any impeller or propeller satisfying the stated conditions and whose blade shape is capable of being expressed by equations of the form given in Section 2.0.

An example of the input data, taken from the HYDRO - 1 impeller, is shown in Table 3. The values of most the variable have dimensions in feet and apply to the prototype impeller (See Table 5).

The following items in the input data require further discussion.

The values of the constants YD and ZD must be chosen to maintain all values of YN(I,NNN), PTY(J) and PTZ(J) positive. This places the origin of the axes XB, YB, ZB and XN, YN, ZN, and XM, YM, ZM outside the fundamental mesh which covers the blade surface.

The value of NN must be at least four (4) more than the maximum

number of points to be calculated in any one row plane on the trailing edge side of the N = 0 plane section. The value of NKKN must be divisible by five (5) and equal to or greater than the maximum value of

$$NTE(I) + 4* MTE(I) + 4 \qquad \ldots \quad 24.$$

The maximum value of this expression occurs where the projected blade area on the X, Y plane has the maximum Y dimension.

The dimension of YB (I,NNN) in the X direction, i.e. I, must be at least 8 more than the total number of row planes required. The other subscripted variables referring to row planes RXLE(I), NLE(I) etc. must have the I^{th} subscript greater than the total number of row planes, by at least four (4).

The dimension of YB(I,NNN) and ZB(I,NNN,J) in the YB direction i.e. NNN, must be at least twice the value of NN.

The machining dimensions can be calculated for points between any two row planes. The input variables controlling this are the values of IP and IPAT. The value of IP selects the beginning point for the calculation and is the $(IP + 4)^{th}$ row plane. The value of IPAT determines the end row plane with I = (IPAT + 4) where the calculation ceases. If the (IP + 4) and (IPAT + 4) row planes lie within the blade surface area and are not on the edge of this surface then the variables associated with the first two and the last two row planes have small errors due to the differentiation in Section 3.4.

Care must be taken when choosing the value of DEVN2, and reference should be made to Section 4.2 for a discussion on its value.

As previously mentioned in Section 4.0 the initial value of RX and also the rate and accuracy of convergence in the two "Regular

Falsi" routines, must be carefully selected.

If the leading and trailing edges are to be adequately defined then the value of PCX must be less than 0.90. This variable PCX determines the point where the spacing of column planes change from SPACX to the smaller spacing of SPACN.

If a progressive print-out of all major calculations and decisions in the programme is needed NTEST should be set to a positive number, otherwise it should be zero or negative.

The programme as written occupied approximately 25,300 words in the store of an IBM 709/7090 II computer with main storage capacity of 32,561 words.

5.2 Output Instructions

The machining technique governs the form of the output instructions. The output for the Hydrojet impeller was chosen to be punched cards, which were later listed. These output instructions are in a form suitable for the machinist of a hand-operated vertical milling machine.

The machining instructions for the back and face surfaces of the blade could not be separated in the computer without increasing storage and running time. Each alternate card of output thus refers to the same blade surface. The deck of output cards may be later processed by an IBM Collator, to separate the alternate cards.

In the output listing the row planes are called stations and are numbered from one (1) at the blade tip. Thus each station is actually the $(I + 4)^{th}$ row plane.

Associated with each point on the blade surface and its machining co-ordinates there is a reference number. This reference number is actually the number of the NK^{th} column plane which passes through the point. All surface points with the same reference number NK are

physically on the same column plane.

The example of the machining instructions given in Table 4 is for the HYDRO - 1 impeller at a station on the back surface. Fig. 7 shows a plot of computed points on the back and face surface of the impeller at selected sections.

5.3 Execution Time

The average time taken by the IBM 709/7090 to calculate the machining co-ordinates for 100 mesh points (i.e. 100 points on both the back and face surface) was approximately 21 seconds. Thus the execution time required for the 3,666 mesh points of the impeller HYDRO - 1 was 765 seconds.

REFERENCES

1. HALE, M.R: The Design of Ducted Impellers using a Vortex line Analysis and an Optimizing Computer Technique. University of Adelaide, Dept. of Mech. Eng. Mech. Eng. R65/3.

2. O'BRIEN, T.P: The Design of Marine Screw Propellers. Hutchinson & Co. Ltd. London. 1962.

3. HASTINGS, C.J: Approximations for Digital Computers. Princeton University Press. 1955.

4. ABBOTT, I.H. and VON DOENHOFF, A.E: Theory of Wing Sections - including a Summary of Aerofoil Data. Dover Publications, Inc., New York, also NACA Rep. 824 - 1945.

5. NEWELL H.E: "Vector Analysis" McGraw Hill. 1955.

Table 1. Impeller Dimensions and Characteristics.

DESIGN PARAMETERS HYDROJET IMPELLER

DESIGN ASSUMPTIONS
BETZ MIN ENERGY CONDITION
CONSTANT AXIAL VELOCITY
NACA PROFILE SHOCK FREE ENTRY

RADIUS	VELOCITY	ROTATION	BLADES	IDEAL EFF	TOTAL EFF	THRUST	SHP
7.50	19.30	1.50	4	0.9733	0.8599	44800.	1807.

TIP CHORD	BOSS CHORD	BOSS RATIO	TIP IMMERSION	ALLOWABLE STRESS
5.000	3.000	0.200	11.50	7250.

RAD FRAC	CHORD	THICKNESS	MEAN LINE	ANGLE BI	LIFT COEF	DRAG/LIFT
1.00	5.000	0.2250	0.0926	15.67	0.249	0.030
0.95	4.875	0.2194	0.0876	16.45	0.241	0.031
0.90	4.750	0.2137	0.0826	17.31	0.233	0.032
0.85	4.625	0.2081	0.0776	18.26	0.225	0.033
0.80	4.500	0.2025	0.0726	19.32	0.217	0.034
0.75	4.375	0.1969	0.0675	20.51	0.207	0.036
0.70	4.250	0.1912	0.0625	21.84	0.197	0.038
0.65	4.125	0.2035	0.0574	23.34	0.187	0.040
0.60	4.000	0.2302	0.0523	25.06	0.175	0.044
0.55	3.875	0.2562	0.0471	27.02	0.163	0.049
0.50	3.750	0.2813	0.0419	29.29	0.150	0.056
0.45	3.625	0.3056	0.0367	31.94	0.136	0.066
0.40	3.500	0.3289	0.0315	35.04	0.121	0.080
0.35	3.375	0.3508	0.0263	38.71	0.104	0.100
0.30	3.250	0.3723	0.0211	43.08	0.087	0.130
0.25	3.125	0.3915	0.0160	48.29	0.069	0.178
0.20	3.000	0.4056	0.0112	54.51	0.050	0.264

Table 1. Continued.

RAD FRAC	ST F	ST B	ST E	ST N	CAVT S	CAVT P	THRUST GRAD	TORQUE GRAD
1.00	0.	0.	0.	0.	0.555	0.347	0.181E 06	0.425E 06
0.95	140.	-127.	113.	113.	0.615	0.340	0.155E 06	0.363E 06
0.90	505.	-550.	385.	386.	0.685	0.333	0.132E 06	0.308E 06
0.85	1149.	-1330.	834.	834.	0.766	0.325	0.111E 06	0.259E 06
0.80	2089.	-2476.	1444.	1441.	0.861	0.317	0.922E 05	0.216E 06
0.75	3392.	-4061.	2229.	2216.	0.973	0.309	0.759E 05	0.177E 06
0.70	5095.	-6113.	3168.	3139.	1.106	0.300	0.616E 05	0.144E 06
0.65	6204.	-7246.	3300.	3246.	1.265	0.303	0.492E 05	0.115E 06
0.60	6454.	-7248.	2758.	2673.	1.457	0.318	0.386E 05	0.906E 05
0.55	6657.	-7247.	2330.	2201.	1.690	0.334	0.296E 05	0.699E 05
0.50	6829.	-7248.	1989.	1800.	1.975	0.349	0.221E 05	0.528E 05
0.45	6976.	-7249.	1717.	1446.	2.327	0.365	0.159E 05	0.387E 05
0.40	7101.	-7247.	1503.	1122.	2.762	0.381	0.110E 05	0.274E 05
0.35	7211.	-7247.	1346.	816.	3.303	0.397	0.719E 04	0.185E 05
0.30	7247.	-7184.	1236.	507.	3.969	0.415	0.433E 04	0.118E 05
0.25	7247.	-7099.	1191.	194.	4.779	0.432	0.228E 04	0.695E 04
0.20	7251.	-7030.	1230.	-135.	5.727	0.446	0.920E 03	0.365E 04

Table 2. - Programme Listing.

```
C     **1330 M R HALE/FOWLER MECH ENG DEPT U OF A TEL 461**
C     **RECT COORDINATES  MACHINING DIMENSIONS**
C     **PROGRAMME NO 0022/7090**
  010 FORMAT(1H4,42H  PATTERN COORDINATES OF HYDROJET IMPELLER)
  015 FORMAT(1H0,47H MACHINING COORDINATES UNIFORM RECTANGULAR GRID)
  020 FORMAT(1H0,15H MODEL SCALE  =,F7.3)
  021 FORMAT(1H ,15H MODEL RADIUS =,F7.3,3HINS)
  025 FORMAT(1H0,20H REFERENCE DISTANCES)
  030 FORMAT(1H0,41H  REF PT TO LINE OF CENTROID IN Y DIRCN =,F7.3)
  035 FORMAT(1H ,41H  REF PT TO LINE OF CENTROID IN Z DIRCN =,F7.3)
  040 FORMAT(1H1,I3,11H STATION NO,9X,16HBACK COORDINATES)
  041 FORMAT(1H1,I3,11H STATION NO,9X,16HFACE COORDINATES)
  045 FORMAT(1H0,30H  RADIAL DISTANCE TO STATION =,F8.3)
  048 FORMAT(1H0,11X,22HMACHINING  COORDINATES,16X,16HBOTTOM OF CUTTER)
  049 FORMAT(1H5,6X,17HPOINTS ON SURFACE)
  050 FORMAT(1H ,9X,1HX,12X,1HY,12X,1HZ,12X,1HX,8X,1HY,8X,1HZ)
  051 FORMAT(1H5,5X,1HX,8X,1HY,8X,1HZ)
  055 FORMAT(1H ,39H  NO REV THOU      REV THOU      REV THOU)
  060 FORMAT(1H ,I4,I4,I5,I8,I5,I8,I5,4X,3F9.3)
  062 FORMAT(1H ,4X,F9.3,4X,F9.3,4X,F9.3)
  065 FORMAT(1H0,18H  ST CHORD WIDTH =,F8.3,7X,11HLE RADIUS =,F6.3)
  066 FORMAT(1H5,3F9.3,I6)
  067 FORMAT(1H ,43X,3F9.3)
  068 FORMAT(1H ,I4)
  070 FORMAT(4E14.7/5I7/5E14.7/3E14.7/5E14.7/4E14.7)
  080 FORMAT(3E14.7/4E14.7/5E14.7/5E14.7/3E14.7/5E14.7/5E14.7)
  090 FORMAT(5F10.5,F8.3,I5)
  091 FORMAT(4F10.3,I8)
      DIMENSIONRXLE(57),RXTE(57),YLE(57),YTE(57),RLE(57),NLE(57),MLE(57)
     1,NTE(57),MTE(57),YB(61,120),Z(2),ZB(57,120,2),YC(2,9),PT(2,9,2),
     2GRAD(2,2),PTX(2),PTY(2),PTZ(2),YYY(2),ZZZ(2)
      COMMONYB
  100 READINPUTTAPE2,070,RAD,RATIO,SCALE,SCALM,IP,IPAT,NN,NKKN,NTEST,
     1DX,SPACX,SPACN,PCX,PERCR,YD,ZD,ALTE,STEP1,STEP2,DEVN1,DEVN2,DEVN3,
```

Table 2

Table 2. - Continued.

```
     2CUTR,XMILR,YMILR,ZMILR
      READINPUTTAPE2,080,COD,CID,CX7,T0,T1,T2,T3,A0,A1,A2,A3,A4,AMO,
     1AMI,ANGO,ANGI,PD,HBC,YBCT,RADLE,Y0,Y1,Y2,Y3,Y4,Y5,Y6,Y7,Y8,Y9
      UNIT=12.0/SCALE
      RADM=RAD*UNIT
      PUNCH010
      PUNCH010
      PUNCH015
      PUNCH015
      PUNCH020,SCALE
      PUNCH020,SCALE
      PUNCH021,RADM
      PUNCH021,RADM
      PUNCH025
      PUNCH025
      PUNCH030,YD
      PUNCH030,YD
      PUNCH035,ZD
      PUNCH035,ZD
C     **COMPUTING END POINTS AT SPECIFIED RADIAL DISTANCES**
      PI=3.1415927
      PITCH=PD*2.0*RADM
      COD=COD*UNIT
      CID=CID*UNIT
      AMO=AMO*UNIT
      AMI=AMI*UNIT
      YR=(1.0-HBC)*COD*COSF(ANGO)+YBCT*AMO*SINF(ANGO)
      XOL=RADM*COSF(YR/RADM)
      YR=(1.0-HBC)*CID*COSF(ANGI)+YBCT*AMI*SINF(ANGI)
      XIL=RATIO*RADM*COSF(YR/(RATIO*RADM))
      YR=-HBC*COD*COSF(ANGO)+YBCT*AMO*SINF(ANGO)
      XOT=RADM*COSF(YR/RADM)
      YR=-HBC*CID*COSF(ANGI)+YBCT*AMI*SINF(ANGI)
      XIT=RATIO*RADM*COSF(YR/(RATIO*RADM))
      IPP=IP+4
      II=IPAT+4
```

Table 2. - Continued.

```
      DO330I=IPP,II
      A=I-5
      X=RADM-DX*A
      DO310M=1,2
      IF(M-1)1000,110,140
  110 IF(X-XOL)130,130,120
  120 RXLE(I)=RADM
      RLE(I)=0.0
      YLE(I)=SQRTF(RADM*RADM-X*X)
      GOTO310
  130 IF(X-XIL)1000,170,170
  140 IF(X-XOT)160,160,150
  150 RXTE(I)=RADM
      YTE(I)=-SQRTF(RADM*RADM-X*X)
      GOTO310
  160 IF(X-XIT)1000,170,170
  170 RB=0.0
      RA=0.0
      RX=X+RADM*PERCR
  180 CA=RX*ATANF(SQRTF(RX*RX-X*X)/X)
      IF(M-1)1000,190,200
  190 K=1
      GOTO600
  195 CB=(1.0-HBC)*CX*COSF(ANG)+YBCT*AM*SINF(ANG)
      GOTO210
  200 K=2
      GOTO600
  205 CB=HBC*CX*COSF(ANG)-YBCT*AM*SINF(ANG)
  210 IF(CA-CB)240,270,220
  220 RA=RX
      IF(RB)1000,230,250
  230 RX=RX-STEP1
      GOTO180
  240 RB=RX
  250 IF(ABSF(CA-CB)-DEVN1)270,270,260
  260 RX=0.5*(RA+RB)
```

Table 2. - Continued.

```
      GOTO180
  270 IF(M-1)1000,280,300
  280 RXLE(I)=0.5*(RA+RB)
      YLE(I)=SQRTF(RXLE(I)*RXLE(I)-X*X)
      RX=RXLE(I)
      K=3
      GOTO600
  290 RLE(I)=RADLE*TX*TX/CX
      GOTO310
  300 RXTE(I)=0.5*(RA+RB)
      YTE(I)=-SQRTF(RXTE(I)*RXTE(I)-X*X)
  310 CONTINUE
      IF(NTEST)330,330,320
  320 WRITE OUTPUT TAPE 3,090,X,RXLE(I),RXTE(I),YLE(I),YTE(I),RLE(I),I
  330 CONTINUE
C     **CALCULATING COORDINATES OF POINTS ON SURFACE**
C     **UNIFORM GRID SPACING**
      III=IPAT+8
      NN2=NN*2
      DO340I=1,III
      DO340N=1,NN2
  340 YB(I,N)=0.0
      DO550I=IPP,II
      A=I-5
      X=RADM-DX*A
      IF(I-5)1000,344,346
  344 NLE(I)=0
      MLE(I)=0
      NTE(I)=0
      MTE(I)=0
      GOTO515
  346 NLE(I)=10*NN
      NTE(I)=10*NN
      RX=RXTE(I)
      K=8
      GOTO600
```

Table 2. - Continued.

```
348 YYTE=(ALTE*SCALM/2.0+DEVN2*TX)*1.0001*SINF(ANG)/SCALE
    DO510M=1,2
    Y=0.0
    DO510N=1,NN
    IF(M-1)1000,350,400
350 IF(N-NLE(I)-1)360,510,510
360 IF(Y-PCX*YLE(I))370,380,380
370 Y=Y+SPACX
    MLE(I)=N
    GOTO450
380 Y=Y+SPACN
    IF(Y-YLE(I))450,390,390
390 NLE(I)=N-1
    GOTO510
400 IF(N-NTE(I)-1)410,510,510
410 IF(Y-PCX*YTE(I))430,430,420
420 Y=Y-SPACX
    MTE(I)=N
    GOTO450
430 Y=Y-SPACN
    IF(Y-(YTE(I)+YYTE))440,440,450
440 NTE(I)=N-1
    GOTO510
450 RX=SQRTF(X*X+Y*Y)
    IF(RX-RATIO*RADM)460,470,470
460 Z(1)=0.0
    Z(2)=0.0
    YA=-YD
    GOTO480
470 K=4
    YA=Y
    IF(M-1)1000,471,472
471 YR=+RX*ATANF(SQRTF(RX*RX-X*X)/X)
    GOTO600
472 YR=-RX*ATANF(SQRTF(RX*RX-X*X)/X)
    GOTO600
```

Table 2. - Continued.

```
  480 IF(M-1)1000,490,495
  490 NNN=NN+N
      GOTO496
  495 NNN=NN-N
  496 ZB(I,NNN,1)=Z(1)
      ZB(I,NNN,2)=Z(2)
      YB(I,NNN)=YA+YD
      IF(NTEST)510,510,500
  500 WRITE OUTPUT TAPE 3,091,ZB(I,NNN,1),YB(I,NNN),ZB(I,NNN,2),X,NNN
  510 CONTINUE
  515 RX=X
      YR=0.0
      K=5
      IF(RX-RATIO*RADM)520,600,600
  520 Z(1)=0.0
      Z(2)=0.0
      YR=-YD
  530 ZB(I,NN,1)=Z(1)
      ZB(I,NN,2)=Z(2)
      YB(I,NN)=YR+YD
      IF(NTEST)550,550,540
  540 WRITE OUTPUT TAPE 3,091,ZB(I,NN,1),YB(I,NN),ZB(I,NN,2),X,NN
  550 CONTINUE
C     **DETERMINATION OF DIRECTION COSINES AT A POINT**
C     **HENCE CORRECTING COORDINATES FOR THOSE AT BOTTOM OF CUTTER**
      DO3000I=IPP,II
      A=I-5
      IA=I-4
      X=RADM-DX*A
      PUNCH040,IA
      PUNCH041,IA
      PUNCH045,X
      PUNCH045,X
      PUNCH048
      PUNCH048
      PUNCH049
```

Table 2.

Table 2. - Continued.

```
      PUNCH049
      PUNCH050
      PUNCH050
      PUNCH051
      PUNCH051
      PUNCH055
      PUNCH055
C     **TRAILING EDGE COORDINATES**
      SPX=12.0*DX
      IF(X+2.0*DX-XOT)1140,1180,1110
 1110 IF(X+DX-XOT)1130,1130,1115
 1115 IF(X-XOT)1120,1120,1400
 1120 GDT=(3.0*YTE(I+4)-16.0*YTE(I+3)+36.0*YTE(I+2)-48.0*YTE(I+1)+
     125.0*YTE(I))/SPX
      GOTO1200
 1130 GDT=(-YTE(I+3)+6.0*YTE(I+2)-18.0*YTE(I+1)+10.0*YTE(I)+3.0*YTE(I-1)
     1)/SPX
      GOTO1200
 1140 IF(X-2.0*DX-XIT)1150,1180,1180
 1150 IF(X-DX-XIT)1170,1160,1160
 1160 GDT=(-3.0*YTE(I+1)-10.0*YTE(I)+18.0*YTE(I-1)-6.0*YTE(I-2)+YTE(I-3)
     1)/SPX
      GOTO1200
 1170 GDT=(-25.0*YTE(I)+48.0*YTE(I-1)-36.0*YTE(I-2)+16.0*YTE(I-3)-
     13.0*YTE(I-4))/SPX
      GOTO1200
 1180 GDT=(YTE(I+2)-8.0*YTE(I+1)+8.0*YTE(I-1)-YTE(I-2))/SPX
 1200 RX=RXTE(I)
      K=6
      GOTO600
 1210 ANGLE=ATANF(GDT)
      PZ=-HBC*CX*SINF(ANG)-YBCT*AM*COSF(ANG)
      BZ=ZD-PZ+CUTR
      FZ=ZD+PZ+CUTR
      FY=YD+YTE(I)-CUTR*COSF(ANGLE)
      BY=YD-YTE(I)+CUTR*COSF(ANGLE)
```

Table 2. - Continued.

```
      PX=X+CUTR*SINF(ANGLE)
      PUNCH067,PX,BY,BZ
      PUNCH067,PX,FY,FZ
C     **POINTS IN BLADE AREA--RENUMBERING POINTS ABOUT LINE OF CENTROID
C     ** AS N=NN  HENCE SELECTING  4 PTS SURROUNDING THE PT ON EACH SIDE
 1400 NA=NN-NTE(I)
      NB=NN-MTE(I)
      NC=NN+MLE(I)
      ND=NN+NLE(I)
      DO2600N=NA,ND
      IF(YB(I,N))1000,2600,1410
 1410 IF(N-NB)1430,1420,1420
 1420 IF(N-NC)1550,1550,1650
 1430 NK=NKKN-4*MTE(I)-NN+N
      SPAC=SPACN
      DO1540KA=1,9
      NKK=NK-5+KA
      NNN=NKK-NKKN+4*MTE(I)+NN
      IF(NNN-NB)1480,1480,1470
 1470 YC(1,KA)=0.0
      GOTO1490
 1480 YC(1,KA)=YB(I,NNN)
      PT(1,KA,1)=ZB(I,NNN,1)
      PT(I,KA,2)=ZB(I,NNN,2)
 1490 III=I+5-KA
      NNN=NK-NKKN+4*MTE(III)+NN
      IF(NNN-(NN-MTE(III)))1530,1530,1500
 1500 IF((NK+4)/5-NK/5)1000,1520,1510
 1510 YC(2,KA)=0.0
      GOTO1540
 1520 NNN=(NK-NKKN)/5+NN
 1530 IF(NNN)1535,1535,1534
 1534 IF(NNN-NN2)1536,1536,1535
 1535 YC(2,KA)=0.0
      GOTO1540
 1536 YC(2,KA)=YB(III,NNN)
```

Table 2

Table 2. - Continued.

```
      PT(2,KA,1)=ZB(III,NNN,1)
      PT(2,KA,2)=ZB(III,NNN,2)
1540  CONTINUE
      GOTO2000
1550  NK=NKKN-5*(NN-N)
      SPAC=SPACX
      DO1640KA=1,9
      NKK=NK-25+5*KA
      NNN=(NKK-NKKN)/5+NN
      IF(NNN-NB)1560,1560,1570
1560  NNN=NKK-NKKN+4*MTE(I)+NN
      IF(NNN)1585,1585,1590
1570  IF(NNN-NC)1590,1580,1580
1580  NNN=NKK-NKKN-4*MLE(I)+NN
      IF(NNN-NN2)1590,1585,1585
1585  YC(1,KA)=0.0
      GOTO1595
1590  YC(1,KA)=YB(I,NNN)
1595  PT(1,KA,1)=ZB(I,NNN,1)
      PT(1,KA,2)=ZB(I,NNN,2)
      III=I+5-KA
      NNN=(NK-NKKN)/5+NN
      IF(NNN-(NN-MTE(III)))1600,1600,1610
1600  NNN=NK-NKKN+4*MTE(III)+NN
      GOTO1630
1610  IF(NNN-(NN+MLE(III)))1630,1620,1620
1620  NNN=NK-NKKN-4*MLE(III)+NN
1630  IF(NNN)1635,1635,1634
1634  IF(NNN-NN2)1636,1636,1635
1635  YC(2,KA)=0.0
      GOTO1640
1636  YC(2,KA)=YB(III,NNN)
      PT(2,KA,1)=ZB(III,NNN,1)
      PT(2,KA,2)=ZB(III,NNN,2)
1640  CONTINUE
      GOTO2000
```

Table 2.

Table 2. - Continued.

```
1650 NK=NKKN+4*MLE(I)-NN+N
     SPAC=SPACN
     DO1730KA=1,9
     NKK=NK-5+KA
     NNN=NKK-NKKN-4*MLE(I)+NN
     IF(NNN-NC)1660,1670,1670
1660 YC(1,KA)=0.0
     GOTO1680
1670 YC(1,KA)=YB(I,NNN)
     PT(1,KA,1)=ZB(I,NNN,1)
     PT(1,KA,2)=ZB(I,NNN,2)
1680 III=I+5-KA
     NNN=NK-NKKN-4*MLE(III)+NN
     IF(NNN-(NN+MLE(III)))1690,1720,1720
1690 IF((NK+4)/5-NK/5)1000,1710,1700
1700 YC(2,KA)=0.0
     GOTO1730
1710 NNN=(NK-NKKN)/5+NN
1720 IF(NNN)1725,1725,1724
1724 IF(NNN-NN2)1726,1726,1725
1725 YC(2,KA)=0.0
     GOTO1730
1726 YC(2,KA)=YB(III,NNN)
     PT(2,KA,1)=ZB(III,NNN,1)
     PT(2,KA,2)=ZB(III,NNN,2)
1730 CONTINUE
C    **ROUTINE FOR DETERMINING COORDINATES OF CUTTER AT EACH XYZ PTS**
2000 DO2570J=1,2
     NNN=10
     DO2480L=1,2
     IF(L-1)1000,2010,2020
2010 SP=12.0*SPAC
     GOTO2030
2020 SP=12.0*DX
2030 IF(NNN-1)1000,2480,2040
2040 IF(YC(L,3))1000,2350,2380
```

Table 2. - Continued.

```
2350 IF(YC(L,4))1000,2360,2370
2360 IF(YC(L,9))1000,2420,2430
2370 IF(YC(L,8))1000,2420,2440
2380 IF(YC(L,7))1000,2390,2450
2390 IF(YC(L,6))1000,2400,2410
2400 IF(YC(L,1))1000,2420,2470
2410 IF(YC(L,2))1000,2420,2460
2420 NNN=1
     GOTO2480
2430 IF(YC(L,6)*YC(L,7)*YC(L,8))1000,2420,2435
2435 GRAD(L,J)=(-25.0*PT(L,5,J)+48.0*PT(L,6,J)-36.0*PT(L,7,J)+16.0*PT(L
    1,8,J)-3.0*PT(L,9,J))/SP
     GOTO2480
2440 IF(YC(L,6)*YC(L,7))1000,2420,2445
2445 GRAD(L,J)=(-3.0*PT(L,4,J)-10.0*PT(L,5,J)+18.0*PT(L,6,J)-6.0*PT(L,7
    1,J)+PT(L,8,J))/SP
     GOTO2480
2450 IF(YC(L,4)*YC(L,6))1000,2420,2455
2455 GRAD(L,J)=(PT(L,3,J)-8.0*PT(L,4,J)+8.0*PT(L,6,J)-PT(L,7,J))/SP
     GOTO2480
2460 IF(YC(L,4))1000,2420,2465
2465 GRAD(L,J)=(-PT(L,2,J)+6.0*PT(L,3,J)-18.0*PT(L,4,J)+10.0*PT(L,5,J)+
    13.0*PT(L,6,J))/SP
     GOTO2480
2470 IF(YC(L,2)*YC(L,4))1000,2420,2475
2475 GRAD(L,J)=(3.0*PT(L,1,J)-16.0*PT(L,2,J)+36.0*PT(L,3,J)-48.0*PT(L,4
    1,J)+25.0*PT(L,5,J))/SP
2480 CONTINUE
     IF(J-1)1000,2485,2490
2485 YYY(J)=2.0*YD-YB(I,N)
     ZZZ(J)=ZD-ZB(I,N,J)
     GOTO2494
2490 YYY(J)=YB(I,N)
     ZZZ(J)=ZD+ZB(I,N,J)
2494 IF(NNN-1)1000,2495,2500
2495 PUNCH068,NK
```

Table 2. - Continued.

```
      GOTO2570
 2500 DEN=SQRTF(1.0+GRAD(1,J)*GRAD(1,J)+GRAD(2,J)*GRAD(2,J))
      IF(J-1)1000,2510,2520
 2510 COSA=-GRAD(2,J)/DEN
      COSB=-GRAD(1,J)/DEN
      COSC=1.0/DEN
      CPX=X+CUTR*COSA
      CPY=YB(I,N)+CUTR*COSB
      CPZ=ZB(I,N,J)+CUTR*COSC
      PTX(J)=CPX
      PTY(J)=2.0*YD-CPY
      PTZ(J)=ZD-CPZ+CUTR
      GOTO2560
 2520 COSA=GRAD(2,J)/DEN
      COSB=GRAD(1,J)/DEN
      COSC=-1.0/DEN
      CPX=X+CUTR*COSA
      CPY=YB(I,N)+CUTR*COSB
      CPZ=ZB(I,N,J)+CUTR*COSC
      PTX(J)=CPX
      PTY(J)=CPY
      PTZ(J)=ZD+CPZ+CUTR
 2560 B=PTX(J)/XMILR
      KX=B
      B=KX
      C=B*XMILR
      KXX=1000.0*(PTX(J)-C)+0.5
      B=PTY(J)/YMILR
      KY=B
      B=KY
      C=B*YMILR
      KYY=1000.0*(PTY(J)-C)+0.5
      B=PTZ(J)/ZMILR
      KZ=B
      B=KZ
      C=B*ZMILR
```

Table 2.

Table 2. - Continued.

```
      KZZ=1000.0*(PTZ(J)-C)+0.5
      PUNCH060,NK,KX,KXX,KY,KYY,KZ,KZZ,PTX(J),PTY(J),PTZ(J)
 2570 CONTINUE
      PUNCH066,X,YYY(1),ZZZ(1),NK
      PUNCH066,X,YYY(2),ZZZ(2),NK
 2600 CONTINUE
C     **LEADING EDGE COORDINATES**
      IF(X+2.0*DX-XOL)2640,2680,2610
 2610 IF(X+DX-XOL)2630,2630,2615
 2615 IF(X-XOL)2620,2620,3000
 2620 GDT=(3.0*YLE(I+4)-16.0*YLE(I+3)+36.0*YLE(I+2)-48.0*YLE(I+1)+25.0*Y
     1LE(I))/SPX
      GOTO2700
 2630 GDT=(-YLE(I+3)+6.0*YLE(I+2)-18.0*YLE(I+1)+10.0*YLE(I)+3.0*YLE(I-1)
     1)/SPX
      GOTO2700
 2640 IF(X-2.0*DX-XIL)2650,2680,2680
 2650 IF(X-DX-XIL)2670,2660,2660
 2660 GDT=(-3.0*YLE(I+1)-10.0*YLE(I)+18.0*YLE(I-1)-6.0*YLE(I-2)+YLE(I-3)
     1)/SPX
      GOTO2700
 2670 GDT=(-25.0*YLE(I)+48.0*YLE(I-1)-36.0*YLE(I-2)+16.0*YLE(I-3)-3.0*YL
     1E(I-4))/SPX
      GOTO2700
 2680 GDT=(YLE(I+2)-8.0*YLE(I+1)+8.0*YLE(I-1)-YLE(I-2))/SPX
 2700 RX=RXLE(I)
      K=7
      GOTO600
 2710 ANGLE=ATANF(GDT)
      PX=X-CUTR*SINF(ANGLE)
      FY=YD+YLE(I)+CUTR*COSF(ANGLE)
      BY=YD-YLE(I)-CUTR*COSF(ANGLE)
      PZ=(1.0-HBC)*CX*SINF(ANG)-YBCT*AM*COSF(ANG)
      BZ=ZD-PZ+CUTR
      FZ=ZD+PZ+CUTR
      PUNCH067,PX,BY,BZ
```

Table 2. - Continued.

```
      PUNCH067,PX,FY,FZ
      CXST=YLE(I)-YTE(I)
      PUNCH065,CXST,RLE(I)
      PUNCH065,CXST,RLE(I)
 3000 CONTINUE
      GOTO100
C     **ROUTINE FOR CALCULATING PROPERTIES OF BLADE SECTIONS **
C     ** ALSO Z ORDINATE FOR A GIVEN X,Y COORDINATE **
  600 CX=COD-(COD-CID)*(RADM-RX)/(RADM*(1.0-RATIO))
      XR=RX/RADM
      IF(RX-0.7*RADM)620,610,610
  610 TX=0.045*CX
      GOTO650
  620 IF(RX-0.65*RADM)640,630,630
  630 TX=0.045*CX7*UNIT
      GOTO650
  640 TX=(T0+T1*XR+T2*(XR**2)+T3*(XR**3))*UNIT
  650 ANG=ATANF(PITCH/(2.0*PI*RX))
      AM=(A0+A1*XR+A2*(XR**2)+A3*(XR**3)+A4*(XR**4))*UNIT
      GOTO(195,205,290,654,654,1210,2710,348),K
  654 DO840J=1,2
      MTEST=0
      XCA=0.0
      XCB=0.0
      XC=(1.0-HBC)*CX-YR/COSF(ANG)
  655 XX=XC/CX
  660 MTEST=MTEST+1
      IF(MTEST-30)669,670,670
  670 Z(1)=0.0
      Z(2)=0.0
      YA=-YD
      GOTO840
  669 IF(XX)661,661,662
  661 XX=0.0
      GOTO664
  662 IF(XX-1.0)665,663,663
```

Table 2. - Continued.

```
663 XX=1.0
664 YO=0.0
    YM=0.0
    GOTO666
665 YO=(1.0-XX)*0.98879*SQRTF(XX)+YO+Y1*XX+Y2*(XX**2)+Y3*(XX**3)
    YO=YO+Y4*(XX**4)+Y5*(XX**5)+Y6*(XX**6)+Y7*(XX**7)+Y8*(XX**8)
    YO=YO+Y9*(XX**9)
    YM=-((1.0-XX)*LOGF(1.0-XX)+XX*LOGF(XX))/0.6930354
666 IF(XX-0.5)668,668,667
667 YO=YO+ALTE*SCALM*(XX-0.5)/(SCALE*TX)
668 XC=XX*CX
    IF(J-1)1000,690,700
690 YDC=(YM-YBCT)*AM+YO*TX
    GOTO710
700 YDC=(YM-YBCT)*AM-YO*TX
710 GL=(1.0-HBC)*CX-XC
    GP=SQRTF(YDC*YDC+GL*GL)
    IF(GL)720,730,760
720 GAMMA=ATANF(YDC/GL)+PI
    GOTO770
730 IF(YDC)740,1000,750
740 GAMMA=-PI/2.0
    GOTO770
750 GAMMA=PI/2.0
    GOTO770
760 GAMMA=ATANF(YDC/GL)
770 DELTA=GAMMA+ANG
    Z(J)=GP*SINF(DELTA)
    YYR=GP*COSF(DELTA)
    IF(YR-YYR)800,840,780
780 XCA=XC
    IF(XCB)1000,790,820
790 XX=XX-STEP2
    GOTO660
800 XCB=XC
    IF(XCA)1000,810,820
```

Table 2. - Continued.

```
  810 XX=XX+STEP2
      GOTO660
  820 IF(XCA-XCB-DEVN3)840,840,830
  830 XC=(XCA+XCB)*0.5
      GOTO655
  840 CONTINUE
      GOTO(1000,1000,1000,400,530,1000,1000,1000),K
 1000 CALL EXIT
      END
```

Table 4. - Output Machining Instructions.

49 STATION NO BACK COORDINATES

RADIAL DISTANCE TO STATION = 4.000

	MACHINING COORDINATES						BOTTOM OF CUTTER		
	X		Y		Z		X	Y	Z
NO	REV	THOU	REV	THOU	REV	THOU			
							3.764	8.995	7.114
405									
406									
407									
408									
409									
410									
415	15	48	58	108	49	118	3.798	8.608	6.243
420	15	64	57	108	48	60	3.814	8.483	6.060
425	15	79	56	109	47	7	3.829	8.359	5.882
430	15	94	55	109	45	81	3.844	8.234	5.706
435	15	109	54	109	44	34	3.859	8.109	5.534
440	15	124	53	108	42	115	3.874	7.983	5.365
445	15	139	52	106	41	74	3.889	7.856	5.199
450	15	154	51	104	40	37	3.904	7.729	5.037
455	15	169	50	102	39	4	3.919	7.602	4.879
460	15	183	49	100	37	99	3.933	7.475	4.724
465	15	198	48	98	36	72	3.948	7.348	4.572
470	15	213	47	96	35	48	3.963	7.221	4.423
475	15	227	46	93	34	27	3.977	7.093	4.277
480	15	241	45	90	33	8	3.991	6.965	4.133
485	16	6	44	90	31	119	4.006	6.840	3.994
490	16	20	43	88	30	103	4.020	6.713	3.853
495	16	34	42	84	29	88	4.034	6.584	3.713
500	16	48	41	78	28	74	4.048	6.453	3.574
505	16	61	40	73	27	64	4.061	6.323	3.439
510	16	74	39	66	26	56	4.074	6.191	3.306

Table 4. - Continued.

515	16	86	48	59	25	52	4.086	6.059	3.177
520	16	98	47	52	24	51	4.098	5.927	3.051
525	16	109	46	44	23	53	4.109	5.794	2.928
530	16	120	45	35	22	58	4.120	5.660	2.808
535	16	130	44	26	21	67	4.130	5.526	2.692
540	16	140	43	17	20	80	4.140	5.392	2.580
545	16	149	42	6	19	96	4.149	5.256	2.471
550	16	157	40	119	18	116	4.157	5.119	2.366
555	16	164	39	106	16	14	4.164	4.981	2.264
560	16	170	38	91	17	42	4.170	4.841	2.167
565	16	174	37	74	16	75	4.174	4.699	2.075
570	16	177	36	53	15	111	4.177	4.553	1.986
575	16	178	35	27	15	27	4.178	4.402	1.902
580	16	174	33	116	14	74	4.174	4.241	1.824
585									
590									
591									
592									
							3.776	3.116	2.331

ST CHORD WIDTH = 4.717 LE RADIUS = 0.046

Table 3. - Input Data for HYDRO - 1 Impeller.

.7500000E+01	.2000000E+00	.5625000E+01	.2250000E+02	
1 53	60 500	10		
.2500000E+00	.1250000E+00	.2500000E-01	.9300000E+00	.6500000E-01
.6000000E+01	.4000000E+01	.2000000E-01		
.1000000E+00	.1000000E-01	.5000000E-03	.5230000E-04	.5000000E-03
.6250000E+00	.2500000E+00	.1250000E+00	.1250000E+00	
.5000000E+01	.3000000E+01	.4250000E+01		
+.4418644E+00	-.4035868E-01	-.7637916E+00	+.4039596E+00	
-.6666175E-02	+.7744783E-01	+.7200185E-01	-.8029886E-01	+.3014936E-01
.9260056E-01	.1116641E-01	.2734877E+00	.9514174E+00	.8812670E+00
.5160000E+00	.8180000E+00	.4888800E+00		
+.1630200E-03	-.1894213E+00	+.4503821E+01	-.3021160E+02	+.1443567E+03
-.4279820E+03	+.7665728E+03	-.8084242E+03	+.4603855E+03	-.1090113E+03

Table 4. - Continued.

POINTS ON SURFACE			
X	Y	Z	
4.000	8.375	6.233	405
4.000	8.350	6.292	406
4.000	8.325	6.253	407
4.000	8.300	6.215	408
4.000	8.275	6.177	409
4.000	8.250	6.140	410
4.000	8.125	5.959	415
4.000	8.000	5.784	420
4.000	7.875	5.613	425
4.000	7.750	5.444	430
4.000	7.625	5.278	435
4.000	7.500	5.116	440
4.000	7.375	4.957	445
4.000	7.250	4.802	450
4.000	7.125	4.649	455
4.000	7.000	4.499	460
4.000	6.875	4.353	465
4.000	6.750	4.208	470
4.000	6.625	4.065	475
4.000	6.500	3.925	480
4.000	6.375	3.787	485
4.000	6.250	3.648	490

POINTS ON SURFACE			
X	Y	Z	
4.000	6.125	3.511	495
4.000	6.000	3.377	500
4.000	5.875	3.246	505
4.000	5.750	3.110	510
4.000	5.625	2.993	515
4.000	5.500	2.872	520
4.000	5.375	2.754	525
4.000	5.250	2.639	530
4.000	5.125	2.529	535
4.000	5.000	2.422	540
4.000	4.875	2.319	545
4.000	4.750	2.220	550
4.000	4.625	2.126	555
4.000	4.500	2.038	560
4.000	4.375	1.955	565
4.000	4.250	1.878	570
4.000	4.125	1.808	575
4.000	4.000	1.749	580
4.000	3.875	1.702	585
4.000	3.750	1.685	590
4.000	3.725	1.690	591
4.000	3.700	1.706	592

Table 5. Nomenclature of Programme Symbols.

Table 5.

ITEM	DESCRIPTION	UNIT	SYMBOL
A0, ..., A4	Coeff. of polynomial-Max. ord. of mean line		a_i
ALTE	Min. allowable T.E. thickness of model	inches	
AM	Max. mean line ordinate	feet	a_m
AMI	" " " " at hub	"	
AMO	" " " " at tip	"	
ANG	Blade pitch angle	radians	β
ANGI	" " " at hub	"	"
ANGO	" " " at tip	"	"
CID	Chord width at hub	feet	
COD	" " tip	"	
COSA	Direction cosines - normal to surface		α
COSB	" " " "		β
COSC	" " " "		γ
CUTR	Rad. of spherical milling cutter	inches	
CX7	Chord width at R0.7	feet	
CX	" " at rad. fraction x	inches	c_x
DELTA	See Fig. 5	radians	$\delta = \beta + \gamma$
DEVN1	Computing accuracy of CB - Sec. 4.1	inches	
DEVN2	Edge allowance on T.E. - Sec. 5.1	"	
DEVN3	Computing accuracy of XC - Sec. 4.2	"	
DX	Dist. between row planes - model	inches	
GAMMA	See Fig. 5	radians	γ
GDT	Grad. of tangent to blade edge in X, Y plane		
GL, GP	See Fig. 5		
GRAD(L,J)	Gradient of surface J in direction L		
HBC	Blade section characteristice (Ref. 3 p 293)		$-\frac{h}{c}$
IP	No. of row plane where calculations begin		
IPAT	" " " end		
KX, KXX	No. of rotn. & parts of lead screw X direc.		
KY, KYY	" " " " Y "		
KZ, KZZ	" " " " Z "		

Table 5(contd.) Nomenclature of Programme Symbols

ITEM	DESCRIPTION	UNIT	SYMBOL
MLE(I)	No. of points, Y=0 to Y=PCX of L.E.		
MTE(I)	" " " " of T.E.		
NKKN	No. ofpoint on the N=0 plane sec. 5.0		
NLE(I)	No. of points from Y=0 to L.E.		
NN	No. of the NNN plane on line of centroids		
NTE(I)	" of points from Y=0 to T.E.		
NTEST	0 Punch 0/P, $+^{ve}$ punch 0/P & intermediate calculation		
PCX	Fraction of CX where spacing is SPACX		
PD	Pitch to diameter ratio		P/D
PERCR	Initial estimate of RX - Sec. 4.1		
PT(L,KA,J)	ZB ord. of points surrounding pt. I,NNN	inches	
PTX (J)	ordinates of bottom of cutter X direction	"	
PTY(J)	" " " " " Y "	"	
PTZ(J)	" " " " " Z "	"	
RAD	Rad. of impeller - prototype	feet	R
RADLE	Rad. of L.E. factor RLE(I) = RADLE $\frac{t^2}{c}$		
RADM	Rad. of blade tip of master template	inches	R_m
RATIO	Ratio of boss to tip radius		
RLE(I)	Rad. of L.E. at section	inches	
RX	Radial distance to point	"	r_x
RXLE(I)	" " " L.E. at row plane	"	
RXTE(I)	" " " T.E. "	"	
SCALE	Scale of prototype to master template		R/R_M
SCALM	Scale of prototype to model		
SPACN	Minimum spacing between column planes	inches	
SPACX	Maximum " " " "	"	
STEPI	Forced convergence interval - Sec. 4.1	"	
STEP2	" " " Sec. 4.2	"	
T0,..,T3	Coeff. of polynomial for max. thickness		t_i
TX	Blade section maximum thickness	feet	t_x
X	X ordinate	inches	x

Table 5(contd) Nomenclature of Programme Symbole

ITEM	DESCRIPTION	UNIT	SYMBOL
XTL	X ordinate of L.E. at hub	inches	
XIT	" " " T.E. " "	"	
XMILR	Pitch of lead screw of miller - x direc.	"	
XOL	X ordinate of L.E. at tip	"	
XOT	" " T.E. " "	"	
XR	Radius fraction		
XX	Fraction of chord		$x/_c$
Y0,..,Y9	Coeff. of polynomial - NACA-16 profile	inches	y_i
Y	Y ordinate	"	
YB(I,NNN)	Y ordinate w.r. to axes XB, YB, ZB	"	
YBCT	Blade section characteristics (Ref. 3 p293)		$\frac{\bar{y}_c}{t}$
YC(L,KA)	Y ordinate of PT(L,KA,J) w.r. to YB	inches	
YD	Distance from X, Z plane to XB, ZB plane	"	
YDC	See Fig. 5	"	y'_c
YLE(I)	Y ordinate of L.E. at section	"	
YM	See Fig. 5.	"	y_m
YMILR	Pitch of lead screw of miller - Y direction	"	
YO	Ordinate of NACA - 16 profile	"	y_o
YR	Circumferencial distance from N = 0 plane	"	
YTE(I)	Y ordinate to T.E. at section	"	
YYTE	Difference in Y of back & face at T.E.	"	
YYY(J)	Y ordinate of point w.r. to machining axes	"	
Z(J)	Z " " " " X,Y,Z axes	"	
ZB(I,NNN,J)	" " " " " XB,YB,ZB	"	
ZD	Distance from X,Y plane XN, YN plane	"	
ZMILR	Pitch of lead screw of miller - z direction	"	
ZZZ(J)	Z ordinate of point w.r. to machining axes	"	

$$DV = YO_{NACA} - YO$$

where YO_{NACA} = Ordinate Value given by NACA - 16 Profile.

$$YO = (1 - XX)\left[\sqrt{0.98879XX}\right] + \sum Y_i\, XX^i$$

where $i=0,1,\ldots,9$

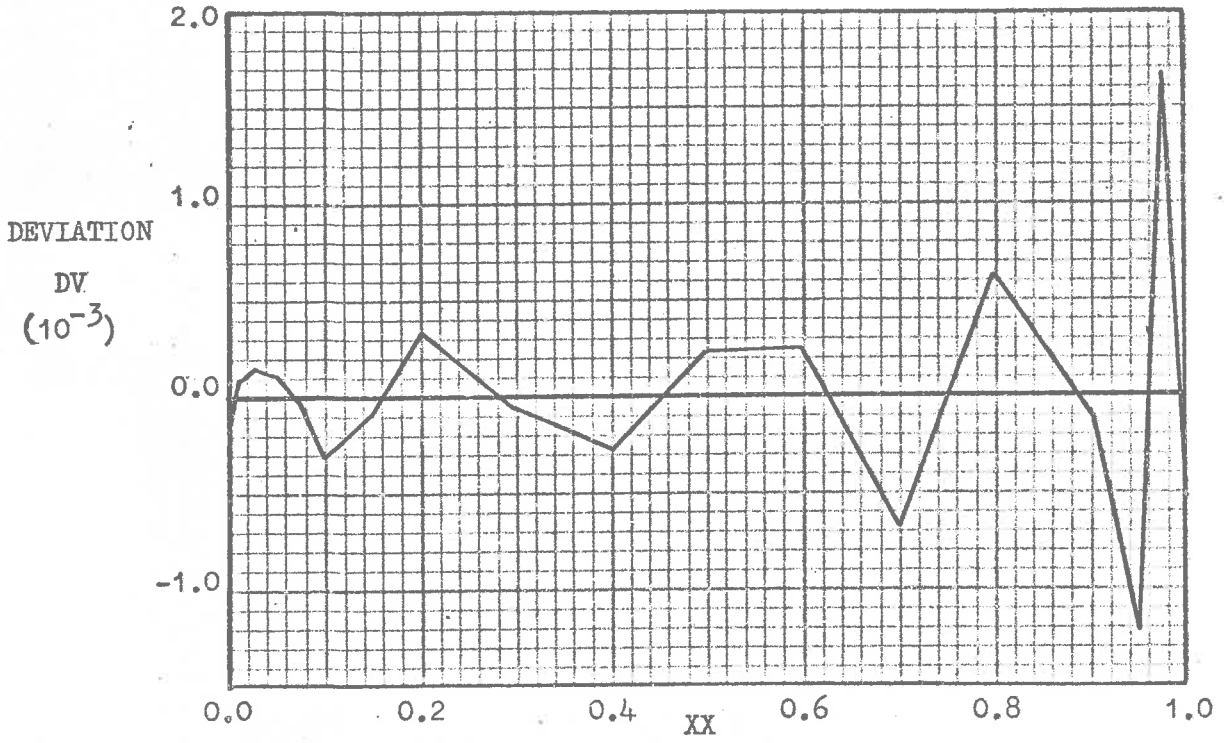

Fig. .1 - Deviation from NACA - 16 Profile of Unit Thickness.

Fig. .1

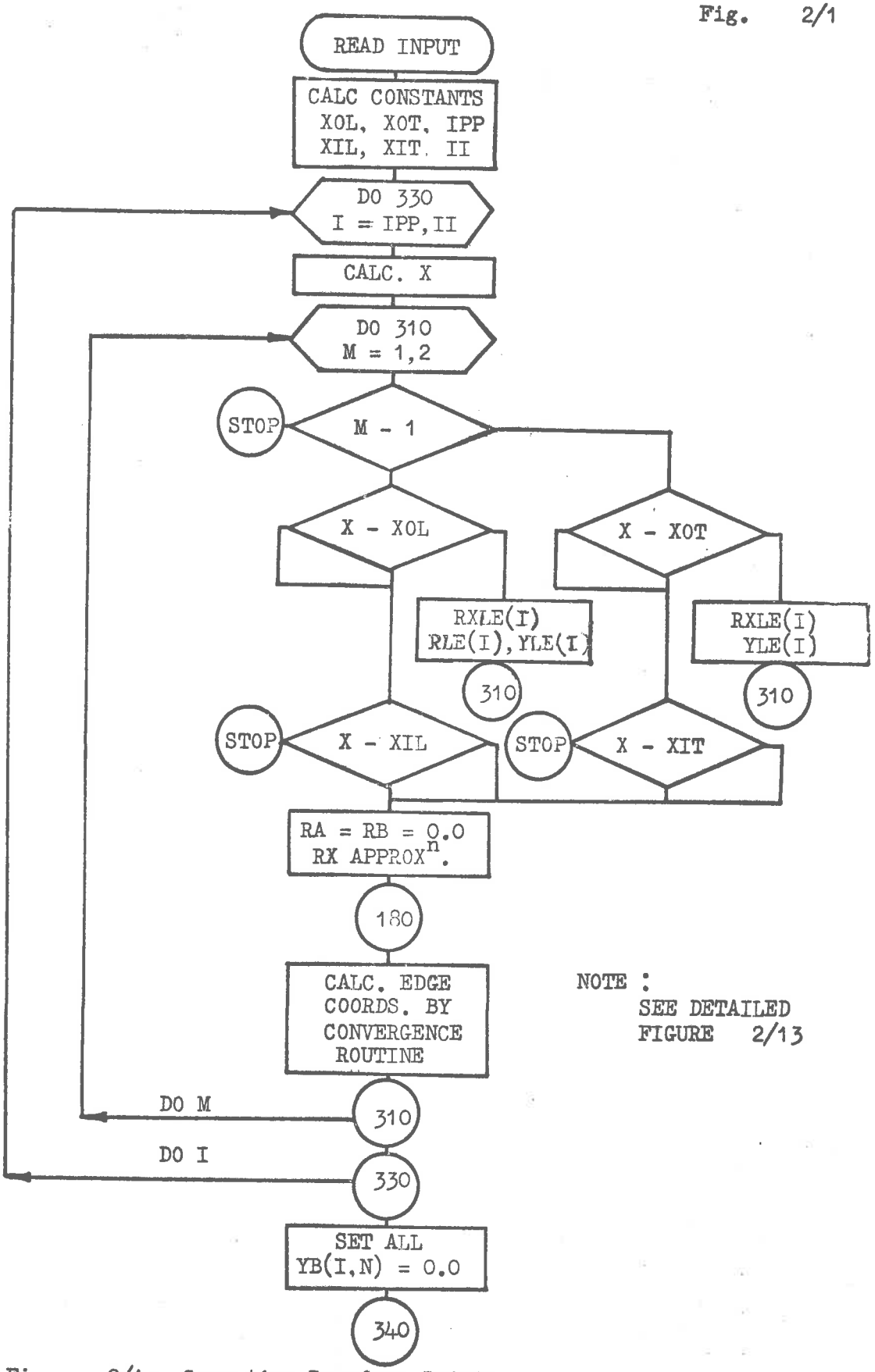

Fig. 2/1- Computing Boundary Points.

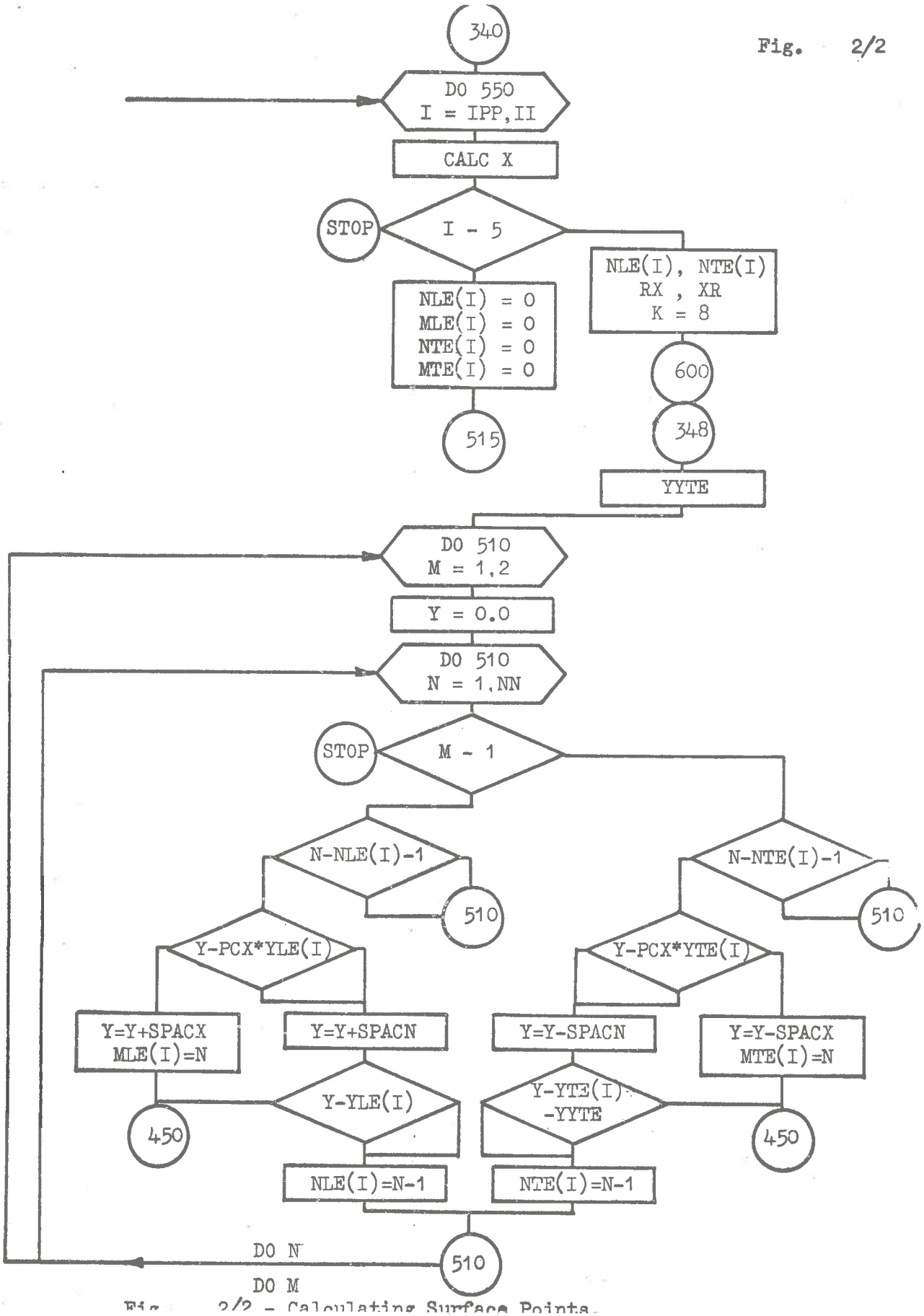

Fig. 2/2 - Calculating Surface Points

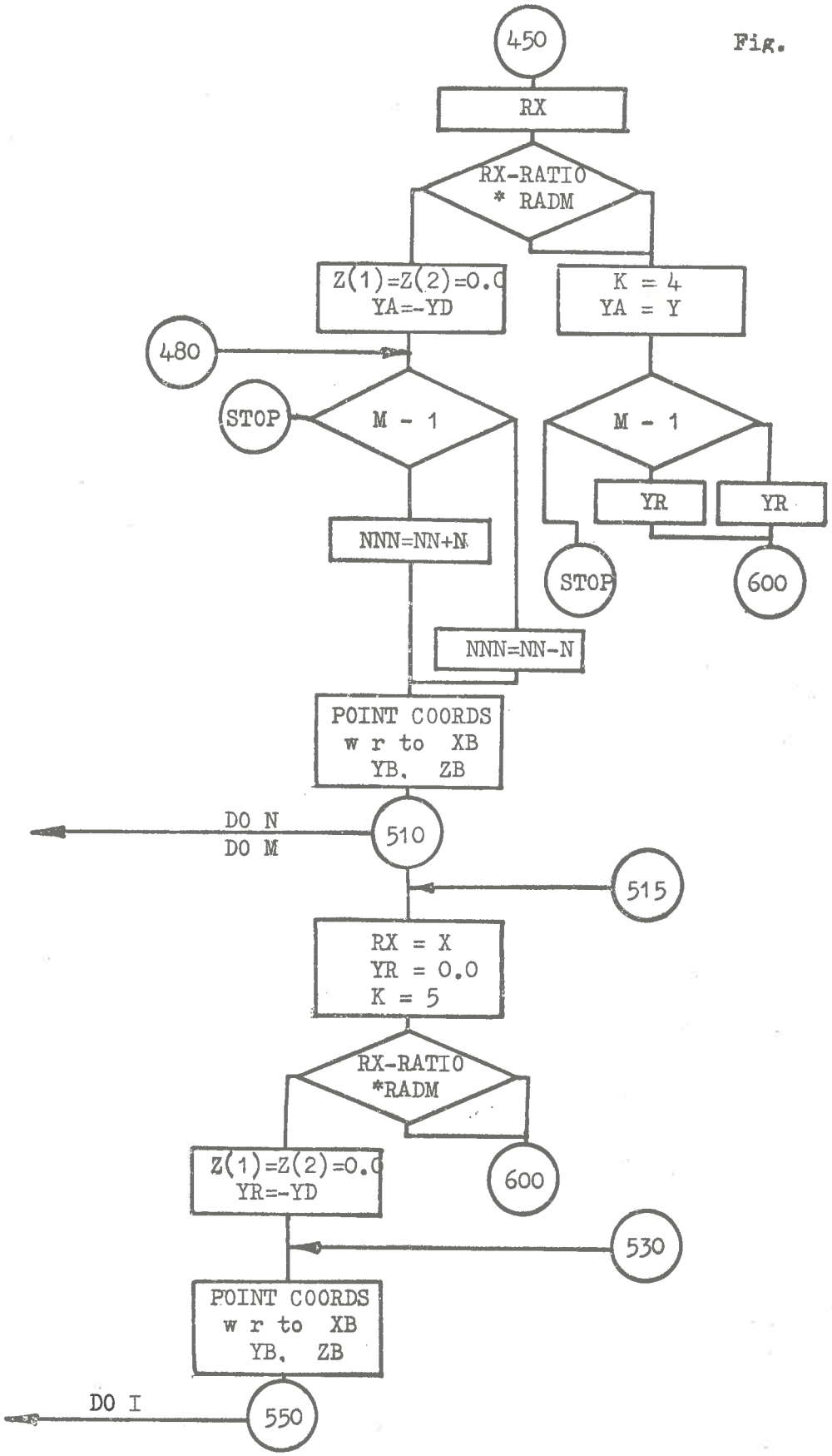

Fig. 2/3 - Calculation of Blade Surface Points.

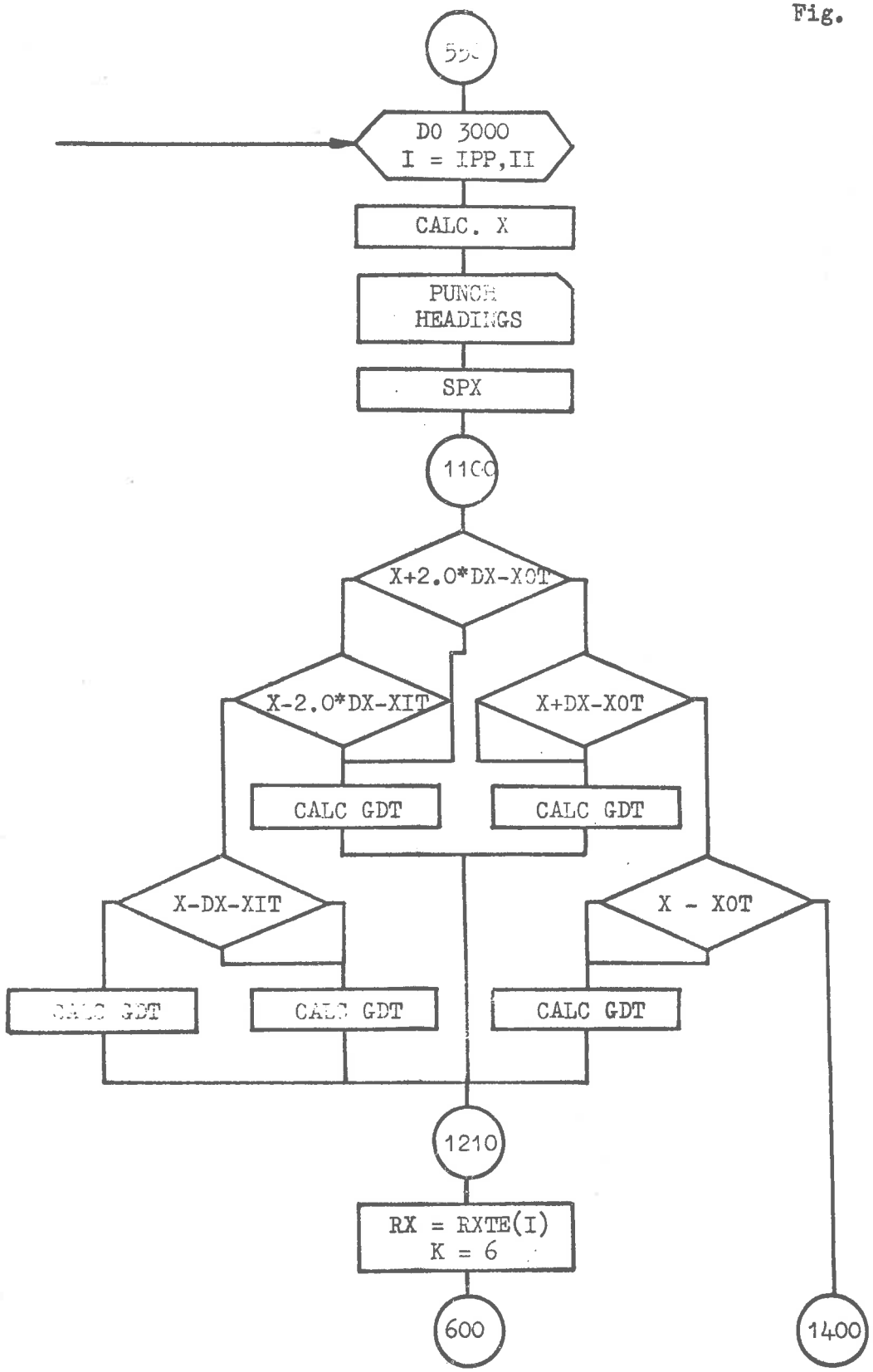

Fig. 2/4 - Trailing Edge Machining Co-ordinates.

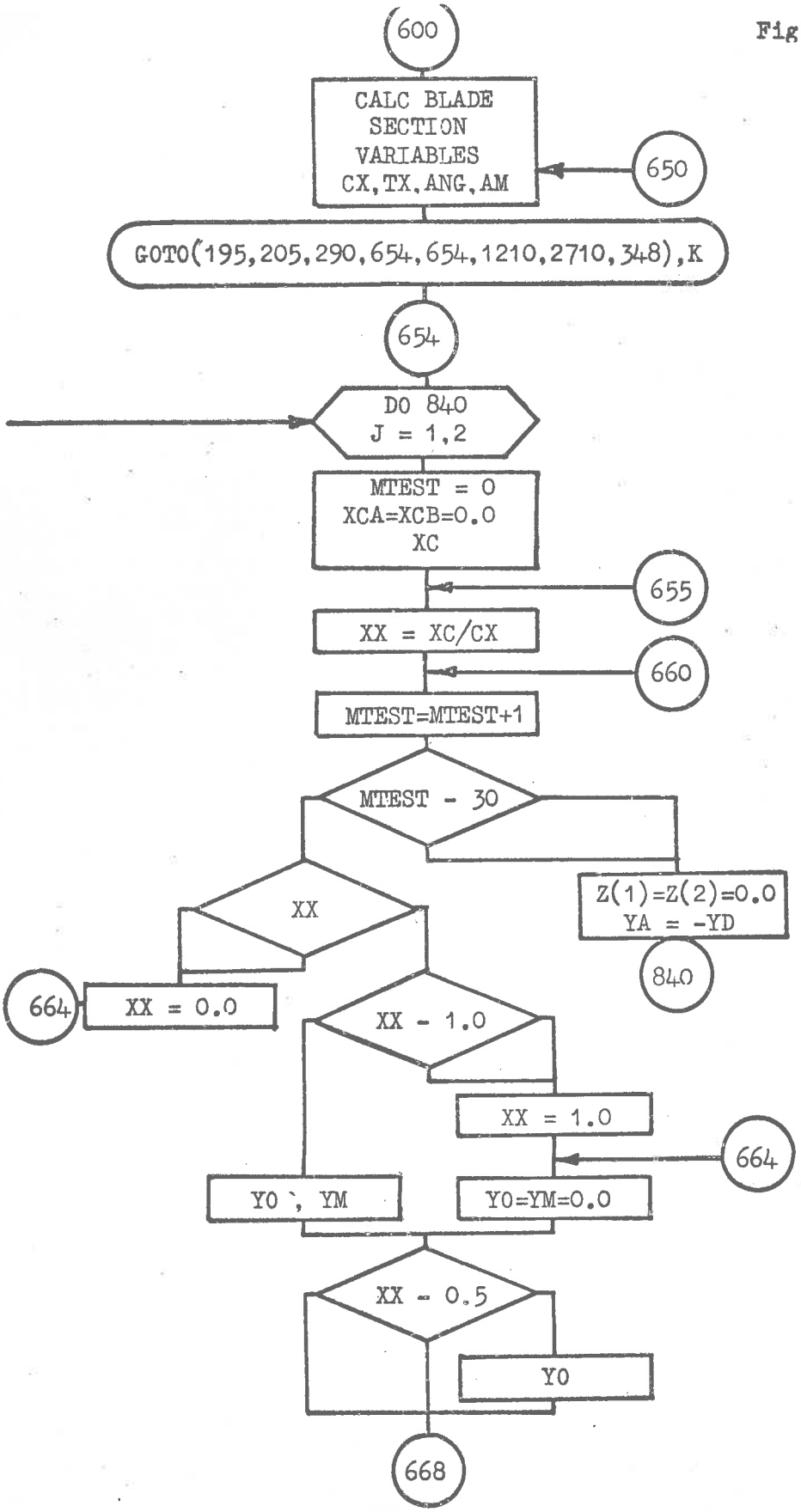

Fig. 2/5 - Routine for Calculating Blade Section Variables.

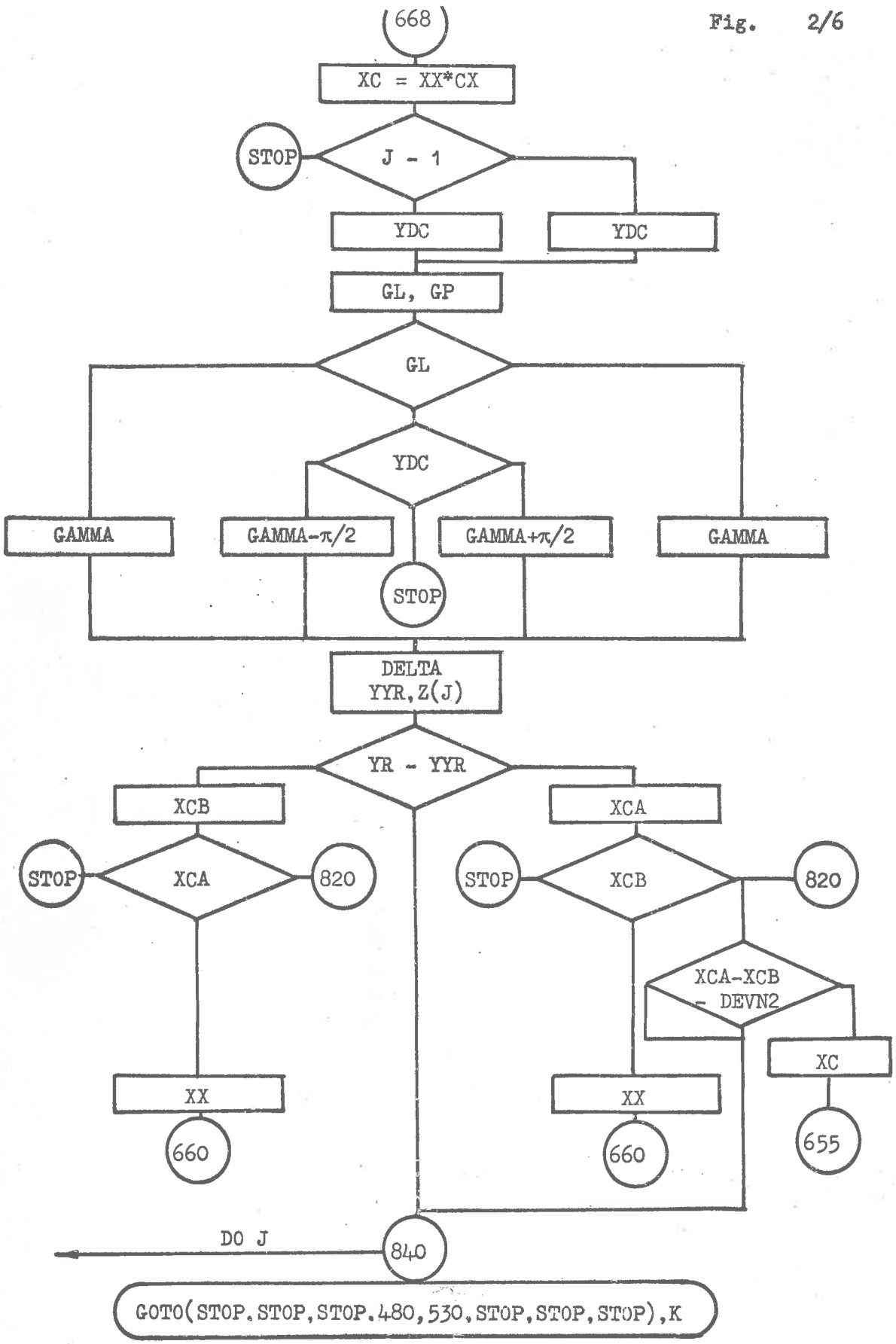

Fig. 2/6 - Routine for Calculating Blade Section Variables and Surface Point Co-ordinates.

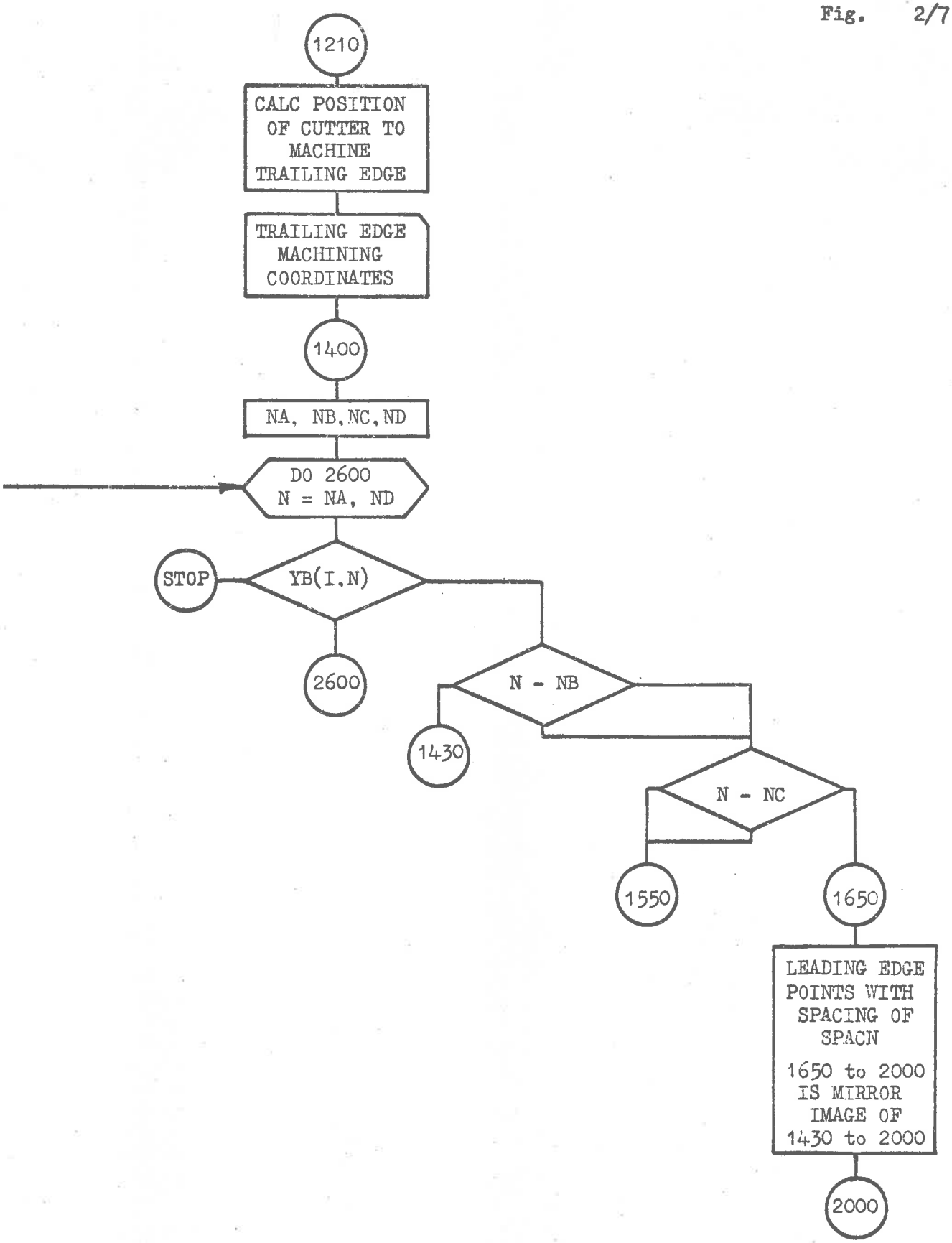

Fig. 2/7 - Determining Region of Surface Points.

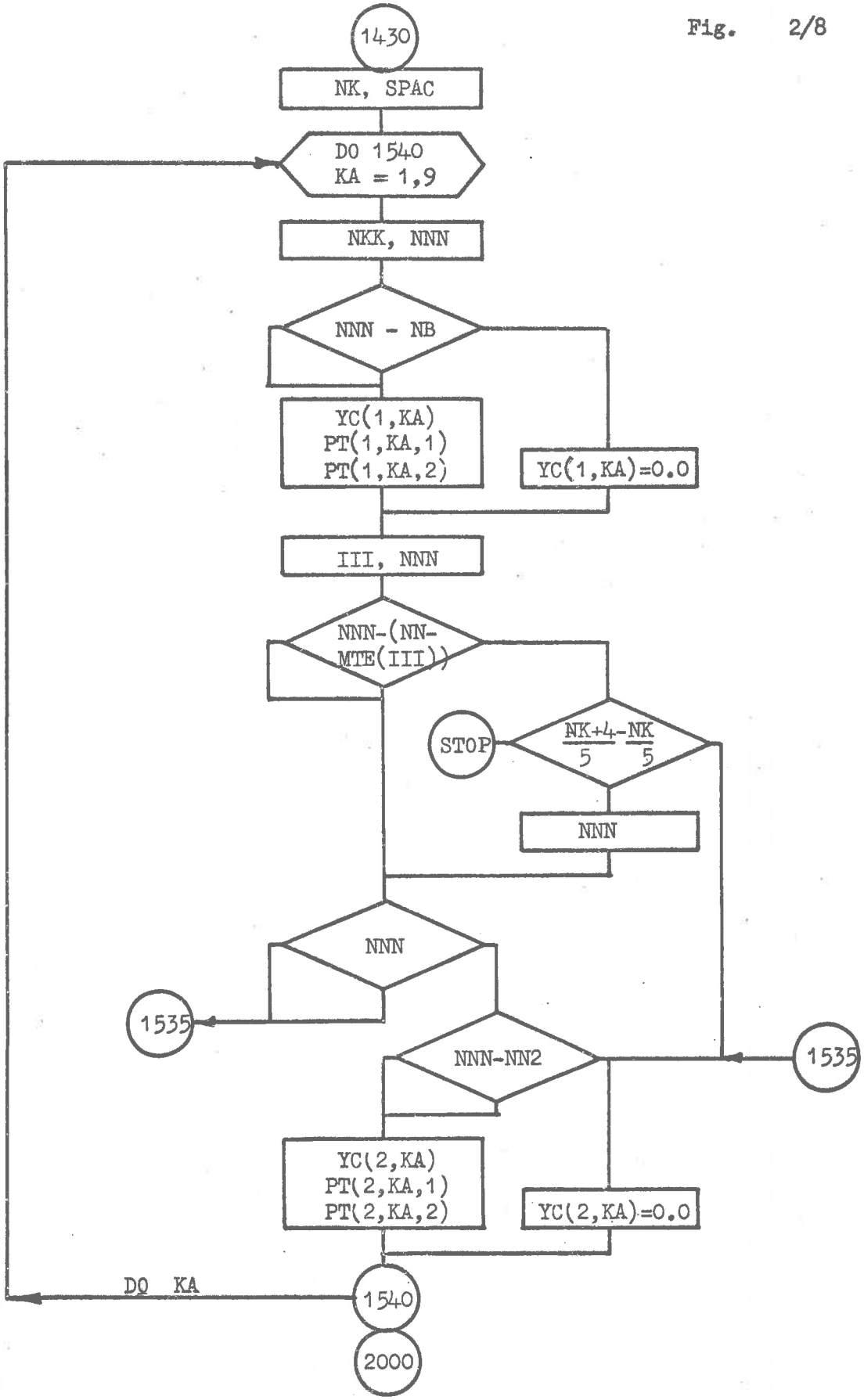

Fig. 2/8 - Locating Neighbouring Surface Points - Region I

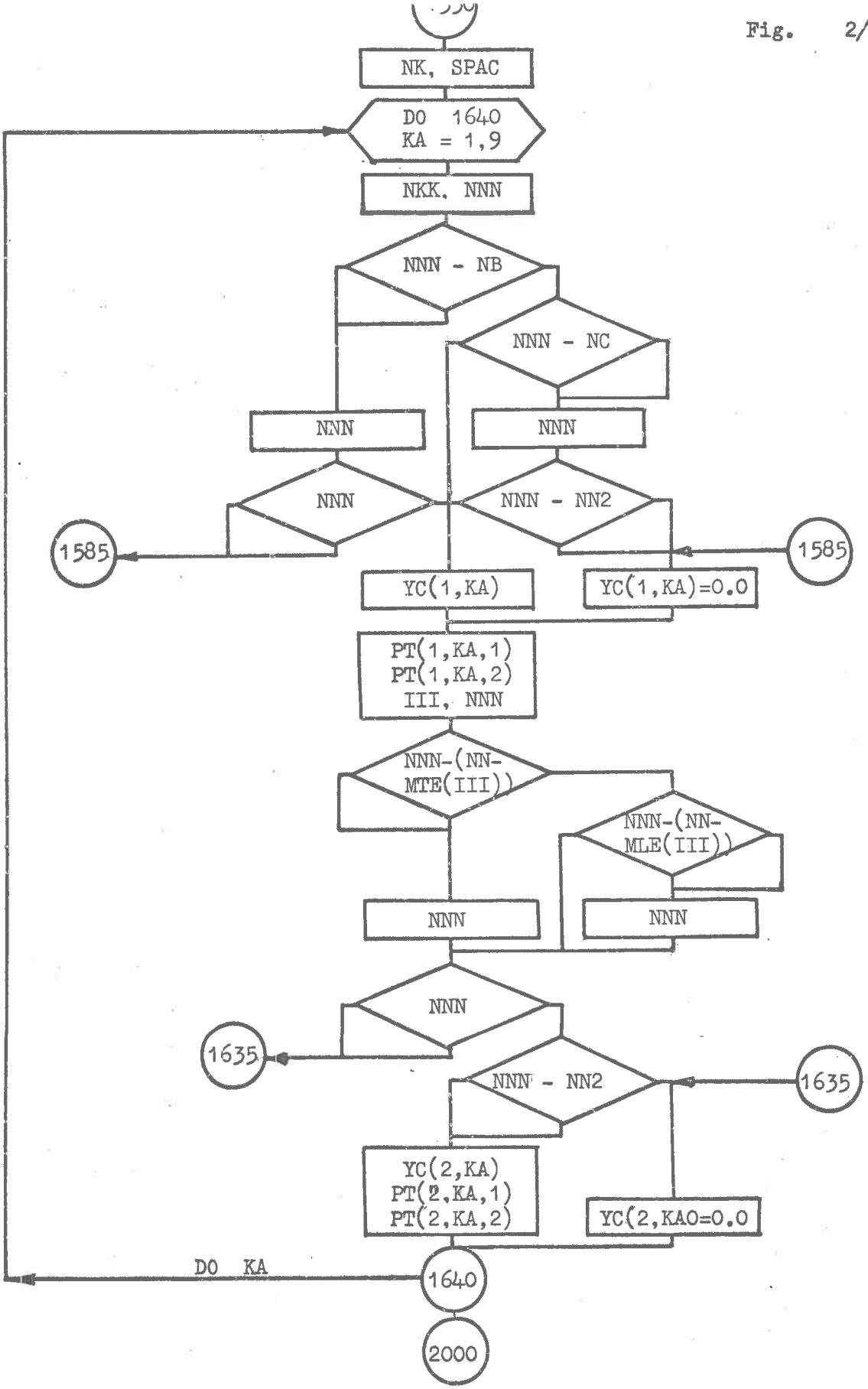

Fig. 2/9 - Locating Neighbouring Surface Points - Region II

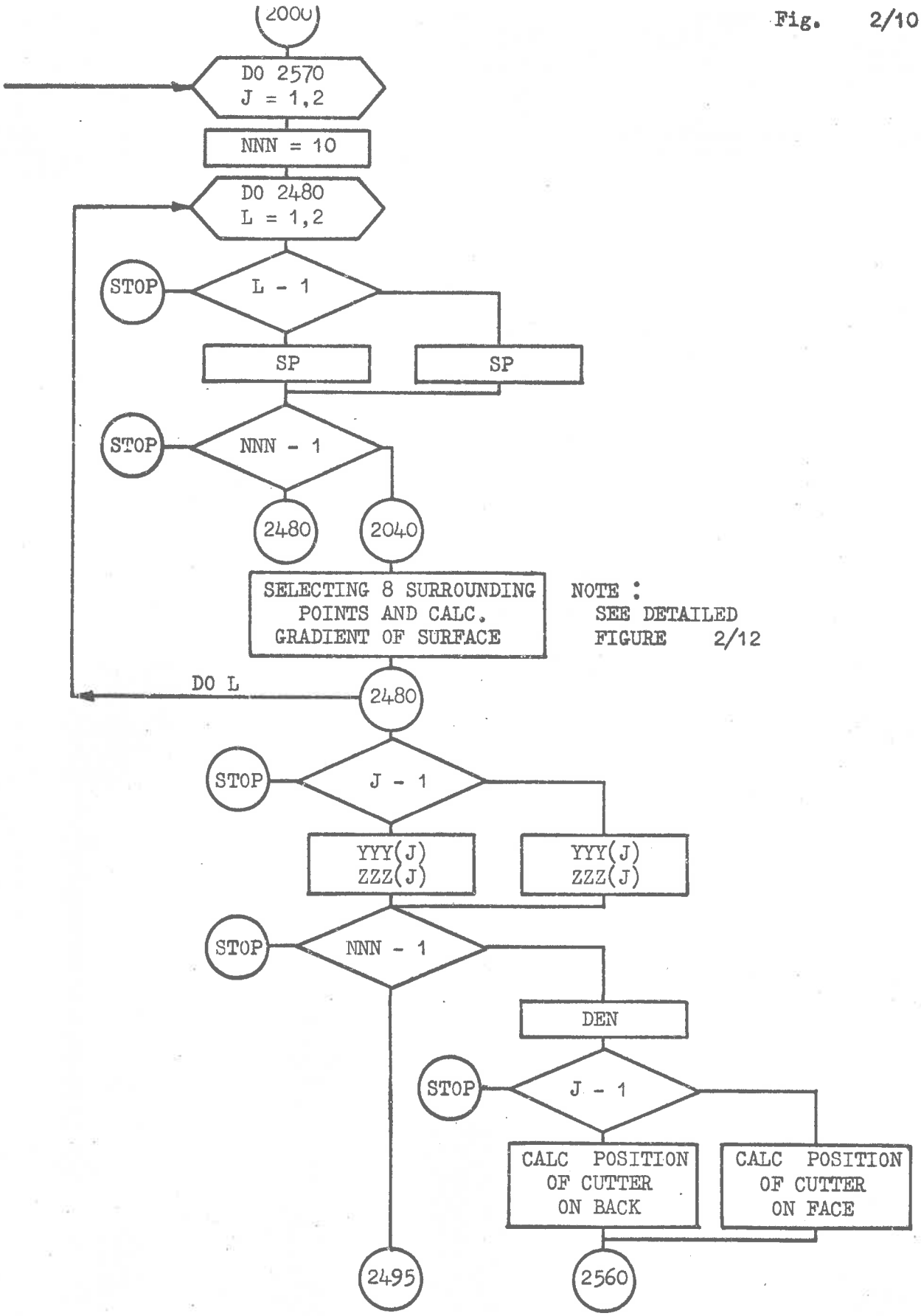

Fig. 2/10 - Calculating Machining Co-ordinates for Surface Points.

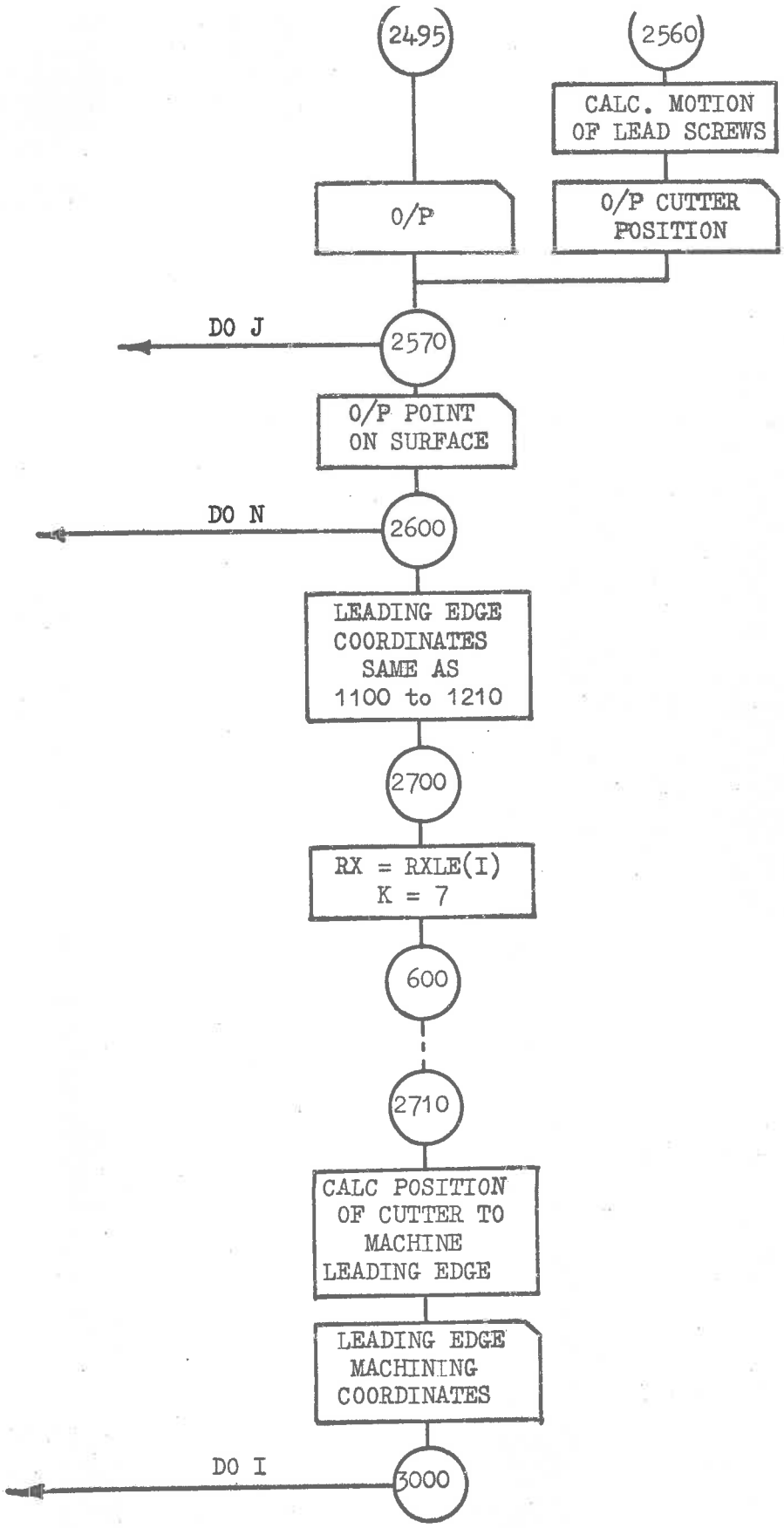

Fig. 2/11 - Output for Machining Instructions.

Fig 2/12

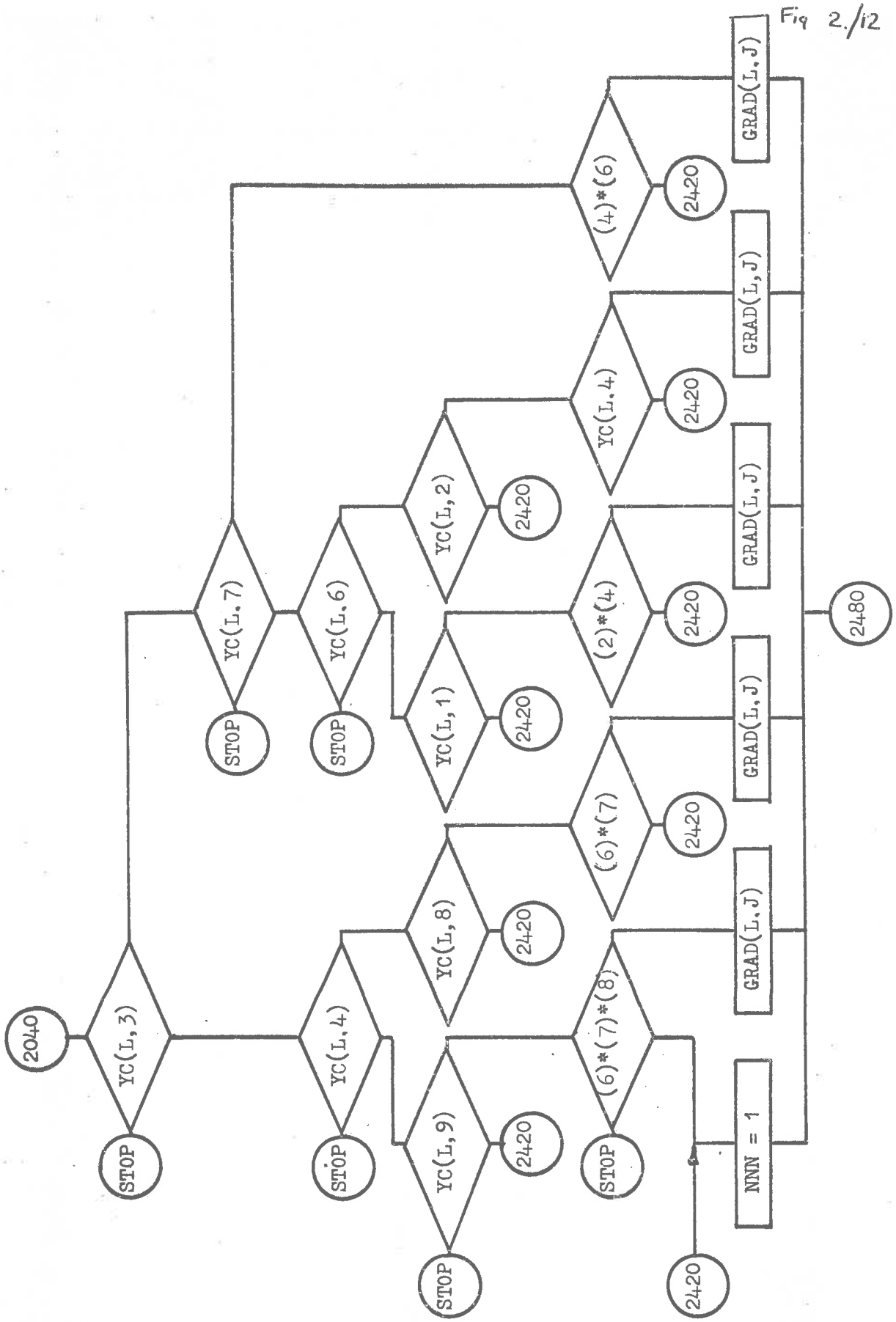

Fig. 2/12 - Calculating Gradient of Surface at a Point.

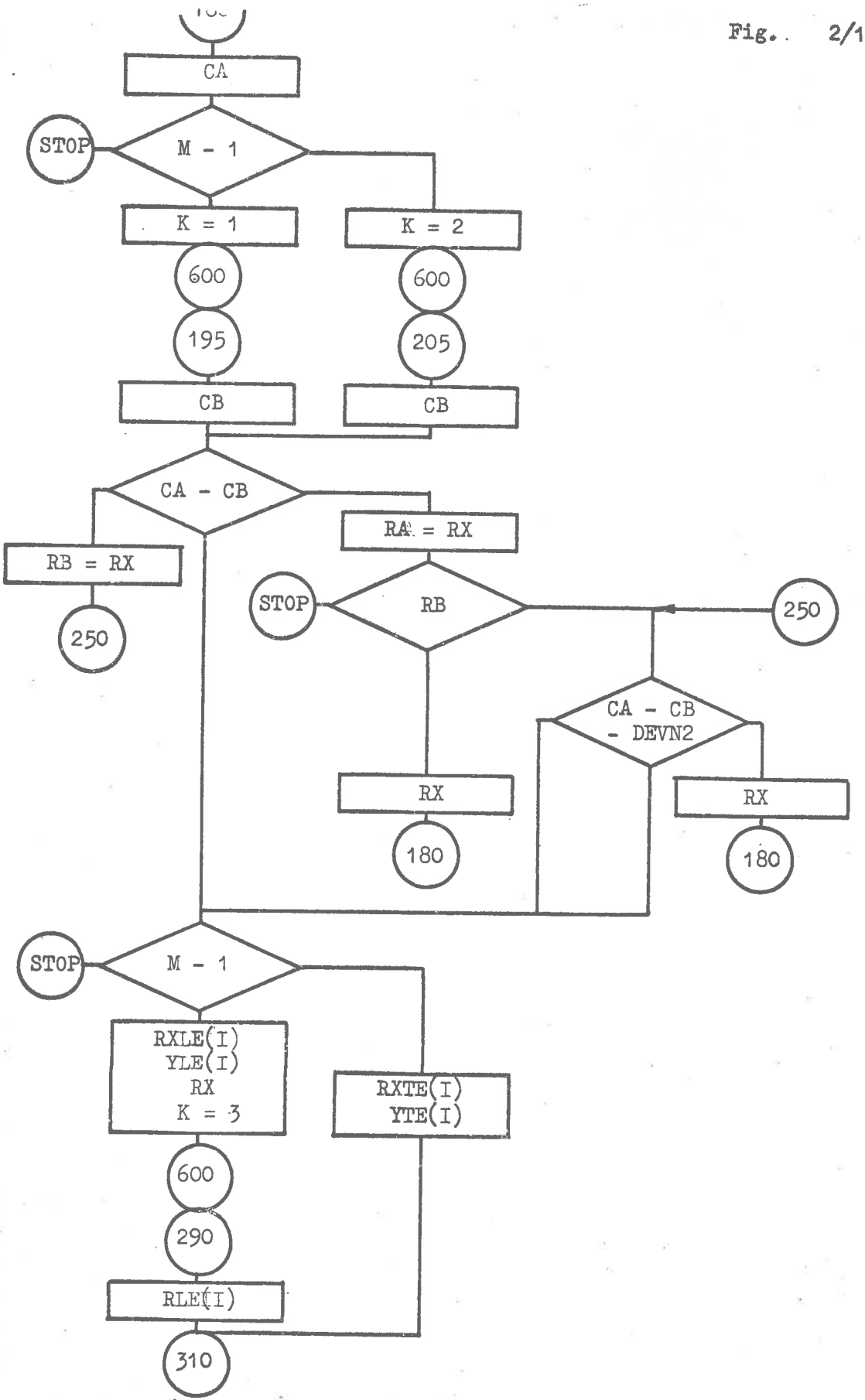

Fig. 2/13 - Convergence Routine for Boundary Points.

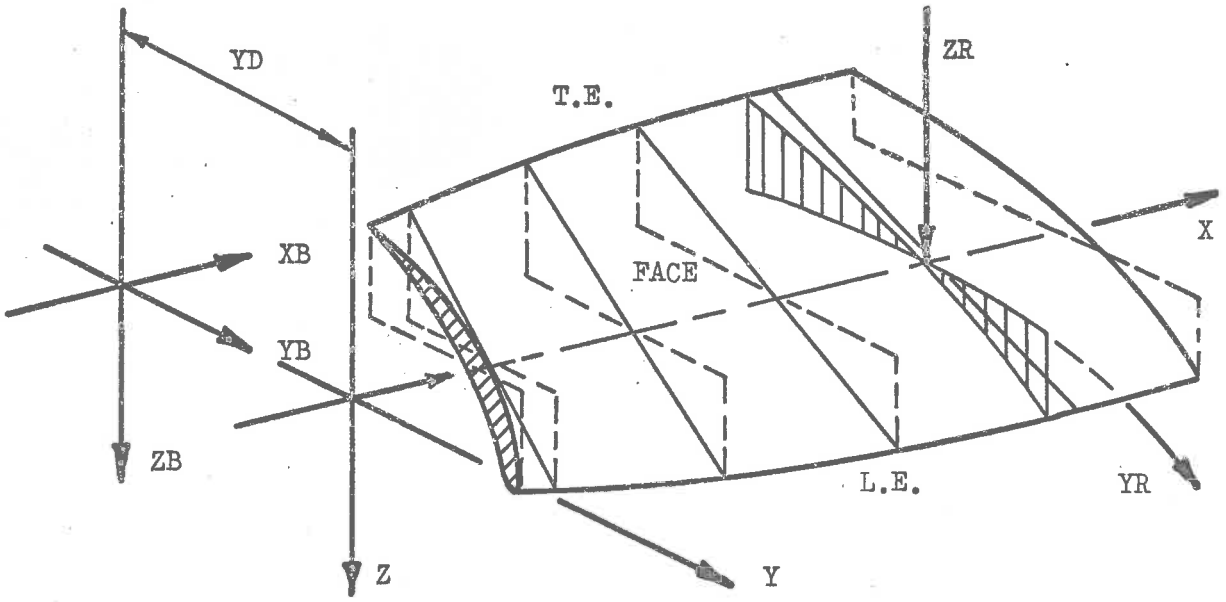

Fig. .3 - Calculation Axes

Fig. .4 - Machining Axes.

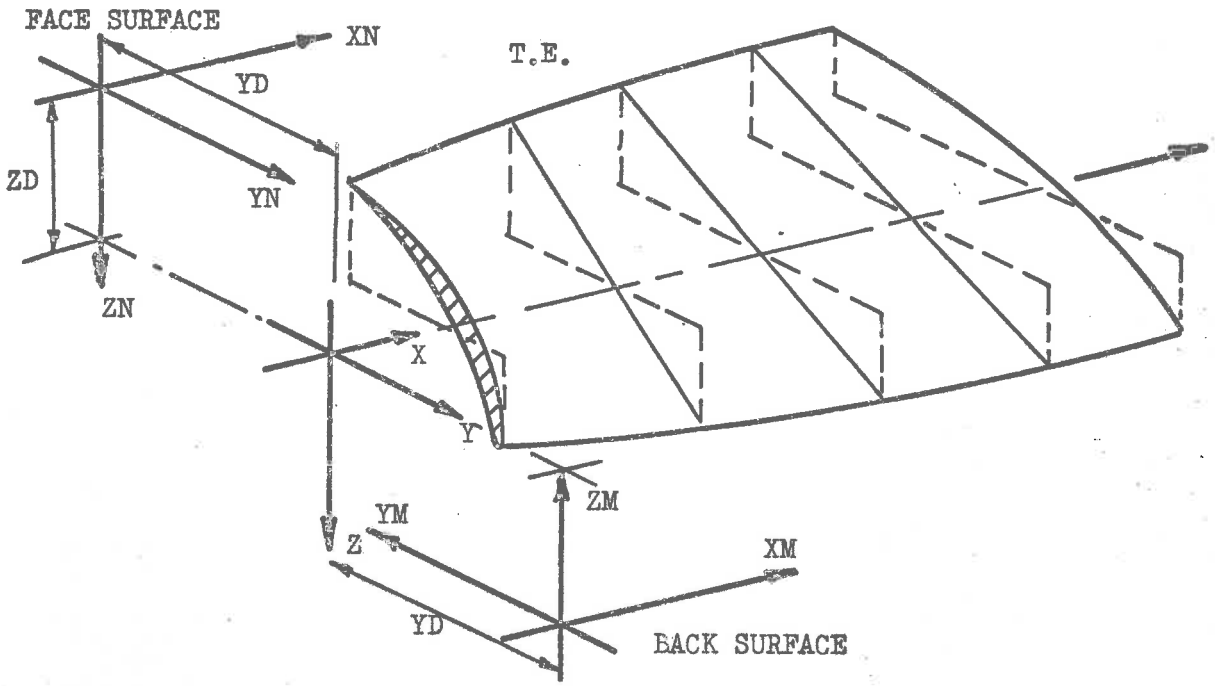

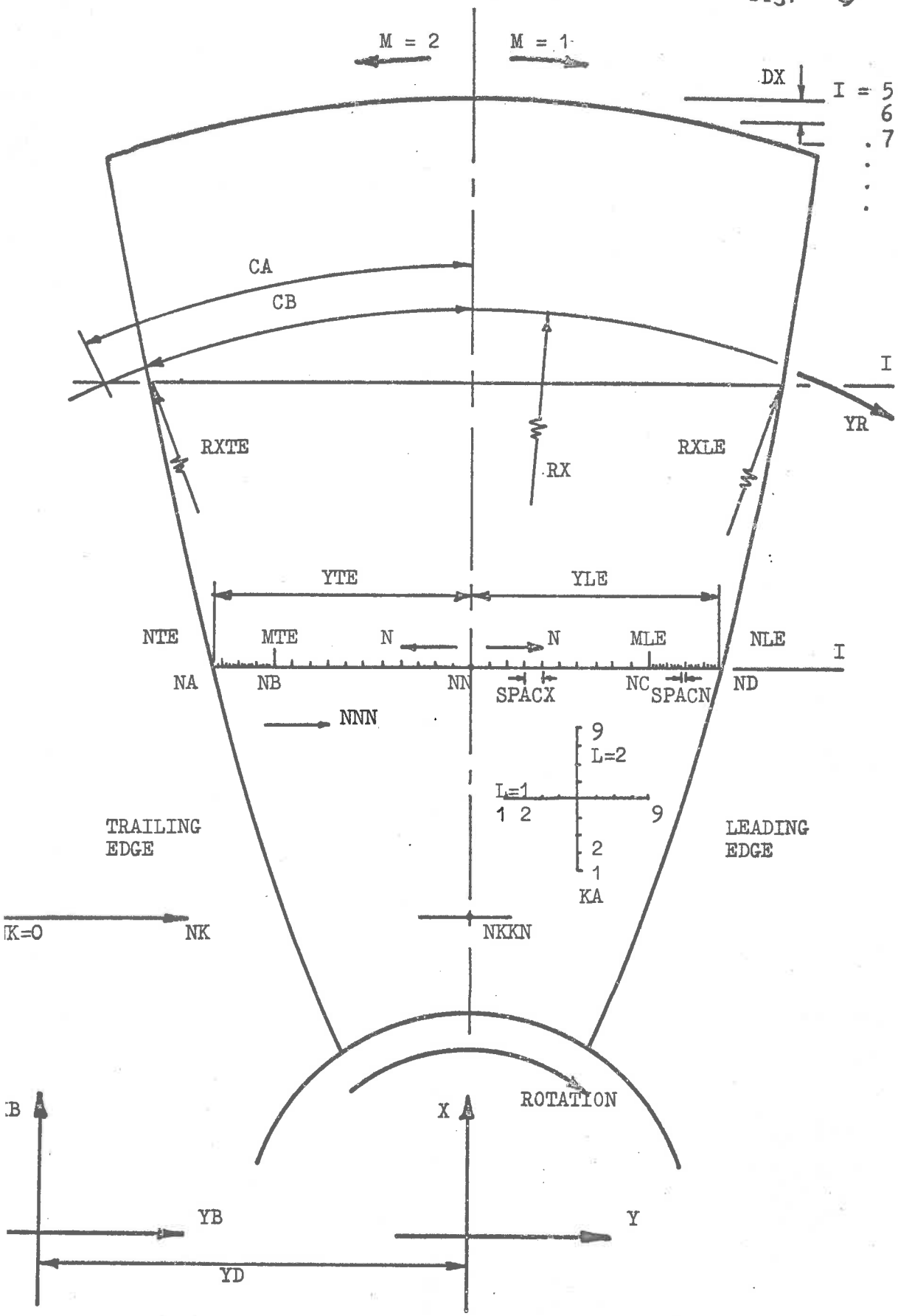

Fig. .5 - Blade Surface Variables.

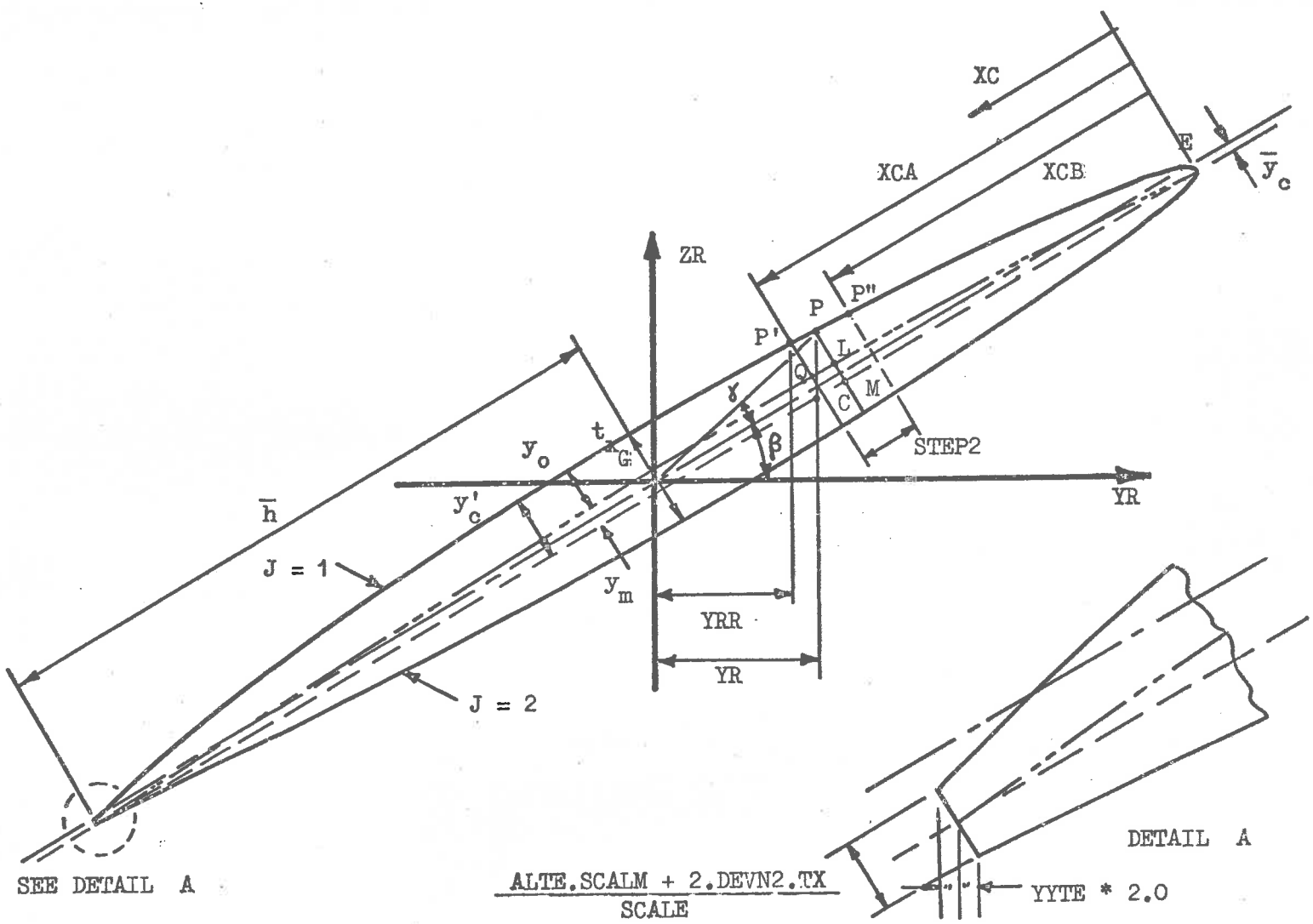

Fig. 6 - Blade Section Variables.

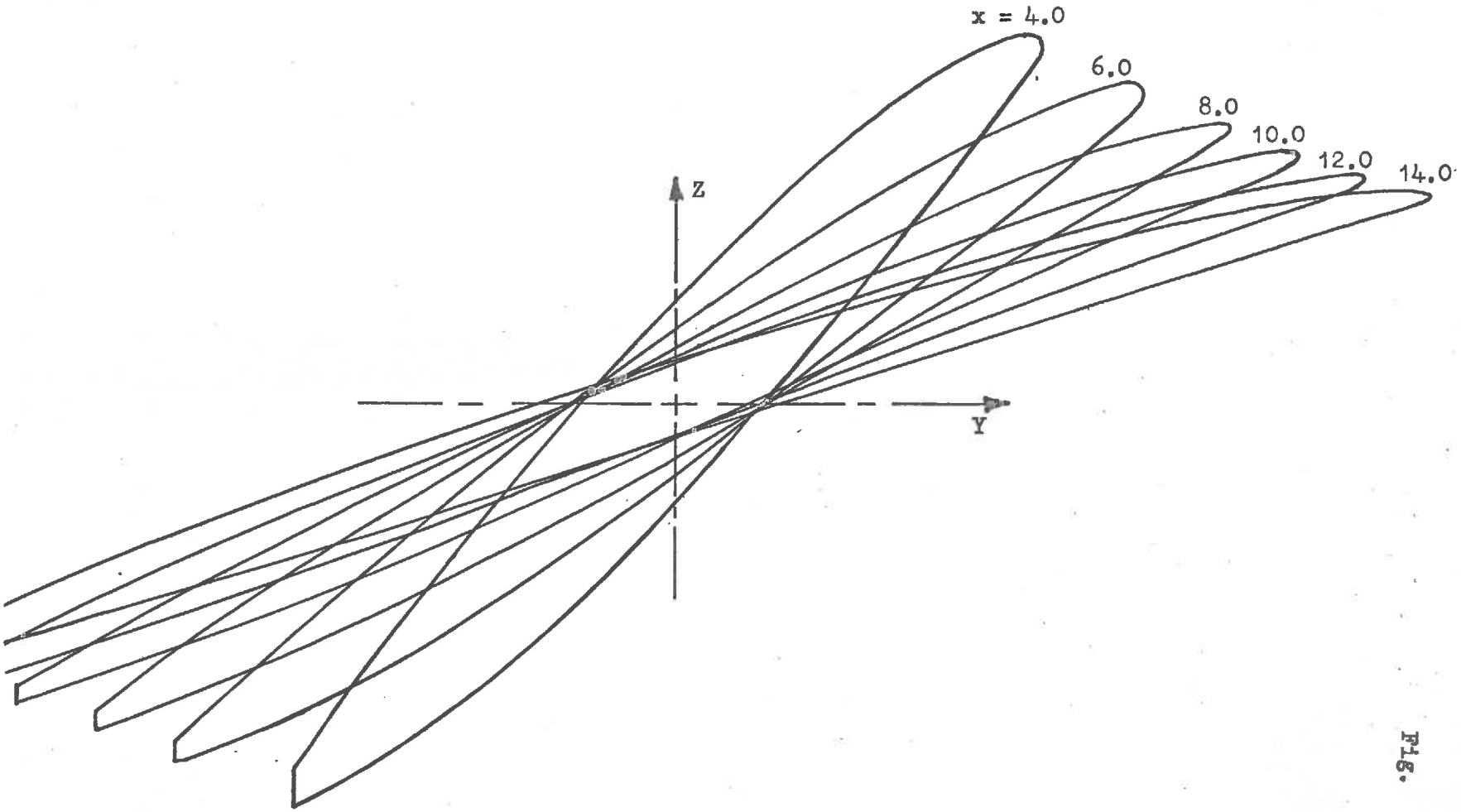

Fig. 7- Computed Blade Surfaces at Selected Stations HYDRO - 1 Impeller.

Fig. 7

APPENDIX A3

MACHINING PROCEDURE FOR THE MODEL IMPELLER.

APPENDIX A3

MACHINING PROCEDURE FOR THE MODEL IMPELLER.

1. The master templates were cast with free cutting alluminium alloy (6% Si, 0.2% Cu, 0% Fe).

2. After rough machining the base of the templates and heat treating them, the surfaces were accurately machined and hand-scraped.

3. To accurately position the templates on the table of a milling machine, it was necessary to machine two surfaces normal to each other and normal to the base of the templates. It was arranged that these surfaces were parallel to the axes which were used to describe the geometry of the impeller blade.

4. A datum jig (Fig. 2.6) was constructed and fixed relative to the above three surfaces to locate the origin from which the machining coordinates were computed. (details in Appendix A2)

5. After having positioned the milling cutter directly over the datum jig, the milling machine positioning dials were pre-set to zero.

6. The surface, as defined by the points, was then machined (Fig.2.6).

7. A small amount of hand filing and scraping was necessary to remove the excess material from between the accurately machined points.

8. The inner and outer cylindrical surfaces of the templates were machined and a dummy hub fitted to the inner surface .

9. The model impeller material was rough machined, heat treated, and bored to final size.

10. A precision indexing table was mounted on the pantograph copying machine to support the model impeller(Fig. 2.7). Care was taken to align the master templates and the model material in the correct position relative to the follower and cutter of the copying machine.

11. The model impeller was then roughly machined all over to within 0.040 of an inch (Fig. 2.8).

12. One surface of all the blades was then finished.

13. Before machining the second side of the blades, the blades were supported from behind with plastic putty to increase the stiffness of the material and reduce deflections when machining (Fig. 2.7).

14. Finally the accuracy and balance of the model was checked (Fig. 2.9).

APPENDIX A4

PROPULSIVE EFFICIENCY OF DUCTED PROPULSION SYSTEM.

APPENDIX A 4

PROPULSIVE EFFICIENCY OF A DUCTED PROPULSION SYSTEM.

Assuming all the losses in the ducting can be expressed as a fraction (ξ) of the total kinetic energy of the fluid at the intake to the duct.

$$\text{duct loss /unit mass flow} = \xi \frac{V_I^2}{2} \qquad \ldots \text{A4.1}$$

Then the total head across the impeller is, referring to figure below.

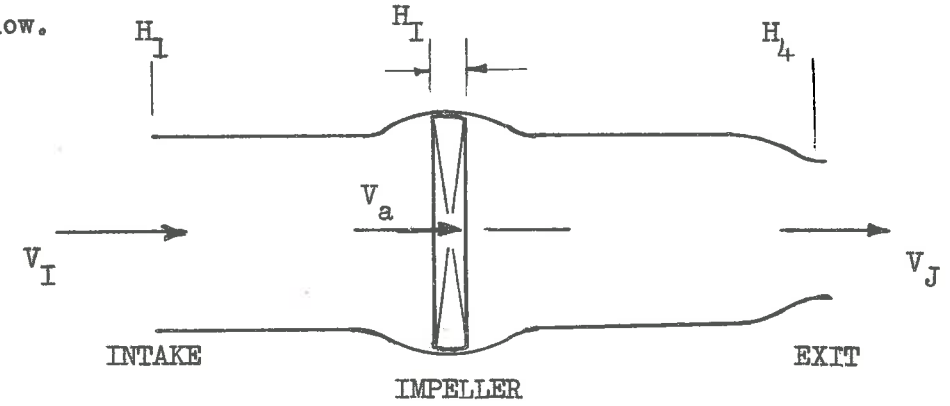

$$H_I = H_4 - H_1 + h \qquad \ldots \text{A4.2}$$

$$= \frac{V_J^2}{2g} - \frac{V_I^2}{2g} + \xi \frac{V_I^2}{2g} \qquad \ldots \text{A4.3}$$

$$= \frac{1}{2g} [V^2_J - V_I^2 (1 - \xi)] \qquad \ldots \text{A4.4}$$

The power supplied to an impeller which has an efficiency η_E

$$P = \frac{1}{\eta_E} g M H_I \qquad \ldots \text{A4.5}$$

where M = mass of fluid flowing per second.

Assuming the intake and jet velocities are uniform, then the thrust developed by unit is equal to rate of change of momentum.

$$T = M (V_J - V_I) \quad \ldots A4.6$$

To estimate the expended horse power delivered by the impeller a hull efficiency factor must be included because the resistance of the ship does not usually equal the thrust of the propulsion unit and the ship's velocity differs from the intake velocity to the propulsion system.

Defining the hull efficiency η_H in the normal way as

$$\eta_H = \frac{(1 - t)}{(1 - w)} \quad \ldots A4.7$$

where t = thrust deduction factor

and w = wake factor

Hence the expended horse power is

$$E.H.P. = \eta_H (V_J - V_I) M V_I \quad \ldots A4.8$$

and the propulsive efficiency η_P of the unit is

$$\eta_P = \frac{E.H.P.}{\text{Power input}} = \eta_E \eta_H \frac{2 V_I (V_J - V_I)}{[V_J^2 - V_I^2(1 - \zeta)]} \quad \ldots A4.9$$

$$= \eta_E \eta_H \frac{2\mu (1 - \mu)}{[1 - \mu^2 (1 - \zeta)]} \quad \ldots A4.10$$

where $\mu = \frac{V_I}{V_J}$

The maximum efficiency for a given ξ is

$$\eta_{P\ opt} = \eta_E \eta_H \frac{1}{[1 + \sqrt{\xi}]} \qquad \ldots A4.11$$

and occurs where $\mu_{opt} = \frac{1}{1 + \sqrt{\xi}}$

The propulsive efficiency can also be expressed in terms of the thrust load coefficient (C_{TL}) of the impeller.

$$\eta_{P\ opt} = \eta_E \eta_H \frac{4\ (C_{TL}\ K_A)}{[\ (C_{TL}\ K_A)^2 + 4\ (C_{TL}\ K_A) + 4\ \xi\ ]} \qquad \ldots A4.12$$

where $C_{TL} = \dfrac{T}{\frac{1}{2} \rho\ Va^2\ A_o}$

$$= 2\ K_A\ [\ \frac{1}{\mu} - 1\ ]$$

where Va = axial velocity at the impeller plane

A_o = area of impeller annulus

K_A = ratio of impeller annulus area to area of duct at intake.

The optimum propulsive efficiency for a given ξ corresponds to a unique value of thrust load coefficient where ,

$$\eta_{P\ opt} = 2\ \eta_E\ \eta_H \frac{1}{[C_{TLopt}\ K_A + 2\ ]} \qquad \ldots A4.13$$

where $C_{TLopt} = \dfrac{2\sqrt{\xi}}{K_A}$

APPENDIX A5

HYDRO-JET PROPULSION REDUCES VIBRATION

by

M.R.Hale and D.H.Norrie

Engineering, 24 July 1964

Hale, M.R., & Norrie, B.E. (1964). Hydro-jet propulsion reduces vibration. *Engineering,* 24 July 1964.

APPENDIX A6

THE ANALYSIS AND CALIBRATION OF THE FIVE - HOLE SPHERICAL PITOT

by

M.R.Hale and D.H.Norrie

UNIVERSITY OF ADELAIDE

DEPARTMENT OF MECHANICAL ENGINEERING

Report Mech. Eng. R66/1

March, 1966.

THE ANALYSIS & CALIBRATION OF THE FIVE-HOLE SPHERICAL PITOT

by M.R. Hale & D. H. Norrie

SUMMARY

The theory of the five-hole spherical pitot is summarized and the reasons for the actual characteristics deviating from the theoretical discussed. An analysis and associated technique for the calibration of the pitot, even in a flow whose direction is only approximately known, is given. The results of the calibration can be put in a form suitable for the reduction of test data by a digital computer. The technique described allows a calibration of high accuracy to be obtained with a simple flow duct and should enable a much wider use to be made of this simple instrument for measuring simultaneously the magnitude and direction of fluid velocity.

1.0 INTRODUCTION.

A variety of instruments are available for determining separately the magnitude and direction of the velocity at a point in a fluid stream. (Ref. 1). There are few, however, which determine simultaneously both magnitude and direction. Of those with this capability the simplest depend on the measurement of pressure at points on the surface of a sphere. Spherical pitots using five holes were used by Taylor (Ref. 2) in 1915, Meyer and Borren (Ref. 3) in 1928 and Gutsche (Ref. 4) in 1931. A 13-hole instrument was early developed by the David Taylor Model Basin (Ref. 2), Krisam (Ref. 5), Jegerow (Ref. 6) & Eckert (Ref. 7) also reported on these pitots. A notable advance was made by Pien (Ref. 8) in 1958, who utilized the fact that three pressure measurements on a great circle of a sphere determine uniquely the velocity component in that plane. By reducing the angular distance between the side and centre holes to 20° from the previously used $40\text{-}50^{\circ}$ Pien also increased the accuracy and range of the instrument. The Pien pitot has subsequently been reported on favourably by Silovic (Ref. 9).

Up to the present, accurate calibration of the instrument has required a flow whose direction is known accurately. This has necessitated the use of a towing tank, in which the relative motion of carriage and water is precisely known, or a very precise wind or water tunnel. It is the purpose of this paper to show that an accurate calibration can be carried out in a flow whose direction is only approximately known. Calibration is thus

possible in a small wind tunnel, water tunnel or duct. Although this paper is concerned with the application of the probe in incompressible flows, it can also be used in compressible flows (Ref. 1, 10) and the technique described below can be adapted to this case.

2.0 THEORY.

The potential solution of the flow around a sphere gives the pressure at a point as:

$$\frac{p - p_o}{\frac{1}{2}\rho V^2} = 1 - \frac{9}{4}\sin^2\beta \qquad \ldots \quad 1.$$

where p = pressure at point considered

p_o = free stream pressure

V = magnitude of velocity vector $\bar{V}$ of free stream

ρ = fluid density

β = angular position of point from stagnation point.

For three equispaced holes a,b,c on a great circle of a sphere (see Fig. 1) Pien (Ref. 8) has shown that:

$$C_{ph} = \frac{p_a - p_b}{\frac{1}{2}\rho V_h^2} = \frac{9}{4}\sin 2\alpha \sin 2\beta_h \qquad \ldots \quad 2$$

$$C_{Ph} = \frac{p_a - p_b}{2p_c - p_a - p_b} = \frac{\sin 2\alpha}{1 - \cos 2\alpha}\tan 2\beta_h \qquad \ldots \quad 3$$

where p_a, p_b, p_c = pressures at a,b, c

C_{ph}, C_{Ph} = pressure coefficients

α = angle between adjacent holes

V_h = Orthogonally projected component of the velocity $\bar{V}$ onto the plane of the great circle.

β_h = angle between V_h and the stagnation point.

From measurements of p_a, p_b, p_c, the value of β_h can be calculated from equation 3, whence V_h can be obtained from equation 2. If on the great circle through c orthogonal to that through a, b, c, two equispaced holes a' and b' are placed as shown in Fig. 1., the component V_v of the velocity $\bar{V}$ in the plane of this circle can be determinad from measurement of p'_a, p'_c, p'_b, by equations analogous to 2 and 3. The three components V_x, V_y, V_z along the sphere axes X, Y, Z of the velocity $\bar{V}$ are then given by:

$$V_x = V_h \cos\beta_h, \quad V_y = V_h \sin\beta_h, \quad V_z = V_v \sin\beta_v \qquad \ldots \quad 4.$$

In Refs. 8 and 9 in place of equation 2, the appropriate relations for

$$\frac{p_c - p_a}{\frac{1}{2}\rho V_h^2}, \qquad \frac{p_c - p_b}{\frac{1}{2}\rho V_h^2}$$

are used. The first or second of these pressure coefficients is taken depending on whether V_h is on one side or the other side of the centre hole. This introduces an unnessary complication. Use of equation 2 is recommended also because its pressure coefficient has a greater variation at any given value of β_h than these other two coefficients, thus giving a greater sensitivity.

3.0 CALIBRATION ANALYSIS.

Equations 2 and 3 are only true if the fluid has no viscosity, the sphere is perfect, the holes are exactly positioned, and the hole size approaches zero. Since none of these conditions is true in practice, calibration of the instrument is necessary to obtain curves of C_{Ph} and C_{ph} versus β_h which are used in place of equations 2 and 3. Similar calibration is necessary for C_{pv} and C_{Pv}.

Ideally, calibration for all combinations of values of C_{ph}, C_{Ph}, C_{pv}, C_{Pv}, β_h, β_v is required at all Reynolds numbers. This is not practical, or in reality necessary. Adequate accuracy can be obtained by using the following approximations.

(1) That the position of an orthogonal set of axes OX, OY OZ (the 'pitot axes') passing through the sphere centre and fixed to the pitot can be found experimentally such that if a, c, b and a', c, b' are assumed to be on the orthogonal planes XOY, XOZ respectively, the maximum error in the computed velocity vector $\bar{V}$ will be minimized within the variation of magnitude and direction of $\bar{V}$ it is wished to consider. These axes can be regarded as the 'best-fit' axes for the holes a, a', c, b, b'. The actual hole positions will clearly be very close to the planes XOY, XOZ for a well-made instrument.

(2) That the relationship between C_{ph}, C_{Ph}, and β_h is independent of V_v and β_v to a high degree of accuracy. In theory, as 2 and 3 indicate, there is complete independence. In practice, there can be a slight dependence. Similarly that the relationship between C_{pv}, C_{Pv}, and β_v is independent of V_h and β_h.

For a perfect instrument and fluid, the velocity $\bar{V}$ will be along the X pitot axis when:

(a) the pressures at a, b, a', b' are equal.

(b) the pressures remain equal at a and b for rotation about OY, and at a' and b' for rotation about OZ.

For the actual case, if a stream of precisely known direction is available, the pitot can be orientated in this stream to obtain the best overall compromise between condition (a) and condition (b) for angular rotations within the range required, thus determining the 'pitot axes' OX, OY, OZ.

If such a stream is not available, the following method can be used.

3.1 Initial Angular Calibration

The pitot is set up in a flow whose direction is approximately known, so that it can be rotated about two axes OY', OZ' which are normal to each other and to the nominal flow direction. OY' and OZ' pass through the sphere centre which remains fixed in space. The axis OX' also passes through the sphere centre and is orthogonal to OY' and OZ'.

The axes OX', OY', and OZ' remain fixed in space and in practice represent the axes of a mounting device or gymbal. The sphere is then orientated about its centre until the best compromise is obtained to condition (b) above. Figs. 2a and 2b indicate the effects of the "lateral tilt" and "rotational tilt" on the pressure difference of a hole pair, and the way in which the shape of the pressure difference curve can be used to indicate the corrective orientation necessary. If OY' and OZ' were truly normal to the flow vector $\bar{V}$ their position relative to the sphere would now closely coincide with the "pitot axes" OY, OZ defined earlier. In practice $\bar{V}$ would only be a few degrees from the direction of X'O so that as a first approximation it can be assumed to be in the direction of X'O. Calibration graphs of C_{ph} and C_{Ph} versus β_h, and C_{pv} and C_{Pv} versus β_v, can now be determined by rotation about OZ', OY'. These pressure coefficients can be assumed to be a first approximation of those which would be obtained by rotation about the pitot axes OZ and OY with $\bar{V}$ being initially exactly along XO. Note that the accuracy of the approximation decreases with increase in the angle of rotation about OZ' and OY', so that the initial orientation and calibration should only be for small values of β_h, and β_v (eg. up to $\pm$ 7°). The magnitude of $\bar{V}$ can be measured to to suffucuent accuracy by a standard bull-nose pitot-tube, which is not very sensitive to a few degrees yaw in the flow.

The error introduced by the flow velocity $\bar{V}$ not being in the calibration plane will be quite small since the velocity in the Calibration plane will differ from V only by $V(1 - \cos\phi)$ where ϕ is the angle of $\bar{V}$ to the calibration plane. Usually ϕ will not be more than a few degrees.

3.2 Orientation of Pitot Axes with reference to Datum Instrument Axes.

On the pitot base there will have been machined location faces. These can be used to define a set of orthogonal axes at the sphere centre, which will be called the datum instrument axes 0XX, 0YY, 0ZZ. The problem is to now determine the orientation or position of the pitot axes with reference to these known instrument axes. As shown below, this orientation can be determined in a stream whose flow direction is only approximately known, by three inversions of the sphere position, providing the pitot is set up in the flow so that the sphere can be rotated about 0XX, 0YY or 0ZZ without the centre of the sphere moving in space.

The direction cosines of the instrument axes 0XX, 0YY, 0ZZ with respect to the (unknown) pitot axes 0X, 0Y, 0Z will be denoted by:

	0X	0Y	0Z
0XX	l_{11}	l_{12}	l_{13}
0YY	l_{21}	l_{22}	l_{23}
0ZZ	l_{31}	l_{32}	l_{33}

The direction cosines of the velocity $\bar{V}$ with respect to the instrument axes 0XX, 0YY, 0ZZ will be denoted by l, m, n.

3.2.1 Rotation about 0XX Axis.

The sphere is initially positioned so that the flow vector $\bar{V}$ is at some estimated angle ψ to the centre hole (of between 5^{o} and 10^{o}). The sphere is then rotated successively by 90^{o} about the instrument axis 0XX, the initial position being that shown in Fig. 1 and denoted by the subscript 1, and the successive positions by subscripts 2,3,4. The direction of rotation is with the 0ZZ axis moving towards the position of the 0YY axis. The velocity $\bar{V}$ becomes with respect to the axes, successively, $\bar{V}_1$, $\bar{V}_2$, $\bar{V}_3$, $\bar{V}_4$ with direction cosines relative to the instrument axes 0XX, 0YY, 0ZZ as shown below.

	0XX	0YY	0ZZ
$\bar{V}_1$	1	m	n
$\bar{V}_2$	1	n	-m
$\bar{V}_3$	1	-m	-n
$\bar{V}_4$	1	-n	m

The direction cosines of $\bar{V}_1$, $\bar{V}_2$, $\bar{V}_3$, $\bar{V}_4$ with respect to the pitot axes 0X, 0Y, 0Z will be

$$\frac{V_{x1}}{V_1}\ ,\ \frac{V_{y1}}{V_1}\ ,\ \frac{V_{z1}}{V_1}\ ,\ \frac{V_{x2}}{V_2} \quad \text{etc.}$$

These can be denoted generally by

$$\frac{V_{ij}}{V_j} \qquad \text{where } i = 1,2,3$$

according to whether V_{ij} is the x,y,z component, and j takes the values 1,2,3,4 according to whether V_j is the magnitude of $\bar{V}_1$, $\bar{V}_2$, $\bar{V}_3$, $\bar{V}_4$. The ratio $\frac{V_{ij}}{V_i}$ will also be denoted by a_{ij}

By the transformation-of axes these direction cosines are given by;

$$a_{i1} = l_{1i}l + l_{2i}m + l_{3i}n \quad \text{with } i = 1,2,3 \quad \ldots \quad 6$$

$$a_{i2} = l_{1i}l + l_{2i}n - l_{3i}m \quad \text{with } i = 1,2,3 \quad \ldots \quad 7.$$

$$a_{i3} = l_{1i}l - l_{2i}m - l_{3i}n \quad \text{with } i = 1,2,3 \quad \ldots \quad 8.$$

$$a_{i4} = l_{1i}l - l_{2i}n + l_{3i}m \quad \text{with } i = 1,2,3 \quad \ldots \quad 9.$$

Since the a_{ij} of equations 6 to 9 can be computed from the pressure readings, the initial angular calibrations, and equation 4, we have a set of 12 equations in the 12 unknowns l_{pq} $(p,q = 1,2,3)$ and l, m, n.

There are also 6 identities between the direction cosines l_{pq} of the type

$$l_{11}^2 + l_{21}^2 + l_{31}^2 = 1 \quad \ldots \quad 10,$$

and a similar relation for the direction cosines l,m,n. There are thus 19 equations available in the 12 unknowns. On solving these equations it is found that they are not all independent and that the following relations exist between the direction cosines a_{ij} :

$$a_{i1} + a_{i3} = a_{i2} + a_{i4} \quad \text{with } i = 1,2,3 \quad \ldots \quad 11.$$

The only explicit solutions for the direction cosines l_{pq} and l,m,n are those for l_{11}, l_{12}, l_{13}, and l. Addition of equations 6 to 9 in respective pairs gives

$$a_{i1} + a_{i3} = 2l_{1i}l \;, \quad i = 1,2,3 \quad \ldots \quad 12.$$

$$a_{i2} + a_{i4} = 2l_{1i}l \;, \quad i = 1,2,3 \quad \ldots \quad 13.$$

Substituting equations 12 and 13 in 10 gives:

$$1 = \frac{1}{2}\left[(a_{11} + a_{13})^2 + (a_{21} + a_{23})^2 + (a_{31} + a_{33})^2\right]\frac{1}{2} \quad \ldots 14.$$

$$1 = \frac{1}{2}\left[(a_{12} + a_{14})^2 + (a_{22} + a_{24})^2 + (a_{31} + a_{34})^2\right]\frac{1}{2} \quad \ldots 15.$$

Since the velocities $(V_x, V_y, V_z, V)_{1,2,3,4}$ are determined experimentally, the experimental values for a_{ij} may not exactly satisfy equation 11. Equations 14 and 15 will yield two experimentally derived values of 1, and substitution respectively into 12 and 13 gives two sets of values for l_{11}, l_{12}, l_{13}. Since the initial angular calibration graphs used to calculate $(V_x, V_y, V_z,)_{1,2,3,4}$ are a first approximation, these values of 1, l_{11}, l_{12}, l_{13} must also be regarded as first approximations.

3.2.2 Inversion about OYY Axis.

The sphere is rotated to the initial position 1 of Section 3.2.1. The velocity $\bar{V}$ will make an angle θ with the XXYY plane as shown in Fig. 3. Since the flow direction is known approximately, an estimate of the value of θ can be made. The sphere is then rotated about OYY so that $\bar{V}$ will make an angle of approximately $-\theta$ with the XXYY plane. The initial and final configurations will be denoted by subscripts 1 and 5.
The components of $\bar{V}_1$ with respect to OXX, OYY, OZZ will be (Fig. 3).

$$V_1 \cos\beta_1 \cos\theta_1; \quad V_1 \sin\beta_1; \quad V_1 \cos\beta_1 \sin\theta_1 \quad \ldots 16.$$

and the corresponding direction cosines of $\bar{V}_1$ will thus be

$$\cos \beta_1 \cos \theta_1; \quad \sin \beta_1; \quad \cos \beta_1 \sin \theta_1 \qquad \ldots \quad 17.$$

The direction cosines l_1, m_1, n_1 of $\bar{V}_1$ with respect to OX, OY, OZ are from equations 17 and 5 using the transformation-of-axes theorem.

$$\begin{aligned} l_1 &= l_{11} \cos \beta_1 \cos \theta_1 + l_{21} \sin \beta_1 + l_{31} \cos \beta_1 \sin \theta_1 \\ m_1 &= l_{12} \cos \beta_1 \cos \theta_1 + l_{22} \sin \beta_1 + l_{32} \cos \beta_1 \sin \theta_1 \\ n_1 &= l_{13} \cos \beta_1 \cos \theta_1 + l_{23} \sin \beta_1 + l_{33} \cos \beta_1 \sin \theta_1 \end{aligned} \qquad \ldots \quad 18.$$

A similar set of equations 19 to that of 18 can be derived for $\bar{V}_5$.

The components of the vector $\bar{V}_6 = \bar{V}_1 - \bar{V}_5$ with respect to OX, OY, OZ are given by

$$\begin{aligned} V_{x6} &= V_1 l_1 - V_5 l_5 \\ V_{y6} &= V_1 m_1 - V_5 m_5 \\ V_{z6} &= V_1 n_1 - V_5 n_5 \end{aligned} \qquad \ldots \quad 20$$

and substituting into equation 20 from 18 and 19 and putting $V_1 = V_5 = V$, and $\beta_1 = \beta_5 = \beta$ to simplify we obtain:

$$\frac{V_{x6}}{V} = (l_{11} \cos \beta \cos \theta_1 + l_{31} \cos \beta \sin \theta_1) - (l_{11} \cos \beta \cos \theta_5 + l_{31} \cos \beta \sin \theta_5)$$

$$\frac{V_{y6}}{V} = (l_{12} \cos \beta \cos \theta_1 + l_{32} \cos \beta \sin \theta_1) - (l_{12} \cos \beta \cos \theta_5 + l_{32} \cos \beta \sin \theta_5)$$

$$\frac{V_{z6}}{V} = (l_{13}\cos\beta\cos\theta_1 + l_{33}\cos\beta\sin\theta_1) - (l_{13}\cos\beta\cos\theta_5 + l_{33}\cos\beta\sin\theta_5) \quad \ldots \quad 21$$

The components of $\bar{V}_6$ are also given by

$$\begin{aligned} V_{x6} &= V_{x1} - V_{x5} \\ V_{y6} &= V_{y1} - V_{y5} \\ V_{z6} &= V_{z1} - V_{z5} \end{aligned} \quad \ldots \quad 22$$

Substituting equation 22 into 21 gives:

$$\begin{aligned} \frac{V_{x1} - V_{x5}}{V\cos\beta} &= l_{11}(\cos\theta_1 - \cos\theta_5) + l_{31}(\sin\theta_1 - \sin\theta_5) \\ \frac{V_{y1} - V_{y5}}{V\cos\beta} &= l_{12}(\cos\theta_1 - \cos\theta_5) + l_{32}(\sin\theta_1 - \sin\theta_5) \\ \frac{V_{z1} - V_{z5}}{V\cos\beta} &= l_{13}(\cos\theta_1 - \cos\theta_5) + l_{33}(\sin\theta_1 - \sin\theta_5) \end{aligned} \quad \ldots \quad 23$$

Since $\theta_5 \simeq \theta_1$ the first term of equation 23 is approximately zero and can be neglected.

Hence equation 23 reduces to:

$$\begin{aligned} \frac{V_{x1} - V_{x5}}{V} &= l_{31}A \\ \frac{V_{y1} - V_{y5}}{V} &= l_{32}A \\ \frac{V_{z1} - V_{z5}}{V} &= l_{33}A \end{aligned} \quad \ldots \quad 24$$

where $A = \cos\beta\,(\sin\theta_1 - \sin\theta_5)$

From the pressure measurements at configurations 1 & 5 and using the initial angular calibrations, $(V_x, V_y, V_z, V)_{1\ \&\ 5}$ can be estimated, and substitution into equation 24 together with the condition that

$$l_{31}^2 + l_{32}^2 + l_{33}^2 = 1 \qquad \ldots \quad 25$$

enables l_{31}, l_{32}, l_{33} to be calculated.

By setting the pitot back to configuration 4 of Section 3.2.1 and inverting to configuration 6, in a similar manner, another set of equations similar to 24 can be obtained from which another set of values of l_{31}, l_{32}, l_{33} can be calculated.

3.2.3. Inversion about OZZ Axis.

By repeating the procedure outlined in Section 3.2.2, but in this case for inversion about the OZZ axis from configuration 1 to configuration 7, values can be obtained for l_{21}, l_{22}, l_{23}, the relevant equations being

$$\frac{V_{x1} - V_{x7}}{V} = l_{21}\,B$$

$$\frac{V_{y1} - V_{y7}}{V} = l_{22}\,B \qquad \ldots \quad 26$$

$$\frac{V_{z1} - V_{z7}}{V} = l_{23}\,B$$

and

$$l_{21}^2 + l_{22}^2 + l_{23}^2 = 1 \qquad \ldots \quad 27$$

A similar inversion about OZZ from configuration 2 to configuration 8 allows a second set of values of l_{21}, l_{22}, l_{23} to be computed.

3.2.4 Iterative Procedure to Increase Accuracy.

By the method outlined in Sections 3.1 and 3.2.1 to 3.2.3, first approximations have been obtained for the angular calibrations with respect to pitot axes, and for the orientation of the pitot axes with respect to datum instrument axes. This orientation being specified by the direction cosines l_{pq} $(p,q = 1,2,3)$. Also first approximations have been obtained to the flow direction.

The pitot can now be reset so that the calculated pitot axis OX is in the calculated flow direction, and the procedure repeated as necessary to obtain both the angular calibrations and the direction cosines to the desired accuracy. For the final angular calibrations it is desirable to obtain graphs of C_{ph} and C_{Ph} versus β_h for several fixed values of β_v, and to average these to obtain the final calibration graphs of C_{ph} and C_{Ph} versus β_h. Similarly for the β_v calibration graphs. On physical grounds it can be seen that the iterative procedure described above will be convergent. In many cases, the first set of results will be sufficiently accurate.

4.0 EFFECT OF REYNOLDS NUMBER.

It has been noted (Ref. 11) that below a Reynolds Number R_n of the order of 10^4 there can be "some trouble with calibration," and "laminar separation and a change of the pressure distribution in the neighbourhood of the pressure holes" is suggested as the cause. Calibrations carried out by the authors in a wind tunnel with a 3/8 inch diameter Spherical pitot (see Fig. 4) show some variation below a R_n of about 1.4×10^4. Above this value the effect of R_n would appear to be small.

5.0 THE UTILIZATION OF CALIBRATION DATA.

The calibrations at $R_n = 1.6 \times 10^4$ obtained by the authors for the 3/8" pitot are shown in Fig. 5. In this form, the calibration data is not suited to the analysis of test results by digital computer. The calibration data can be expressed for computer analysis by determining the difference between theoretical and experimental results in a polynomial form as follows:--

Thus

$$\left(\frac{p_a - p_b}{\frac{1}{2}\rho V^2}\right)_{\text{expt'al}} = \frac{9}{4}\left(\sin 2\alpha \sin 2\beta_h\right) - \sum_i a_i \beta_h{}^i \qquad \ldots \quad 28$$

$$(\tan 2\beta_h)_{expt'al} = \frac{(p_a - p_b)(1-\cos 2\alpha)}{(2p_c - p_a - p_b)\sin 2\alpha} - \sum_i b_i \left[\frac{(p_a - p_b)}{2p_c - p_a - p_b}\right]^i_{expt'l} \quad \ldots \quad 29$$

where the last right-hand-side terms are best-fit polynomials. This numerical procedure allows the calibrations to be incorporated into a data reduction programme for test results.

REFERENCES

1. DEAN, R.C. — Aerodynamic Measurements. M.I.T Press. 1953

2. JANES, C.E. — Instruments & Methods for Measuring the Flow of Water around Ships & Ship Models. David Taylor Model Basin Report 487, March'48

3. MEYER, H — Onderzoek betreffend de meetmethode met de pitot-buis van Dr. Ing.J.J. Borren (Investigation on the Method of Measurement with Pitot Tube, Designed by Dr. J.J. Borren) De Ingenieur p.173. 7 July 1928.

4. GUTSCHE, F — Das Zylinderstaurohr (The Cylindrical Pitot Tube) Schiffbau, Shiffart and Hafenbau pp.13-19, v. 32, n.1, January, 1931

5. KRISAM, F — Speed & Pressure Recording in Three-Dimensional Flow. NACA-TM 688, October, 1932

6. JEGEROW, G. — Measurement of Direction, Velocity & Pressure in a Three-Dimensional Current. R.T.P Translation No.2498, Durand Reprinting Comm., California Institute of Technology.

7. ECKERT, B. — Experiences with Flow-Direction Instruments NACA-TM 969, March, 1941.

8. PIEN, P.C. — The Five-Hole Spherical Pitot Tube. David Taylor Model Basin Report 1229 May 1958

9. SILOVIC, V — The Five Hole Spherical Pitot Tube for Three Dimensional Wake Measurement. Hydro-Og Aerodynamisk Laboratorium. (Lyngby, Denmark) Report No.Hy-3, May, 1964)

10. ROBERT, B.G. — Static Response of Hemispherical Head, Differential Pressure Incidence Meter from March No 1.6 to 2.6 Weapons Research Establishment Technical Notes HSA 46 Nov. 1959. Extension of the Calibration to 30^{o} Incidence and Mach. No 2.75. WRE Tech. Note HSA 72 January 1961.

11. van MANEN, J.D. — Unsteady Propeller Forces. Proceedings of 10th International Towing Tank Conference, Vol.1. pp. 151-155, 1963.

Fig. 1.

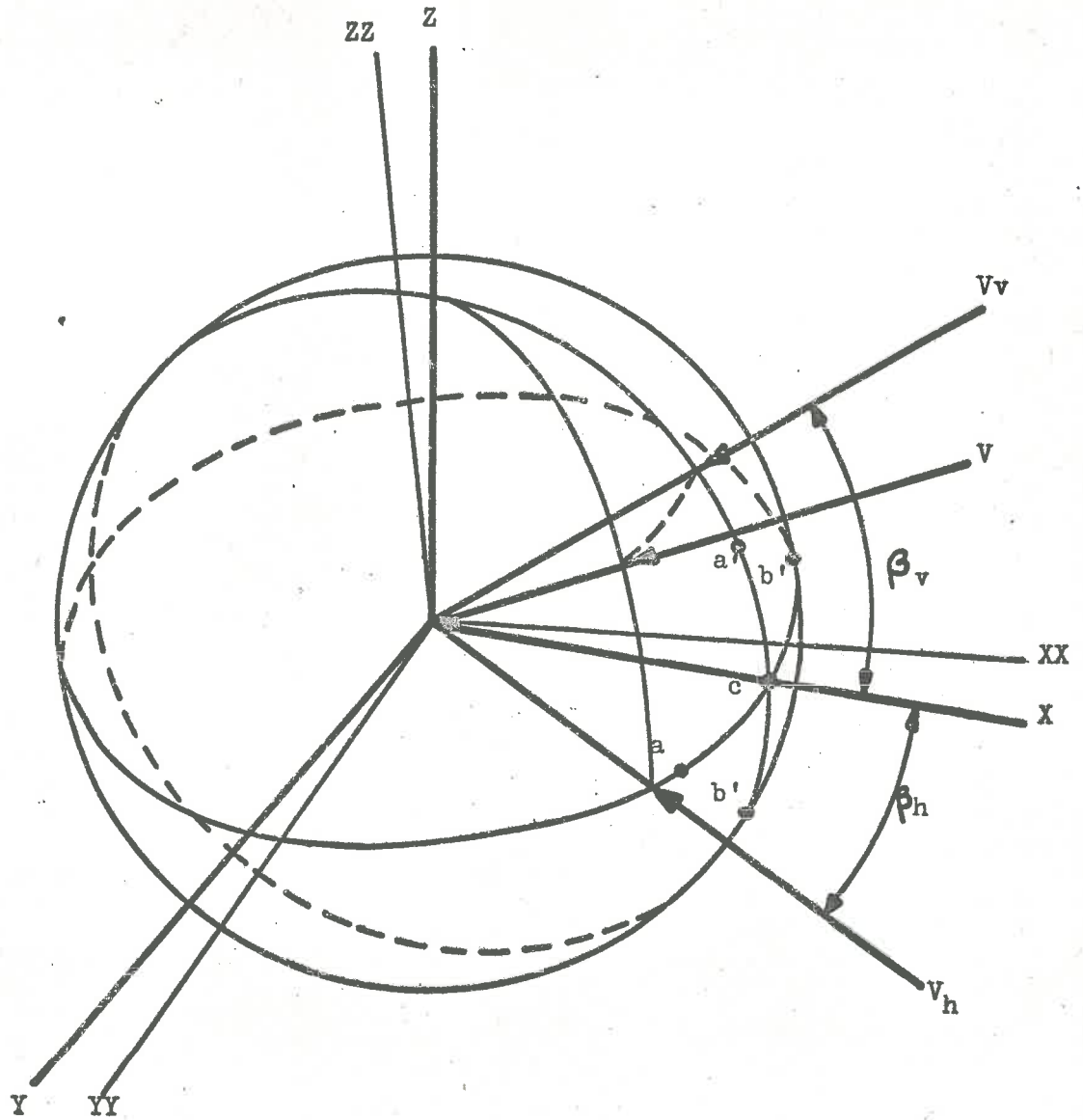

Fig. 1. - Orientation of Velocity components and pressure points to the Axes.

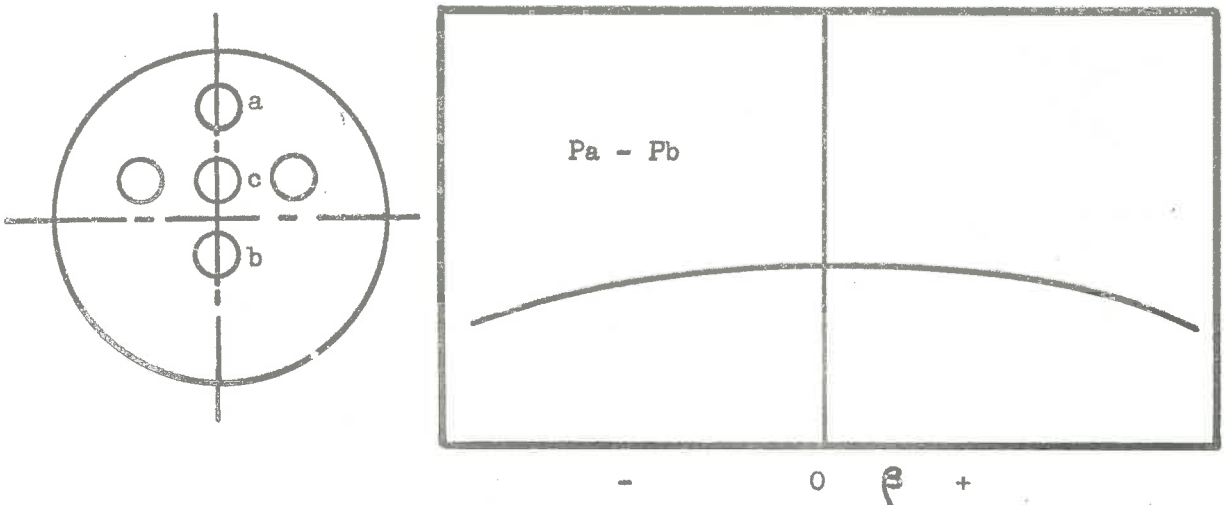

Fig. 2a - Effect of "lateral Tilt" on Pressure Difference (Pa - Pb)

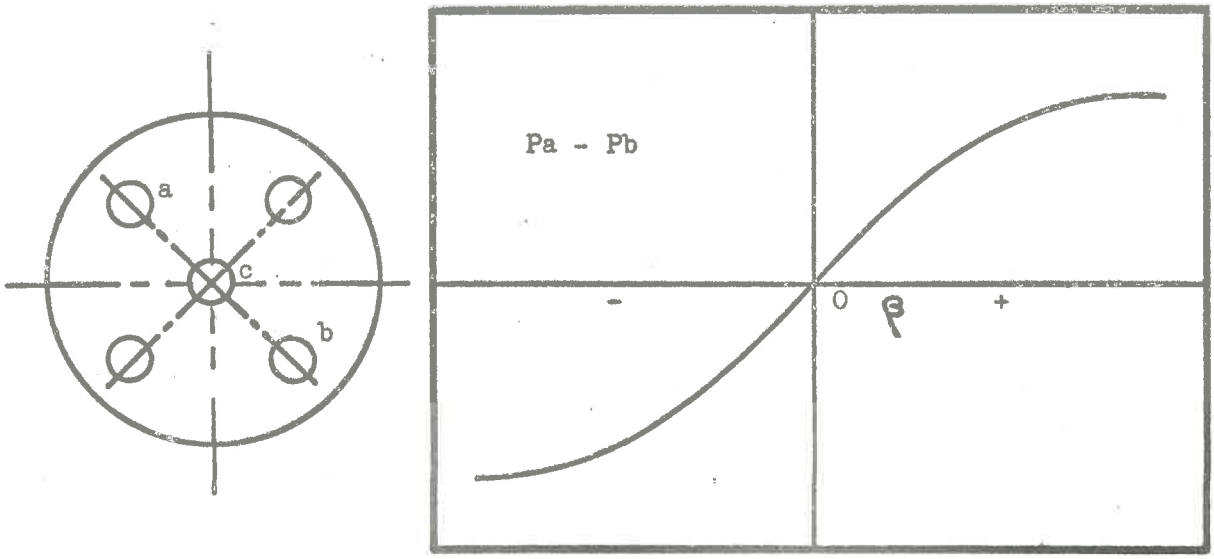

Fig. 2b - Effect of "rotational tilt" on Pressure Difference (Pa - Pb)

Fig. 3.

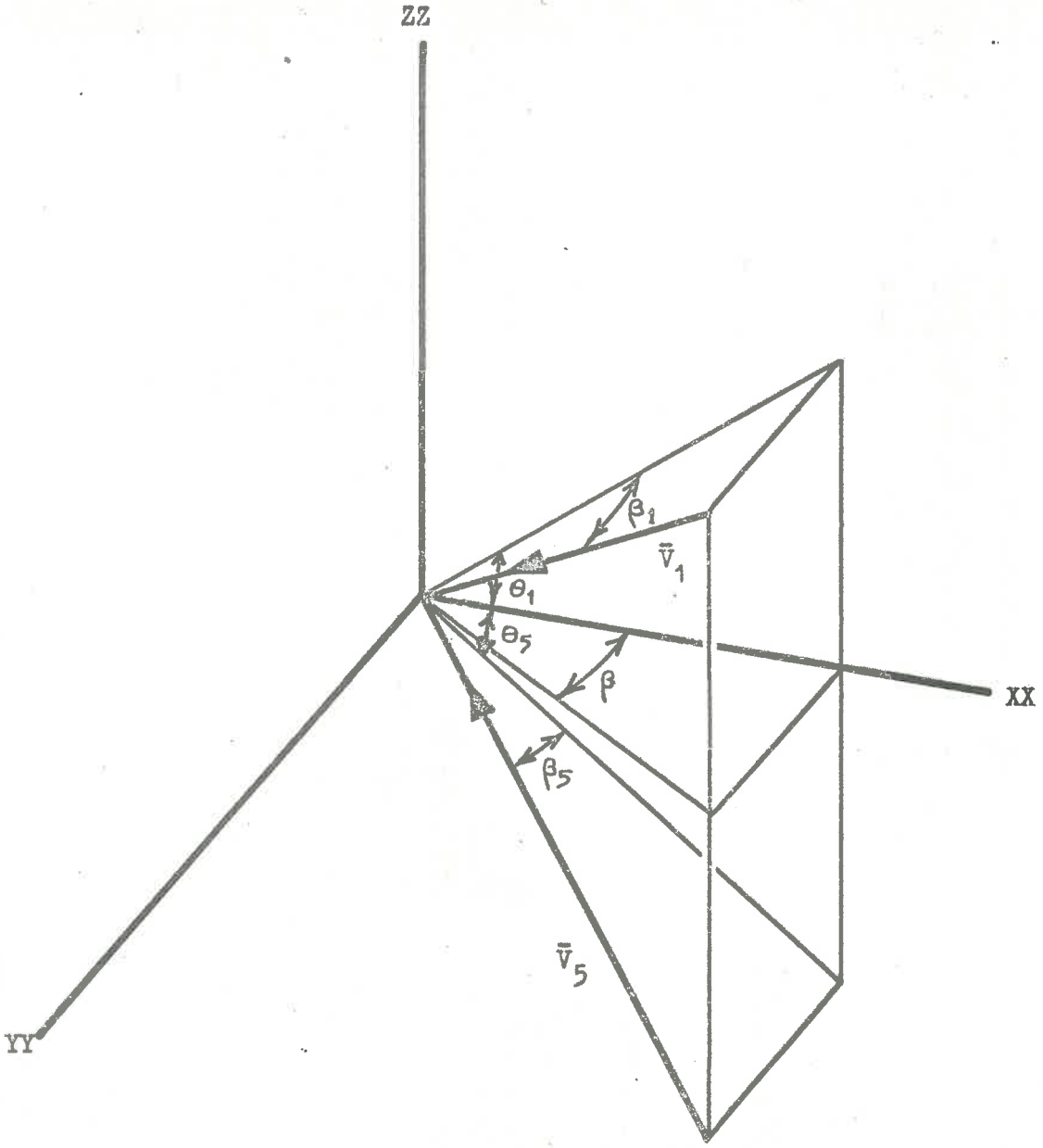

Fig. 3 - Inversion about OYY Axis.
Notation of Velocity Components with respect to the Instrument Axes.

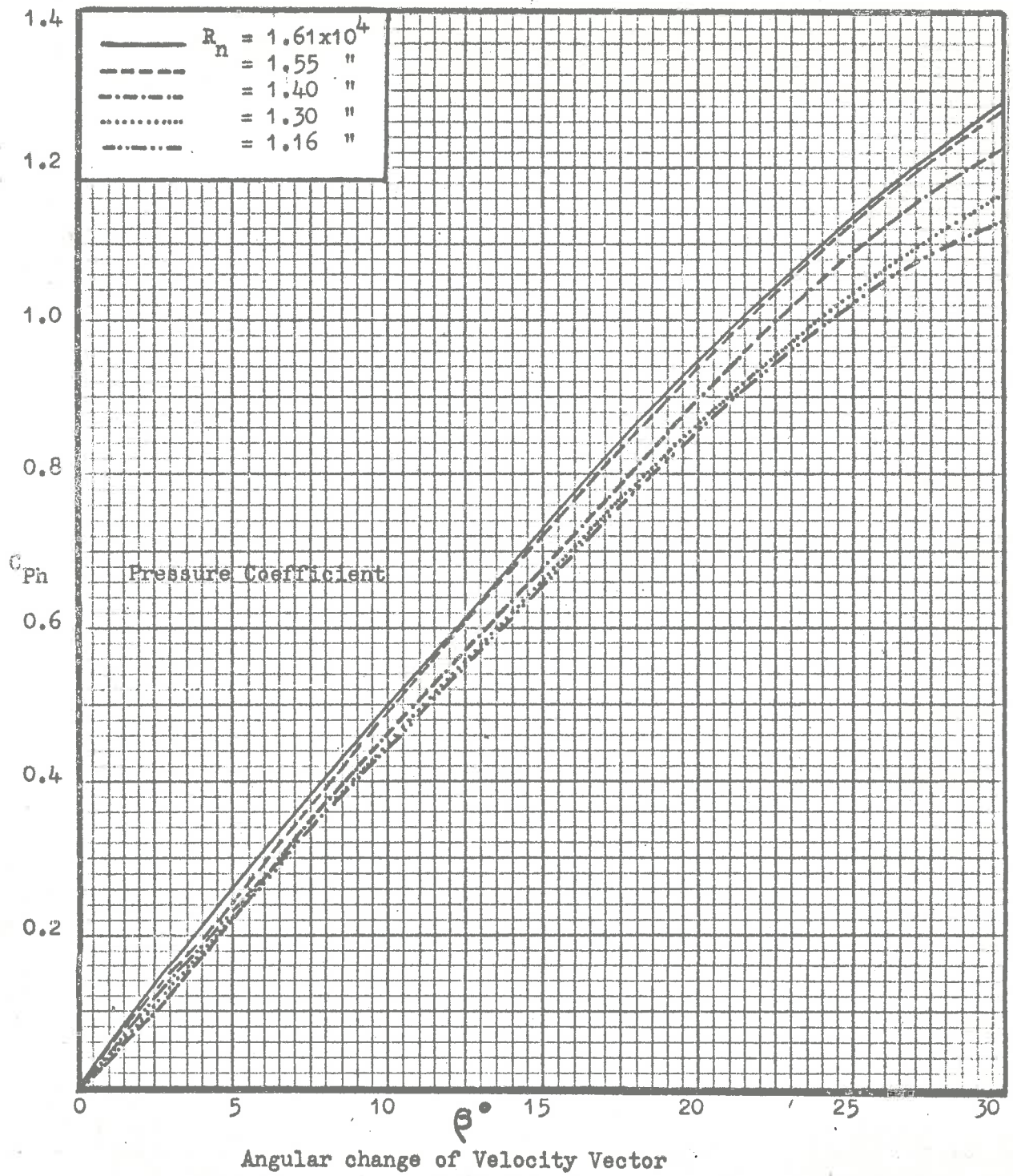

Fig. 4 - Effect of Reynolds Number on Pressure Coefficient.

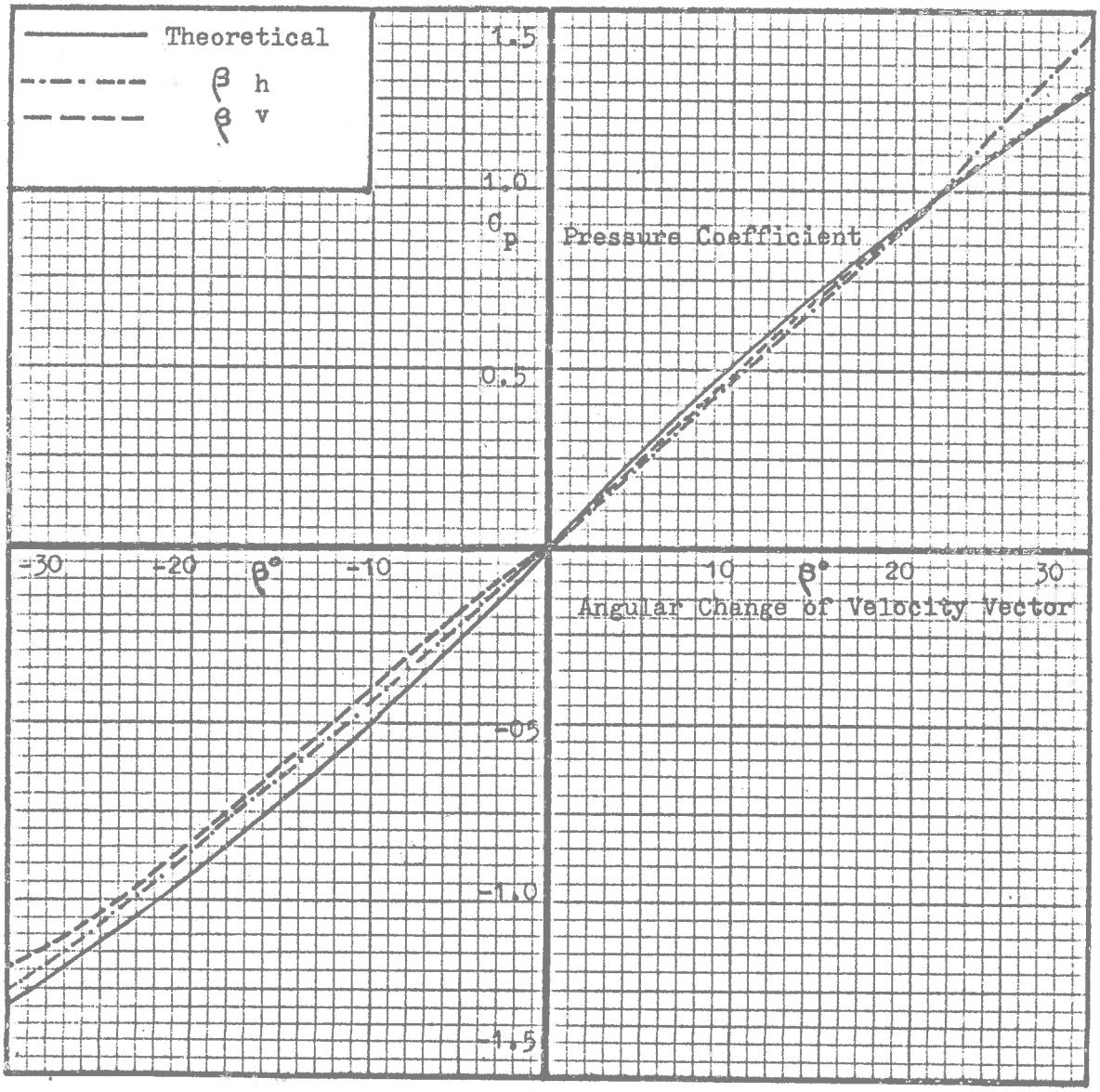

Fig. 5.1 - Typical Calibration Curve for 3/8" Pitot.

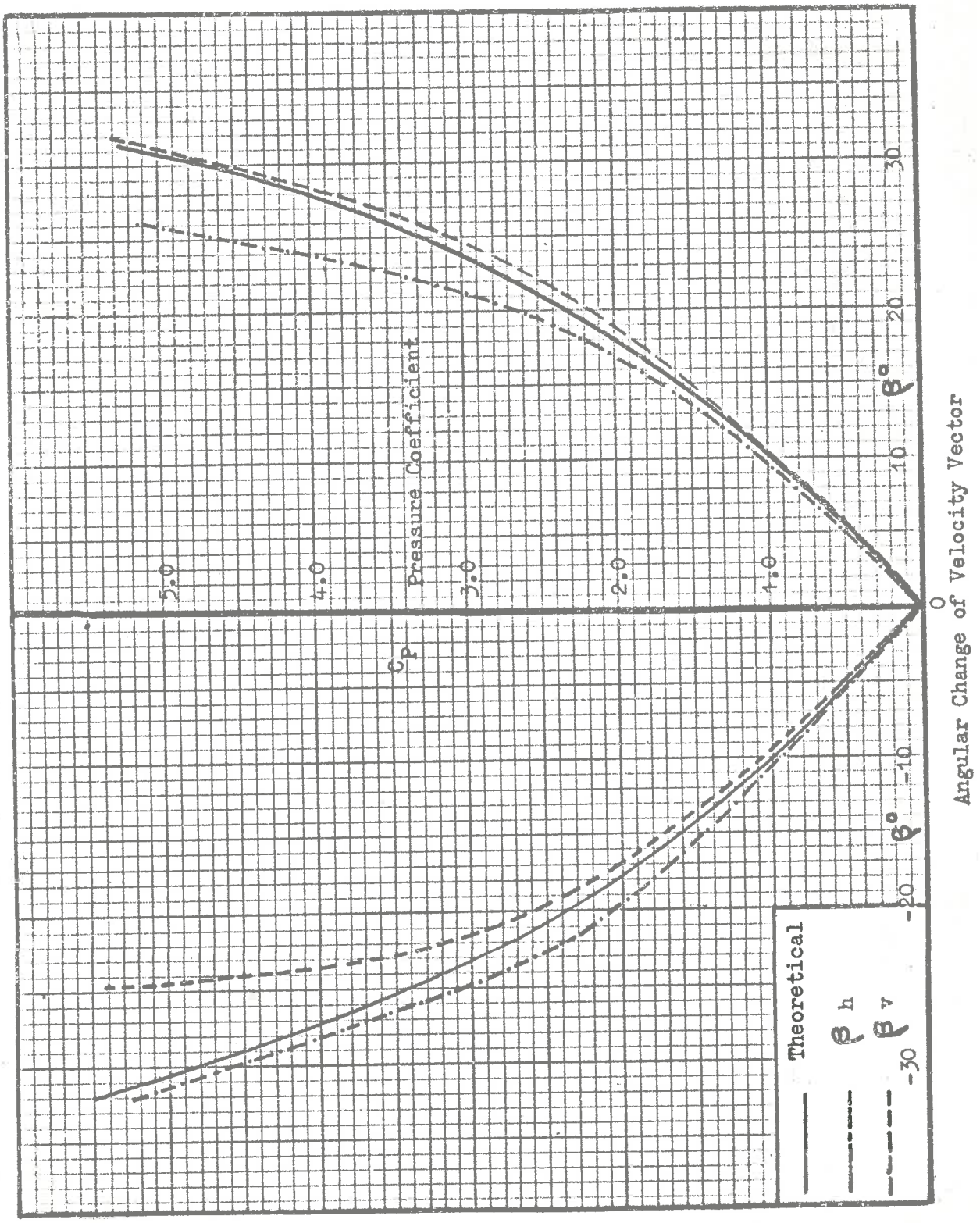

Fig. 5.2 - Typical Calibration Curve for 3/8" Pitot.

APPENDIX A7

MOVADAS - DATA ACQUISITION SYSTEM.

APPENDIX A7

A7.0 MOVADAS - DATA ACQUISITION SYSTEM

MOVADAS - (Modulated Voltage Analogue Data Acquisition System) is a Frequency Modulated Recording System based on the Standard Bandwidth IRIG Specifications as follows:

Tape speed	ips	60	30
Carrier frequency	Kc/S	54	27
Modulation range	% of carrier	±40	±40

MOVADAS consists of the following basic units:

(1) Signal Amplifiers and conditioning units.

- (i) D.C. Voltage pre-amplifiers.
- (ii) Driver Amplifier and High-pass Filter.
- (iii) Voltage-frequency (V-F) Converters.
- (iv) Programming switch.
- (v) Event Marker.
- (vi) Reference frequency.

(2) High speed tape recorder.

A simplified layout of MOVADAS is given in Fig. A7.1.

A7.1 SIGNAL AMPLIFIERS AND CONDITIONING UNITS

(1) D.C. Voltage Pre-amplifiers

The circuit for the D.C. Pre-amplifier was based on the conventional type of balanced differential transistor amplifier.

The circuit as shown in Fig. A7.9.1 was designed using the experience gained within the Mechanical Engineering Department at Adelaide over the past years. By careful selection of the components, it was possible to reduce the voltage drift and the amplifier noise level, due to changes in either ambient temperature or the supply voltage, to quite small values.

A brief specification of the D.C. Pre-amplifiers is as follows:

Input impedance	73 KΩ
Output "	230 Ω
Voltage gains up to	7000
Input noise level	4 μV
Common mode rejection ratio	Excellent
Offset voltage	0v
Linear O/P voltage swing	±3 volts
Frequency response (flat)	DC-17KC (at least)
Supply voltage	18v DC

The first stage transistors (2S501 or 2S502, low noise transistors) were selected using the following technique,

(i) Each transistor (T_1) was compared with a fixed or control transistor (T_2), and the value of the load resistor RV1 in the figure below was measured after RV1 was adjusted to give voltage e_o equal to 0 volts.

(ii) The transistors were paired according to equal load resistor RV1.

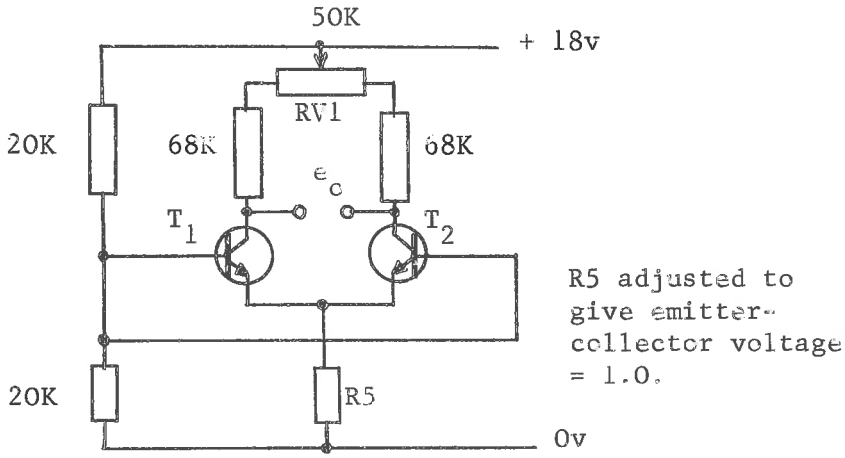

(iii) The pairs with maximum gains were selected for the pre-amplifiers.

All the transistors in the amplifiers were symmetrically mounted in a circular aluminium block the function of which was to act as a heat sink for uniform temperature. Metallic-oxide film, high-stability resistors were used throughout to maintain stability and to reduce the noise level.

The amplifier power supply regulation circuit and strain gauge voltage and balance circuit are given in Figs. A7.9.2 and A7.9.3.

(2) Driver Amplifier and High Pass Filter

This provided either DC or AC coupled inputs through two Nuvistor triodes in push-pull cathode follower configuration.

The triodes gave a high input impedance and a low output impedance to connect directly to two push-pull transistor amplifier stages (Ref. A7.1). The gain control was obtained by feedback. The output voltage from an emitter follower to the V-F converter was limited by the forward conduction of silicon diodes.

The circuit diagram is shown in Fig. A7.2.1 and A7.2.2.

(3) Voltage-Frequency Converter

The IRIG specification as follows was adopted.

Carrier frequency	54 Kc/s at 60"/s
Modulation range	±40% of carrier frequency
Input voltage	±1.4 volts for f.s.d.

Each V-F converter consisted of:

(i) Input stage

(ii) Modulator

(iii) Schmitt Trigger

(iv) Binary divider/flip-flop plus output stage.

The circuit diagrams are given in Figs. A7.3.1 to A7.3.6.

(i) Input Stage

Provided approximately 10,000Ω input impedance through an OC 140 emitter follower. This was temperature compensated by another OC 140 in the emitter circuit.

(ii) Modulator

This was a free-running voltage controlled R-L multivibrator adjusted to 54 Kc/s at zero input. The allowable linear deviation from this centre frequency was ±40%. The input signal was fed in through two 10mH

inductances, each one coupled to an emitter follower. A further emitter follower supplied a low output impedance to the Schmitt trigger.

(iii) Schmitt Trigger

This unit converted the Modulator output voltage to a "square" wave form.

(iv) Binary divider/Flip-flop

At a recording speed of 30 ips both inputs A & B at this stage were connected to output B of the Schmitt Trigger to provide a binary division prior to the flip-flop.

At 60 ips both outputs A & B of the Schmitt were connected to inputs A & B respectively of the Flip-flop which acted as a signal clean-up stage.

A low impedance output stage followed to match that of the Record/Reproduce tape head.

(4) Programming Switch

This unit controlled the recording sequence and inserted pulses of known amplitudes to identify the recorded information, i.e. run and channel identification. An instantaneous calibration of the V-F converter was also provided, immediately prior to the recording of real data.

Format details of the recorded information can be found in a following Section A7.4.

A block diagram of the programming switch is given in Fig. A7.6.1 and the circuit of the basic monostable multivibrator used is given in Fig. A7.6.2.

The programming switch inserted the identification marks simultaneously on all active channels, except that channel which recorded the reference frequency [see (6) following].

(5) Event Marker

An FM signal changing from a static level of 54 Kc/s to a transient value of 70 Kc/s upon occurrence of a cyclic "Event" was recorded on a separate data channel during each recording sequence.

The event was signified by the interruption of a light beam impinging on a photo-cell.

An OC 71 transistor, which had the paint removed from its cover, was used as the photocell.

The voltage signal was fed into an AC coupled, two-stage pulse amplifier which provided a heavy positive pulse to the monostable multivibrator.

A variable pulse length was provided by the switching of a capacitor C3. (Refer Fig. A7.5.2).

The stages following were identical to those of the V-F converter.

The circuit diagrams are shown in Figs. A 7.5.1 and A7.5.2.

(6) Reference Frequency

This was required for the analogue-to-digital conversion and was a 50 Kc/s, F-M signal recorded on a separate track of the magnetic tape.

The unit was controlled by a Venner Crystal Oscillator Type TS 25.

The basic layout for this unit is given in Fig. A7.4.

A7.2 HIGH SPEED TAPE RECORDER

An Epsylon Multitrack high speed tape recorder was modified to take 0.500 of an inch tape width at speeds of 60 and 30 ips. The magnetic heads were replaced with DRICO Series 50, Record/Reproduce heads to IRIG 7 track specifications.

A7.3 ANALOGUE - DIGITAL CONVERSION

The recorded F.M. information was converted into binary information at the rate of 4000 samples per second at an analogue tape speed of 60 ips. The recording mode of the digital information was compatible with IBM 7090 digital computer

i.e.	Packing density	200 bits per inch
	MOVADAS Data word	12 reading bits plus 2 parity bits
	Computer word	36 bits or three MOVADAS data words
	Record length	324 words

Because the A-D Converter used for the conversion was programmed to accept multiplexed telemetery data, the resulting structure of each computer record was as follows:

Each recorded track was converted separately and the digital information was recorded end-for-end on the digital tape or"transmittal tape."

The list of numbers which represented a complete single recorded run was termed a file. After each file an end of file

mark was recorded on the digital tape.

In the first record of a file, between the first (1) and the twenty-fourth (24) MOVADAS word, a time word of three (3) MOVADAS words in length was automatically inserted. The time word had the following structure, in octal notation.

$$4000_8,\ XXXX_8,\ YYYY_8$$

where $XXXX_8$ was greater than 40_8

$YYYY_8$ was greater than 4000_8

This information was a real time count and was redundant in the subsequent analysis.

After every twenty-fourth MOVADAS word the time word was repeated until the end of file.

A7.4 FORMAT OF RECORDED INFORMATION, ANALOGUE AND DIGITAL

The form of the input voltage to the V-F converter in MOVADAS, on automatic record mode, is sketched in Fig. A7.10.

The corresponding F.M. signal and digital output is also given in Fig. A7.10.

It was found necessary to commence each recording by a period of constant voltage, i.e. constant frequency on the F.M. signal, because the A-D Converter had to be manually operated.

The identification pulses prior to the recorded data represented the run number and channel (or track) number in binary form.

The run number consisted of five bits of information giving run numbers from 0 to 31 and the channel identification consisted of three bits. After this information a series of calibration voltages followed, enabling an instantaneous calibration to be made of the V-F converter.

The identification pulses and calibration voltages were applied to all active channels simultaneously. This was necessary because the recorded data from several tracks had to be phase compared in subsequent analysis.

The information recorded on the digital tape is as sketched in Fig. A7.10. The list of digits which constitutes a single experimental reading was termed a file and was terminated with an end of file mark. It should be noted that due to the programming switch in MOVADAS, the actual digital pulses were not ideally 'square cornered.' The initial discontinuity and leading edge was as desired, but oscillations did exist on the pulse top and trailing edge. These irregularaties presented difficulties, when developing a technique for detecting the identification pulses during computer analysis of the data.

The bit structure of the recorded digital data is quoted in Section A7.3 and details of the analysis of the data are given in Appendix A8.

REFERENCE

A7.1 GRIGSON, C.W.B. Some Precision Direct-Coupled Transistor Amplifier and Approximate Design.
Electronic Engineering, July-August 1964 Vol.36 Nos.437, 438

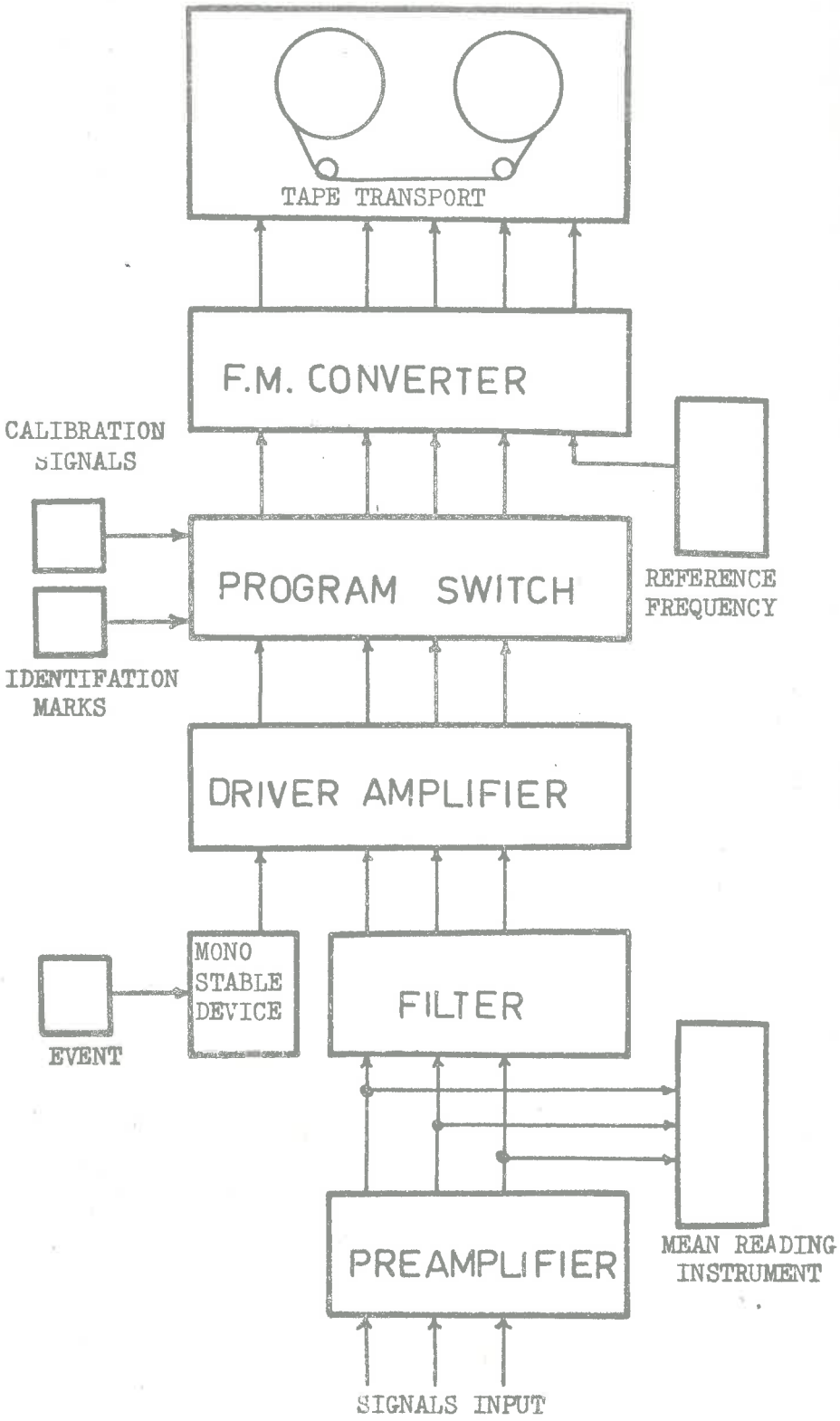

Fig. A7.1 - Layout of Movadas

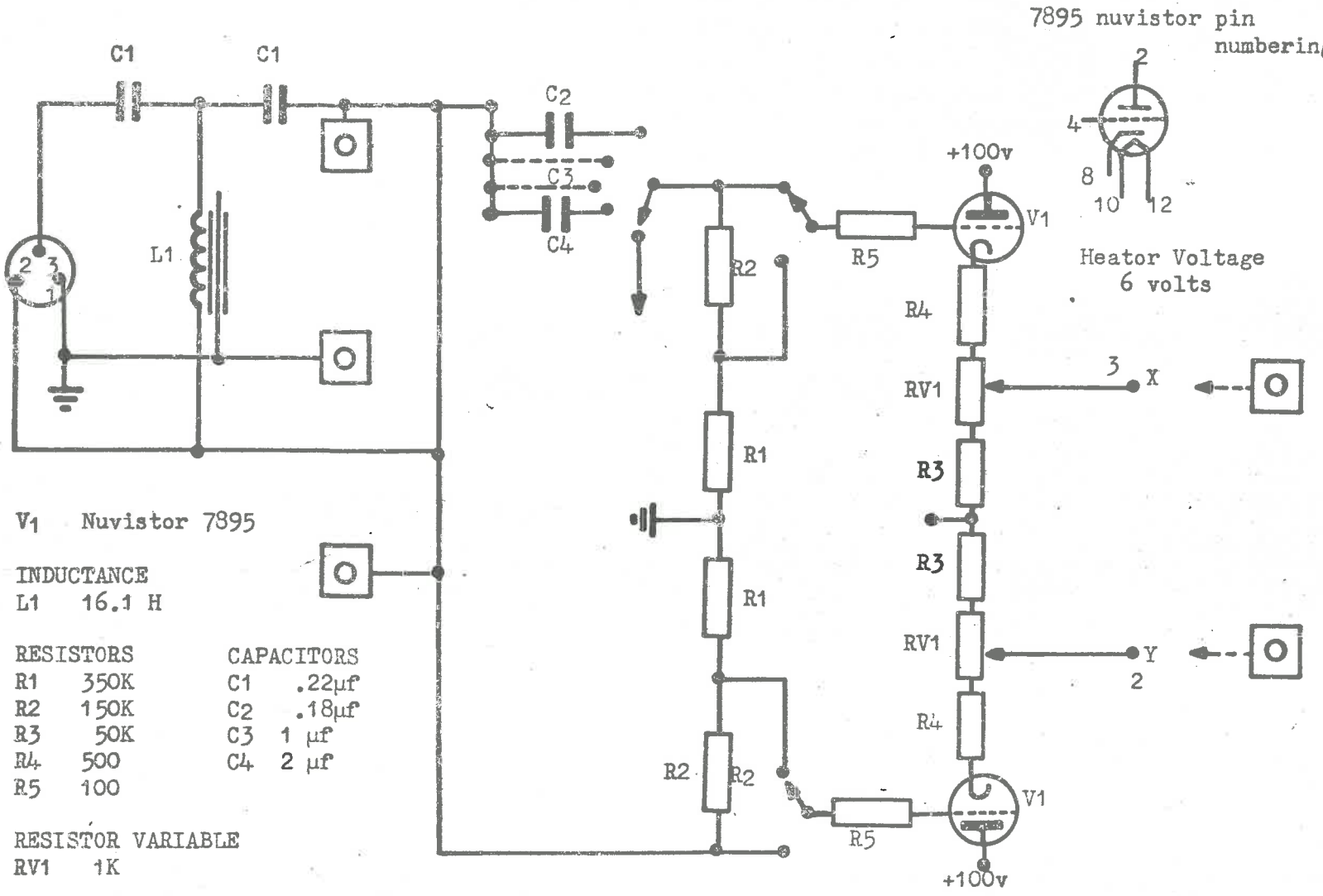

Fig.A2.1 - Driver Amplifier
Filter and High Input Impedance Stage

Fig.A2.1

TRANSISTORS

T1 2S 303
T2 2S 703
T3 2S 303

DIODES

D1 10D4
D2 10D4

RESISTORS

R1 390
R2 390
R3 Variable so RV2
R4 works at 0.V
R5 between T1 & T2
R6 33K
R7 5.6K
R8 1K
R9 1.2K
R10 1K
R11 220
R12, R13, R14, R15, R16 } Gain setting resistor selected

RESISTORS VARIABLE

RV1 10K fine } balance
RV2 500 coarse }

CAPACITORS

C1, C2, C3, C4, C5 } Selected for each gain Setting

Fig. 2.2 - Driver Amplifier Amplification Stage.

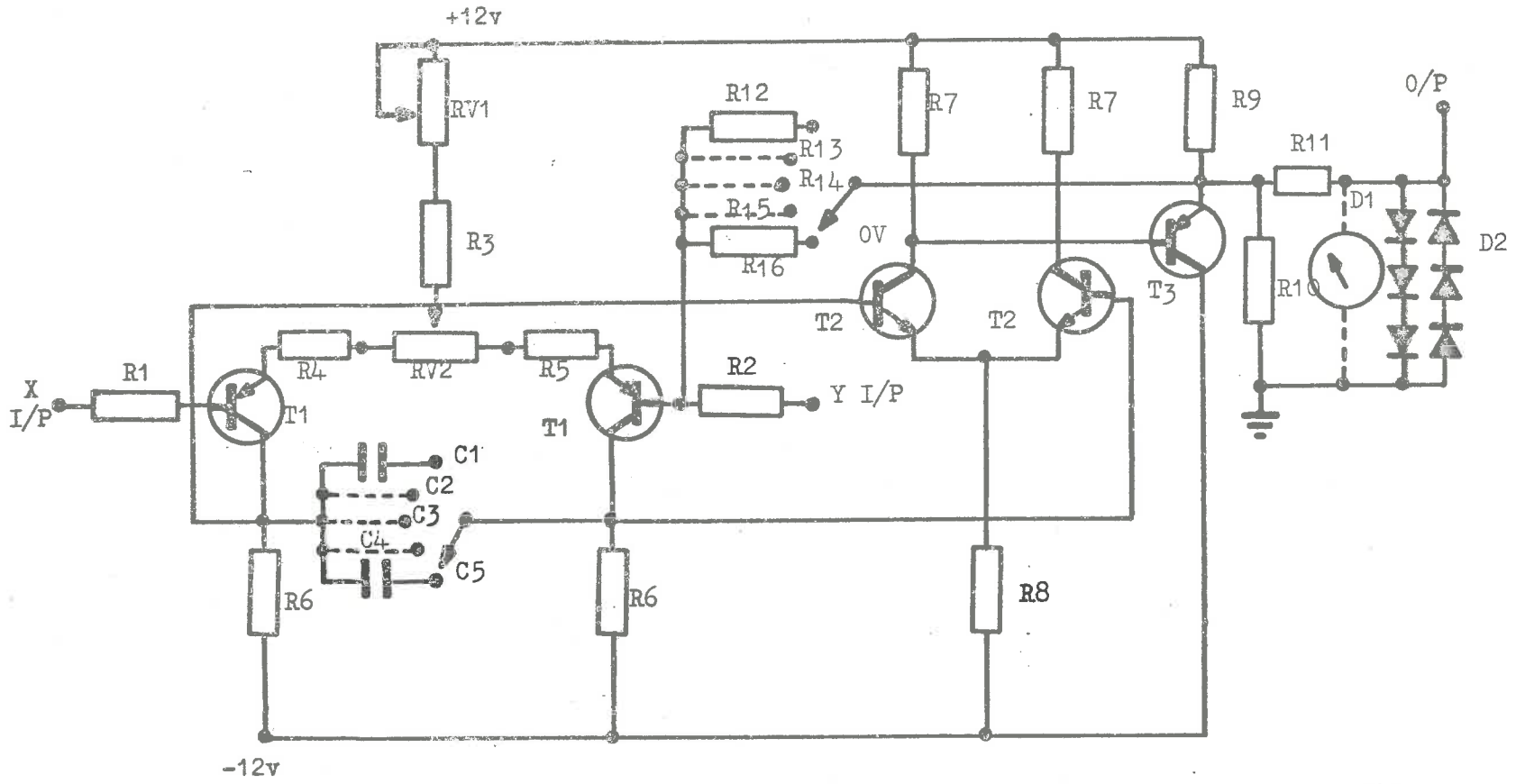

Fig.A7.2.2 - Driver Amplifier
Amplification Stage.

Fig.A7.2.2

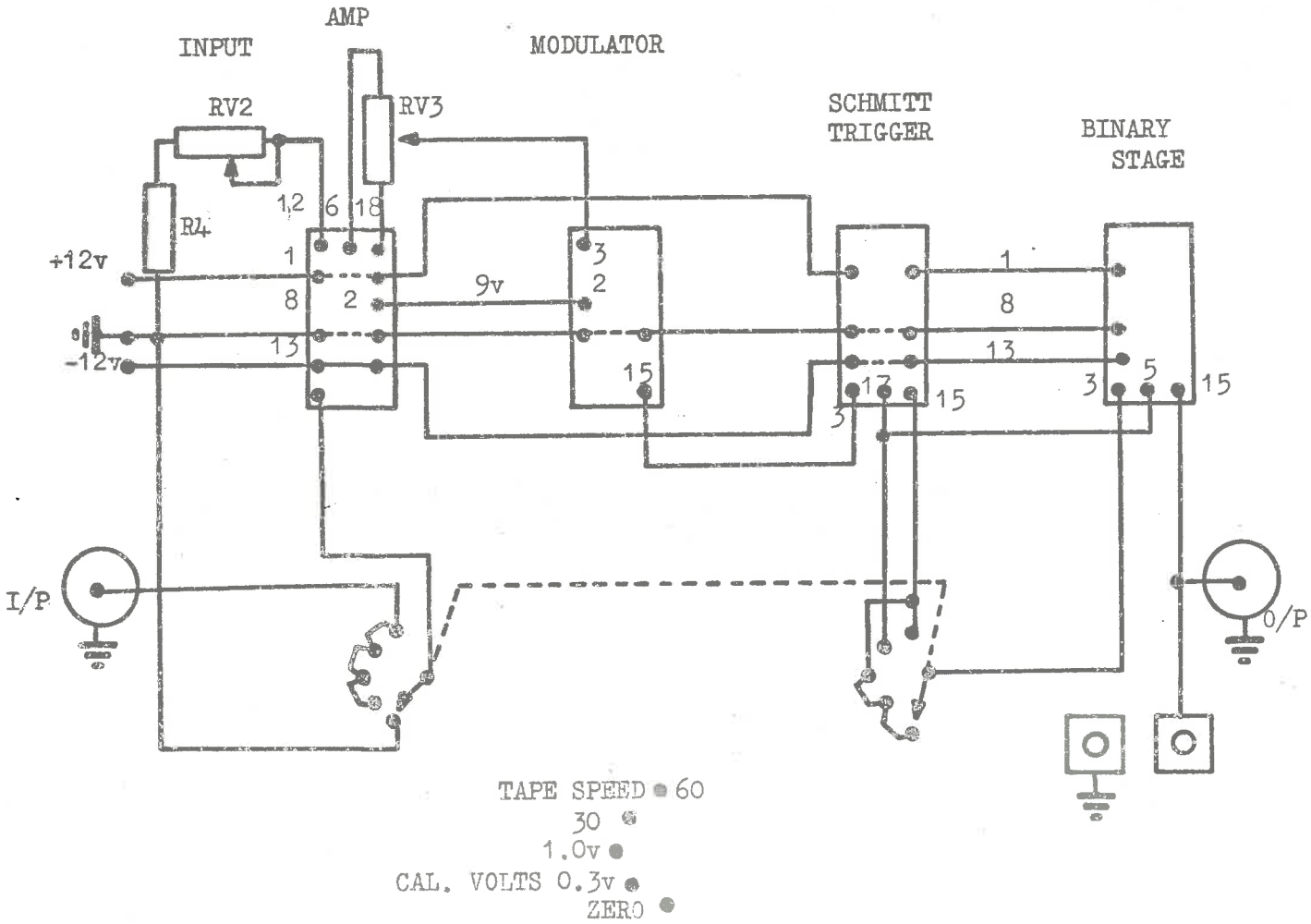

RESISTORS

R4 2.7K to 3.3K

RESISTOR VARIABLE

RV2 5K sensitivity
RV3 100 zero set

Fig. A7.3.1 - V-F Converter

Block Diagram of Wiring between Basic Cards.

Fig. A7.3.1

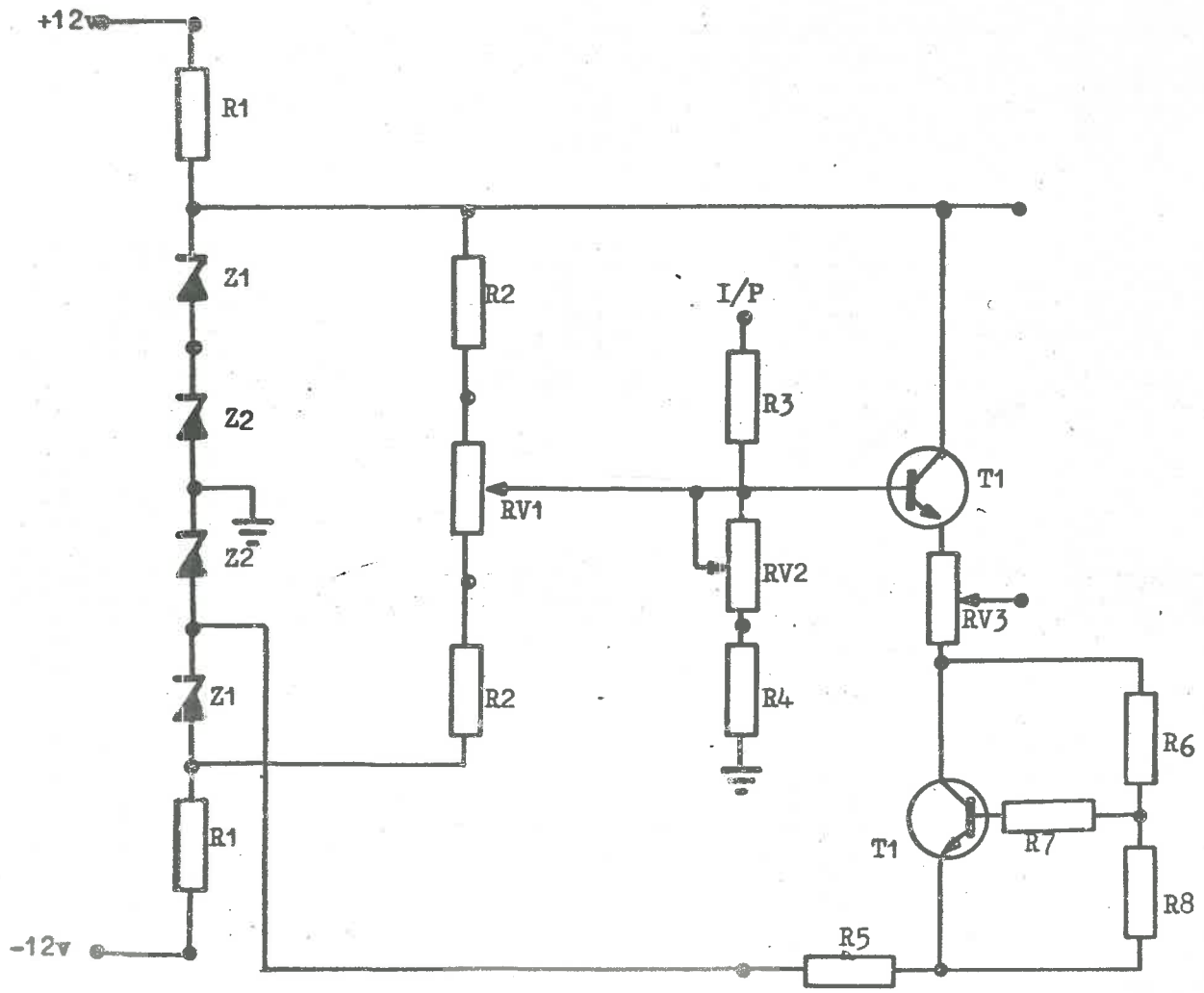

Fig.A7.3.2 - V - F Converter
Input Amplifier

TRANSISTORS
T1 0C140

ZENER DIODE
Z1 1Z4.7T5
Z2 1Z5.6T5

RESISTORS
R1 33
R2 100K Electrosil
R3 10K
R4 2.7K to 3.3K
R5 0-330
R6 47K
R7 33K
R8 100K

RESISTORS VARIABLE
RV1 25K
RV2 5K
RV3 100

Fig.A7.3.2

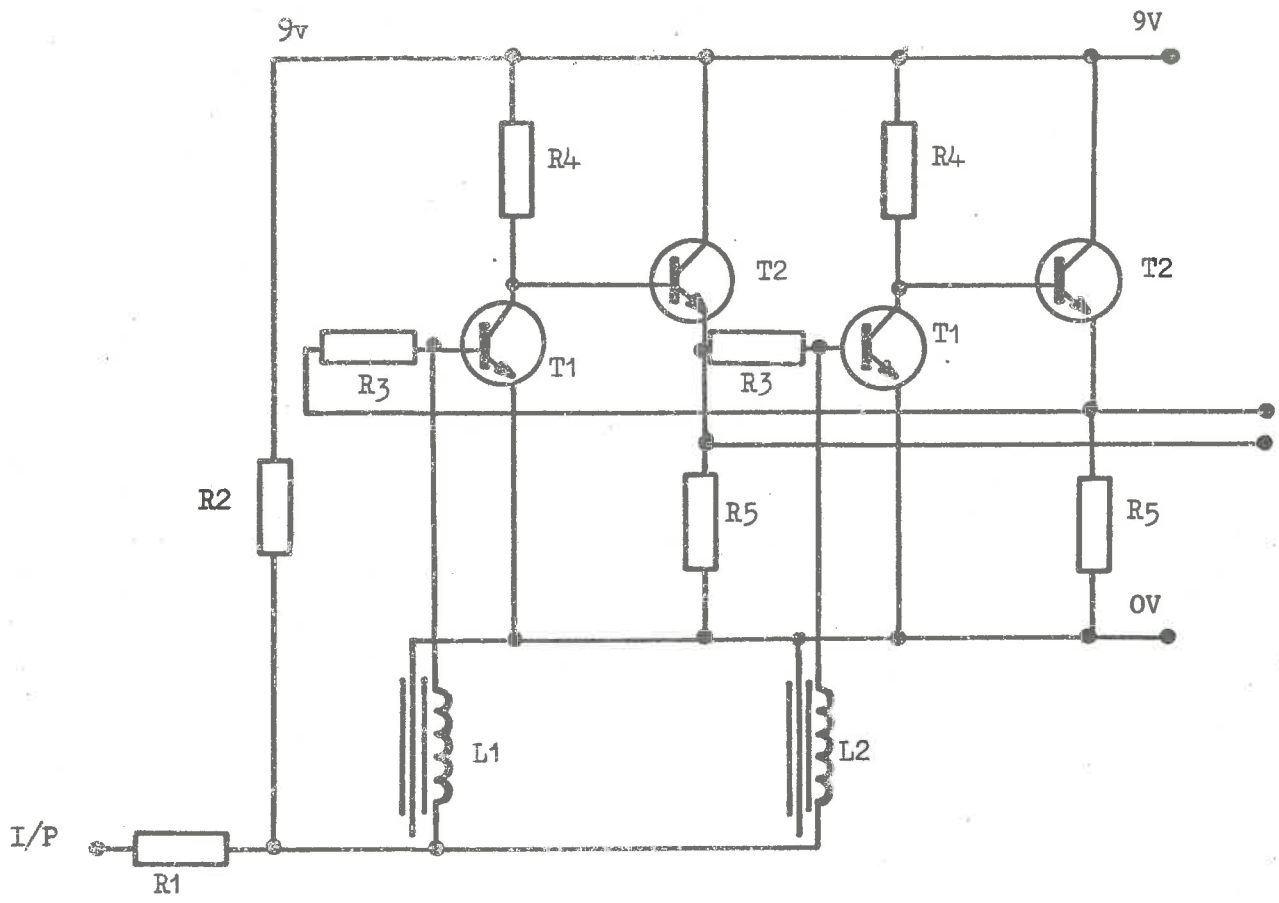

TRANSISTORS
T1 2S703
T2 OC140

INDUCTANCE
L1 10mH
L2 10mH

RESISTORS
R1 100 high stability
R2 100 " "
R3 12K " "
R4 4.7K " "
R5 3.3K

Fig.A7.3.3 - V-F Converter

Astable Multivibrator - Voltage Controlled Modulator.

Fig.A7.3.3

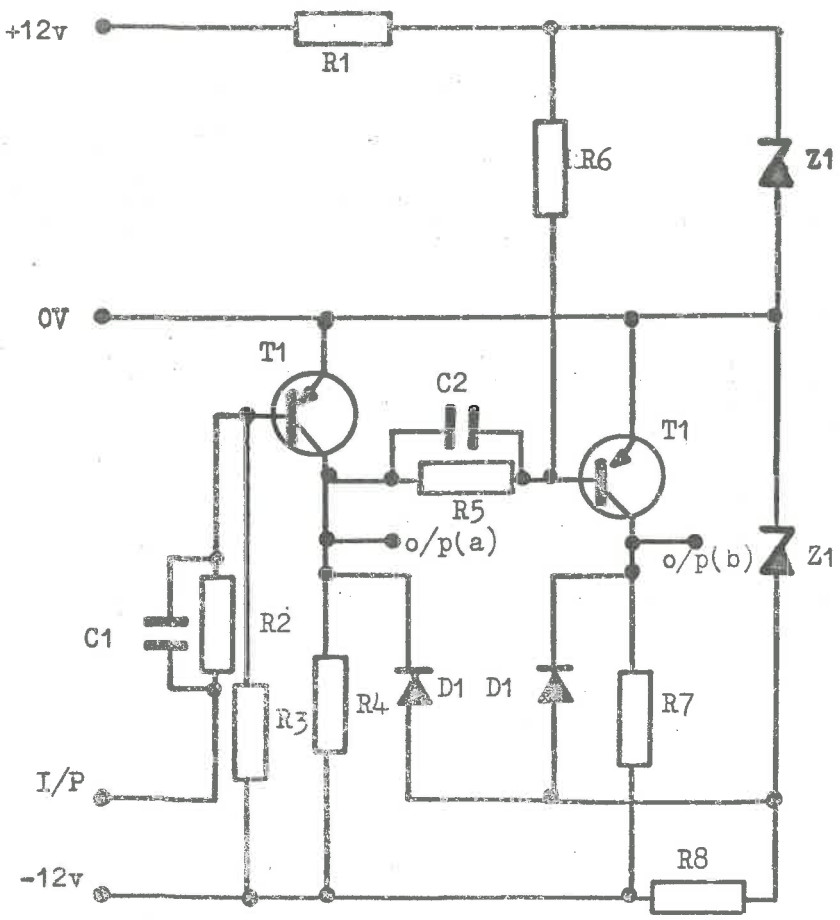

Fig. AZ3.4 - V-F Converter
Schmitt Trigger.

TRANSISTORS
T1 2N1309

ZENER DIODE
Z1 Z2A5.6

DIODE
D1 1N914

RESISTORS
R1 560
R2 22K
R3 82K
R4 3.9K
R5 15K
R6 68K
R7 3.9K
R8 150

CAPACITORS
C1 180pf
C2 180pf

Fig. AZ3.4

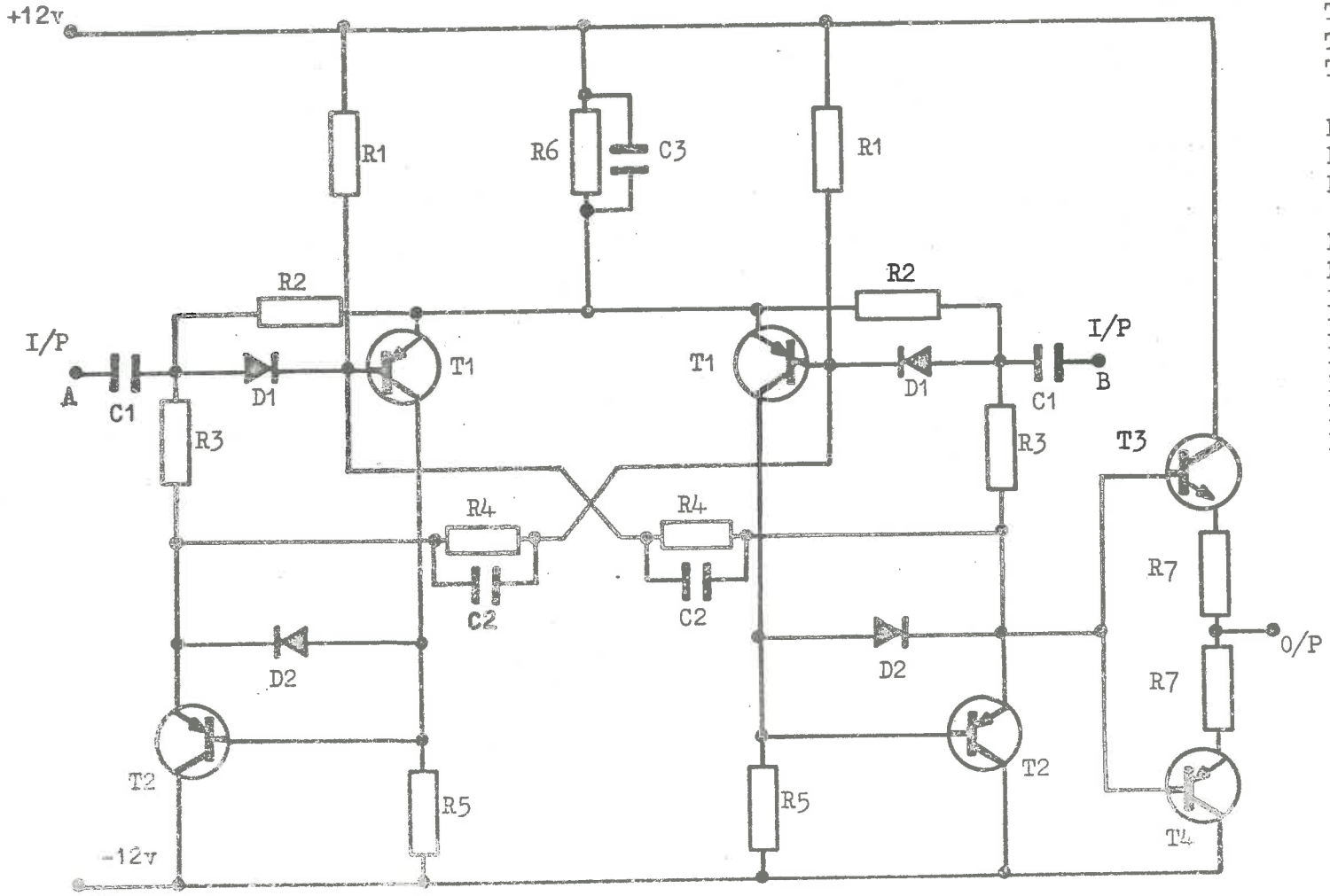

Fig.A7.3.5 - V-F Converter
Binary Divide/Astable Multivibrator

TRANSISTORS
T1 ASZ2ON
T2 ASZ2ON
T3 2N1308
T4 2N1309

DIODES
D1 1N914
D2 1N914

RESISTORS
R1 10K
R2 2.7K
R3 39K
R4 56K
R5 4.7K
R6 68
R7 1K

CAPACITORS
C1 180pf
C2 100pf
C3 8µf

Fig.A7.3.5

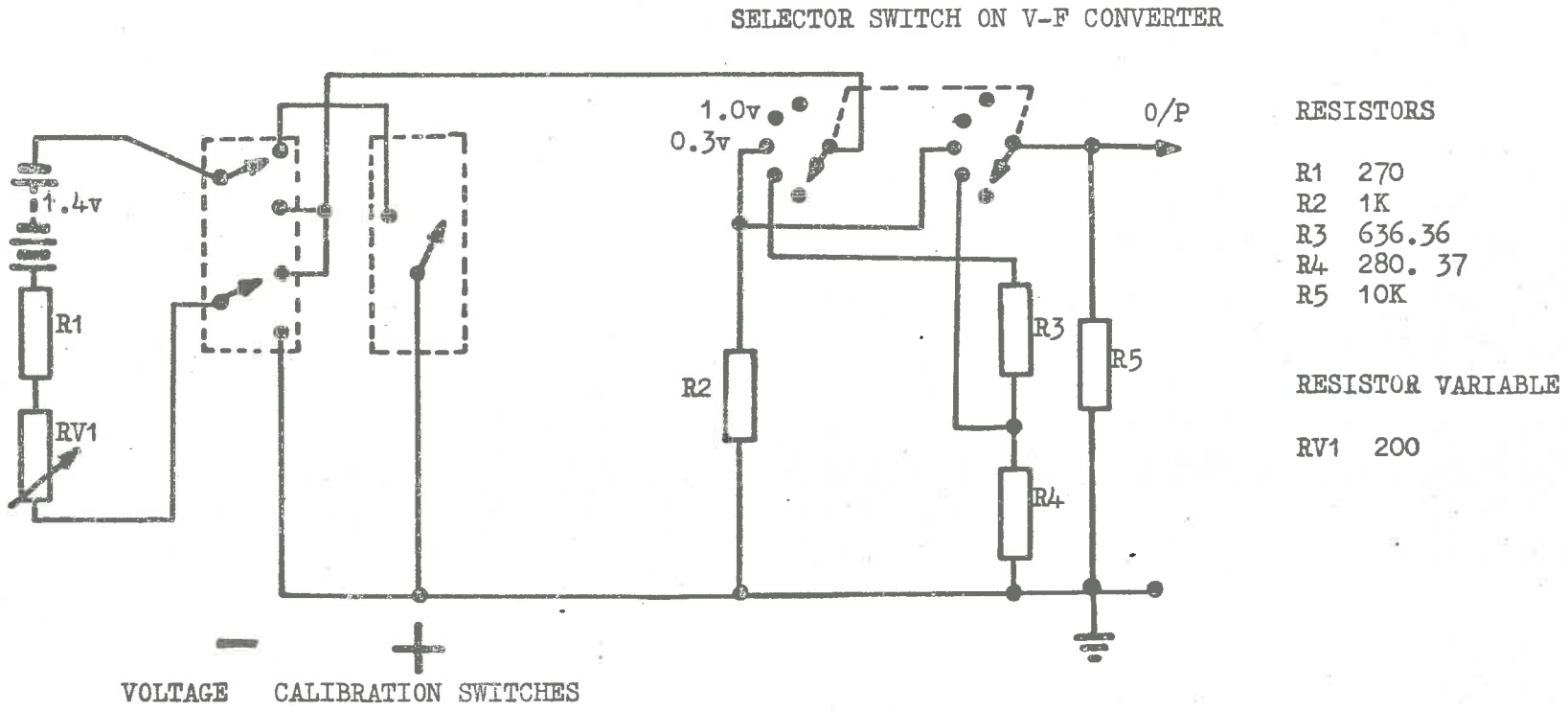

Fig. A7.3.6 - V-F Converter
Calibration Voltage Supply.

Fig. A7.3.6

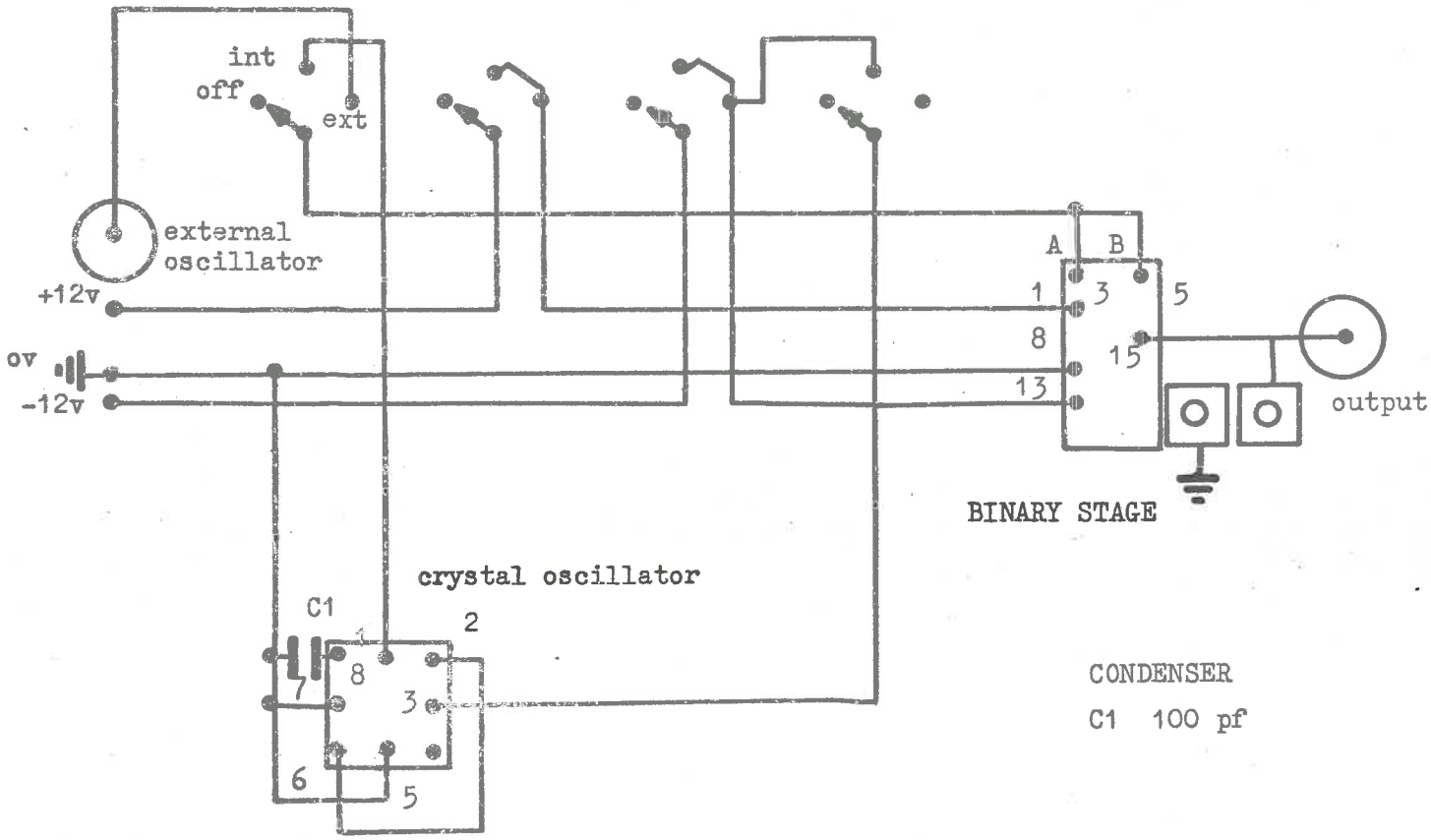

Fig.A7.4 - Reference Frequency
Block Diagram of Wiring between Basic Cards.

Fig.A7.4.

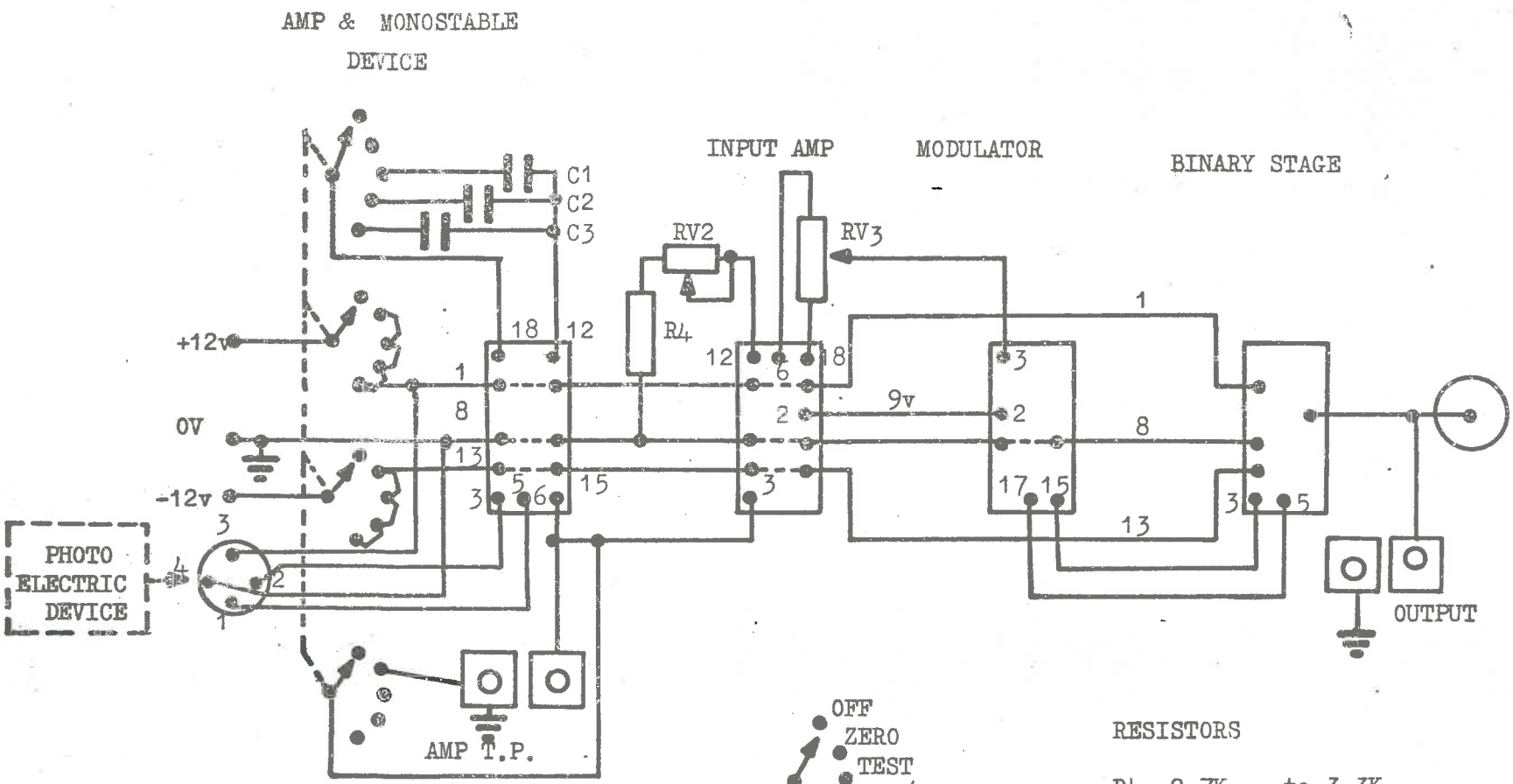

CAPACITORS

C1 64μf
C2 0.47μf
C3 1μf

RESISTORS

R4 2.7K to 3.3K

RESISTORS VARIABLE

RV2 5K sensitivity
RV3 100 zero set

Fig.A7.5.1 - Event Marker

Block Diagram of Wiring between Basic Cards.

Fig.A7.5.1

RESISTORS

R1	10K
R2	56K
R3	10K
R4	82K
R5	1K
R6	5.6K
R7	1K
R8	10K
R9	1meg
R10	33K
R11	5.6K
R12	2.2K
R13	33K
R14	2.2K
R15	560
R16	5.6K

CAPACITORS

C1	0.047µf
C2	100µf
C3	2.5µf
C4	0.01µf
C5	4700pf
C6	Variable time delay
C7	0.01µf
C8	1.0µf
C9	25µf

TRANSISTORS

T1	0C71
T2	0C74N
T3	AF114N
T4	2S303
T5	0C71

Paint removed to make transistor light sensitive

DIODE

D1	1N914

Fig. 5.2 - Event Marker
Amplifier and Monostable Multivibrator.

Fig. 5.2

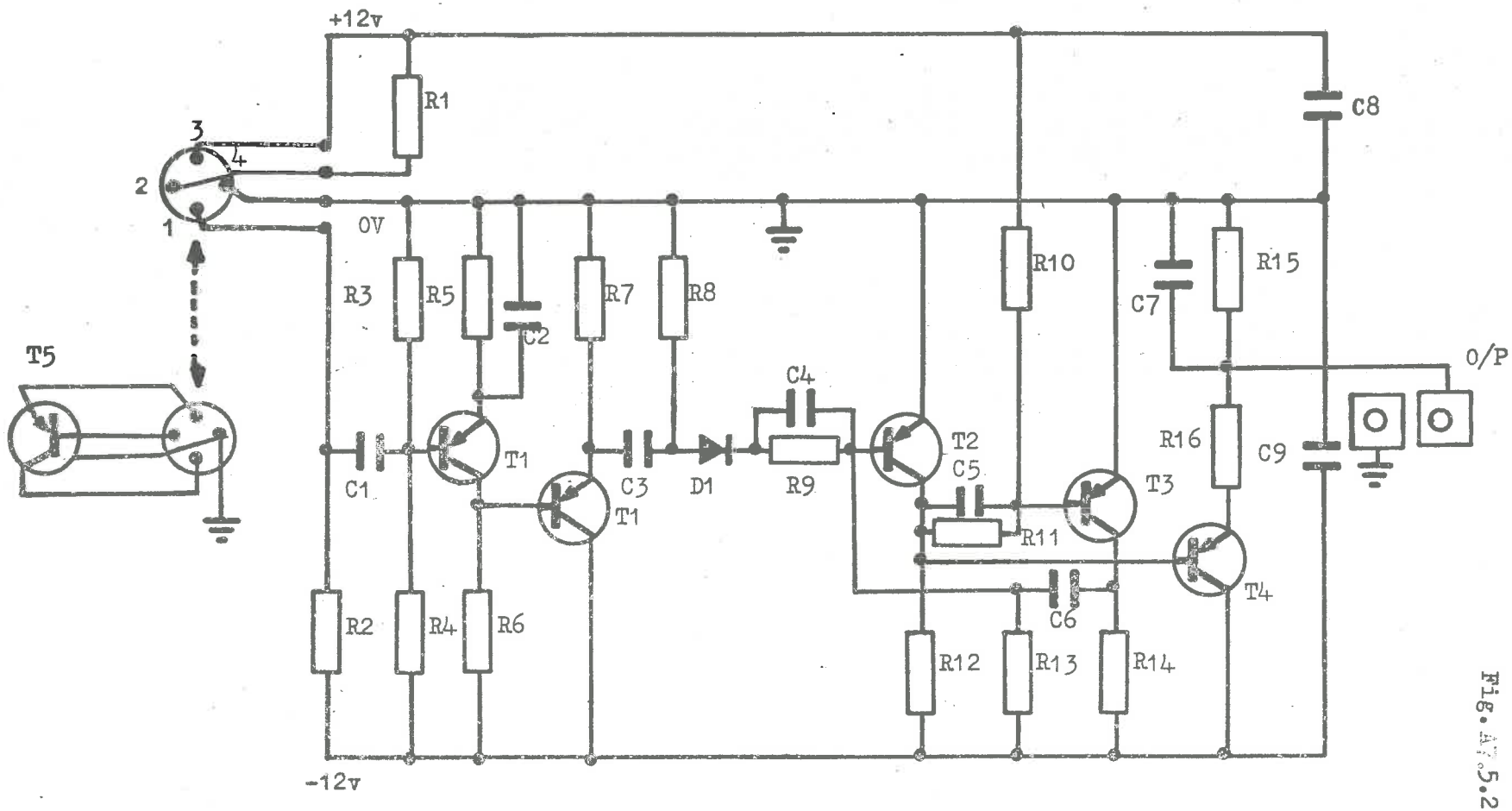

Fig.A7.5.2 - Event Marker
Amplifier and Monostable Multivibrator.

Fig. A7.5.2

TRANSISTORS

T1	OC71
T2	AD140
T3	OC71
T4	AC128
T5	2N3638

ZENER DIODE

Z1	1Z30	T5

RESISTORS

R1	68 Ω
R2	1 K
R3	10 K
R4	15 K
R5	10 K

CAPACITORS

C1	1 µf
C2	1 µf
C3	1000 µf
C4	.68 µf

MONOSTABLE DEVICE

F/F1
F/F2
F/F3
F/F4

RELAYS SIEMENS

RL 1	6500/416
RL 2	"
RL 3	"
RL 4	"
RL 5	"
RL 6	6500/418

RL 1, Rl 2 } Connect Record/Reproduce Heads to V-F Converters

RL 3, RL 4 } Controls Tape Recorder Operation

RL 5 Connects Driver Amplifier and V-F Converters

RL 6 Controls Drive Coil of Uni-selector

Fig. 6.1 - Programme Switch
Block Diagram of Basic Cards.

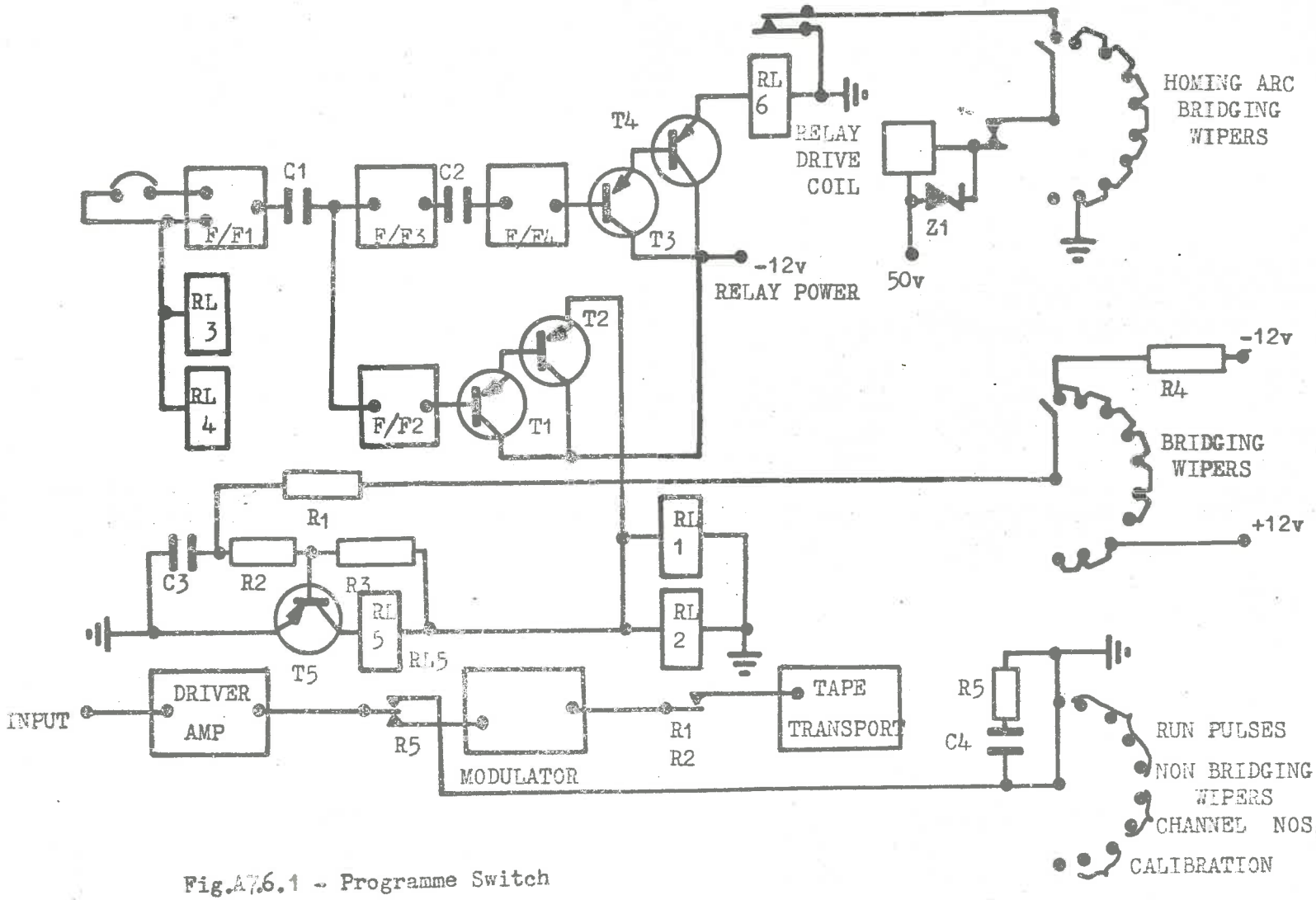

Fig.A7.6.1 - Programme Switch

Block Diagram of Basic Cards

Fig.A7.6.1

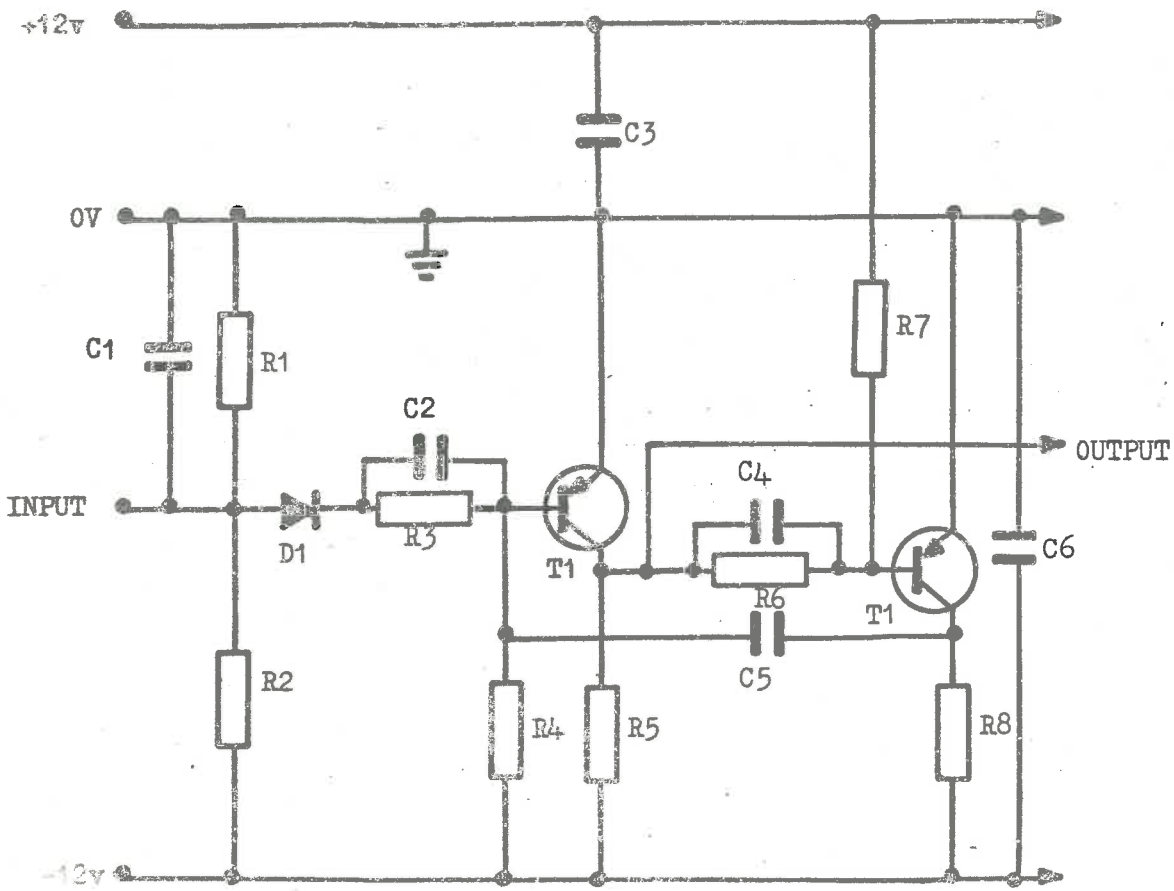

TRANSISTOR

T1 0C74N

DIODE

D1 1N914

RESISTOR

R1	10K
R2	39K
R3	1m
R4	33K
R5	2.2K
R6	1m
R7	33K
R8	2.2K

CAPACITOR

C1	560pf
C2	0.01µf
C3	25µf
C4	0.01µf
C5	time delay
C6	250µf

Fig. A7.6.2 - Programme Switch
Monostable Multivibrator.

Fig. A7.6.2

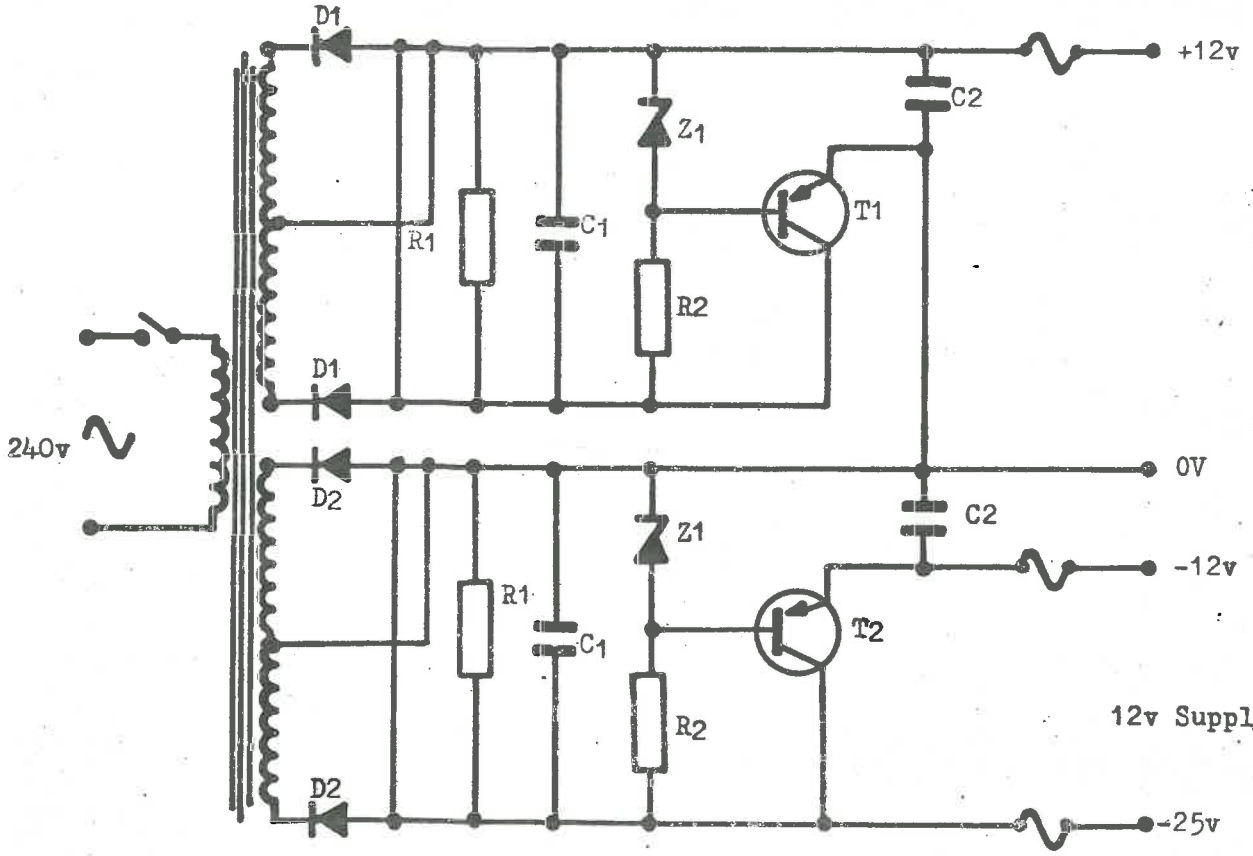

TRANSISTORS
T1) OC22 or
T2) AD140

ZENER DIODES
Z1 1Z12T5

DIODES
D1 1S023
D2 1S023

RESISTORS
R1 1K 1 watt
R2 390 1 watt

CAPACITORS
C1 500 µf
C2 640 µf

12v Supply +12v -12v 750 ma Fuse

Battery charge +12v -25v 1 amp fuse

Fig.A7.8.1 - D.C. Power Supply ± 12 volts.

Fig.A7.8.1

VALVES

V1 6x4
V2 6x4
V3 6u8 two in one valve
V4 6u8 " " "
V5 5651

RESISTORS

R1 100KΩ
R2 47KΩ
R3 100KΩ
R4 47KΩ
R5 220KΩ
R6 220KΩ
R7 1KΩ
R8 33KΩ
R9 3.3KΩ
R10 1KΩ
R11 1mΩ
R12 1mΩ
R13 39KΩ
R14 33KΩ
R15 6.8KΩ

RESISTORS VARIABLE

RV1 10KΩ
RV2 10KΩ

CAPACITORS

C1 70µf
C2 .02µf
C3 2.0µf
C4 0.1µf
C5 40µf

Fig. 8.2 - D.C. Power Supply
High Tension ± 100v

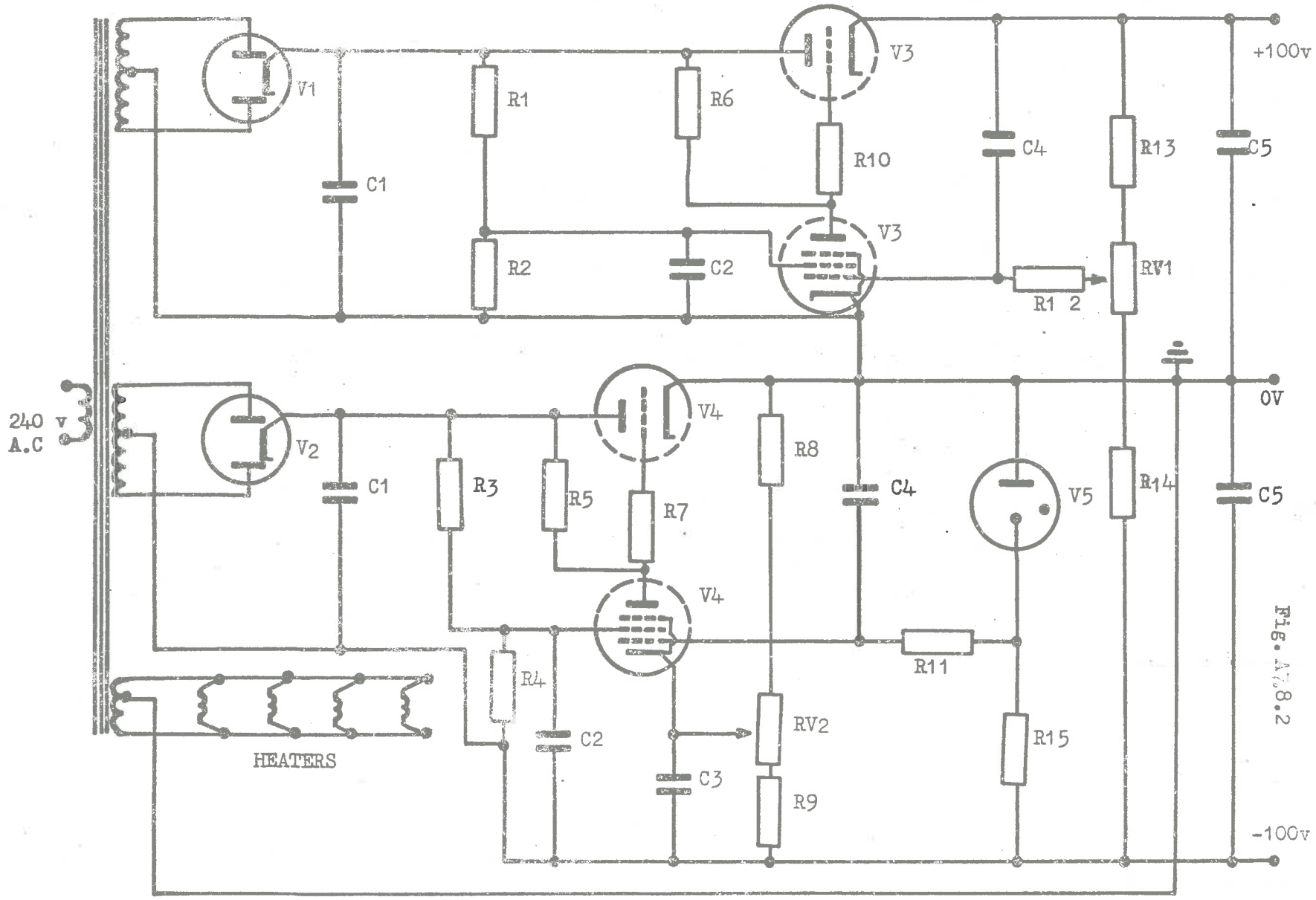

Fig. A7.8.2

Fig. A7.8.2 - D.C. Power Supply. High Tension ± 100v

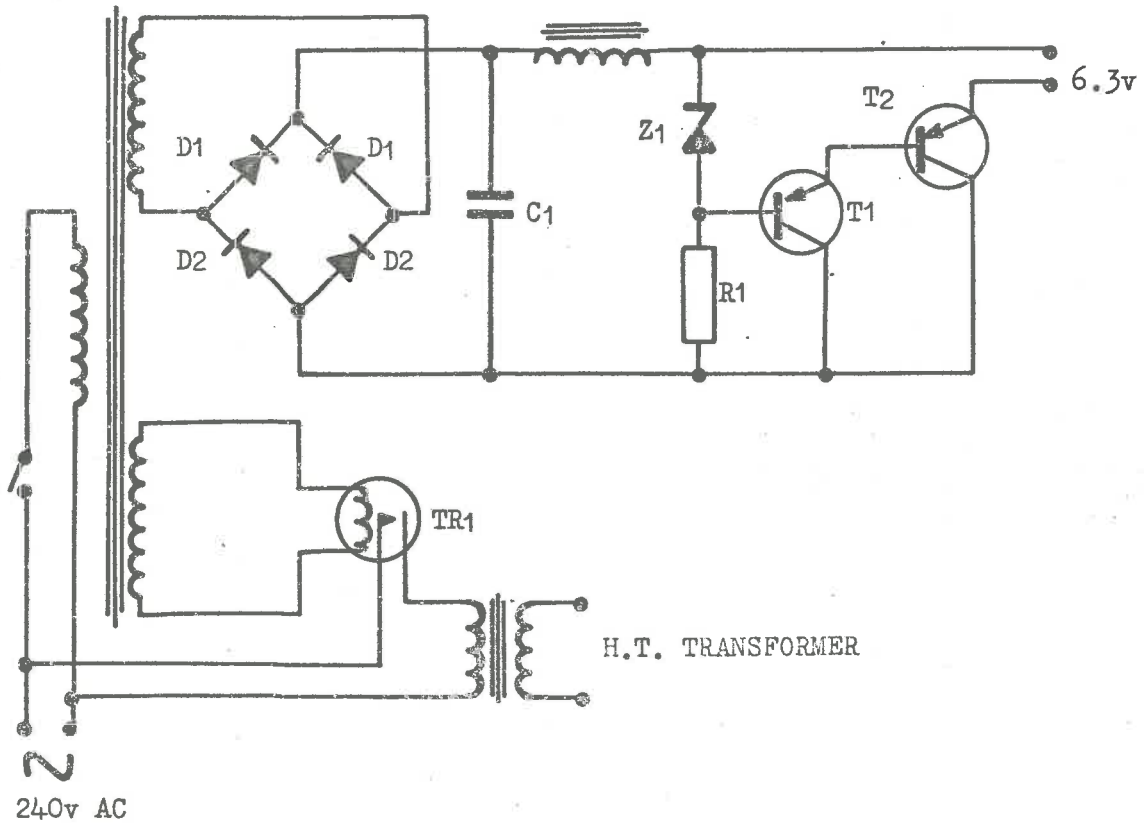

TRANSISTORS
T1 OC74N
T2 AD140

ZENER DIODE
Z1 1Z6.3T5

DIODES
D1 0A210
D2 0A210

RESISTORS
R1 180 1 watt

CAPACITORS
C1 4000µf

THERMAL RELAY
TR1 VLS631

Fig.A78.3 - DC Power Supply
Heaters of Driver Amplifier.

Fig.A78.3

RESISTORS

R1	50K Ω	high stability
R2	100K	" "
R3	100K	" "
R4	50K	" "
R5	25K	" "
R6	40K	" "
R7	50K	" "
R8	1K	" "
R9	100K	" "
R10	2.7K	" "
R11, R12	gain setting	
R13, R14, R15	feed back selected	

TRANSISTORS

T1	2S501
T2	2S703
T3	2N3566

VARIABLE RESISTORS

RV1	5K Ω w/w Amp Balance
RV2	100 Ω Slide Wire
RV3	5K Ω w/w Amp Balance

ROTATING PRE AMP ONLY

RV1	1K Ω
RV3	1K Ω

Fig. 9.1 - D.C. Pre-Amplifiers
Basic Circuit Diagram.

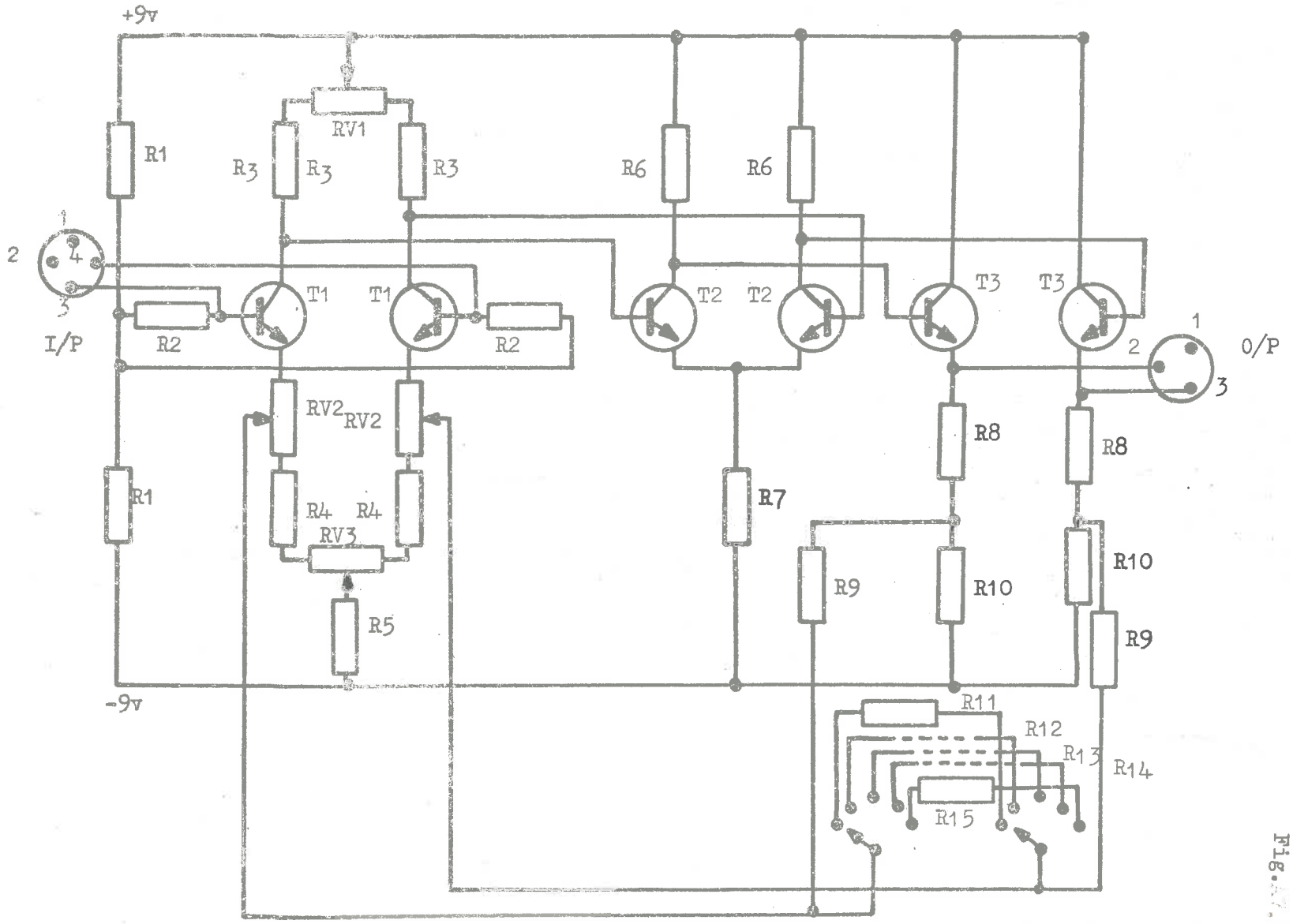

Fig. A7.9.1 - D. C. Pre-Amplifiers
Basic Circuit Diagram.

Fig. A7.9.1

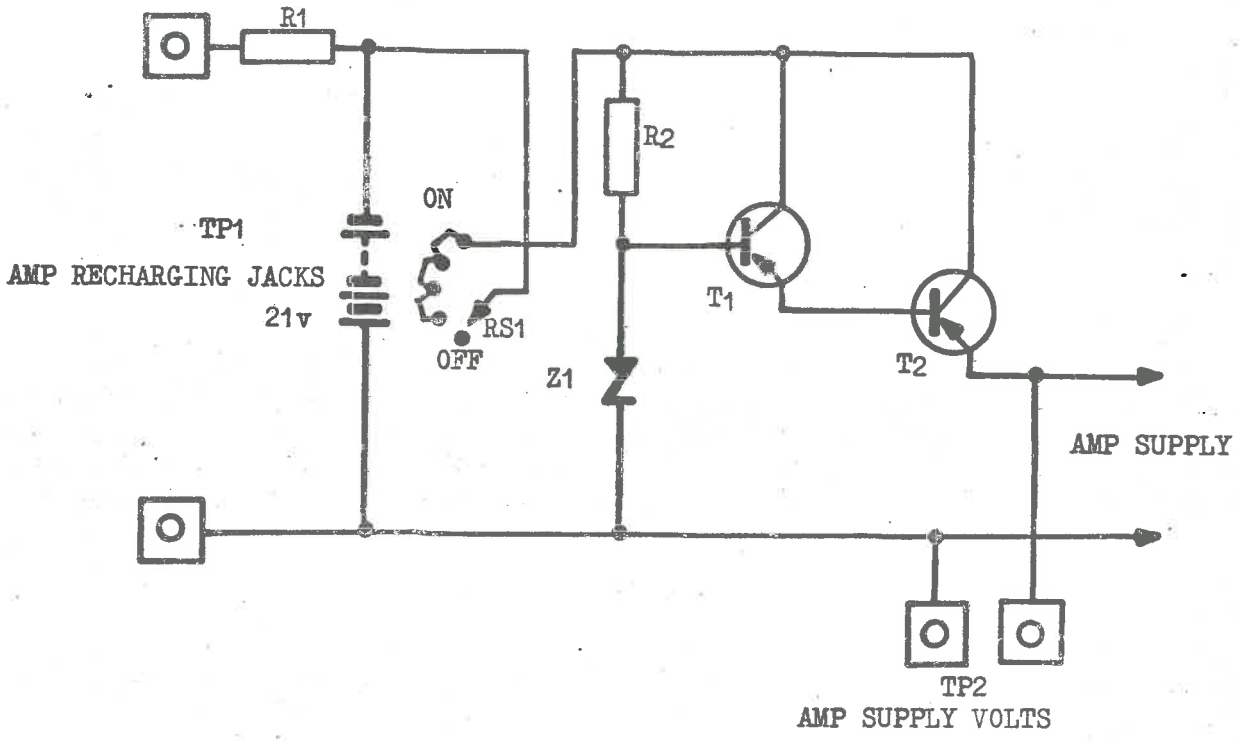

TRANSISTORS

T1	AF 114N
T2	AC 128

ZENER DIODE

Z1	1Z18T5

RESISTORS

R1	12 KΩ
R2	1.5 KΩ

Fig.A7.9.2 - D.C. Pre-Amplifiers
Amplifier Regulated Voltage Supply.

Fig.A7.9.2

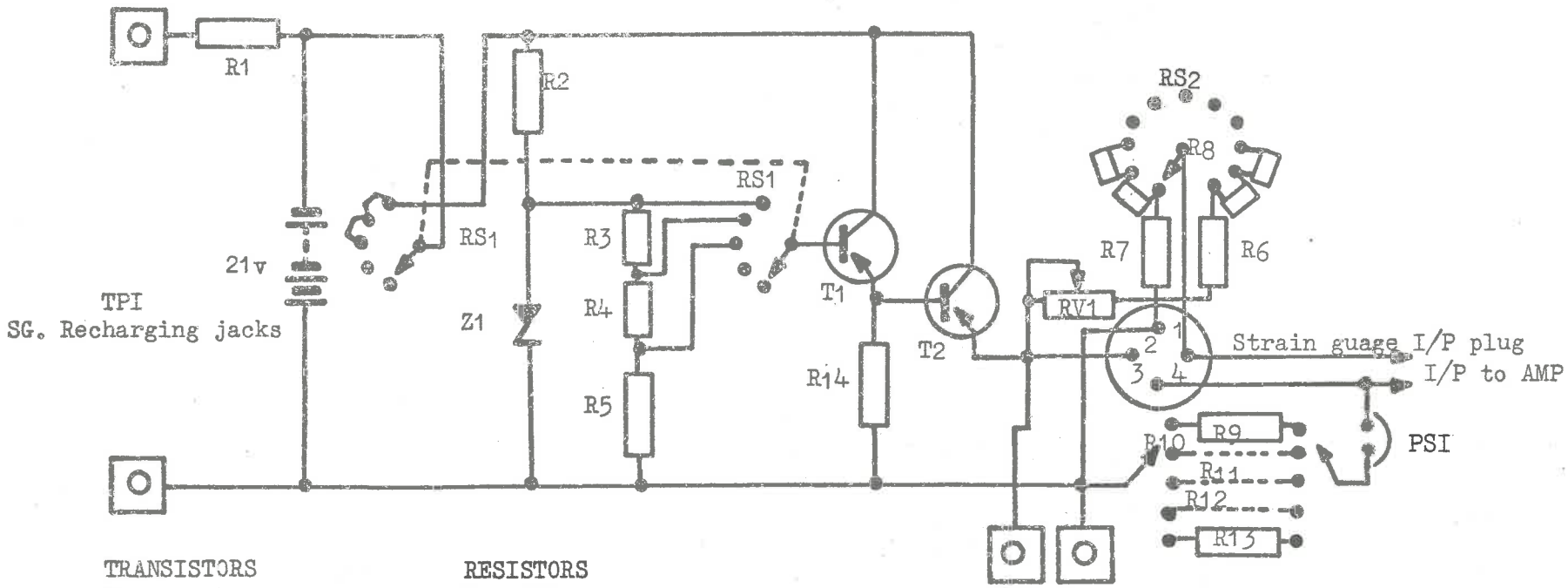

TRANSISTORS
T1 AF114N
T2 OC22 or AD140

ZENER DIODE
Z1 IZ18T5

RESISTOR VARIABLE
RV1 300 w/w

RESISTORS
R1 390
R2 1.5K
R3 27K
R4 1.2K
R5 6K
R6 10K 1%
R7 10K 1%
R8 10 of each 100
R9 to R13 Calibration Resistors
R14 8.2K

Fig.A7.9.3 - D.C. Pre Amplifiers

Strain Guage Regulated Power Supply and Balance Circuit.

Fig.A7.9.3

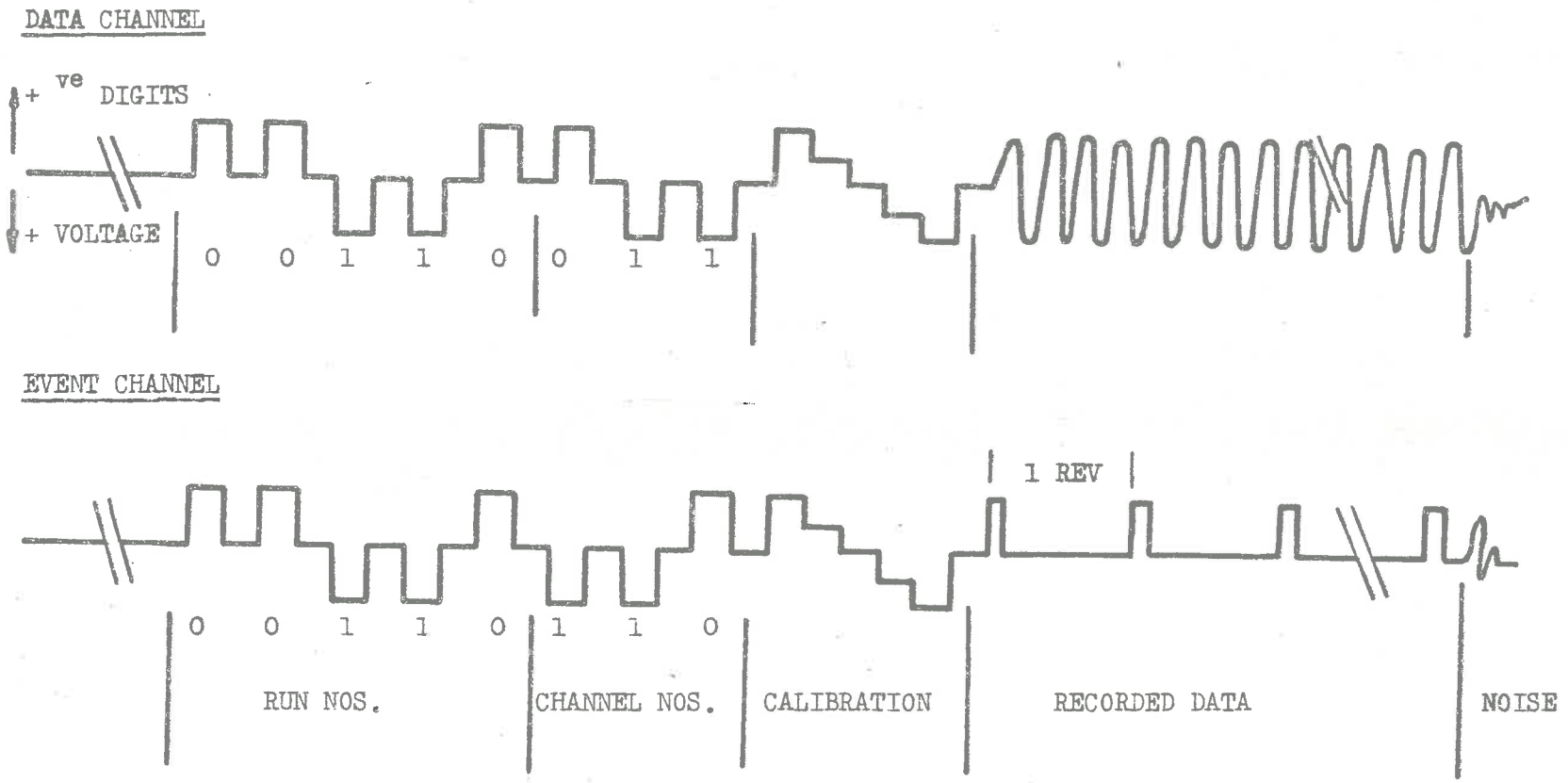

Fig. A7.10 Characteristics of a Single File from MOVADAS

Fig. A7.10

APPENDIX A8

COMPUTING PROCEDURE

APPENDIX A8.

COMPUTING PROCEDURE.

A8.1

COMPUTING SEQUENCE.

The information recorded on magnetic tape by MOVADAS (Appendix A7) was a Frequency Modulated (FM) wave. Before this could be processed by a digital computer, the information had to be converted to an array of numbers in Binary Coded Decimal (BCD) format which represented the recorded signal sampled at equal intervals of time. The FM Analogue to Digital (A-D) Conversion was carried out at the Mathematical Services Division of Weapons Research Establishment, South Australia. Subsequent analysis of the data was conducted on the digital computers at the University.

The analysis of the data was divided into the following stages.

(1) PROGRAM CONVERT (Table A8.1).

The digital information, in the form discussed in Sections A7.3 and A7.4 of Appendix A7 was firstly decoded into a format compatible with the word structure of the computers, and then data files were recognized from the identification pulses. This conversion was necessary because the output from the A-D Converter was to IBM 7090 format which was incompatible with that of the CDC Computers at the University.

As mentioned in Section A7.4 of Appendix A7, the analogue information was simultaneously applied to all active channels of MOVADAS and recorded on separate tracks of the magnetic tape. Included in this analogue information were the identification pulses, i.e. run and channel numbers and instantaneous V-F

Converter calibrations. The analogue information from each track was converted separately to digital information at the same sampling frequency of 4000 samples per second. After A-D conversion, digital files were then written consecutively, 'end for end' on the digital tape. The occurence of the last calibration voltage pulse was taken as the time zero origin, and was thus accurate to 1/4000 of a second. Hence a digital sample from one channel counted from the time origin had a corresponding sample at the same instant of time on all other channels.

The digital samples after time zero origin were selected and recorded, together with various identification numbers, on to another magnetic tape for subsequent analysis by program CONTROL.

(2) PROGRAM CONTROL (Table A8.2).

Using the recorded data from program CONVERT and input instructions in the form of punched cards, the analysis was as follows:--

Subroutine SYNC

This routine selected from the digital file of an experimental data channel an array of numbers which corresponded to a given number of recorded cycles.

As previously mentioned, the digital information recorded from program CONVERT contained all samples from the time zero origin. From the digital event file, the particular locations of the event pulses from the time origin were determined. The corresponding points on the data files were also

located. Thus, it was possible to select from the complete digital file an array of numbers between any two event pulses.

Subroutine CONV and REDFA.

The data was converted into real values of the measured variable (pressure) because the sensitivities of each unit in the recording system were known. The values of the transducers and amplifiers sensitivities were supplied to the program from card input information. The V-F converter sensitivity was obtained from the known instantaneous calibration levels which preceded the recorded data. (Section A7.4, Appendix A7.)

Subroutine FASQW

A Fourier analysis (Ref. A8.1) was performed on the data as selected in subroutine SYNC above.

The phase of the Fourier component was with respect to the event pulse. The Fourier coefficients were corrected in magnitude and phase because of the non-linear frequency response of the high-pass filter used in the recording instrumentation (Section 4.2).

The program printed the following results for each blade frequency harmonic --

(a) The magnitude of the actual pressure.

(b) The pressure coefficient.

(c) Phase with respect to the position of the impeller blades.

Subroutine CALMAX

From the calculated Fourier components the actual pressure signal was synthesized. From this synthesized wave,

the maximum and minimum pressures and their phase angles were determined. The wave form was also plotted using the following subroutine MEKPLT.

Subroutine MEKPLT

This is an automatic plotting routine developed for a line printer to plot the values stored in a double subscripted array. This routine provides automatic scaling and choice of origin for up to 10 separate functions plotted on the one sheet. The coordinate axes are anotated and the user may specify the titles for each axis. The input instructions are given at the beginning of subroutine MEKPLT in Table A8.2.

A8.2 PROGRAM INPUT INSTRUCTIONS.

The programs are listed in Table A8.1 and A8.2.

The definitions of the input variables are as follows:--

(1) PROGRAM CONVERT

ITAPTRN	Transmittal or digital tape number
ITAPCON	The output tape number written by CONVERT
NNSER	Series run number
LIST	Control on type of output required
	- ve lists the data points
	0 lists the data points and writes on to magnetic tape
	+ ve writes on magnetic tape only
LLEST (N M)	Array of numbers to specify the number of files to be listed, and skipped and listed..... etc.

(2) PROGRAM CONTROL

ITAPA	No. of the F.M. analogue tape
ITAPT	No. of the transmittal or digital tape
ITAPCON	No. of the tape recorded by program CONVERT
ITAPSYN	Extra file identification if required
NPI	Number of the cycle of the event at which the analysis is to begin
NP	Number of cycles over which the analysis is to be conducted
LIST	- ve or 0 lists the data points over one cycle and also the Fourier components of the total number of cycles that were investigated. These Fourier components are not corrected for the effect of the high-pass filter.
	+ ve does not list the above
ICHN	No. of the data channel to be investigated
NTYPE	Identification for the type of data
KKD	No. of Fourier coefficients required per revolution of the impeller
VOLTC(I),I=1.5	Value of the 5 voltage signals which were supplied automatically to the F.M. Converters on recorded mode (Appendix, A7.)
GI	Sensitivity of the transducer
REV	Rotational speed of the impeller (rpm)
SETANG	Angle between the position where the event occured and the position of the transducer

WAKEANG	Angle, at which the wake pattern is set with respect to the transducer
FMOD(I), I=1,7	Magnification ratio of the high-pass filter at the frequency of the blade harmonics
FPHASE(I), I=1,7	Phase angle for the filter at the frequency of the blade harmonics
AAPHA(I), I=1,8	Comments which will form the title to the output information
NSER	Series run number
IRUN	Run number for the experimental reading and also the digital file number
NOCHN(I), I=1,7	The numbers associated with the channels of information to be investigated. The event channel number must precede the data channels
IG2, IG3, IG4	Gain switch positions on the recording instruments. The gain figures are given in the program as GG2(I) GG3(I), GG4(I).

A8.3 THE FOURIER ANALYSIS ROUTINE FASQW

A mathematical derivation for this method of Fourier Analysis is given in Ref. A8.1. Briefly it is as follows:--

The Fourier Series expansion of a continuous function f(t) in the range $0 \leqslant t \leqslant 2c$ is,

$$f(t) = a_o + \sum_{n=1}^{\infty} \left(a_n \operatorname{Cos} \frac{n\pi t}{c} + b_n \operatorname{Sin} \frac{n\pi t}{c} \right) \qquad \ldots A8.1$$

where $a_o = \frac{1}{2c} \int_o^{2c} f(t)\, dt$

$$a_n = \frac{1}{c} \int_o^{2c} f(t) \operatorname{Cos} \frac{n\pi t}{c}\, dt$$

and $$b_n = \frac{1}{c} \int_o^{2c} f(t) \operatorname{Sin} \frac{n\pi t}{c}\, dt$$

An estimate a_n' of a_n for a series of N equally spaced points $f(h, k,)$ where h is the sampling interval and k = 0,1,.....N-1 is:--

$$a_n' = \frac{2}{N-1} \sum_{k=0}^{N-1} W_k\, f(h,k) \operatorname{Cos} k\theta \qquad \ldots A8.2$$

where W_k = weighting coefficients

and $\theta = \frac{2\, n\, \pi}{N-1}$

Consider now a series defined by

$$a_n'' = \frac{2}{N-1} \sum_{k=0}^{N-1} W_k\, f(h,k) \frac{\operatorname{Cos} k\theta}{|\operatorname{Cos} k\theta|} \qquad \ldots A8.3$$

and since $\frac{\operatorname{Cos} k\theta}{|\operatorname{Cos} k\theta|}$ is mathematically represented by

$$\frac{4}{\pi} \sum_{j=1}^{\infty} \frac{(-1)^{j-1}}{2j-1} \operatorname{Cos} (2j-1)k\theta \qquad \ldots A8.4$$

Then equation A8.3 can be expressed by

$$a_n'' = \frac{4}{\pi} \sum_{j=1}^{\infty} \frac{(-1)^{j-1}}{2j-1}\, a'_{(2j-1)\, n} \qquad \ldots A8.5$$

A similar solution is given for b_n'' and b_n' (Ref. A8.1). The ratio Cos k θ /|Cos k θ| for a fixed θ and varying k is obtained by sampling the squarewave of frequency θ at intervals of k in time.

After summation of the series in equation A8.3 the linear system equation A8.5 is solved by back substitution.

This method of solving for the Fourier components is faster than the normal methods.

A8.4 MAJOR SYMBOLS USED IN THE PROGRAM.

Y	is the one dimensional data list
N	is the number of data points in the data list
K	is the number of estimates of a_k and b_k required
YS	is the two dimensional array for (a_k'', b_k'')
YC	is the two dimensional array for (a_k', b_k')

A8.5 REFERENCE

A8.1 CLARKE, A.P Computation of the Coefficients of a Fourier Series Expansion of a Function defined by Sampled Data Points.
Weapons Research Establishment, Sth. Aust.
T.M TRD 71 ADDS.

```
      PROGRAM CONVERT
C     CONVERTS MAG TAPE FROM A-D CONVERTER   INFORMATION RECORDED
C     INITIALLY ON MOVADAS
C     CONVERTS THE LIST OF NUMBERS IN EACH FILE NAMED FROM IBM 7090
C     FORMAT TO CDC 3200 OR 6400 FORMAT
C     THE TIME WORDS ARE REMOVED, FILES THAT ARE NOT DATA FILES ARE
C     REJECTED, IDENTIFICATION AND CALIBRATION PULSES ARE LOCATED AND
C     DECODED, THE TRUE DATA IS PLACED ON MAG TAPE WITH THE NECESSARY
C     IDENTIFICATION
C     DATA OUTPUT IN BLOCKS OF 864 NUMBERS WITH DUMMY EOF AFTER EACH
C     BLOCK (-1,100,-10)
C     AFTER THE LAST BLOCK A DUMMY EOF IS (-2,-200,-20)
C      THIS IS FOLLOWED BY A TRUE END OF FILE
      INTEGER SHIFT
      INTEGER VAL
      DIMENSIONINPT(486),VAL(1836),IFILE(8),ICAL(5)
      DIMENSIONLLEST(12,2)
      DIMENSIONIV(3),IW(3)
    5 FORMAT(55X,10HEOF SENSED)
    6 FORMAT(10X,22HEOF WRITTEN ON OUTTAPE)
   10 FORMAT(10X,33HPARITY ERROR DETECTED AND IGNORED)
   15 FORMAT(20X,19HCONVERTED RECORD NO,I5)
   20 FORMAT(1X,20HTOTAL NUMBER RECORDS,I6)
   25 FORMAT(1H-,11HFILE NUMBER,I6)
   30 FORMAT(1X,20I5)
   35 FORMAT(24I3)
   40 FORMAT(50X,22HDATA FILE NOT DETECTED)
   45 FORMAT(5X,9HRECORD NO,I5)
   50 FORMAT(4I5)
   55 FORMAT(20H TRANSMITTAL TAPE NO,I6,3X,15HCONVERT TAPE NO,I6)
   60 FORMAT(1X,9I5)
   65 FORMAT(50X,25HEOF DETECTED BEFORE IDENT)
   70 FORMAT(7X,14HGOOD DATA FILE)
   75 FORMAT(15X,18HLOOKING FOR IDENTS)
   80 FORMAT(10X,10HFILE IDENT,I5,3H  =,I2,4X,11HNO OF STEPS,I3)
   85 FORMAT(3X,12HSKIP FILE NO,I5)
   90 FORMAT(50X,29HCALIBRATION SIGNALS INCORRECT)
   95 FORMAT(9I5)
   96 FORMAT(20I5)
   97 FORMAT(3I5)
      IV(1)=-1
      IV(2)=-100
      IV(3)=-10
      IW(1)=-2
      IW(2)=-200
      IW(3)=-20
C      READS TRANSMITTAL AND CONVERT TAPE NOS, SERIAL NO OF DATA,
C      LIST   +VE  IF MAG TAPE ONLY IS REQUIRED
C     LIST   ZERO   FOR MAG TAPE AND LIST OF POINTS
C      LIST    -VE  FOR LIST OF POINTS ONLY
      READ(60,50)ITAPTRN,ITAPCON,NNSER,LIST
      WRITE(61,55)ITAPTRN,ITAPCON
      IF(LIST)103,102,102
  102 REWIND11
```

```
  103 CALL DENS(10,1,REJ)
C     READS NO OF FILES TO BE LISTED, SKIPPED, LISTED, SKIPPED,.....ETC
      READ(60,35)((LLEST(N,M),M=1,2),N=1,12)
      NOFILE=0
      DO106N=1,12
      IF(LLEST(N,1).EQ.0.AND.LLEST(N,2).EQ.0)1000,104
  104 IF(LLEST(N,1))1000,105,109
  105 IF(LLEST(N,2))1000,1000,107
  106 CONTINUE
  107 LL=LLEST(N,2)
      DO108LT=1,LL
      NOFILE=NOFILE+1
      WRITE(61,85)NOFILE
  108 CALL SKIP(10)
      GOTO106
  109 NL=LLEST(N,1)
      DO990LT=1,NL
      NOREC=0
      NODIS=0
      IDENT=0
      IP=0
      JS=0
      KFILE=1
      JTEST=1
      JDTEST=6
      IYD=35
      IIYD=50
      NOFILE=NOFILE+1
      WRITE(61,25)NOFILE
      BUFFERIN(10,1)(INPT(1),INPT(486))
  100 CALL UNITST(10,K)
      GOTO(100,136,110,120),K
  110 IF(IP)1000,985,950
  120 WRITE(61,10)
  136 NOREC=NOREC+1
      WRITE(61,45)NOREC
C     BY MASKING   BREAKS THE WORD INTO TWO WORDS
      DO140I=1,486
      J=2*I-1+JS
      VAL(J)=SHIFT(INPT(I),-12)
  140 VAL(J+1)=AND(INPT(I),7777B)
      BUFFERIN(10,1)(INPT(1),INPT(486))
      NUM=972+JS
C     CHECKING FOR TIME WORDS AND REMOVING THEM
      IF(AND(VAL(JS+971),4000B).EQ.4000B.AND.AND(VAL(JS+972),40B).EQ.40B
     1.AND.AND(VAL(JS+1),4000B).EQ.4000B)150,170
  150 II=1+JS
      III=969+JS
      DO160I=II,III
  160 VAL(I)=VAL(I+1)
      NUM=NUM-3
      GOTO200
  170 IF(AND(VAL(JS+972),4000B).EQ.4000B.AND.AND(VAL(JS+1),40B).EQ.40B.A
     1ND.AND(VAL(JS+2),4000B).EQ.4000B)180,200
```

```
180 II=1+JS
    III=969+JS
    DO190I=II,III
190 VAL(I)=VAL(I+2)
    NUM=NUM-3
200 I=1+JS
210 IF(AND(VAL(I),4000B).EQ.4000B.AND.AND(VAL(I+1),40B).EQ.40B.AND.AND
   1(VAL(I+2),4000B).EQ.4000B)220,235
220 NUM=NUM-3
    DO230J=I,NUM
230 VAL(J)=VAL(J+3)
235 I=I+1
    IF(I-NUM+2)210,210,237
237 WRITE(61,15)NOREC
    IF(JS)1000,236,250
236 JS=864
    GOTO100
250 GOTO(400,455,700),KFILE
400 IF(NOREC-3)405,405,450
    CHECKING FOR A DATA FILE,  IE, INITIAL POINTS ARE APPROX. CONSTANT
405 DO420I=36,864,18
    IF(IABS(VAL(I)-VAL(I-18))-IYD)420,420,410
410 JTEST=JTEST+1
420 CONTINUE
    GOTO(1000,900,430),NOREC
430 IF(JTEST-JDTEST)445,440,440
440 WRITE(61,40)
    CALL SKIP(10)
    GOTO990
445 WRITE(61,70)
450 KFILE=2
    L=39
455 WRITE(61,75)
500 L=L+1
    IF(L-903)520,520,510
510 L=39
    GOTO900
    IDENTIFYING THE IDENTIFICATION PULSES
520 IF(IABS(VAL(L)-VAL(L-1))-IIYD)500,500,525
525 IF(IABS(VAL(L)-VAL(L-10))-IIYD)500,500,530
530 IF(IABS(VAL(L)-VAL(L-20))-IIYD)500,500,535
535 IF(IABS(VAL(L-1)-VAL(L+1))-IYD)540,540,545
540 IF(IABS(VAL(L-1)-VAL(L+2))-IYD)500,500,545
545 LTEST=1
    CHECKING THAT IT IS A PULSE
    DO555M=20,40
    MN=L+M
    IF(IABS(VAL(MN)-VAL(MN-1))-IYD)555,555,550
550 LTEST=2
555 CONTINUE
    GOTO(575,560,1000),LTEST
    ANOTHER CHECK FOR THE PULSE
560 DO570M=40,60
    MN=L+M
```

```
      IF(IABS(VAL(MN)-VAL(MN-1))-IYD)570,570,565
  565 LTEST=3
  570 CONTINUE
      GOTO(1000,575,500),LTEST
C     KEEPS RUNNING COUNT OF THE NO OF DISCONTINUITIES AND SQUARE PULSES
  575 IF(NODIS-16)590,640,640
  590 NODIS=NODIS+1
      IF(NODIS/2-(NODIS+1)/2)600,630,1000
  600 IDENT=IDENT+1
      IF(VAL(L)-VAL(L-1))620,1000,610
  610 IFILE(IDENT)=0
      GOTO630
  620 IFILE(IDENT)=1
  630 L=L+100
      WRITE(61,80)IDENT,IFILE(IDENT),NODIS
      GOTO500
  640 IDENT=IDENT+1
      ISUM=0
C     DETERMINING THE CALIBRATION LEVELS
      DO670I=20,80
      IAL=I+L
  670 ISUM=ISUM+VAL(IAL)
      SUM=ISUM
      ICAL(IDENT-8)=SUM/61.0
      IF(IDENT-13)675,680,1000
  675 L=L+100
      GOTO500
C     DECODES RUN AND CHANNEL NOS
  680 IIRUN=IFILE(1)*16+IFILE(2)*8+IFILE(3)*4+IFILE(4)*2+IFILE(5)
      IICHN=IFILE(6)*4+IFILE(7)*2+IFILE(8)
      WRITE(61,60)NNSER,IIRUN,IICHN,(ICAL(I),I=1,5),ITAPCON
      WRITE(61,97)(IV(I),I=1,3)
C     CHECK ON VALUES FOR CALIBRATION
      IF(ICAL(1).GT.ICAL(3).AND.ICAL(5).LT.ICAL(3))684,984
C     VARIOUS OUTPUT FORMATS DEPENDING ON THE VALUE OF LIST
  684 IF(LIST)690,685,685
  685 WRITE(11,95)NNSER,IIRUN,IICHN,(ICAL(I),I=1,5),ITAPCON
      WRITE(11,97)(IV(I),I=1,3)
  690 KFILE=3
      LLL=L+250
      IP=0
      DO695J=LLL,1728
      IP=IP+1
  695 VAL(IP)=VAL(J)
      IF(864-IP)720,100,100
  700 DO710J=865,1728
      IP=IP+1
  710 VAL(IP)=VAL(J)
  720 IF(LIST)730,735,740
  730 WRITE(61,30)(VAL(I),I=1,864)
      WRITE(61,97)(IV(I),I=1,3)
      GOTO750
  735 WRITE(61,30)(VAL(I),I=1,864)
      WRITE(61,97)(IV(I),I=1,3)
```

```
 740 WRITE(11,96)(VAL(I),I=1,864)
     WRITE(11,97)(IV(I),I=1,3)
 750 IP=IP-864
     DO760J=1,IP
 760 VAL(J)=VAL(J+864)
     GOTO100
 900 DO910I=1,864
 910 VAL(I)=VAL(I+864)
     GOTO100
 950 IF(IDENT-13)985,955,1000
 955 IF(LIST)960,965,970
 960 WRITE(61,30)(VAL(I),I=1,IP)
     WRITE(61,97)(IW(I),I=1,3)
     GOTO980
 965 WRITE(61,30)(VAL(I),I=1,IP)
     WRITE(61,97)(IW(I),I=1,3)
 970 LLL=IP+1
     DO975I=LLL,864
 975 VAL(I)=0
     WRITE(11,96)(VAL(I),I=1,864)
     WRITE(11,97)(IW(I),I=1,3)
 980 WRITE(61,20)NOREC
     WRITE(61,5)
     GOTO990
 984 WRITE(61,90)
     CALL SKIP(10)
     GOTO990
 985 WRITE(61,65)
     WRITE(61,20)NOREC
 990 CONTINUE
     GOTO105
1000 CALL DENS(10,2,REJ)
     IF(LIST)1002,1001,1001
1001 END FILE 11
     WRITE(61,6)
1002 STOP
     END
```

```
      PROGRAM CONTROL (INPUT,TAPE60=INPUT,OUTPUT,TAPE61=OUTPUT,TAPE02)
C     COMPLETE FOURIER ANALYSIS OF DATA FROM MOVADAS CONVERTED
C      TO CDC 6400 WORD STRUCTURE
      COMMONIY(4321),Y(4321),ITAPCON,NSER,IRUN,NOCHN(8),ICAL(5)
      COMMONVOLTC(5),NPI,NP,NPD,NPTS,LIST,ISTOP
      COMMON NTEST,CAL(5),NPERD,MI,MF
      COMMON FMOD(7),FPHASE(7),REV,SETANG,WAKEANG
      COMMON G1,G2,G3,G4
      COMMON AAPHA(8),KKD
      DIMENSION GG2(5),GG3(2),GG4(10)
  010 FORMAT(9I3)
   11 FORMAT(1H0,12I5)
  095 FORMAT(4I5)
  096 FORMAT(1H1,15HCONVERT TAPE NO,I5)
  097 FORMAT(1H ,13HANOLOGUE TAPE,I3,4X,16HTRANSMITTAL TAPE,I6)
  098 FORMAT(3I3/3I3/5F10.3)
  099 FORMAT(E10.3)
  100 FORMAT(8A10)
  101 FORMAT(1H ,8A10)
  110 FORMAT(3I3)
  120 FORMAT(F6.0,2F6.1)
  130 FORMAT(7F6.3)
  140 FORMAT(7F6.1)
  180 FORMAT(1H0,7H SERIAL,5X,3HRUN,5X,7HCHANNEL,5X,4HTYPE,3X,10HNO PERI
     1ODS,3X,10HBLADE COEF,3X,9HNO POINTS,3X,21HINITIAL - MAX PERIODS)
  190 FORMAT(1H0,I6,4(5X,I5),2(8X,I5),I9,I8)
C     ***************************************************************
C     CALIBRATION VALUES FOR PREAMP 2 | FM 1
      GG2(1)=107.1
      GG2(2)=379.0
      GG2(3)=771.0
      GG2(4)=1170.0
      GG2(5)=2440.0
      GG3(1)=0.1008
      GG3(2)=1.0
      GG4(1)=10.21
      GG4(2)=14.46
      GG4(3)=20.60
      GG4(4)=31.13
      GG4(5)=41.07
      GG4(6)=57.73
      GG4(7)=82.44
      GG4(8)=103.1
C     ***************************************************************
      READ(60,095)ITAPA,ITAPT,ITAPCON,ITAPSYN
      READ(60,098)NPI,NP,LIST,ICHN,NTYPE,KKD,(VOLTC(I),I=1,5)
      READ(60,099)G1
      READ(60,120)REV,SETANG,WAKEANG
      READ(60,130)(FMOD(I),I=1,7)
      READ(60,140)(FPHASE(I),I=1,7)
  205 READ(60,100)(AAPHA(I),I=1,8)
      IF(ENDFILE 60)1000,200
  200 READ(60,010)NSER,IRUN,(NOCHN(I),I=1,7)
      READ(60,110)IG2,IG3,IG4
```

```
      G2=GG2(IG2)
      G3=GG3(IG3)
      G4=GG4(IG4+1)
      ISTOP=1
      WRITE(61,096)ITAPCON
      WRITE(61,097)ITAPA,ITAPT
      WRITE(61,101)(AAPHA(I),I=1,8)
      WRITE(61,011)NSER,IRUN,(NOCHN(I),I=1,7),NPI,NP,LIST
      NTEST=1
      CALL SYNC
      GOTO(220,1000),ISTOP
  220 GOTO(221,205),NTEST
  221 CALL CONV
      GOTO(230,205),NTEST
  230 CALL REDFA
      WRITE(61,096)ITAPCON
      WRITE(61,100)(AAPHA(I),I=1,8)
      WRITE(61,097)ITAPA,ITAPT
      WRITE(61,180)
      WRITE(61,190)NSER,IRUN,ICHN,NTYPE,NPD,KKD,NPTS,NPI,NPERD
      CALL FASQW
      GOTO205
 1000 STOP
      END


      SUBROUTINE SYNC
C     SYNCHRONIZE DATA CHANNEL WITH EVENT MARKER SELECTS FILES, PERIODS,
C     AND DATA POINTS
      DIMENSION IX(3)
      DIMENSIONNPT(50)
      COMMONIY(4321),Y(4321),ITAPCON,NSER,IRUN,NOCHN(8),ICAL(5)
      COMMONVOLTC(5),NPI,NP,NPD,NPTS,LIST,ISTOP
      COMMON NTEST,CAL(5),NPERD,MI,MF
      COMMON FMOD(7),FPHASE(7),REV,SETANG,WAKEANG
      COMMON G1,G2,G3,G4
      COMMON AAPHA(8),KKD
    6 FORMAT(10X,44HIDENTIFICATION BETWEEN DATA BLOCKS INCORRECT)
   10 FORMAT(1H ,35HCONVERT TAPE IS NOT THE TAPE CALLED/10H TAPE READ,I5
     1/12H TAPE CALLED,I5)
  020 FORMAT(1H ,27HDATA POINT APPEARS IN ERROR,I8,3X,5HPOINT/15H ORIGIN
     1AL POINT,I6,3X,12HCORRECTED TO,I6/23H SURROUNDING POINTS ARE,5I8)
  035 FORMAT(1H0,8X,7HPERIODS,15X,16HNUMBER OF POINTS,12X,6HPERIOD)
  036 FORMAT(67H SELECT  INITIAL  MAX    SELECT  INITIAL  FINAL  TOTAL
     1  VARIATION)
  040 FORMAT(1H ,I5,I8,I7,I10,2I8,I7,I8,I6)
  050 FORMAT(1H0,10HERROR TYPE,3(2X,I5))
  060 FORMAT(1H0,7HCHAN NO,I6)
  070 FORMAT(1H0,10I5)
  080 FORMAT(1X,20I5)
   95 FORMAT(9I5)
   96 FORMAT(20I5)
   97 FORMAT(3I5)
      NOCHN(8)=0
```

```
      NT=5
      IYD=5
      IIYD=50
      NPTDD=5
      INTPOL=100
  100 REWIND02
      DO115N=1,4321
  115 IY(N)=0
C     READS MAG TAPE AND SELECTS FILE REQUIRED FOR EVENT MARKER.
  118 READ(02,95)NNSER,IIRUN,IICHN,(ICAL(I),I=1,5),ITAPCO
      IF(ENDFILE 02)1000,117
  117 IF(ITAPCON-ITAPCO)600,119,600
  119 IF(IRUN-IIRUN)150,120,150
  120 IF(NOCHN(1)-IICHN)150,160,150
  150 CALL SKIP(02)
      GOTO118
  160 NPF=NP+NPI
      NPERD=0
      NTOTE=0
      KTEST=1
      DO105I=1,50
  105 NPT(I)=0
      M=-863
      MM=0
C     READS DATA POINTS FROM FILE OF EVENT MARKER.
  170 M=M+864
      MM=MM+864
      READ(02,97)(IX(I),I=1,3)
      IF(IX(1).EQ.-1.AND.IX(2).EQ.-100.AND.IX(3).EQ.-10)162,161
  161 IF(IX(1).EQ.-2.AND.IX(2).EQ.-200.AND.IX(3).EQ.-20)174,900
  162 READ(02,96)(IY(I),I=M,MM)
      IF(ENDFILE 02)174,171
  171 IF(MM-3456)170,170,172
  172 CALL SKIP(02)
  174 N=9
  175 N=N+1
      IF(N-MM+30)178,245,245
  178 IF(IY(N)-1000)240,240,180
C     DETERMINING THE EVENT PULSES.
  180 IF(IABS(IY(N)-IY(N-1))-IYD)175,175,181
  181 IF(IABS(IY(N)-IY(N-4))-IYD)175,175,182
  182 IF(IABS(IY(N)-IY(N-9))-IYD)175,175,183
  183 IF(IABS(IY(N-1)-IY(N+1))-IYD)173,173,189
  173 IF(IABS(IY(N-1)-IY(N+2))-IYD)175,175,189
  189 LTEST=1
C     CHECKING TO MAKE SURE IT IS AN EVENT PULSE
      DO185M=4,14
      MN=N+M
      IF(IABS(IY(MN)-IY(MN-1))-IYD)185,185,184
  184 LTEST=2
  185 CONTINUE
      GOTO(200,186,1000),LTEST
  186 DO188M=15,25
      MN=N+M
```

```
      IF(IABS(IY(MN)-IY(MN-1))-IYD)188,188,187
  187 LTEST=3
  188 CONTINUE
      GOTO(1000,200,240),LTEST
  200 IF(IY(N)-IY(N-1)-IYD)220,220,205
  205 IF(IY(N)-IY(N-1)-IIYD)175,175,210
C     NOTES NO. OF PERIOD AND NO. OF  POINT WHERE IT OCCURED.
  210 NPERD=NPERD+1
      NPT(NPERD)=N
  220 N=N+15
      GOTO175
  240 NTOTE=N-1
  245 REWIND02
C     CHECK THAT PERIODS DID OCCUR.
      IF(NPERD)250,250,255
  250 IERR=0003
      NTEST=2
      WRITE(61,050)IERR,NPERD,NTOTE
      GOTO335
C     CHECK THAT VARIATION IN NO. OF POINTS PER PERIOD IS ACCEPTABLE
  255 NMIN=NPT(2)-NPT(1)
      NMAX=NMIN
      NN=NPERD-1
      DO290N=2,NN
      NPTD=NPT(N+1)-NPT(N)
      IF(NMAX-NPTD)260,270,270
  260 NMAX=NPTD
      GOTO290
  270 IF(NMIN-NPTD)290,290,280
  280 NMIN=NPTD
  290 CONTINUE
      IF(NMAX-NMIN-NPTDD)305,305,300
  300 IERR=004
      WRITE(61,050)IERR,NMIN,NMAX
      NTEST=2
      GOTO335
C     CHECK THAT DESIRED NO. OF PERIODS IS OBTAINABLE
  305 IF(NPERD-NPF)310,320,320
  310 IERR=005
      WRITE(61,050)IERR,NPERD,NPF
      NPP=NPERD
      GOTO330
  320 NPP=NPF
  330 NPD=NPP-NPI
      IF(NPD)331,331,332
  331 NTEST=2
      GOTO335
C     HENCE DETERMINE  NO. OF INITIAL AND FINIAL POINTS, (TOTAL NO.
C     OF POINTS)
  332 MI=NPT(NPI)
      MF=NPT(NPP)
      NPTS=MF-MI+1
      WRITE(61,035)
      WRITE(61,036)
```

```
      WRITE(61,040)NPD,NPI,NPERD,NPTS,MI,MF,NTOTE,NMIN,NMAX
  335 K=1
  340 K=K+1
      IF(NOCHN(K))370,1001,380
  370 IERR=006
      WRITE(61,050)IERR,K,K
      GOTO1000
  380 WRITE(61,060)NOCHN(K)
      REWIND02
      DO360N=1,4321
  360 IY(N)=0
C     SELECT DATA FILE DESIRED FROM MAG.TAPE
  390 READ(02,95)NNSER,IIRUN,IICHN,(ICAL(I),I=1,5),ITAPCO
      IF(ENDFILE 02)1000,391
  391 IF(IRUN-IIRUN)430,400,430
  400 IF(NOCHN(K)-IICHN)430,435,430
  430 CALL SKIP(02)
      GOTO390
  435 KTEST=1
      M=-863
      MM=0
C     READ DATA FROM MAG. TAPE
  440 M=M+864
      MM=MM+864
      READ(02,97)(IX(I),I=1,3)
      IF(IX(1).EQ.-1.AND.IX(2).EQ.-100.AND.IX(3).EQ.-10)442,441
  441 IF(IX(1).EQ.-2.AND.IX(2).EQ.-200.AND.IX(3).EQ.-20)500,900
  442 READ(02,96)(IY(I),I=M,MM)
      IF(ENDFILE 02)500,450
  450 IF(MM-3456)440,440,460
  460 CALL SKIP(02)
  500 GOTO(510,340),NTEST
  510 WRITE(61,070)NSER,IIRUN,IICHN,(ICAL(I),I=1,5),NPTS,NPD
C     CHECK FOR ERRORS IN DATA AND INTERPOLATES FOR THE POINT.
      DO512I=MI,MF
      IF(IABS(2*IY(I-1)-IY(I-2)-IY(I))-INTPOL)512,511,511
  511 IYY=IY(I)
      IY(I)=(IY(I-1)+IY(I+1))/2
      WRITE(61,020)I,IYY,IY(I),IY(I-2),IY(I-1),IY(I),IY(I+1),IY(I+2)
  512 CONTINUE
      IF(LIST)515,515,340
  515 IF(MF-MI-79)520,530,530
  520 WRITE(61,080)(IY(M),M=MI,MF)
      GOTO340
  530 MM=MI+79
      WRITE(61,080)(IY(M),M=MI,MM)
      MM=MF-79
      WRITE(61,080)(IY(M),M=MM,MF)
      GOTO340
  600 WRITE(61,10)ITAPCO,ITAPCON
      GOTO1000
  900 WRITE(61,6)
 1000 ISTOP=2
 1001 REWIND02
```

```
      RETURN
      END


      SUBROUTINE CONV
C     CONVERT DATA POINTS INTO FLOATING POINT  NUMBERS.
      COMMONIY(4321),Y(4321),ITAPCON,NSER,IRUN,NOCHN(8),ICAL(5)
      COMMONVOLTC(5),NPI,NP,NPD,NPTS,LIST,ISTOP
      COMMON NTEST,CAL(5),NPERD,MI,MF
      COMMON FMOD(7),FPHASE(7),REV,SETANG,WAKEANG
      COMMON G1,G2,G3,G4
      COMMON AAPHA(8),KKD
      II=0
      DO100I=MI,MF
      II=II+1
  100 Y(II)=IY(I)
      DO300I=1,5
  300 CAL(I)=ICAL(I)
      RETURN
      END


      SUBROUTINE REDFA
C     FROM CALIBRATION VALUES DETERMINES BEST FIT  STRAIGHT LINES AND
C     CONVERTS DIGITS TO REAL VALUES OF THE MEASURED VARIABLE.
      COMMONIY(4321),Y(4321),ITAPCON,NSER,IRUN,NOCHN(8),ICAL(5)
      COMMONVOLTC(5),NPI,NP,NPD,NPTS,LIST,ISTOP
      COMMON NTEST,CAL(5),NPERD,MI,MF
      COMMON FMOD(7),FPHASE(7),REV,SETANG,WAKEANG
      COMMON G1,G2,G3,G4
      COMMON AAPHA(8),KKD
      PI=3.1415927
      XP=CAL(1)+CAL(2)+CAL(3)
      XN=CAL(3)+CAL(4)+CAL(5)
      YP=VOLTC(1)+VOLTC(2)+VOLTC(3)
      YN=VOLTC(3)+VOLTC(4)+VOLTC(5)
      ZP=CAL(1)**2+CAL(2)**2+CAL(3)**2
      ZN=CAL(3)**2+CAL(4)**2+CAL(5)**2
      WP=CAL(1)*VOLTC(1)+CAL(2)*VOLTC(2)+CAL(3)*VOLTC(3)
      WN=CAL(3)*VOLTC(3)+CAL(4)*VOLTC(4)*CAL(5)*VOLTC(5)
      AP=(ZP*YP-WP*XP)/(3.0*ZP-XP*XP)
      AN=(ZN*YN-WN*XN)/(3.0*ZN-XN*XN)
      BP=(3.0*WP-XP*YP)/(3.0*ZP-XP*XP)
      BN=(3.0*WN-XN*YN)/(3.0*ZN-XN*XN)
      SEN=1.0/(G1*G2*G3*G4)
      CALINT=(AP-AN)/(BN-BP)
      DO290I=1,NPTS
      IF(Y(I)-CALINT)270,280,280
  270 Y(I)=(Y(I)*BN+AN)*SEN
      GOTO290
  280 Y(I)=(Y(I)*BP+AP)*SEN
  290 CONTINUE
      RETURN
      END
```

```
      SUBROUTINE FASQW
C     DETERMINES FOURIER COEFFICIENTS OF THE VARIABLE.
      DIMENSION PRESC(7),PANG(7)
      DIMENSION YS(250,2),YC(250,2)
      DIMENSION PMOD(250),PPHI(250)
      COMMONIY(4321),Y(4321),ITAPCON,NSER,IRUN,NOCHN(8),ICAL(5)
      COMMONVOLTC(5),NPI,NP,NPD,NPTS,LIST,ISTOP
      COMMON NTEST,CAL(5),NPERD,MI,MF
      COMMON FMOD(7),FPHASE(7),REV,SETANG,WAKEANG
      COMMON G1,G2,G3,G4
      COMMON AAPHA(8),KKD
  120 FORMAT(1H1,16X,47HFOURIER COEFFICENTS OF COMPLETE DATA ANALYSISED)
  125 FORMAT(1H0,10X,38HFOURIER COEFFICENTS AT BLADE FREQUENCY)
  130 FORMAT(1H0,9X,5HINDEX,8X,6HCOSINE,13X,4HSINE,12X,7HMODULUS,9X,5HPH
     1ASE//)
  135 FORMAT(1H0,82H BLADE HARMONIC    PRESSURE    PRESSURE COEFFICIENT
     1   PHASE ANGLE          PERCENT)
  136 FORMAT(1H ,21X,5H(PSI),28X,13H(LEAD DEGREE)//)
  140 FORMAT(11X,I4,3(4X,E14.7),4X,F6.1)
  145 FORMAT(1H0,6X,I2,10X,F8.5,9X,F8.5,13X,F7.2,12X,F6.1)
  150 FORMAT(1H8,27H COUNTING ERROR EXIT CALLED)
      KK=NPD*KKD
      N=NPTS
      PI=3.1415927
      THETA=2.0*PI/FLOAT(N-1)
      Y(1)=0.5*Y(1)
      DO50K=1,KK
      ALPHA=PI/(FLOAT(K)*THETA)
      BETA=1.0
      YS(K,1)=0.0
      YS(K,2)=0.0
      DO50J=1,2
      L=1
      BETA=BETA+ALPHA/2.
      GAMMA=BETA
      DO50I=1,N
      IF(FLOAT(I)-GAMMA)20,20,11
   11 DELTA2=FLOAT(I)-GAMMA
      GAMMA=GAMMA+ALPHA
      IF(L-1)96,12,13
   12 L=2
      YS(K,J)=YS(K,J)+.5*Y(I-1)-DELTA2*(Y(I)+Y(I-1))-0.5*Y(I)
      IF(I-N)50,14,96
   13 L=1
      YS(K,J)=YS(K,J)-.5*Y(I-1)+DELTA2*(Y(I)+Y(I-1))+0.5*Y(I)
      IF(I-N)50,14,96
   14 A=YS(K,J)-0.5*Y(I)
      YS(K,J)=1.57079632*A/FLOAT(N-1)
      GOTO50
   20 M=L
      IF(M-1)30,30,45
   30 YS(K,J)=YS(K,J)+Y(I)

  560 PHI=90.0

      WRITE(61,80)
      PI=3.1415927
      DO100I=1,IBH

      END
```

```
      IF(I-N)50,39,50
   39 A=YS(K,J)-0,5*Y(I)
      YS(K,J)=1,57079632*A/FLOAT(N-1)
      GOTO50
   45 YS(K,J)=YS(K,J)-Y(I)
      IF(I-N)50,49,50
   49 A=YS(K,J)+0,5*Y(I)
      YS(K,J)=1,57079632*A/FLOAT(N-1)
   50 CONTINUE
      JJ=(2*KK)/3-1
      YC(KK,1)=YS(KK,1)
      YC(KK,2)=YS(KK,2)
      J=KK-1
      JX=J
      DO95L=1,JX
      YC(J,1)=YS(J,1)
      YC(J,2)=YS(J,2)
      IF(L-JJ)95,70,70
   70 DO91LL=1,L
      M=J+LL
      KA=M/J
      MM=M
   71 IF(MM-J)91,80,72
   72 MM=MM-J
      GOTO71
   80 KKA=KA
   73 IF(KKA-2)90,91,74
   74 KKA=KKA-2
      GOTO73
   90 YC(J,1)=YC(J,1)-YC(M,1)/(FLOAT(KA*(-1)**((KA/2)+2)))
      YC(J,2)=YC(J,2)-YC(M,2)/(FLOAT(KA))
   91 CONTINUE
   95 J=J+1
      DO97K=1,KK
      C=SQRTF(YC(K,1)**2+YC(K,2)**2)
      PHI=ATANF(YC(K,2)/YC(K,1))*180.0/PI
      PHI=ABSF(PHI)
      IF(YC(K,2))470,510,540
  470 IF(YC(K,1))480,490,500
  480 PHI=180,0+PHI
      GOTO98
  490 PHI=270,0
      GOTO98
  500 PHI=360,0-PHI
      GOTO98
  510 IF(YC(K,1))520,530,530
  520 PHI=180,0
      GOTO98
  530 PHI=0,0
      GOTO98
  540 IF(YC(K,1))550,560,98
  550 PHI=180,0-PHI
      GOTO98
  560 PHI=90,0
```

```
 98 PMOD(K)=C
    PPHI(K)=360.0-PHI
 97 CONTINUE
    DEN=1.940/1728.0
    RAV=REV/60.0
    DIA=8.0
    CONS=(DEN*(RAV*DIA)**2)/12.0
    WRITE(61,125)
    WRITE(61,135)
    WRITE(61,136)
    M=0
    J=4*NPD
    DO570K=J,KK,J
    M=M+1
    A=M*4
    PRESS=PMOD(K)/FMOD(M)
    PPHASE=PPHI(K)+FPHASE(M)+A*SETANG
    GOTO566
564 PPHASE=PPHASE-360.0
566 IF(PPHASE.LT.360.0)569,564
569 PRESK=PRESS/CONS
    PRESC(M)=PRESS
    PERCENT=PRESC(M)*100.0/PRESC(1)
    WRITE(61,145)M,PRESC(M),PRESK,PPHASE,PERCENT
570 PANG(M)=PPHASE
    IBH=KK/(NPD*4)
    CALL CALMAX(PRESC,PANG,CONS,IBH,AAPHA)
    IF(LIST)580,580,99
580 WRITE(61,120)
    WRITE(61,130)
    DO590K=1,KK
590 WRITE(61,140)K,YC(K,1),YC(K,2),PMOD(K),PPHI(K)
    GOTO99
 96 WRITE(61,150)
    NTEST=2
 99 RETURN
    END


    SUBROUTINE CALMAX(Y,ANG,CONS,IBH,ALPHA)
C   DETERMINES  PEAK TO PEAK VALES, AND PHASE OF SYNTHESIZED WAVE.
    DIMENSION PP(100)
    DIMENSION Y(7),ANG(7)
    DIMENSION ALPHA(8)
 50 FORMAT(1H0)
 60 FORMAT(1H0,10F10.5)
 70 FORMAT(1H0,22X,24HVALUES OF TOTAL PRESSURE)
 80 FORMAT(1H0,70HMAX PRESSURE - ANGLE     MIN PRESSURE - ANGLE     PR
   1ESSURE COEFFICIENT)
 90 FORMAT(1H0,2(F10.5,F10.1,5X),4X,F10.5)
    WRITE(61,70)
    WRITE(61,80)
    PI=3.1415927
    DO100I=1,IBH
```

```
      A=ANG(I)*PI
  100 ANG(I)=A/180.0
      DANG=0.0
      PMAX=0.0
      PMIN=0.0
  150 P=0.0
      DO200I=1,IBH
      A=4*I
  200 P=P+Y(I)*COSF(ANG(I)*DANG*A)
      IF(P.GT.PMAX)300,400
  300 PMAX=P
      ANGMAX=DANG*180.0/PI
      GOTO600
  400 IF(P.LT.PMIN)500,600
  500 PMIN=P
      ANGMIN=DANG*180.0/PI
  600 IF(DANG.GE.(PI/2.0))800,700
  700 DANG=DANG+0.0005
      GOTO150
  800 PDIFF=PMAX-PMIN
      PK=PDIFF/(2.0*CONS)
      WRITE(61,90)PMAX,ANGMAX,PMIN,ANGMIN,PK
      DA=PI/180.0
      DO900N=1,100
      B=N-1
      DANG=B*DA
      PP(N)=0.0
      DO900I=1,IBH
      A=4*I
  900 PP(N)=PP(N)+Y(I)*COSF(ANG(I)+DANG*A)
      WRITE(61,50)
      WRITE(61,50)
      WRITE(61,50)
      WRITE(61,60)(PP(N),N=1,100)
      CALL MEKPLT(PP,100,1,1,1,ALPHA          ,10H  DEGREES ,10HPRESS
     1COEF,11,0,1H,)
      RETURN
      END


      SUBROUTINE SKIP(LU)
C     ROUTINE TO SKIP A FILE.
      DIMENSION IX(3)
   97 FORMAT(3I5)
  100 READ(02,97)(IX(I),I=1,3)
      IF(ENDFILE02)1000,200
  200 IF(IX(1).EQ.-1.AND.IX(2).EQ.-100.AND.IX(3).EQ.-10)400,300
  300 IF(IX(1).EQ.-2.AND.IX(2).EQ.-200.AND.IX(3).EQ.-20)900,1000
  400 DO500I=1,44
  500 READ(02,97)(IX(I),I=1,3)
      GOTO100
 1000 STOP 02
  900 RETURN
      END
```

```
      SUBROUTINE MEKPLT(YPT,IMAX,IMIN,JMIN,JMAX,GTITLE,XTITLE,YTITLE,
     1FACTOR,GP0,GP1,GP2,GP3,GP4,GP5,GP6,GP7,GP8,GP9)
C     GENERAL PURPOSE PLOTTING ROUTINE, AUTOMATIC SCALING, NO.OF PLOT
C     COMBINED UP TO 10,
C     YPT = NAME OF ARRAY TO PLOT WITH DIMENSIONS (IMAX,JMAX)
C     PLOTS POINTS FROM THE IMIN VALUE OF THE ARRAY YPT TO IMAX VALUE
C     PLOTS ONLY THE JMIN TO JMAX ARRAY OF POINTS IN YPT.
C     GTITLE = NAME OF GRAPH
C     XTITLE = NAME OF X AXIS
C     YTITLE = NAME OF Y AXIS
C     FACTOR = SCALE FACTOR TO CHANGE THE VALUES OF THE SUBSCRIPT I OF
C      YPT(I,J) TO A GIVEN QUANTITY
C     GP0,     GP9 = CHARACTER TO DESIGNATE THE PARTICULAR GRAPH
C     J OF YPT(I,J)
      DIMENSION GTITLE(8)
      DIMENSION YPT(IMAX,10),APT(100,10),ALPHA(100),BETA(10),IBETA(6)
   10 FORMAT(1H1,30X,8A10)
   20 FORMAT(1H ,20X,2H I,10A10)
   30 FORMAT(1H ,20X,2HI=,10A10,1HI)
   40 FORMAT(1H ,I18,4H =I ,100A1,3HI- )
   50 FORMAT(1H ,20X,2HI ,100A1,1HI)
   60 FORMAT(1H ,A10,10X,2HI ,100A1,1HI)
   61 FORMAT(1H ,4X,I4,12X,2HI ,100A1,1HI)
   62 FORMAT(1H ,2X,4H* 10,14X,2HI ,100A1,1HI)
   70 FORMAT(1H ,18X,I4,16X,I4,16X,I4,16X,I4,16X,I4,16X,I4)
   71 FORMAT(1H ,73X,I4)
   72 FORMAT(1H ,71X,4H* 10)
   80 FORMAT(1H ,65X,A10)
   90 FORMAT(1H )
  100 FORMAT(1H ,5HYDIV=,E16.9,5X,5HXDIV=,E16.9)
C     CALCULATE RANGE OF VALUES OF VARIABLE Y
      AMAX=YPT(IMIN,1)
      AMIN=YPT(IMIN,1)
      DO94K=JMIN,JMAX
      DO94I=IMIN,IMAX
      IF(YPT(I,K),GT.AMAX)91,92
   91 AMAX=YPT(I,K)
      GOTO94
   92 IF(YPT(I,K),LT.AMIN)93,94
   93 AMIN=YPT(I,K)
   94 CONTINUE
      RY=AMAX-AMIN
C     CALCULATE FACTOR TO EXPAND RANGE TO .GT. 50
      IF(RY.GT.50)95,96
   95 RF=1.0
      IRF=1
      GOTO97
   96 RF=50/RY
      IRF=ALOG10(RF)+1.0
      RF=10**IRF
   97 AMAX=AMAX*RF
      AMIN=AMIN*RF
```

```
      DO98I=IMIN,IMAX
      DO98K=JMIN,JMAX
   98 YPT(I,K)=YPT(I,K)*RF
      PRINT 10,(GTITLE(I),I=1,8)
      PRINT90
C     CALCULATE RANGE OF VALUES OF VARIABLE X
      IRX=IMAX-IMIN+1
      IF(IRX.LT.100)110,180
C     FOR .LT. 100 POINTS, CALCULATE 'BEST FIT' X-RANGE, AND NO. SPACES/
  110 IRX5=(IRX+4)/5
  120 IF(IRX5.EQ.(5*(IRX5/5)))140,130
  130 IRX5=IRX5+1
      GOTO120
  140 IRX=5*IRX5
      IC=100/IRX
      RC=IC
      RC=1/RC
      IXMIN=IRX5*(IMIN/IRX5)
      DO170K=JMIN,JMAX
      DO170I=1,100,IC
      IXGRAD=IXMIN+(I-1)/IC
      IF(IXGRAD.LT.IMIN)170,150
  150 IF(IXGRAD.GT.IMAX)170,160
C     DISTRIBUTE POINTS OVER THE FIELD OF 100 SPACES
  160 APT(I,K)=YPT(IXGRAD,K)
  170 CONTINUE
      GOTO250
C     FOR .GT. 100 POINTS, CALCULATE 'BEST FIT' X-RANGE AND NO. POINTS/S
  180 IRX5=(IRX+4)/5
  190 IF(IRX5.EQ.(20*(IRX5/20)))210,200
  200 IRX5=IRX5+1
      GOTO190
  210 IRX=5*IRX5
      IC=IRX5/20
      RC=IC
      IXMIN=IRX5*(IMIN/IRX5)
      DO240K=JMIN,JMAX
      DO240I=1,100
      IXGRAD=IMIN+(I-1)*IC
      IF(IXGRAD.LT.IMIN)240,220
  220 IF(IXGRAD.GT.IMAX)240,230
C     DISTRIBUTE POINTS OVER THE FIELD OF 100 SPACES
  230 APT(I,K)=YPT(IXGRAD,K)
  240 CONTINUE
  250 RY=AMAX-AMIN
C     CALCULATE 'BEST FIT' Y-RANGE
      IRY=RY
  260 IF(IRY.EQ.(50*(IRY/50)))280,270
  270 IRY=IRY+1
      GOTO260
  280 C=IRY/50
C     CHOOSE MIN Y VALUE
      IYMIN=AMIN
      IRY5=IRY/5
```

```
  284 IF(IYMIN.EQ.(IRY5*(IYMIN/IRY5)))285,286
  286 IYMIN=IYMIN-1
      GOTO284
  285 YMIN=IYMIN
      YMAX=YMIN+50.0*C
      IF(YMAX.LT.AMAX)270,287
C     PRINT GRADUATION MARKS ACROSS TOP
  287 DO290K=1,10
  290 BETA(K)=10H          I
      PRINT20,(BETA(K),K=1,10)
C     PRINT LINE ACROSS TOP
      DO300K=1,10
  300 BETA(K)=10H----------
      PRINT30,(BETA(K),K=1,10)
      DO410J=1,51
      DO310K=1,100
C     SET WHOLE FIELD BLANK
  310 ALPHA(K)=1H
      YGRAD=YMAX-(J-1)*C
      YGRAD2=YGRAD-C
      IF(IRX.LT.100)320,330
  320 IXDIV=100/IRX
      GOTO340
  330 IXDIV=1
C     IF Y-VALUE LIES BETWEEN VALUES OF 2 LINES, SET A POINT ON LOWEST L
  340 DO365K=JMIN,JMAX
      DO365I=1,100,IXDIV
      IX=I*RC
      IF(IX.LT.IMIN)365,341
  341 IF(IX.GT.IMAX)365,342
  342 IF(APT(I,K),LE.YGRAD)345,365
  345 IF(APT(I,K),GT.YGRAD2)350,365
  350 GOTO(500,501,502,503,504,505,506,507,508,509)K
  500 ALPHA(I)=GP0
      GOTO365
  501 ALPHA(I)=GP1
      GOTO365
  502 ALPHA(I)=GP2
      GOTO365
  503 ALPHA(I)=GP3
      GOTO365
  504 ALPHA(I)=GP4
      GOTO365
  505 ALPHA(I)=GP5
      GOTO365
  506 ALPHA(I)=GP6
      GOTO365
  507 ALPHA(I)=GP7
      GOTO365
  508 ALPHA(I)=GP8
      GOTO365
  509 ALPHA(I)=GP9
      GOTO365
  365 CONTINUE
```

```
      PY10=ALOG10(YMAX)
      IF(IRF.GT.0)366,367
  367 IPY10=ALOG10(YMAX)
      YGRAD=YGRAD/(10**IPY10)
      IPY10=IPY10-2
      IF(YGRAD.LT.0.0)371,372
  371 IYGRAD=100*YGRAD-1.0E-01
      GOTO368
  372 IYGRAD=100*YGRAD+1.0E-01
      GOTO368
  366 IPY10=-IRF
      IF(YGRAD.LT.0.0)373,374
  373 IYGRAD=YGRAD-1.0E-01
      GOTO368
  374 IYGRAD=YGRAD+1.0E-01
  368 IF(J.EQ.25)370,380
  370 PRINT60,YTITLE,(ALPHA(I),I=1,100)
      GOTO410
  380 IF(J.EQ.26)381,382
  381 PRINT61,IPY10,(ALPHA(I),I=1,100)
      GOTO410
  382 IF(J.EQ.27)383,385
  383 PRINT62,(ALPHA(I),I=1,100)
      GOTO410
  385 IF((J-10*(J/10)-1),EQ.0)390,400
  390 PRINT40,IYGRAD,(ALPHA(I),I=1,100)
      GOTO410
  400 PRINT50,(ALPHA(I),I=1,100)
  410 CONTINUE
C     PRINT LINE ACROSS BOTTOM
      PRINT30,(BETA(K),K=1,10)
C     PRINT GRADUATION MARKS ACROSS BOTTOM
      DO430K=1,10
  430 BETA(K)=10H          I
      PRINT20,(BETA(K),K=1,10)
C     PRINT X-GRADUATIONS
      XMAX=IMAX
      IPX10=ALOG10(XMAX)
      IX10=IPX10
      PFAC=ALOG10(FACTOR)
      IF(PFAC.LT.0.0)600,650
  600 IPFAC=1.0-PFAC+1.0E-01
      FAKTOR=FACTOR*(10**IPFAC)
      IPFAC=-IPFAC
      GOTO700
  650 IPFAC=PFAC+1.0E-01
      FAKTOR=FACTOR/(10**IPFAC)
  700 DO440I=1,6
      BETA(I)=(IXMIN+(I-1)*IRX5)*FAKTOR
      BETA(I)=BETA(I)/(10**IX10)
  440 IBETA(I)=100*BETA(I)+1.0E-01
      IPX10=IPX10-2+IPFAC
      PRINT70,(IBETA(I),I=1,6)
      PRINT71,IPX10
```

```
      PRINT72
      PRINT90
      PRINT80,XTITLE
C     PRINT VALUES OF LINE AND SPACE
      XDIV=IRX5/20*FACTOR
      YDIV=C/RF
      PRINT100,YDIV,XDIV
      RETURN
      END
```